Title
Evaluating Cool Impervious Surfaces: Application to an Energy-Efficient Residential Roof and to City Pavements

Author
Rosado, Pablo Javier

Publication Date
2016

Peer reviewed|Thesis/dissertation

Evaluating Cool Impervious Surfaces: Application to an Energy-Efficient Residential Roof and to City Pavements

by

Pablo Javier Rosado

A dissertation submitted in partial satisfaction of the

requirements for the degree of

Doctor of Philosophy

in

Engineering – Mechanical Engineering

in the

Graduate Division

of the

University of California, Berkeley

Committee in charge:

Professor Carlos Fernandez-Pello, Co-chair
Dr. Ronnen M. Levinson, Co-chair
Professor Alice M. Agogino
Professor Catherine P. Koshland

Spring 2016

Evaluating Cool Impervious Surfaces: Application to an Energy-Efficient Residential Roof and to City Pavements

Abstract

Evaluating Cool Impervious Surfaces: Application to an Energy-Efficient Residential Roof and to City Pavements

by

Pablo Javier Rosado

Doctor of Philosophy in Engineering – Mechanical Engineering

University of California, Berkeley

Professor Carlos Fernandez-Pello, Co-chair

Dr. Ronnen M. Levinson, Co-chair

Summer urban heat island (UHI) refers to the phenomenon of having higher urban temperatures compared to the those in surrounding suburban and rural areas. Higher urban air temperatures lead to increased cooling demand, accelerates the formation of smog, and contributes to the generation of greenhouse gas emissions. Dark-colored impervious surfaces cover a significant fraction of an urban fabric, and as hot and dry surfaces, are a major contributor to the UHI effect. Adopting solar-reflective ("cool") roofs and cool pavements, and increasing the urban vegetation, are strategies proven to mitigate urban heat islands. These strategies often have an "indirect" effect (ambient cooling) and "direct" effect (change in solar energy flux entering the conditioned space) on the energy use of buildings. This work investigates some elements of the UHI mitigation strategies, specifically the annual direct effect of a cool roof, and the direct and indirect effects of cool pavements.

The first topic researched in this paper consists in an experimental assessment of the direct effects from replacing a conventional dark roof with a highly energy-efficient cool roof. The study measures and calculates the annual benefits of the cool roof on the cooling and heating energy uses, and the associated emission reductions. The energy savings attributed to the cool roof are validated by measuring the difference between the homes in the heat loads that entered the conditioned space through the ceiling and HVAC ducts. Fractional annual cooling energy savings (26%) were 2.6 times the 10% daily cooling energy savings measured in a previous study that used a white coating to increase the albedo of an asphalt shingle roof by the same amount (0.44). The improved cooling energy savings (26% vs. 10%) may be attributed to the cool tiles above-sheathing ventilation, rather than to its high thermal mass. The roof also provided energy savings during the heating season, yielding fractional annual gas heating savings of 4% and electric heating savings of 3%. The slightly positive fractional annual heating energy savings likely resulted from the tile roofs high thermal capacitance,

which increased the overnight temperature of the attic air. Thus cool tile roofs should be perceived as a technology that provides energy and environmental benefits during the cooling season as well as the heating season.

The second topic investigates the direct and indirect effects of cool pavements on the energy use of California's building stock. First, a simple urban canyon model was developed to calculate the canyon albedo after the user provides the solar position, canyon orientation, and dimensions of the canyon walls, road, and setbacks. Next, a method is presented to correct the values of temperature changes obtained from previous urban climate models to values that would be obtained from canyon geometries that distinguish between road and setbacks (e.g. sidewalk, front yard).

The new canyon model is used to scale the temperature changes obtained from a recent urban climate model that simulated the climatological impact of cool pavements on various California cities. The adjusted temperature changes are then combined with building energy simulations to investigate the effect of cool pavements on the cooling, heating, and lighting energy uses of buildings as well as the environmental impact related to these energy uses. Net (direct + indirect) conditioning (cooling + heating) energy savings and environmental savings from cool pavements were smaller in residential buildings than in commercial buildings. Additionally, residential buildings strongly dominate the building stock in all of the evaluated cities. Therefore, even though most cities yielded conditioning energy and environmental savings, they were small due to the minuscule savings from the residential buildings. When increasing the albedo by 0.20 of all public pavements in different California cities, Los Angeles was the city with the largest savings, yielding only 0.60% in Primary Energy Demand and 0.30% in Global Warming Potential (GWP). Some of the cities experienced even a small net penalty in GWP of up to 0.20%.

Dedicado a mi familia Rosado Ramírez, mi esposa Rebeca y mi hijo amado Pablo Andrés.

Table of Contents

List of Figures

List of Tables

Abbreviations

AC air conditioning

AFUE annual fuel utilization efficiency

ARB Air Resources Board

BCZ building climate zone

CAT Canyon Air Temperature

CBECS Commercial Building Energy Consumption Survey

CEC California Energy Commission

CEUS Commercial End-Use Survey

COP coefficient of performance

CRRC Cool Roof Rating Council

DOE Department of Energy

DX direct exchange

EP EnergyPlus

EPA Environmental Protection Agency

FCU fan coil unit

GHG greenhouse gas emissions

HVAC heating, ventilation, and air conditioning

LBNL Lawrence Berkeley National Laboratory

LCA life cycle assessment

LDT Local Daylight Time

LST Local Standard Time

MLUCM multi-later urban canopy model

MZ VAV multi-zone variable air volume

NLCD National Land Cover Data

NREL National Renewable Energy Laboratory

PACU precision air conditioning unit

RECS Residential Energy Consumption Survey

SEER Seasonal Energy Efficiency Ratio

SHGC solar heat gain coefficient

SLUCM single-layer urban canopy model

SR solar reflectance

SZ CAV single-zone constant air volume

TEB Town Energy Budget

TUF-IOBES Temperature of Urban Facets Indoor-Outdoor Building Energy Simulator

UAM Urban airshed model

UCM urban canyon model

UCPRC University of California Pavement Research Center

UHI urban heat island

USC University of Southern California

USGS United States Geological Survey

WBT White Box Technologies

WRF Weather Research and Forecasting

ZCSC Zoning Code of Sacramento County

Acknowledgments

First of all, I would like to thank my parents Pablo F. and Cindy for their unconditional support and immeasurable love they have given to my sister and me throughout our lives as we pursued our personal and professional goals. To my dear sister Liza for always being there for me and believing in me; my life has been so much fun and so great simply because you are in it. I am also immensely grateful to the Lord for my wife Rebeca M. Rosado; she came to my life exactly when I was going through the roughest patch in my graduate school years, when I was contemplating giving up on pursuing a PhD. I am so thankful to her for being so supportive and standing by me since then. Most of all, thank you Rebeca for the greatest blessing of making me the father of our baby boy Pablo Andrés Rosado Cordero. This final stretch in completing the dissertation would have been impossible to finish if you and our moms had not carry all of the burden that comes after having a newborn baby.

I want to thank my research advisor Ronnen Levinson, who allowed me to join the Heat Island Group at the end of my first year in Berkeley. He trained me and taught me so much in the past six years. I really appreciate his exceptional guidance on my academic and professional career. To other current and past members of the Heat Island Group: Haley, George, Mel, Hugo, Paul, Sharon, Jane, and Jordan. Thank you for your inputs, help, and great times.

I also want to thank the other dissertation committee members—Carlos Fernandez-Pello, Catherine Koshland, and Alice Agogino—for their assistance and helpful feedback on my research and dissertation. Additionally, I want to thank Carlos for allowing me to be a GSI in his Heat Transfer class; and Alice for allowing me to be a Reader in her Introduction to Product Development class.

Life in Berkeley could not have been as fun as it was if it wasnt for the great and special friends I made during this time. Thank you Jessica, Diana, Amneris, Lucas, Michelle, Andres, Romina, Shuk, John, and the awesome friends I met through LAGSES.

Finally, I want to thank the institutions, fellowships, and people that has made not only my research possible, but supported my financial needs during my life in Berkeley. Starting with the GEM Fellowship, the SUPERB REU program and its directors Beatriz Lopez-Flores and Meltem Erol, the Alfred P. Sloan Foundation Minority Ph.D. Program, and all the funding that Yawo, Shareena, Donna, and Lisa Pruitt were able to secure for me many times through the Mechanical Engineering Department.

The cool roof study was supported by the California Energy Commission (CEC) through its Public Interest Energy Research Program (PIER). It was also supported by the Assistant Secretary for Energy Efficiency and Renewable Energy, Office of Building Technology, State, and Community Programs, of the U.S. Department of Energy under Contract No. DE-AC02-05CH11231. I wish to thank Michael Spears and Woody Delp, and the Windows

and Envelope Materials Group (Lawrence Berkeley National Laboratory); Victor Gonzalez, Tony Seaton, Terry Anderson, Darius Assemi, Mike Bergeron and Karl Gosswiller (Granville Homes Inc.); Ming Shiao and Richard Snyder (CertainTeed Corp.); Annette Sindar and Greg Peterson (Eagle Roofing Products); Danny Parker (Florida Solar Energy Center); and Hashem Akbari (Concordia University).

The cool pavement study was possible thanks to the funding from the California Air Resources Board under Contract 10-321. I especially thank Tabetha Willmon and Courtney Smith, formerly of the California Air Resources Board for their support during the project. This work was also supported by the Assistant Secretary for Energy Efficiency and Renewable Energy, Office of Building Technology, State, and Community Programs, of the U.S. Department of Energy under Contract No. DE-AC02-05CH11231.

CHAPTER 1

Introduction

1.1 Problem overview

Summer urban heat island (UHI) is the phenomenon of having higher urban temperatures compared to those in surrounding suburban and rural areas. Higher urban air temperatures lead to increased cooling demand, accelerate the formation of smog, and contribute to the generation of greenhouse gas emissions. Dark-colored impervious surfaces cover a significant fraction of an urban fabric, and as hot and dry surfaces, are a major contributor to the UHI effect. Adopting solar-reflective ("cool") roofs and cool pavements, and increasing the urban vegetation are strategies shown to mitigate urban heat islands. These strategies often have an "indirect" effect (ambient cooling) and "direct" effect (change in solar energy flux entering the conditioned space) on the energy use of buildings. This work investigates specific elements of the UHI mitigation strategies, specifically the annual direct effect of a cool roof, and the direct and indirect effects of cool pavements.

Past studies have measured the benefits of residential cool roofs, particularly their impact on reducing cooling energy use. Some of the roofs previously researched are highly efficient cool roofs as they not only have high solar reflectance but also high thermal capacitance, which cools the roof even further. The first topic studied in this thesis consists of an experimental assessment of the direct effects from replacing a conventional dark roof with a highly energy-efficient cool roof. The study measures and calculates the annual benefits of the cool roof on the cooling and heating energy uses, and the associated emission reductions.

Most of the prior studies that examined the climatological and energy effects of cool pavements include the contributions from other UHI mitigation strategies (cool roofs and urban vegetation). Only a few past studies have focused on the individual contributions of cool pavements. This paper also investigates the total effect (direct and indirect) of cool pavements on the energy use of California's building stock by combining building energy simulations with recent efforts that simulated the climatological impact of cool pavements.

1.2 Past studies

1.2.1 Direct effect of residential cool roofs

The influence of cool roofs on a building's conditioning energy use has been most commonly studied through building energy simulations. There are relatively few experiments that have measured the building energy impact of cool roofs and most have been on commercial buildings. Some of the previous measurement work on residential homes calculated cool roof savings by measuring pre- and post-retrofit data periods with similar weather patterns (periods with similar profiles of air temperature and sunlight). However, the weather during the pre-retrofit (dark roof) period will never fully match the post-retrofit (cool roof) period and the results are not perfectly comparable. Other studies compared buildings of different size, occupancy patterns and/or in separate locations.

Parker et al. [1] makes the first attempt to compare different cool roof technologies on real-size, side-by-side, unoccupied identical homes. All the homes were controlled to have the same thermostat settings, occupancy patterns, and HVAC equipment. This way the only difference in the interior thermal loads was the heat gained through the roofs. The study measured the cooling benefits of the cool roofs for one summer month.

1.2.2 Direct and indirect effects of cool pavements

Prior studies that investigated the climatological impact of UHI mitigation strategies like cool roofs, cool pavements, and urban vegetation, demonstrated that they can help reduce the convective heating of the city air, which reduces the air temperature and decreases the cooling load in buildings. More recently, other investigations have employed atmospheric models to simulate the individual contribution of cool pavements on decreasing the air temperature. Separately, other studies have used building energy simulations to estimate the direct effect of cool pavements. However, there is a need to understand the total effect on building energy use attributed only to the adoption of cool pavements.

1.2.3 Canyon geometries defined in urban canyon models

Many 2D urban canyon models (UCMs) are coupled with atmospheric models to assess the urban heat islands and their effect on the regional climate. Some past studies have employed these atmospheric/UCM systems to simulate the effect of cool pavements on the local urban climate. Most of these UCMs consider three types of canyon surfaces—roof, wall, and floor. In real urban canyons, the floor is composed of a road and surrounding setbacks (e.g. sidewalk, front yard). Therefore, it would be helpful to have a method to correct the predictions from the atmospheric/UCM systems to better represent realistic canyon floor geometries.

1.2.4 Novel contributions: Cool roof measurements, building energy simulations, and canyon models

The studies performed to date leave room for new research related to the annual energy impact of residential cool roofs and on the overall building energy effect of cool pavements. This dissertation focuses on these two areas and sets out to answer the following questions:

- What are the cooling benefits a cool tile roof will provide over a dark shingle roof in a hot California climate?
- Will the cool tile roof benefit or penalize the heating energy use during the cold season?
- Can the results from urban climate simulations done using current 2D urban canyon models be adjusted to values that would be obtained from realistic urban geometries?
- What is the overall effect of cool pavements on a building's energy use?
- By how much do cool pavements affect the citywide energy use?

1.3 Physics

1.3.1 Effect of roofs in conditioning energy use

The albedo, ρ, of a roof is the fraction of solar energy that is reflected from the roof's surface; in opaque surfaces, solar absorptance, α, can then be calculated as ($\alpha = 1 - \rho$). The absorbed energy heats up the roof and a portion of the heat flows downward. In homes with an attic space, that heat flows to the bottom of the roof (attic ceiling) and is convected to the attic air and emitted to the other attic surfaces. Part of that heat added to the attic space will eventually be conducted through the ceiling and through the HVAC ducts located in the attic, increasing the thermal load in the conditioned space. Hence, increasing the albedo of the roof can help decrease the flow of heat from the roof to the interior.

Roofs with high thermal capacitance (e.g. concrete or clay tiles) remain cooler under the sun and thus reduce the downward heat flow. When tiles are offset from the roofing deck, natural convection below the tiles ("above-sheathing ventilation") can enhance cooling of the roofing system, which helps cool the building.

1.3.2 Direct and indirect effects of pavements on a building's energy use

Cool pavements reduce convective heating of the outside air. This reduction lowers the outside air temperature and changes the temperature difference across the building envelope.

This indirect effect of cool pavements is expected to reduce cooling loads and increase heating loads. Cool pavements also increase their direct effect – related to the reflected sunlight that strikes neighboring walls and windows – which can increase the cooling load and decrease heating load. The increase in reflected sunlight transmitted through the windows may also reduce the need for artificial lighting.

1.3.3 Characteristics of an urban canyon alter the impact of cool pavements

The ability of sunlight to enter into an urban canyon, reach the floor, and be reflected back to the sky depends on the solar position, canyon orientation, and albedos and dimensions of the canyon surfaces. The fraction of canyon-reflected sunlight to entering sunlight can be interpreted as the *canyon albedo*.

The reduction in the air temperature in a city is proportional to the reduction in the canyon's solar heat gain, which in turn is proportional to the decrease in the canyon's solar absorptance. Reducing the solar absorptance of the canyon is equivalent to increasing the canyon albedo. Cool pavements can help increase the canyon albedo. However, the magnitude of the change in canyon albedo is sensitive to the view factor from the pavement to the sky[1].

1.4 Investigations

1.4.1 Measure annual impact of a cool roof

This work presents a study which measured the difference in HVAC energy use between a home with a dark roof (dark asphalt shingles) and a home with the most efficient residential cool roof currently available in California's market (high-reflectance concrete tiles). The homes were side-by-side, nearly-identical, and unoccupied. The experiment was monitored for one year and accounts for the annual cool roof energy and cost savings, and emission and peak-hour demand reductions. The energy savings attributed to the cool roof are validated by measuring the difference between the homes in the heat loads that entered the conditioned space through the ceiling and HVAC ducts.

1.4.2 Scale results of urban climate models to better represent urban canyon floors

This paper describes a model developed to calculate the urban canyon albedo given the user-defined solar position, canyon orientation, and dimensions of the canyon walls, road,

[1]View factor (a.k.a. configuration factor or shape factor) from surface A to surface B is the fraction of radiant energy leaving surface A that is intercepted by surface B.

and setbacks. Next, a method is presented to correct the values of temperature changes obtained from previous urban climate models to values that would be obtained from urban canyon geometries that distinguish between road and setbacks.

1.4.3 Overall effect of cool pavements on conditioning energy use

The newly developed canyon model is used to scale the temperature changes obtained from a recent urban climate model that simulated the climatological impact of cool pavements on various California cities. The adjusted values are then combined with building energy simulations to investigate the overall effect of cool pavements on the annual energy uses on residential and commercial buildings. The results are used to estimate the citywide effect on different California urban areas.

1.5 Heat island mitigation strategies in California

As global climate change manifests throughout California, the state is evaluating and implementing strategies to reduce greenhouse gas (GHG) emissions, mitigate urban heat islands, and improve air quality. The California Air Resources Board (ARB) has set in place short-term and long-term GHG emissions reduction targets and air pollution standards. In addition, California introduced in 2006 the Global Warming Solutions Act (Assembly Bill 32), which requires the state to reduce GHG emissions to 1990 levels by 2020. The Heat Island Group in Lawrence Berkeley National Laboratory (LBNL) have been conducting various projects to advance the science and implementation of strategies that will help meet the GHG emissions goals and improve the states environmental challenges. Two of the projects are summarized below.

1.5.1 Urban Heat Island Mitigation project

LBNL conducted a project titled *Urban Heat Island Mitigation Phase 2* funded by the California Energy Commission (CEC). The project studied various voluntary measures to reduce emissions and mitigate UHIs through implementing strategies such as cool roofs, cool pavements, cool walls, and urban vegetation. The work included cool roof and cool pavements demonstration projects in Fresno, California (cool roof) and in Davis, California (cool pavements) to quantify their energy and environmental benefits. The team also created a database of cool roof retrofit projects with accompanying energy savings analysis; conducted ethnographic case studies with several homeowners to understand why they installed cool roofs and how they selected a product; developed and presented courses on cool roofs and cool pavements; studied the effect of trees on community albedo; and created a residential roofing survey instrument to better understand the decision of homeowners (Haley et al. 2011).

1.5.2 Pavement Life Cycle Assessment Decision Tool project

To help meet the state's GHG emission reduction targets and air pollution standards, the California Environmental Protection Agency and the ARB are evaluating the environmental impact of statewide adoption of cool pavements. A collaborative research effort between Lawrence Berkeley National Laboratory (LBNL), University of California Pavement Research Center (UCPRC), University of Southern California (USC), and thinkstep Inc. is currently developing a pavement life cycle assessment (LCA) decision support tool.

The tool helps decision makers assess the energy and environmental consequences of constructing, using, and maintaining a pavement choice over a 50-year cycle. Given the city of interest, the fraction of the pavement's area to modify, and two pavement scenarios, the tool reports the differences in:

- two LCA indicators: global warming potential and smog potential;
- three life-cycle flows: PM2.5, feedstock energy, and primary energy demand without feedstock energy; and
- annual site electricity and natural gas uses (cooling, heating, and lighting).

The "use" phase of pavements is responsible for their indirect and direct effects on a city's building stock energy use, including annual site electricity (cooling, heating, and lighting) and nature gas (heating) uses.

1.6 Thesis overview

1.6.1 The big picture

This thesis includes my contribution to the *Urban Heat Island Mitigation Phase 2* project and to the *Pavement LCA Decision Tool* project. The first topic of the thesis is presented in Chapter 3, and measures the annual impact of an energy-efficient cool roof. This cool roof study constitutes one of the voluntary measures studied for the UHI Mitigation Phase 2 project. The second topic includes: a) the development of a canyon model to correct the temperature predictions of climate models (Chapter 4), and b) the simulation and analysis of the total (direct + indirect) effect of cool pavements during their use phase (Chapters 5 and 6). The concluding remarks address the results from both topics (Chapter7). The appendices provide supporting material for the two topics presented in the dissertation. Additionally, the last appendix presents the computer code that describe the urban canyon model that was developed.

The impact of cool pavements during their non-use phase (material, transportation, and construction), the design and execution of the pavement LCA tool, and the life-cycle impact of cool pavements are not investigated since they are outside the scope of this thesis.

1.6.2 Topic one: comparing two different roof technologies in side-by-side homes

Chapter 3 presents a demonstration project conducted in Fresno, California to quantify the benefits of cool roofs. The temperatures, heat flows, and energy uses in two similar single-family, single-story homes built side by side were measured for a year to assess cool-roof benefits. The "cool" house had a reflective cool concrete tile roof (initial albedo 0.51) with above-sheathing ventilation, and nearly twice the thermal capacitance of the standard dark asphalt shingle roof (initial albedo 0.07) on the "standard" house.

Cool-roof energy savings in the cooling and heating seasons were computed two ways. Method A divides by HVAC efficiency the difference (standard – cool) in ceiling + duct heat gain. Method B measures the difference in HVAC energy use, corrected for differences in plug and window heat gains.

1.6.3 Topic two: effects of cool pavements on the energy use of current California building stock

In developing the pavement LCA tool, the project collaborators from USC applied a regional climate model to derive the sensitivity of citywide mean air temperature to pavement albedo change. However, the temperature sensitivities they provided needed to be adjusted to values that would be obtained from realistic urban canyon floor dimensions and solar position of a particular city. Chapter 4 presents an urban canyon model developed to correct the temperature sensitivities. The model calculates the solar downward and solar upward radiances through the canyon ceiling, and computes the canyon albedo as the ratio of upward to downward irradiance. Additionally, the chapter presents a method to scale the temperature sensitivities of a particular city to represent the city's street construction standards and its building stock.

The corrected temperature sensitivities were applied when simulating building energy use to estimate the indirect effect of cool pavements. The prototypes used in the building simulations were also modified with external horizontal surfaces to mimic neighboring pavements and estimate their direct effect. Chapter 5 describes the methodology followed for a) simulating the effects (direct + indirect) of cool pavements on building energy use, b) deriving the sensitivities of a building's electric and gas uses to changes in the local and citywide pavement albedo, and c) estimating their citywide impact on California cities.

Chapter 6 includes the results obtained from the building energy simulations.

1.6.4 Conclusions

The conclusions of these study are reported in Chapter 7.

CHAPTER 2

Literature Review

2.1 Impact of high-albedo surfaces

2.1.1 Mitigate urban heat islands, improve air quality, and reduce greenhouse gas emissions

Reduce city air temperature. Millstein and Menon [2] modelled the entire United States at 25 km resolution for 12 years to investigate the regional climate consequences of a widespread deployment of cool roofs and cool pavements. They employ Weather Research and Forecasting (WRF) Model version 3.2.1 for their modelling and each urban grid cell was treated as a 2-D surface without including the effects of urban geometry and surface-atmosphere interactions. Overall, annual outgoing radiation increased by 0.16 ± 0.03 W/m^2 (mean $\pm$ 95% confidence interval) and afternoon summertime temperature in many urban locations was reduced by 0.11 to 0.53°C (some urban areas did not show statistically significant temperature changes).

Additionally, Santamouris [3] performed a meta-analysis of meteorological simulations in many U.S. cities and found that each 0.10 rise in urban albedo (mean solar reflectance of the entire city) decreases average outside air temperature by about 0.3°C, and lowers peak outside air temperature by 0.6 to 2.3°C.

Furthermore, Rosenfeld et al. [4] estimated that in the Los Angeles basin, the urban heat island excess temperature could be reduced by about 0.5°C if the solar reflectance of all its pavements could be raised to 0.35 from 0.10.

Offset global warming, reduce GHG emissions, and improve air quality. Using cool roofs and pavements in a city immediately reduces the flow of thermal radiation into the troposphere ("negative radiative forcing"), offsetting the global warming induced by emission of greenhouse gases [5, 6]. Most recently, Akbari et al. [7] estimated that increasing by 0.01

the albedo of 1 m^2 of urban surface provides a one-time (not annual) offset of 4.9 to 12 kg CO_2.

Akbari et al. [8] noted that urban trees and high-albedo surfaces can improve air quality and decelerate the formation of smog, as smog forms more slowly at lower air temperatures.

2.1.2 Direct and indirect effect on a buildings conditioning energy use

Cooling savings. Akbari et al. [8] estimated that 5 to 10% of the urban electricity demand in cities is used to compensate for the 0.5 to 3.0°C increase in urban temperature attributed to the UHI effect. They also estimated that 20% of the national cooling demand can be avoided through a large-scale implementation of heat island mitigation strategies (cool roofs, cool pavements, and urban trees).

Annual direct and indirect effects from cool surfaces and green areas. Taha [9] employed the Colorado State University Mesoscale Model (CSUMM) to simulate the indirect cooling effect of higher albedo of urban surfaces and increased urban vegetation. The study found peak afternoon air temperature reductions of 0.5 to 1.5°C. Results were fed into a DOE-2 building energy model and obtained peak power demand reductions of up to 10%. Akbari and Konopacki [10] used the simulations from Taha [9] to estimate the indirect energy use effect of heat island reduction strategies for 240 locations in the United States. Akbari and Konpacki modelled three common building types (residence, office, and retail store). Each building was characterized in detail by Pre-1980 (old vintage) or 1980+ (new vintage) construction standards. They also simulated the direct effect on energy use from cool roofing materials and from neighboring trees. The study found that for all building types, over 75% of the total annual savings were from the direct effects.

Heating penalties. During winter, buildings may have a larger heating demand to compensate for the colder outside air in the presence of cool pavements. Hence, it is important to evaluate for different locations and climates the net annual impact of cool pavements in the conditioning energy use. Taha et al.[11] accounted for heating penalty in building energy simulations in 10 different U.S. cities by increasing the roof and pavement albedos by 0.15 and increasing the city-average vegetative fraction by 0.03 to 0.04. The gas heating penalties ranged from 0 (office areas in Miami, FL) to 3,519 MJ per 100 m^2 of roof area (residential areas in Philadelphia, PA). Is important to note that the heating penalties outweighed the cooling benefits only in the residential areas of New York, NY and Philadelphia, PA[1].

[1]Net energy savings in Taha et al. [11] account for both the direct effect from cool roofs and shade trees as well as the indirect effect from high-albedo urban surfaces.

2.2 Simulated and measured direct benefits of cool roofs

2.2.1 Effects of increased roof albedo on conditioning energy use

2.2.1.1 Simulations

Residential cooling savings and heating penalties in different climates. Akbari et al. [12] simulated in the DOE-2 building energy software, the annual cooling and heating energy uses of a variety of building prototypes in 11 U.S. cities. They found that raising the albedo of an RSI-3.3 asphalt-shingle roof by 0.30 reduced the annual cooling energy use of a single-story home by 6 to 15%, and increased annual heating energy use by 0 to 5%.

Synnefa [13] also estimated the effect of cool roofs on the energy loads in residential buildings in various climatic conditions (27 cities around the world were represented). The climatic conditions included Mediterranean, humid continental, subtropical arid, desert conditions, etc. The study modelled a single-story, flat roof (100 m^2 roof area) residential prototype using TRNSYS (a software environment used to simulate transient systems [14]). Increasing the solar reflectance reduced the cooling loads by 18 to 93% and peak cooling demand in air-conditioned buildings by 11 to 27%. These reductions were greater in poorly or non-insulated buildings. In all the locations studied, the heating penalties were less than the cooling benefits. For the case of Los Angeles, the cooling energy was reduced by 39% when increasing the roof albedo by 0.40 and 59% when increased by 0.65.

Energy use, cost, and emission savings. Using building energy simulations, local energy prices, and local electricity emission factors, Levinson and Akbari [15] estimated the potential benefits from the US widespread adoption of cool roofs in commercial buildings. In the study, they utilized building energy simulations, local energy prices, and local electricity emission factors. Increasing the roof albedo to 0.55 from 0.20 yielded nationwide mean annual savings per conditioned roof area of 5.02 kWh/m^2 (cooling energy), 0.065 $therm/m^2$ (heating penalties), 3.02 kg/m^2 (CO2 reduction), 4.81 g/m^2 (NO_x reduction), 12.4 g/m^2 (SO_2 reduction), and 61.2 $\mu g/m^2$ (Hg reduction).

2.2.1.2 Measurements

Residential cooling savings. Parker and Barkaszi [16] measured daily cooling energy uses in summer before and after applying white roof coatings to nine occupied single-story Florida homes. The homes varied in floor area, attic insulation, roof type, and HVAC capacity. Savings ranged from 2 to 40% and averaged 19%. In a home with RSI-3.3 (R-19) ceiling insulation, increasing the albedo of an asphalt shingle roof by 0.44 (to 0.59 from 0.15) reduced daily cooling energy use by 10%, and lowered peak cooling power demand by 16%.

Miller et al. [17] measured cooling energy uses in three pairs of Northern California homes. Each pair of homes had color-matched standard (lower albedo) and cool (higher albedo) roofs. The first pair had brown concrete tile roofs with albedos of 0.10 (standard)and 0.40 (cool); the second, brown metal roofs with albedos of 0.08 (standard) and 0.31 (cool); and the third, gray-brown shingle roofs with albedos of 0.09 (standard) and 0.26 (cool). After adjusting for widely disparate occupancy patterns, summer daily cooling energy savings were estimated to be about 9% in the homes with the cool tile and cool metal roofs; savings for the cool shingle roof were unclear.

2.2.2 Effects of roofs with high thermal capacitance and above-sheathing ventilation on conditioning energy use

2.2.2.1 Simulations

Comparing tile roof to shingle roof. De With et al. [18] studied the thermal benefits of tiled roofs with above-sheathing ventilation and of the high thermal mass of roof tiles. The study simulates the thermal benefits of a tiled roof over a shingle roof under hot climatic conditions typical of California. The thermal mass of the tile provided 6% annual savings. When the tiles rest on battens to provide ventilation under the tile array, the benefits are up to 14%. The study showed that the thermal mass of tiles and below tile ventilation reduces the heat that is conducted into the attic space.

2.2.2.2 Measurements

Comparing summer heat flows through a flat tile roof assembly to a shingle roof. Miller and Kosny [19] measured the summer daily heat flows through a flat tile roof on double battens (tile albedo = 0.13) and through a shingle roof (albedo = 0.09) each installed over a modestly insulated ceiling [RSI-0.9 (R-5)] in a test assembly. The heat flow through the tile roof was only half that through the shingle roof, even though the solar absorptance (1 – albedo) of the tile was only 4% lower than that of the shingle.

Comparing summer cooling energy use of seven different roof types in identical, unoccupied, side-by-side homes. The first attempt to quantify the influence of cool roofs on cooling energy use on identical, unoccupied, side-by-side homes happened in Fort Meyers, Florida [1]. The study spanned for one month during summer. The research measured the effect on the cooling energy use of seven different roofing types installed in seven single-family homes with identical floor plans, orientation, and ceiling insulation [RSI-3.3 (R-19)]. Six of the seven roofs had natural ventilation in the attic while the seventh had an unvented attic. The control scenario was a dark gray shingles roof (albedo = 0.08). It was compared to white shingles (albedo = 0.24), terra cotta barrel tile (0.35), white barrel tile (0.74), flat white tile (0.77), and white metal (0.66). Results indicate that the three white highly reflective roofs (barrel tile, flat tile, metal) reduced cooling energy use by 18 to 26%

and peak demand by 28 to 35%. The savings from the terra cotta tile roof were between 3 and 9%; savings from the white shingles were between 3 and 5%.

2.3 The effects of pavements on building energy use

Section 2.1 summarized past studies that investigated the combined impact of different UHI mitigation strategies (cool roofs, cool pavements, and urban vegetation). The studies described in this section investigated the individual contribution of cool pavements on building energy use.

2.3.1 Indirect effect

Estimated savings from utility-measured energy use. Pomerantz et al. [20] developed a method to estimate the energy savings that might be achieved in a large city by increasing the mean pavement albedo. The technique is restricted to the indirect effect, and uses the power demand recorded by the utilities and the cooling degree hours to define a simple linear equation particular to a city. Results showed that for Sacramento, California, the electrical energy savings from increasing the pavement albedo by 0.20 are 2 kWh per year per square meter of modified city surface.

Estimated peak power savings. Taha [21] used the Colorado State University Mesoscale Model (CSUMM) model and Urban Airshed Model (UAM) to simulate the mesoscale meteorology and ozone air quality in the South Coast Air Basin Area in California. With Taha's results, Pomerantz et al. [22] estimated that if the albedo of all the pavements in Los Angeles (1250 km^2 of pavement) was raised by 0.25, it could save 100 MW of peak power.

2.3.2 Direct effect

In addition to the indirect effect cool pavements may have on building energy use, the sunlight reflected from the pavements may strike the walls and windows of adjacent buildings, which could increase the thermal load.

Direct effect as a function of building age, canyon geometry, and window-to-wall ratio. Yaghoobian and Kleissl [23] applied the Temperature of Urban Facets Indoor-Outdoor Building Energy Simulator (TUF-IOBES) to investigate the effects of reflective pavements on the energy use of office buildings in Phoenix, Arizona. They studied the sensitivity of building energy use to change in pavement albedo by canyon height-to-width ratio, building age, window-to-wall ratio, and window type. In one case study, having a window-to-wall ratio of 47% and modifying the pavement albedo to 0.50 from 0.10 increased the cooling loads up to 11%; the impact on the annual heating loads was small. The authors

note that building conditioning energy use consequences from cooler pavements depends on building construction, building operation, and location.

Sailor et al. [24] modelled the direct effect of cool pavements on three-story buildings when increasing the pavement albedo to 0.46 from 0.17 in Houston, Texas and in Phoenix, Arizona. Their work combined EnergyPlus building energy modelling with Canyon Air Temperature (CAT) urban canyon model, and found that cooling energy increased with pavement albedo. The effect was stronger for buildings having windows with greater solar heat gain coefficient and for wider roads (road-to-wall view factor increases with road width).

2.4 Canyon characteristics in urban canyon models

Many urban canyon models (UCMs) are coupled with atmospheric models to assess the near-surface heat islands and their effect on the regional climate in an urban area [9, 25]. 2-D urban canyon models parameterize the thermal properties and dimensions of the urban canyon surfaces (roofs, walls, and floor). These models generally treat the canyon floor as a uniform surface, not distinguishing between the road and segments (surface between road and wall).

UCMs that consider canyon floor as one uniform surface. Masson [26] presents one of the first attempts to use a well-known canyon geometry to represent a city in an atmospheric model. He developed the Town Energy Budget (TEB) scheme to represent the energy exchanges between the canyon surfaces (roofs, walls, and floor) and the atmosphere. Kusaka et al. [27] developed a single-layer canyon model for energy and momentum exchange between the urban surfaces and the atmosphere. Their work is one of the pioneers in considering the canyon orientation and solar position, which is used to calculate the portions of the canyon that are in shade. Later, Kusaka and Kimura [28] incorporated the single-later canyon model into an atmospheric model to describe the impact of the urban canyon model on an idealized urban heat island simulation. Martilli et al. [29] developed a multi-layer canyon model to explore the impact of the urban buildings on the airflow modelled in an atmospheric model; this model is more sophisticated than any of the former models as it characterizes the buildings density and properties as a function of height.

Dividing the canyon surfaces into multiple equal-size segments. In real urban settings, the road forms only a fraction of the canyon floor. Fortuniak [30] developed a model in which the canyon walls and floor are divided into multiple equally wide segments and each segment can be assigned its own albedo. The model examines the impact of the solar position, canyon geometry, and canyon orientation on the albedo of the canyon. It also considers multiple reflections between the canyon surfaces, hence, when the number of segments is large, running the model can be time-consuming.

2.5 Conclusion

The aforementioned studies have advanced our understanding on the impacts of cool surfaces on mitigating urban heat islands. In the case of cool roofs, most of the studies have concentrated on their impact during summertime. However, they leave room for new research related to the annual impact of not only highly reflective roofs, but of energy-efficient roof assemblies. The first topic of this dissertation describes a demonstration project that was set to examine the annual benefits of an energy-efficient cool roof, and will by presented in Chapter 3.

As mentioned earlier in this chapter, the majority of the past studies on UHI mitigation strategies that involve cool pavements include other urban surfaces. Very few studies have explore the individual contributions of cool pavements on the urban climate. Additionally, there is a need to understand the direct effect of cool pavements on building energy use using realistic pavement geometries on different types of buildings. The second topic of this dissertation (Chapters 4 - 6) focuses only on cool pavements. This study combines the indirect and direct effects of cool pavements on building energy use to assess their overall energy impact in different California climates.

CHAPTER 3

Cool Roof Study

3.1 Introduction

[1]The number and size of air-conditioned homes in hot climates has risen significantly over the past 20 years, increasing U.S. residential cooled floor area by 71% [32]. Boosting the albedo of a building's roof can save cooling energy in summer by reducing solar heat gain, lowering roof temperature, and decreasing heat conduction into the conditioned space and the attic ducts. It may also increase the use of heating energy in winter. Prior research has indicated that net annual energy cost savings are greatest for buildings located in climates with long cooling seasons and short heating seasons, especially those buildings that have distribution ducts in the attic [12, 13, 15, 33–35].

Cool roofs decrease summer afternoon peak demand for electricity [10, 12, 36], reducing strain on the electrical grid and thereby lessening the likelihood of brownouts and blackouts. Reducing peak cooling load can also allow the installation of a smaller, less expensive air conditioner. This is referred to as a "cooling equipment" saving [36]. Smaller air conditioners are also typically less expensive to run, because air conditioners are more efficient near full load than at partial load.

High thermal capacitance and/or subsurface natural convection ("above-sheathing ventilation") in the roof system can further cool the building [1, 18, 37, 38]. Note that above-sheathing ventilation (air flow in the space between sheathing, or roof deck, and the roofing product) is usually driven by buoyancy,rather than wind, because building codes typically require the airspace at the eave (bottom edge) of the roof to be closed for fire protection [39].

Two of the most popular roofing product categories in the western U.S. residential roof-

[1]The majority of the material presented in this chapter was published in 2014 in the Energy & Buildings Journal Vol 80 [31].

ing market are fiberglass asphalt shingles (hereafter, "shingles") and clay or concrete tiles (hereafter, "tiles"). Surveys by *Western Roofing Insulation & Siding* found that shingles and tiles comprised 50% and 27% of 2007 sales, respectively, and 61% and 15% of projected 2015 sales [40, 41]. Substituting a light-colored tile for a dark asphalt shingle reduces the roof's solar heat gain, roughly doubles its thermal capacitance [42], and provides above-sheathing ventilation. In a mild-winter climate where heating is needed primarily in the morning, this substitution may even decrease heating energy use in winter. This is possible because increasing the roof's thermal capacitance keeps the attic warmer overnight, while high roof albedo has little consequence after sunset.

The work presented in this chapter constitutes the cool roof demonstration project conducted as part of the *Urban Heat Island Mitigation Phase 2* project. The study compares two side-by-side, single-story, single-family houses in Fresno, California. Fresno is located in the state's Central Valley, a hot climate in which homes use air conditioning from approximately May to October. The first house had a standard dark asphalt shingle roof, and the second a cool concrete tile roof; they are otherwise quite similar in construction and use. The homes served as show models and were open to the public every day from 09:00 to 17:00 local time (LT). By monitoring temperatures, heat flows, and energy consumption in these air-conditioned houses, it was possible to investigate the extent to which over the course of a year the cool roof reduces (a) roof and attic temperatures; (b) conduction of heat into the conditioned space and into HVAC ducts in the attic; (c) cooling and heating energy uses; and(d) peak-hour power demand. The study also compares measured cooling energy savings to cooling energy savings calculated from heat flow and temperature measurements, to evaluate whether a simplified experimental configuration without power meters can be used in future cool roof experiments.

3.2 Theory

While the tested homes share similar floor and elevation plans, differences other than roof construction, such as those in plug load (appliances and lights), fenestration (window area, orientation, construction, and coverings), and occupancy, can influence building conditioning energy use. Here, two ways were derived to isolate the energy savings attributable to the cool roof.

3.2.1 Heat balance

The conditioned space (hereafter, "room") can gain or lose heat through its envelope (ceiling, wall, floor, and windows), and gain heat from internal sources, including plug loads (appliances, lighting) and people. Conditioned air can also gain or lose heat as it flows through the attic ductwork from the air conditioner or furnace to the room. Denoting the rates of heat gain (power) in the room and ductwork as q_{room} and q_{duct}, the building's

combined heat load is

$$q_{load} \equiv q_{room} + q_{duct} \tag{3.1}$$

The rate q_{HVAC} at which the furnace or air conditioner must remove heat to regulate room air temperature (positive in the cooling season, negative in the heating season) is

$$q_{HVAC} = q_{load} \tag{3.2}$$

q_{room} is disaggregated in gains from the ceiling, plug load, windows, and other sources (e.g., walls, floor, infiltration and occupants), such that

$$q_{room} = q_{ceiling} + q_{plug} + q_{window} + q_{other}. \tag{3.3}$$

The rate of heat gain through the ceiling, $q_{ceiling}$, is the product of ceiling area and the ceiling heat flux (power/area). The rate of plug load heat gain, q_{plug}, equals the plug load electric demand. The rate of heat gain through the windows, q_{window}, can be estimated from solar irradiance and the area, construction, orientation, and coverings of windows. The rate of heat gain through attic ductwork is

$$q_{duct} = \dot{m} c_p |\delta T_{supply} + \delta T_{return}| \tag{3.4}$$

where $\dot{m}$ and c_p are the mass flow rate and specific heat capacity of the duct air, δT_{supply} is the temperate rise (outlet inlet) along the supply duct, and δT_{return} is the temperature rise along the return duct. Note that neglecting minor thermal storage in the duct work, duct heat gain vanishes when the HVAC system is off ($\dot{m}$=0). If duct temperature rises have not been measured, q_{duct} can be estimated as

$$q_{duct} = \overline{U} A_{duct} \frac{\theta out - \theta in}{\ln\left(\frac{\theta out}{\theta in}\right)} \tag{3.5}$$

where $\overline{U}$ is the thermal transmittance of the duct wall, A_{duct} is duct surface area, inlet temperature depression $\theta_{in} = T_{atticair} - T_{inlet}$, and outlet temperature depression $\theta_{out} = T_{atticair} - T_{outlet}$ [43]. In the supply duct, can be estimated from room air temperature and HVAC equipment specifications of temperature drop across the evaporT_{inlet}ator (often approximately 10^oC) and rise across the furnace; in the return duct,T_{inlet} can be approximated by room air temperature. Air temperature at the outlet of either duct can be estimated from

$$\frac{T_{outlet} - T_{atticair}}{T_{inlet} - T_{atticair}} = \exp\left(-\frac{\overline{U} A_{duct}}{\dot{m} c_p}\right). \tag{3.6}$$

The rate of HVAC heat removal during the cooling season is

$$q_{cooling} \equiv q_{HVAC,cooling} = C \times P_{cooling} \tag{3.7}$$

where C is the coefficient of performance (COP) of the cooling equipment (compressor and fan) and $P_{cooling}$ is its electric power demand. Similarly, the rate of HVAC heat removal in the heating season is

$$q_{heating} \equiv q_{HVAC,heating} = -\eta \times P_{heating} \tag{3.8}$$

where η is the annual fuel utilization efficiency (AFUE) of the furnace and $P_{heating}$ is its rate of fuel energy consumption. Note that while $P_{cooling}$ includes electric fan power, $P_{heating}$ does not. COP can be computed from Seasonal Energy Efficiency Ratio (SEER) by applying the SEER-to-EER conversion given by Hendron and Engebrecht [44] and the unit conversion EER = COP 3.412 BTU$h^{-1}W^{-1}$ to obtain

$$C = \frac{-0.02 \times SEER^2 + 1.12 \times SEER}{3.412} \tag{3.9}$$

3.2.2 Energy savings

Consider two buildings, one with a standard roof and the other with a cool roof, that are otherwise matched in size and shape, and in particular have the same ceiling and duct areas. Defining $\Delta x \equiv x_{standard} - x_{cool}$,

$$\Delta q_{HVAC} = \Delta q_{load}. \tag{3.10}$$

The difference in heat load can be disaggregated as

$$\Delta q_{load} = \Delta q_{room} + \Delta q_{duct} = \Delta q_{ceiling} + \Delta q_{plug} + \Delta q_{window} + \Delta q_{other} + \Delta q_{duct}. \tag{3.11}$$

If the duct wall is well-insulated, or the duct air flow rate is high, the air temperature drop from inlet to outlet of each duct will be small. This can be tested by checking whether expression on the right hand side of Eq. 3.6 is close to unity. If further (a) the supply ducts in each building share the same inlet temperature, wall thermal transmittance, and wall area; (b) the same is true of the return ducts, and (c) both HVAC systems are on, then it follows from Eq. 3.5 that

$$\Delta q_{duct,supply} = \overline{U} A_{suply} \Delta T_{atticair} \tag{3.12}$$

and

$$\Delta q_{duct,return} = \overline{U} A_{return} \Delta T_{atticair}. \tag{3.13}$$

This permits estimation of $\Delta q_{duct} = \Delta q_{duct,supply} + \Delta q_{duct,return}$ without measuring or calculating duct inlet and outlet temperatures. If the buildings' HVAC systems share the same COP C and AFUE η, then

$$\Delta q_{cooling} = C \times \Delta P_{cooling} \tag{3.14}$$

and

$$\Delta q_{heating} = -\eta \times \Delta P_{heating}. \tag{3.15}$$

The HVAC power savings (standard building cool building) in the cooling and heating seasons are

$$\Delta P_{cooling} = \frac{\Delta q_{cooling}}{C} = \frac{\Delta q_{load}}{C} \tag{3.16}$$

and

$$\Delta P_{heating} = -\frac{\Delta q_{heating}}{\eta} = -\frac{\Delta q_{load}}{\eta} \tag{3.17}$$

respectively.

To distinguish conditioning power savings attributable to the roof from those that result from differences in plug, window, or other heat loads, the cool-roof cooling power savings in the cooling season are defined as

$$\Delta P_{cooling,roof} \equiv \frac{\Delta q_{ceiling} + \Delta q_{duct}}{C} \tag{3.18}$$

and the cool-roof heating power savings in the heating season (potentially negative) as

$$\Delta P_{heating,roof} \equiv -\frac{\Delta q_{ceiling} + \Delta q_{duct}}{\eta} \tag{3.19}$$

This first approach – **"Method A"** – estimates cool-roof cooling and heating power savings from measured ceiling heat gain and calculated duct heat gain.

Our second approach – **"Method B"** – calculates cool-roof cooling and heating power savings from measured HVAC power savings after correcting for differences in plug, window, and other heat loads. If $\Delta q_{other} = 0$, combining Eqs. 3.11, 3.16 and 3.18 yields the cooling (compressor + fan) power savings attributable to the cool roof,

$$\Delta P_{cooling,roof} = \Delta P_{cooling} - \frac{\Delta q_{plug} + \Delta q_{window}}{C}, \tag{3.20}$$

while combining Eqs. 3.11, 3.17 and 3.19 yields the heating fuel energy savings rate attributable to the cool roof,

$$\Delta P_{heating,roof} = \Delta P_{heating} + \frac{\Delta q_{plug} + \Delta q_{window}}{\eta}. \tag{3.21}$$

Since $P_{heating}$ excludes electric fan power, and AFUE η also neglects fan power, neither method includes cool-roof fan power savings in the heating season. This value is estimated as

$$\Delta P_{fan,heating,roof} = \Delta P_{fan,heating} \times \frac{\overline{\Delta P}_{heating,roof}}{\overline{\Delta P}_{heating}}. \tag{3.22}$$

where bar denotes mean over the heating season. If the envelope of each home is well insulated, room heat gains (or losses) that occur while the HVAC system is off will warm or cool the rooms surfaces and air, influencing the conditioning load when the HVAC system later operates. Therefore, daily, cooling season, and heating season site energy savings are each evaluated by integrating power savings over all hours in the day or season, including those times in which the HVAC system is off. That is, site energy savings

$$\Delta E \equiv \int \Delta P dt. \tag{3.23}$$

This assumption appears safe in the cooling season, because the mid-morning period during which there is typically a substantial ceiling heat gain without HVAC operation is immediately followed by late-morning to early-evening HVAC operation. In the heating season, this assumption may overestimate cool-roof heating energy penalties, because the HVAC system operates primarily in the early morning, nearly 12 hours after the sun has set and during a period where the cool roof will have minimal impact on the attic/duct heat balance (see Appendix A).

Cool-roof energy savings are assumed to be zero on days when HVAC systems are off in both homes.

3.2.3 Other savings

The following savings are all annual.

3.2.3.1 Source energy savings

If substituting a cool roof for a standard roof yields cooling (compressor + fan) site energy savings $\Delta E_{cooling,roof}$, heating fuel site energy savings $\Delta E_{heating,roof}$, and heating fan site energy savings $\Delta E_{fan,heating,roof}$, the source energy savings will be

$$\Delta s = r_e(\Delta E_{cooling} + \Delta E_{fan,heating,roof}) + r_g \Delta E_{heating}. \tag{3.24}$$

where r_e and r_g are the source-to-site energy ratios for electricity and natural gas, respectively.

3.2.3.2 Energy cost savings

The energy cost savings will be

$$\Delta c = d_e(\Delta E_{cooling} + \Delta E_{fan,heating,roof}) + d_g \Delta E_{heating}. \tag{3.25}$$

where d_e and d_g are the prices of electricity and natural gas, respectively.

3.2.3.3 Emission reduction

The reduction in emission of pollutant i will be

$$\Delta p_i = f_{e,i} \frac{\Delta E_{cooling} + \Delta E_{fan,heating,roof}}{\eta_t} + f_{g,i} \Delta E_{heating}. \tag{3.26}$$

where $f_{e,i}$ is its electricity emission factor (mass of pollutant i per unit electricity supplied to the grid), $f_{g,i}$ is its natural gas emission factor (mass of pollutant i per unit gas energy consumed), and η_t is the grids transmission efficiency.

3.2.3.4 Peak-hour power demand reduction

Utilities may define hours of peak electrical demand. For example, the California Public Utilities Commission classifies noon – 6 pm LDT, Monday – Friday, May – October as peak demand hours for nonresidential users [45]. The peak-hour demand reduction on a given day is the ratio of cooling energy saved during those hours to the time interval spanned.

3.3 Experiment

3.3.1 Overview

Temperatures, heat flows, and HVAC (compressor + fan) energy uses are compared over the course of 12 months in two adjacent and similar homes in California's Central Valley, one with a standard roof and the other with a cool roof. Monthly rates of natural gas use for heating are obtained from utility statements.

Cool roof energy savings in the cooling and heating seasons are computed via both Method A (difference in ceiling + duct heat gain, divided by COP or AFUE) and Method B (difference in HVAC energy use, corrected for differences in plug and window heat gains). Seasonal and annual site energy savings, source energy savings, energy cost savings, and emission reductions are calculated with local source-to-site energy ratios, energy prices, and emission factors. Peak-hour power demand reduction is also computed.

(a) Standard home

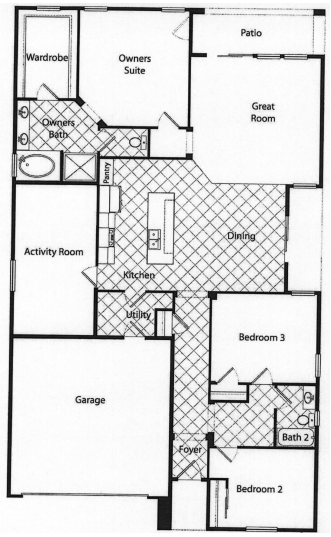

(b) Cool home

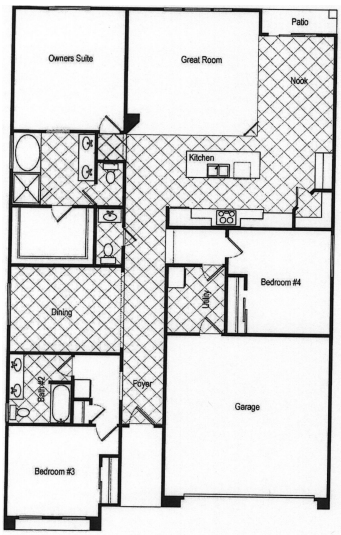

Figure 3.1: Floor plans for (a) the standard home and (b) the cool home.

3.3.2 Construction

Two side-by-side, single-story, single-family homes built by Granville Homes in Fresno, CA in summer/fall 2010 have been made available for this study. The buildings are oriented with the front door facing east and the length of the home running east-west. Hence, one side of each roof faces south and the other north, each at a pitch of about 20°. The houses are similar in floor plan (Figure 3.1) and elevation plan (Figure 3.2a) with the main difference being that one has a standard roof ("standard home") and the other has a cool roof ("cool home"). The homes serve as show models and are open to the public every day from 09:00 to 17:00 LDT. Lighting as well as other appliances are scheduled to turn on during business hours. Each home has additional plug loads drawn by a flat screen TV and a sound system, though the TV and sound system in the standard home were not operated in winter.

The standard home has an asphalt shingle roof (CertainTeed Autumn Blend) measured following ASTM C1549 [46] to have an initial SR of 0.07 (Figure 3.2b). Shingles are glued and nailed on an underlayment covering the roof deck (Figure 3.3a).

The cool home has a flat concrete tile roof (Eagle Roofing model 4258, CRRC PID 0918-0008) rated with initial SR 0.51 and three-year-aged SR 0.47 [47].[2] Each row of flat tiles rests on a horizontal batten and on a lower row of tiles, allowing air to circulate between the tiles and underlayment (Figure 3.3b). Air enters at the eave and is exhausted at the ridge.

[2]The albedos reported for each roofing product are beam-normal, air mass 1.5 solar reflectance outputs of a Devices & Services Solar Spectrum Reflectometer.Because this metric tends to overestimate the solar reflectance of spectrally selective surfaces, the true albedo of the cool tile roof is likely 0.03-0.05 lower than rated [48, 49].

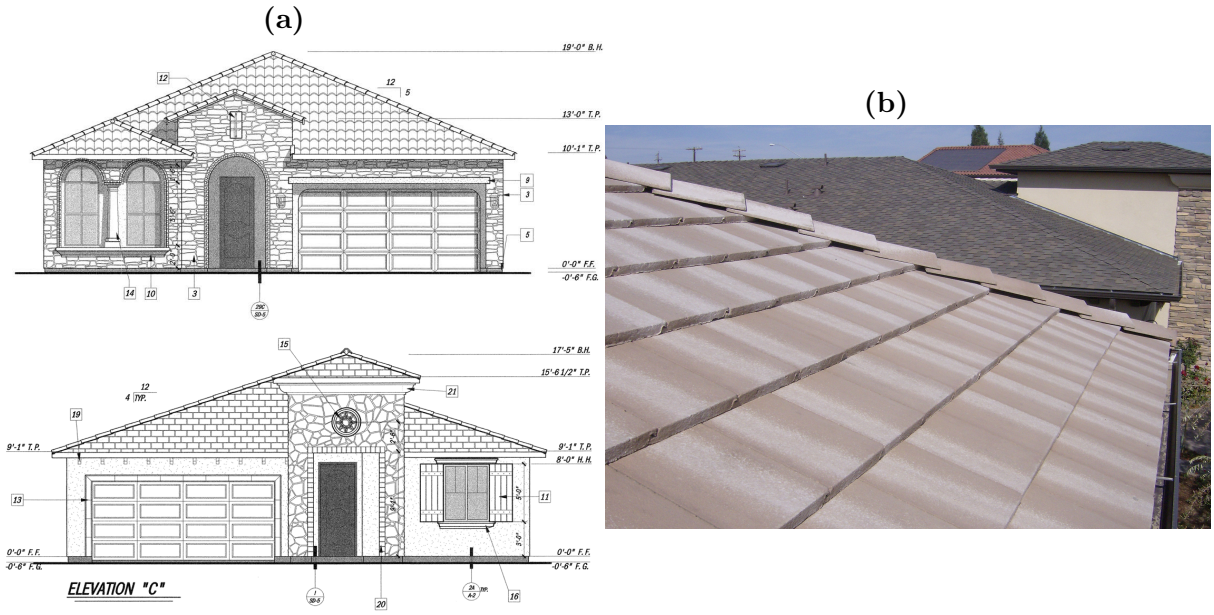

Figure 3.2: Plans and image of adjacent single-family homes in Fresno, CA, showing (a) elevations of homes with cool roof (top) and standard roof (bottom); and (b) cool concrete tile roof (foreground) and standard asphalt shingle roof (background)

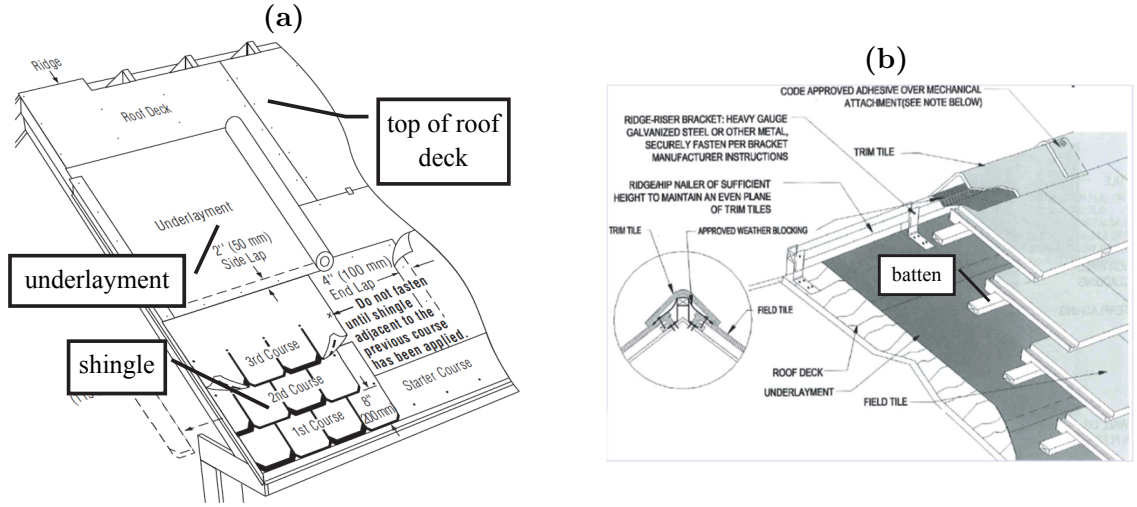

Figure 3.3: Diagrams of installation assembly layers over roof deck for (a) asphalt shingles [50] and (b) flat tiles [51].

Based on CRRC-reported measurements for the tile product, and CRRC-reported measurements for comparable asphalt shingle products, the initial thermal emittance of each roof was about 0.9.

The homes are built with the AC compressor placed at the back of the house next to the wall facing west; the furnace and ventilation fan are placed in the attic, approximately at the center of the floor plan. The ducts (RSI-1.1) run through a prefabricated truss support system located in the attic, supplying every room of the home. Each home is also equipped with a return grill, located outside the master bedroom. For attic ventilation, squared static gable vents are located on the west side of both attics, facing the backyard. Eave and profile-specific attic vents (OHagin's Inc., Rohnert Park, CA) provide additional attic ventilation. Each attic floor is covered with blown cellulose insulation of thermal resistance 3.3 $m^2 \cdot K \cdot W^{-1}$ (RSI-3.3) [19 $ft^2 \cdot^\circ F \cdot h \cdot \mathrm{BTU}^{-1}$ (R-19)].[3] Wall insulation is also RSI-3.3 (R-19), and the ventilation duct insulation is RSI-1.1 (R-6). Windows are double-paned.

Each home has a SEER-14 (∼COP 3.5) air conditioner and an AFUE 92% gas furnace. Table 3.1 further details each home's roof, attic, envelope, and HVAC system.

3.3.3 Instrumentation and data acquisition

Sensors and data loggers were installed between 27 August and 14 December 2010. Each home has been instrumented to measure external and internal temperatures, ceiling heat flux, and electricity use, while a roof-mounted station on the standard house records weather.

In a clear summer day in Fresno, the south face of a 20° pitch roof receives more direct irradiance than the north face at mid-day, when the sun is south-southeast to south-southwest, but less irradiance in the early morning (sun east-northeast) and early evening (sun west-northwest). On a clear winter day, the south face receives more direct irradiance all day, because the sun stays in the southern hemisphere (Figure 3.4). For example, at solar noon on the summer solstice (June 21), when the solar altitude is 77°, the north face of a 20° tilt roof receives 16% less direct sunlight than the south face. At solar noon on the winter solstice (solar altitude 30°), the north face receives 78% less direct sunlight than the south face [57]. Since this can make the north face of the roof cooler than the south face, sensors were placed on both the north and south sides of each house to assess building temperatures, and to explore the downward propagation of north-south temperature differences (see Appendix B).

Table 3.2 summarizes the type and location of all sensors installed.

[3] Attic insulation thermal resistance was chosen to represent median-age housing stock, rather than new construction. In 2011, the median year of construction for homes in the US Pacific census division (California, Oregon, Washington, Hawaii,and Alaska) was 1976 [52].

Table 3.1: Home construction and HVAC equipment.

Property	**Standard Home**	**Cool Home**
Living floor area (also ceiling area) (m^2)	187	189
Number of stories	1	Same
Ceiling height (m)	2.74	3.05
Ratio of distribution duct inner surface area to ceiling area	35% [a]	Same
Frame construction	Wood	Same
Roof		
Roofing product		
Type	Asphalt shingle	Concrete tile
Make and model	CertainTeed Autumn Blend Presidential Shake	Eagle Roofing flat tile - Bel Air/ 4258 Ridgecrest-Color Bonded/ Color-Tan, Cream
CRRC product ID	NA	0918-0008
Initial albedo	0.07	0.51
Initial thermal emittance	0.90 (estimated)	0.93
Mass per deck area (kg/m^2) [lb/ft^2]	17.3 [3.55]	47.4 [9.70]
Thermal capacity per deck area ($kJ/m^2{\cdot}K$) [b]	21.8	39.8
Waterproofing layer and deck	43 lb/100 ft^2 (2.1 kg/m^2) black felt over 0.5" (13 mm) CDX plywood sheathing	Same
Rise to run [slope]	4:12 [18.4°]	5:12 [22.6°]
Air gap height under roofing product (cm)	No gap	1.9–4.4
Attic		
Total ventilation area (m^2)	1.66	1.62
Gable end vent – qty. × area (m^2)	2 × 0.25	4 × 0.17
Eave vent – qty. × area (m^2)	20 × 0.04	19 × 0.04
O'Hagin Dormer vent – qty. area (m^2)	6 × 0.06	3 × 0.06
Radiant barrier	None	Same
Insulation		
Thermal resistance ($m^2{\cdot}K/W$) [$ft^{2}{\cdot}°F{\cdot}$ h/BTU]		
Roof	3.3 [19]	Same
Exterior wall	3.3 [19]	Same
Ducts	1.1 [6]	Same
Windows		
Construction	Double-pane, low-E	Same
Thermal transmittance ($W/m^2{\cdot}K$)	1.9–2.0	1.6–1.7
Area (m^2)		
South	3.25	4.74
East	1.86	3.4
West	11.9	11
North	9.38	2.32
Total	26.3	21.5
HVAC system		
Air conditioner [c]		
Make and model	Lennox 14ACX-042-230-11	Lennox 14ACX-048-230-11
SEER (BTU/Wh)	14	Same
Estimated COP (Wh/Wh)	3.5	3.5
Nominal cooling capacity (kW) [ton]	12.3 [3.5]	14 [4]
Gas furnace [d]		
Make and model	Lennox G51MP-48C-090	Same
Annual Fuel Utilization Efficiency (AFUE) (%)	92.1	Same

[a] Estimated following ASHRAE Standard 152P, Method B, based on the number of supply and return registers [53].
[b] Assumes specific heats of 1.26 $kJ/m^2{\cdot}K$ (asphalt shingle) and 0.84 $kJ/m^2{\cdot}K$ (lightweight concrete) [54].
[c] Lennox Merit Series 14ACX Units [55].
[d] Lennox G51MP Series [56].

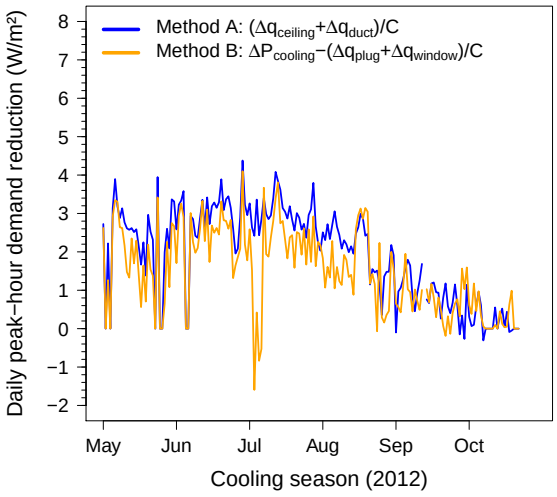

Figure 3.4: Sun path chart for Fresno, CA [58]

Table 3.2: Instrumentation

Measurement(s)	Sensor(s)	Location(s)
Outdoor air temperature and relative humidity	NeuroLogic Research, Model 1200A, with Model 40 Rain and Sun Guard	On weather station tower at the top of west wall of standard home
Global horizontal solar irradiance	Blue-enhanced photodiode pyranometer (LI-COR LI-200SA)	On weather station tower at the top of west wall of standard home
Wind speed and direction	Three-cup anemometer (Weather Instruments, Model A70-SL), potentiometric wind vane (Model A70-DL)	On weather station tower at the top of west wall of standard home
Roof surface temperature × 4	Omega thermistors, model TH-44006-40-T	Standard and cool homes, north and south sides: under shingle of the standard roof; inside hole drilled into back of tile
Attic temperature × 12	Omega thermistors, model TH-44006-40-T	Standard and cool homes, north and south sides: roof bottom (surface); attic air (midway between roof bottom and attic floor); attic floor (surface)
Room temperature × 4	Omega thermistors, model TH-44005-120-T	Standard and cool homes: center of ceiling surface; air near thermostat
Return air temperature and relative humidity × 2	Pure Choice Inc., model The Nose Monitor	Standard and cool homes: ceiling level air near the two return grilles
Ceiling heat flux (power/area) × 2	Hukseflux, HFP01-100-PT	Standard and cool homes, south side: attic floor beneath the cellulose insulation
Electricity use × 6	Continental Control Systems LLC, Watt Node Logger WNC-3Y-208-FT10 pulse counter transducer with split-core current transformers (CCS, CTS Series)	Standard and cool homes: AC compressor; ventilation fan; total building power
Data logger × 2	Echelon, iLon SmartServer 2.0	Standard and cool homes
Logger expansion × 2	Control Solutions, AddMe II^{TM}, AM2-MX30, 30-point Lon Works I/O node	Standard and cool homes

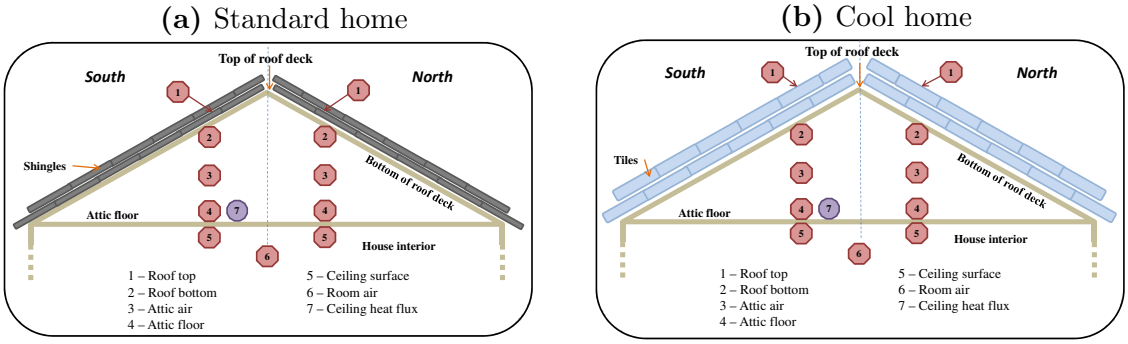

Figure 3.5: Temperature and heat flux sensor locations in (a) the standard home and (b) the cool home.

3.3.3.1 Roof

To measure the roof top temperature of the standard home, a thermistor was placed under a shingle on each side of the house (north and south), approximately at the center of each side (Figure 3.5a). On the cool roofed home the roof top temperature was measured with a thermistor placed near the surface of a tile on each side of the roof (Figure 3.5b). To do so, a small hole was drilled at the back of the tile extending nearly to the top of the tile; the thermistor was embedded and epoxied inside this hole. This shielded the sensor from direct sunlight, wind and outside air.

3.3.3.2 Attic

Each attic was instrumented with vertical arrays of thermistors on both the north and south side. At each side, a sensor was attached to the underside of the roof deck to measure the roof bottom, another was suspended at mid-attic height, and a third was attached to the attic floor (Figure 3.5). The vertical profile was positioned mid-way along the home's east-west axis. A heat flux sensor was taped on the south side of the attic floor close to the thermistor under the insulation to measure the heat flux through the ceiling.

3.3.3.3 Room

Inside each home are two sensors, each of which measures both temperature and relative humidity. These are located at ceiling level near the ceiling-mounted return grill. Two additional thermistors were installed inside of each home. One was placed on the ceilings surface below the heat flux sensor, and the other next to the thermostat of the HVAC system. The latter is used to measure room air temperature.

3.3.3.4 Weather station

A weather station was mounted on a tower fixed at the top of the west end wall of the standard roof home and extends 1.5 m above roof line. The tower has a combined and self-contained temperature and relative humidity transmitter. The sensors of the transmitter are shielded by a cylindrical PVC rain and sun guard to prevent wetting of the humidity sensor and keep direct sunlight from shining on the sensors. A three-cup anemometer and a precision potentiometric wind vane are mounted at the top of the tower. A blue-enhanced photodiode pyranometer was also installed at the top of the tower to measure global horizontal solar irradiance.

3.3.3.5 Electric power monitoring devices

Three split-core current transformers (accuracy $\pm 1\%$) were connected to the power meter of each home, measuring currents drawn by the AC compressor, ventilation fan, and entire house. The transformers are directly connected to a digital energy meter which reports power demand.

3.3.3.6 Data acquisition system

Two data loggers, one in each home, are used to acquire measurements. Each one has a multiplexer to increase the number of inputs. The data loggers are connected to the internet for data transfer. They are both located in the master bedroom walk-in closet, inside the panel that contains the internet wiring for each home. The data loggers are programmed to scan instantaneous readings every 30 seconds; data is transmitted hourly.

3.3.4 Estimation of window heat gain

Monthly window heat fluxes (energy/area) were evaluated with the Sustainable By Design window heat gain tool [59], using window solar heat gain coefficients (SHGC) and orientations reported in building plans. The SHGC of each window and its covering (curtain or blind) was estimated using WINDOW software [60] assuming surface-normal solar incidence. Each monthly heat gain (energy per area) was then multiplied by window area and divided by its time interval (seconds in a month) to calculate its contribution to the rate of window heat gain, Q_{window} (power/area).

3.3.5 Building operation

From January to April 2011, the team tested the operation of the homes, the instrumentation and the retrieval of data. Measurements have been recorded and analyzed since May 2011, but in July 2011, the AC in the standard home started leaking refrigerant from a loose valve. This forced its compressor to overwork to satisfy the cooling demand. The problem was identified and addressed in April 2012 when an HVAC professional recharged

the refrigerant in the standard home's AC, and verified that each home's AC was operating property.

During the cooling season of 2012 (May – October), the indoor air temperature in each home was set to 25°C. During the heating season (November 2012 - April 2013), indoor temperatures were set to 20°C from 7:00 LST to 23:00 LST and 13°C at other times.

3.3.6 Study period

This study analyzes nearly a full year of measurements collected from May 2012 through April 2013, during which time the HVAC system was monitored to ensure proper operation. About 7% of the data in this 12-month period—12 days in early January and 13 days in late April—was lost when communications were interrupted. In calculation of cumulative energy savings, daily energy savings for the 12 missing days in January are interpolated, while daily energy savings for the 13 missing days in late April are set to zero.

3.3.7 Local source-to-site-energy ratios, energy prices, and emission factors

Method A and Method B site energy savings are converted to source energy savings and energy cost savings using the source-to-site energy ratios and site energy prices in Table 3.3. They are also converted to CO_2, NO_x, and SO_2 emission reductions using the emission factors in Table 3.4 and a grid efficiency assumed to be 90%.

Table 3.3: Source-to-site energy ratios and site energy prices in Fresno, CA.

	Electricity	**Natural gas**
Source-to-site energy ratio	3.34 [a]	1.047 [a]
Site energy price ($/kWh)	0.298 [b]	0.0325 [c]

[a] US average [61].
[b] Average Tier 3 (131% to 200% of baseline) electricity price in Fresno from March – October 2012 [62].
[c] Average Tier 1 (up to 100% of baseline) natural gas price in Fresno (November 2012 – April 2013) [62], converted from $/therm at 29.3 kWh/therm.

Table 3.4: Year-2009 total and non-baseload output emission factors per unit electricity supplied to the grid in US EPA eGRID subregion WECC California [63]; and non-regional natural gas combustion site emission factors per unit fuel energy consumed [64].

	CO_2 (kg/kWh)	**NO_x (g/kWh)**	**SO_2 (g/kWh)**
Total electricity	0.299	0.19	0.0826
Non-baseload electricity	0.451	0.146	0.0143
Natural gas	0.18	0.141	0.000887

Peak-hour demand reduction in the cooling season is calculated as the mean rate of cooling energy savings during peak-demand hours, defined by the California Public Utilities Commission for nonresidential users as noon – 6 pm LDT, Monday – Friday, May – October [45]. (While the utility does not yet apply time of use rates to its residential customers, any peak-demand hour savings benefits the grid).

3.4 Results

3.4.1 Representative summer and winter days

3.4.1.1 Weather

July 6, 2012 and January 21, 2013 were selected as representative sunny days in summer and winter, respectively. The maximum and minimum outside air temperatures on July 6, 2012 were similar to the average maximum and minimum values on July 6 from 1995 through 2011. However, the maximum outside air temperature on January 21, 2013 (sunny) exceeded the historical average for that day of year, because winter days in Fresno are often cloudy or rainy [65][66]. On the summer day, about two weeks after the summer solstice, outside air temperature ranged from 14.3°C (04:53 LST) to 36.3°C (15:14 LST); global horizontal solar irradiance peaked at 990 W/m^2 (12:07 LST), with 14.6 hours from sunrise to sunset and 8.40 kWh/m^2 of solar irradiation. On the winter day, about one month after the winter solstice, outside air temperature ranged from 1.3°C (06:05 LST) to 24.3°C (14:16 LST); solar irradiance peaked at 577 W/m^2 (12:03 LST), with 10.1 hours from sunrise to sunset and 3.45 kWh/m^2 of solar irradiation (Figure 3.6).

3.4.1.2 Maximum building temperatures, ceiling heat gain, and duct heat gain

The cool home's higher roof albedo lowers its maximum attic air temperature, ceiling heat gain rate, and duct heat gain rate, which can reduce need for cooling energy in summer, and increase need for heating energy in winter.

For example, on the summer day, maximum roof top, roof bottom, and attic air temperatures in the cool home were 13.8, 14.3, and 10.5°C lower than in the standard house. In the standard home, the roof top, roof bottom, and attic air temperatures reached their maxima at 12:42, 13:35, and 14:37 LST; in the cool home, the corresponding maxima were attained 68, 64, and 47 min later (Figure 3.7; ESM Table C 3). Maximum rates of ceiling, duct, and ceiling + duct heat gain in the cool home were 1.50, 0.89, and 2.4 kW lower than in the standard house (Figures 3.8 and 3.9; ESM Table C 3).

On the winter day, maximum roof top, roof bottom, and attic air temperatures in the cool home were 11.0, 10.6, and 6.9°C lower than in the standard house. In the standard home, the roof top, roof bottom, and attic air temperatures reached their maxima at 13:06, 14:19, and 14:47 LST; in the cool home, the corresponding peaks were attained 65, 64, and

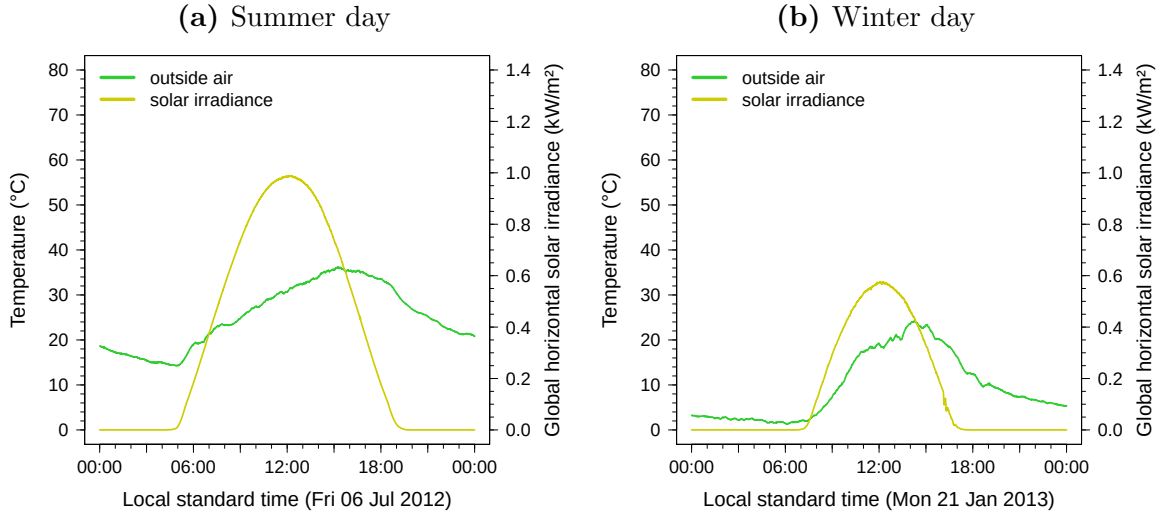

Figure 3.6: Outside air temperature and global horizontal solar irradiance on (a) a sunny summer day (6 July 2012) and (b) a sunny winter day (21 January 2013).

37 min later. Maximum ceiling, duct, and ceiling + duct rates of heat gain in the cool home were 0.83, 1.33, and 1.17 kW lower than in the standard house.

On each day, the lags between peak temperatures in the cool and standard houses (e.g., time of roof top peak temperature in the cool house minus time of roof top peak temperature in the standard house) are expected consequences of the higher thermal capacity of the tile roof. Differences in maximum temperatures (standard – cool) are greater on the summer day than on the winter day because they occur in the afternoon, when there is more sunlight in summer than in winter. The same remarks also apply to ceiling.

3.4.1.3 Minimum building temperatures, ceiling heat gain, and duct heat gain

The cool homes higher roof thermal capacity raises its minimum attic air temperature, ceiling heat gain rate, and duct heat gain rate, which can increase need for cooling energy in summer, and reduce need for heating energy in winter.

On the summer day, minimum roof top, roof bottom, and attic air temperatures in the cool home were 2.1, 2.4, and 2.4°C *higher* than in the standard house; these minima were reached in the early morning, when cooling power demand is low. In the standard home, the roof top, roof bottom, and attic air temperatures reached their minima at 04:53, 05:09, and 05:17 LST; in the cool home, the corresponding minima were attained 14, 34, and 32 min later (Figure 3.7;ESM Table C 4). Minimum rates of ceiling, duct, and ceiling + duct heat gain in the cool home were 0.44, 0, and 0.44 kW higher than in the standard house (Figures 3.8 and 3.9; ESM Table C 4).

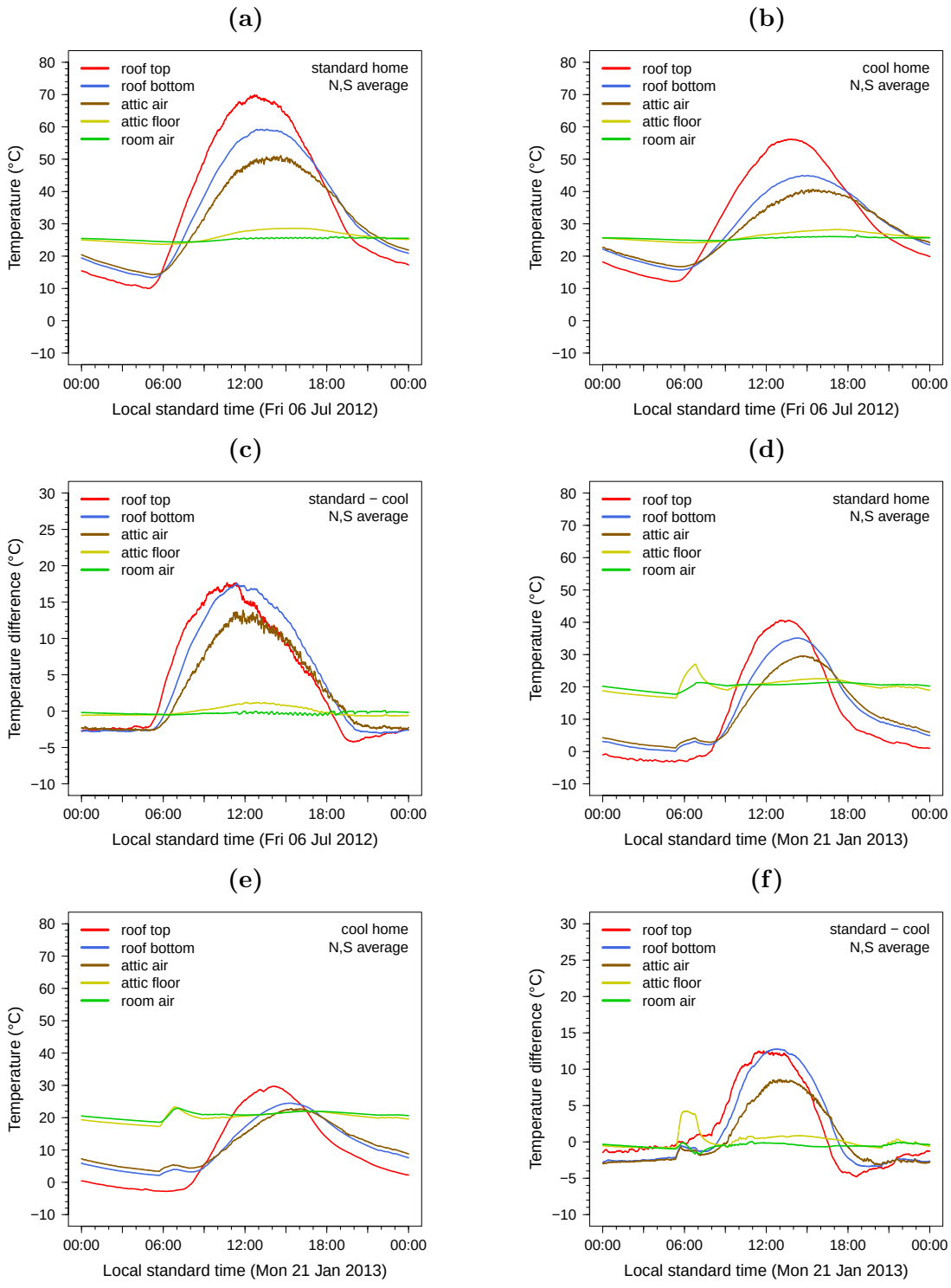

Figure 3.7: Roof top, roof bottom, attic air, attic floor, and room air temperatures and temperature differences on (a-c) the summer day and (d-f) the winter day. Label "N, S average" applies to roof and attic temperatures.

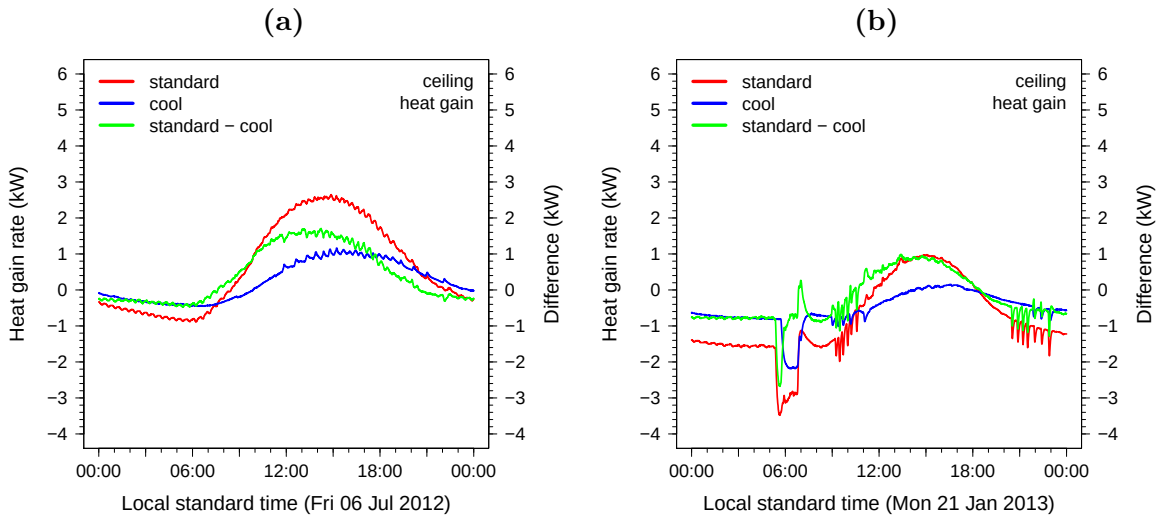

Figure 3.8: Rates of ceiling heat gain on (a) the summer day and (b) the winter day.

On the winter day, minimum roof top, roof bottom, and attic air temperatures in the cool home were 0.4, 2.1, and 2.3°C *higher* than in the standard house. In the standard home, the roof top, roof, and attic air temperatures reached their minima at 05:15, 05:19, and 05:18 LST; in the cool home, the corresponding minima were attained 57, 21, and 24 min later. Minimum rates of ceiling, duct, and ceiling + duct heat gain in the cool home were 1.32, -0.12, and 1.20 kW higher than in the standard house.

On each day, the minimum roof top, roof bottom, and attic air temperatures in the cool house are greater than those in the standard house because the tile roof is slower than the shingle roof to cool to the outdoor air and night sky. The differences in minimum temperatures (cool – standard) on the summer day (2.1 to 2.4°C) are comparable to those on the winter day (0.7 to 2.3°C) because the minima occur long after sunset.

3.4.2 Daily solar irradiation and maximum outdoor air temperature

Clear-day global horizontal solar irradiation was up to three times greater in summer in Fresno than in winter, ranging from 2.9 kWh/m^2 (December) to 8.8 kWh/m^2 (June). Dips in daily solar irradiation indicate that cloudy days were more common in the heating season (Nov - Apr) than in the cooling season (May - Oct) (Figure 3.10).

Clear-day maximum outdoor air temperature was up to 32°C higher in summer than in winter, ranging from about 11°C (December) to 43°C (June) (Figure 3.10).

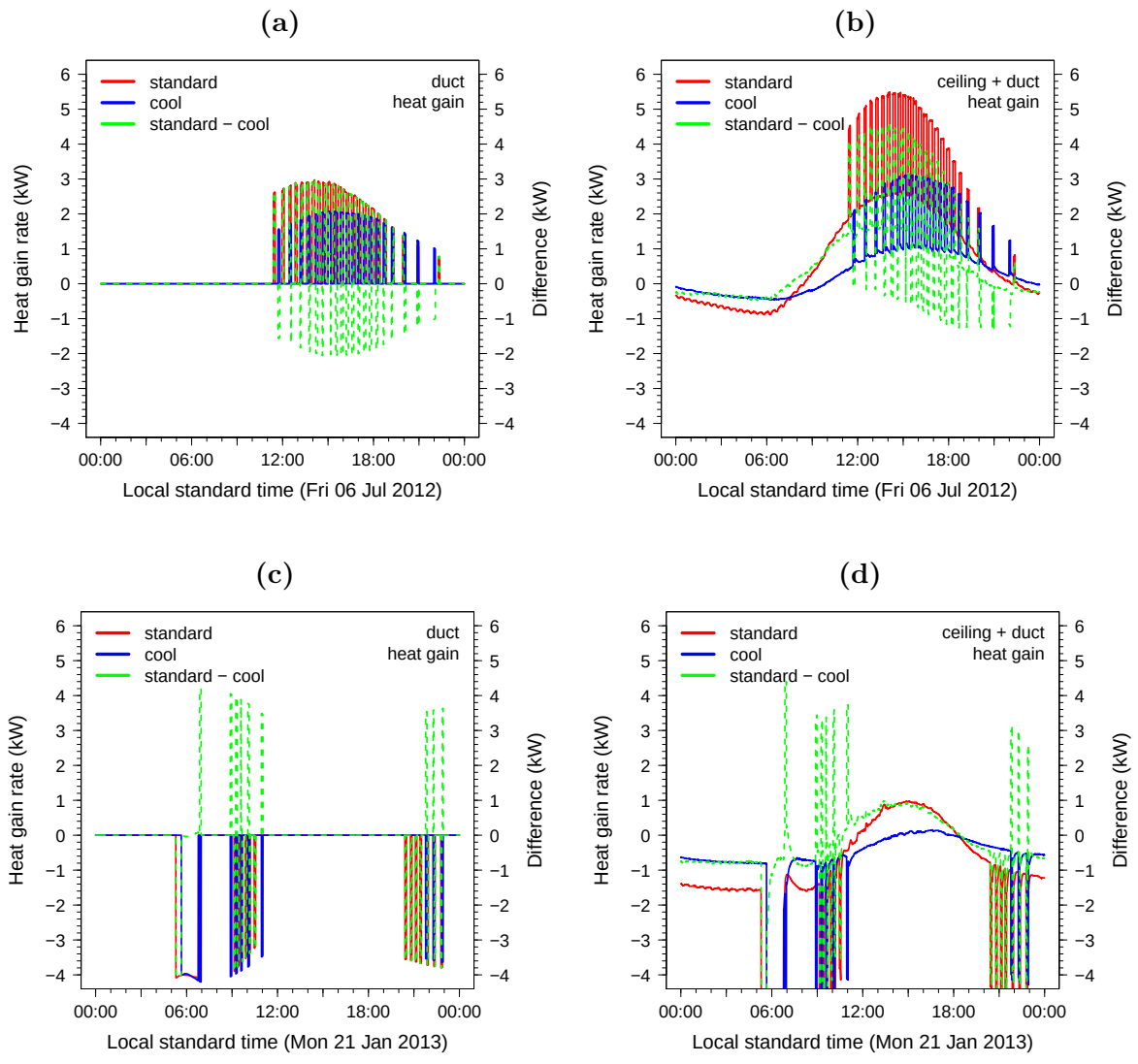

Figure 3.9: Rates of duct and ceiling + duct heat gain on (a-b) the summer day and (c-d) the winter day.

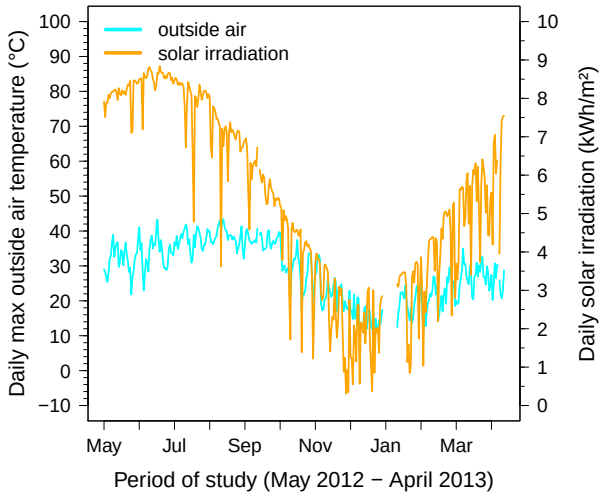

Figure 3.10: Daily maximum outside air temperature and daily solar irradiation over the period of study.

3.4.3 Seasonal reduction in daily mean temperatures and heat gains

Seasonal mean reductions (standard – cool) in roof top, roof bottom, and attic air temperatures in the cooling season were about 3.4°C, 3.7°C, and 2.4°C, roughly twice those the heating season (Table 3.5). Ordinarily, one would expect to find the greatest temperature difference between standard (lower albedo) and cool (higher albedo) roofs at roof top, where sunlight is absorbed. In this experiment, above-sheathing ventilation cooling the deck of the cool tile roof may have made the temperature difference (standard – cool) at roof bottom (underside of roof deck) larger than that at roof top (just below tile surface). Daily maximum and mean roof top, roof bottom, and attic air temperatures are detailed in Figure 3.11.

Cooling-season mean rates of whole-ceiling and duct heat gain in the standard home were about 310 W and 130 W lower in the cool home than in the standard home. However, heating-season mean rates of ceiling and duct heat gain were about 46 W and 32 W greater in the cool home than in the standard home (Table 3.5). The higher heating-season mean ceiling and duct heat gains in the cool home are attributed to the higher thermal capacity of the cool tile roof, which keeps the attic air under the cool roof warmer at night and early morning than that under the standard roof (Figure 3.11f). In fact, the daily mean ceiling heat gain is greater in the cool house than in the standard house on most days between early November and late February, or roughly two thirds of the heating season (Figure 3.12a).

Daily mean plug load heat gains were about the same in each house during the cooling season, but substantially higher in the cool house than in the standard house during the

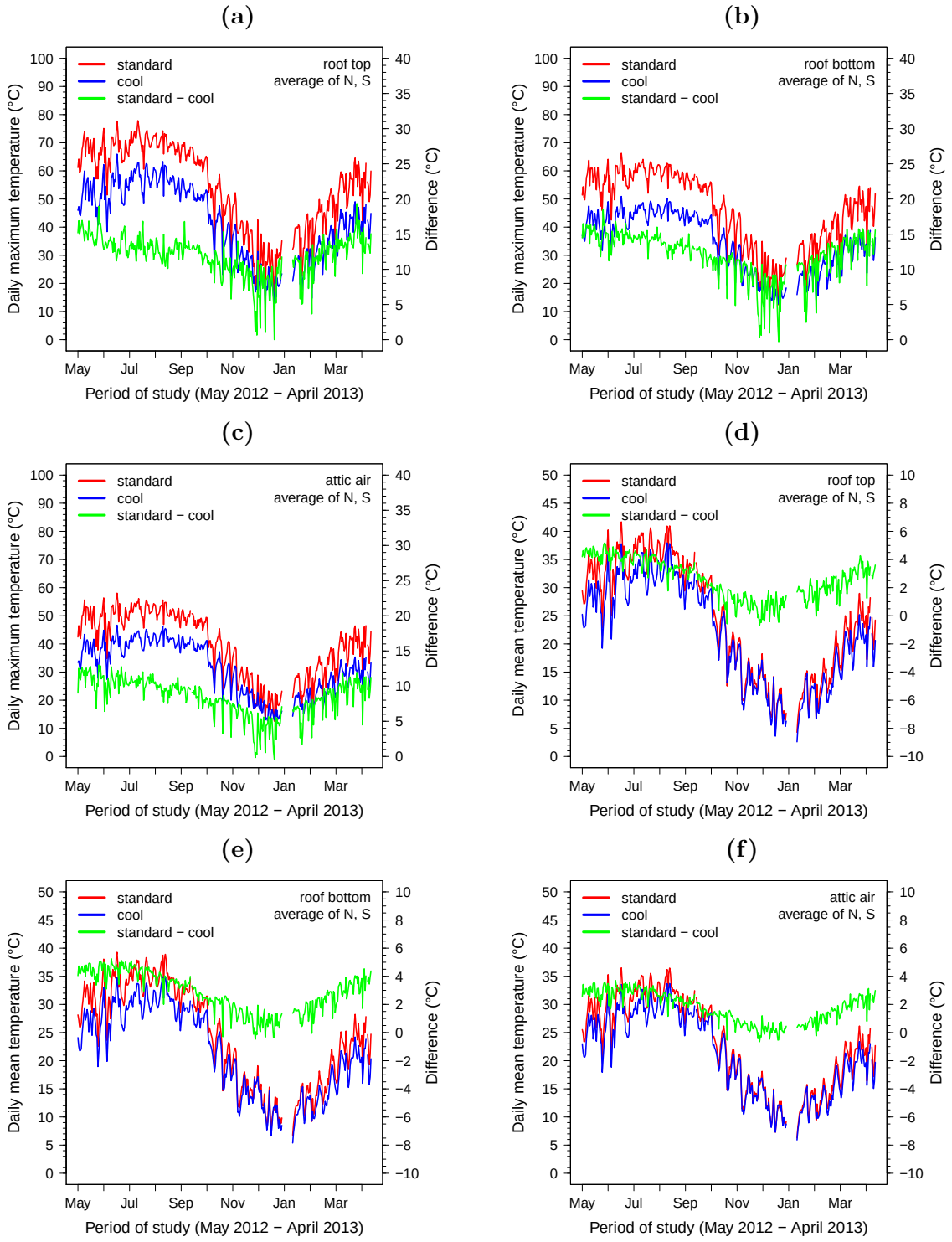

Figure 3.11: Daily (a - c) maximum and (d - f) mean temperatures at roof top, roof bottom, and attic air.

Table 3.5: Seasonal mean reductions (standard – cool) in daily maximum and daily mean temperatures and heat gain rates.

	Cooling season (May to Oct)		**Heating season (Nov to Apr)**	
	Max	Mean	Max	Mean
Roof top temperature (°C)	13	3.4	10.8	1.7
Roof bottom temperature (°C)	13.5	3.7	10.2	1.9
Attic air temperature (°C)	9.8	2.4	6.9	1
Ceiling heat gain rate (W)	1370	311	805	-46
Duct heat gain rate (W)	819	129	0	-32
Ceiling + duct heat gain rate (W)	2190	440	805	-78

heating season, simply because the television and stereo in the standard house were turned off in winter (Figure 3.12c).

Estimated daily mean window heat gains in the cool home always exceeded those in the standard home (Figure 3.12d). Window heat differences were smallest in December and January, the months with least insolation (Figure 3.10).

3.4.4 Daily and cumulative energy savings in the cooling and heating seasons

Figure 3.13 shows in each season (cooling, heating) the daily and cumulative values of cool-roof energy savings per unit ceiling area.[4]

In the cooling season, Method A reports ceiling and duct heat gain savings divided by COP, while Method B subtracts from HVAC (compressor plus fan) electricity savings the difference (standard – cool) in plug load and window heat gains divided by COP. Cool-roof energy savings are assumed to be zero on days when HVAC systems are off in both homes. Method A and Method B agree well in the cooling season, with an especially close match from May through July (Figures 3.13a,3.13b). Cumulative cooling energy predicted by Method A (2.89 kWh/m^2) are 2% higher than those calculated from Method B (2.82 kWh/m^2) (Figure 3.13b), which is very close.

Figure 3.14 compares Method A and Method B daily energy savings for each day and each week of the cooling season. Agreement is especially good on a weekly basis.

In the heating season, Method A switches sign, since the HVAC supplies, rather than removes, heat [3.17], while Method B adds to fuel savings the difference in plug load and window heat gains divided by AFUE. Method A over-predicts Method B in the heating season, especially from November through January (Figure 3.13c and Figure 3.13d). Cumulative

[4]Ceiling area means the area of the ceiling of the top floor of the building.

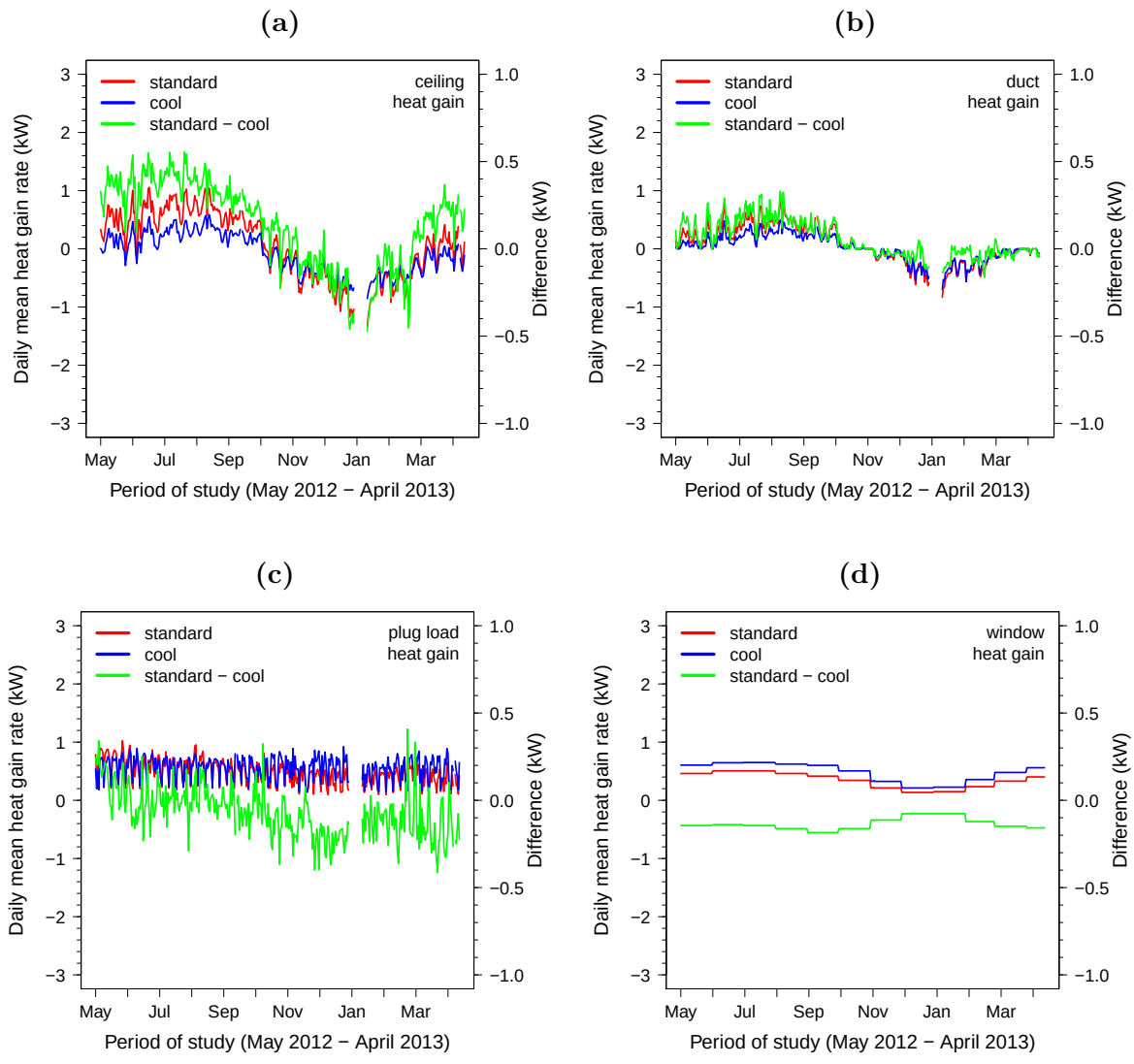

Figure 3.12: Daily mean rates of (a) ceiling, (b) duct, (c) plug load and (d) window heat gain.

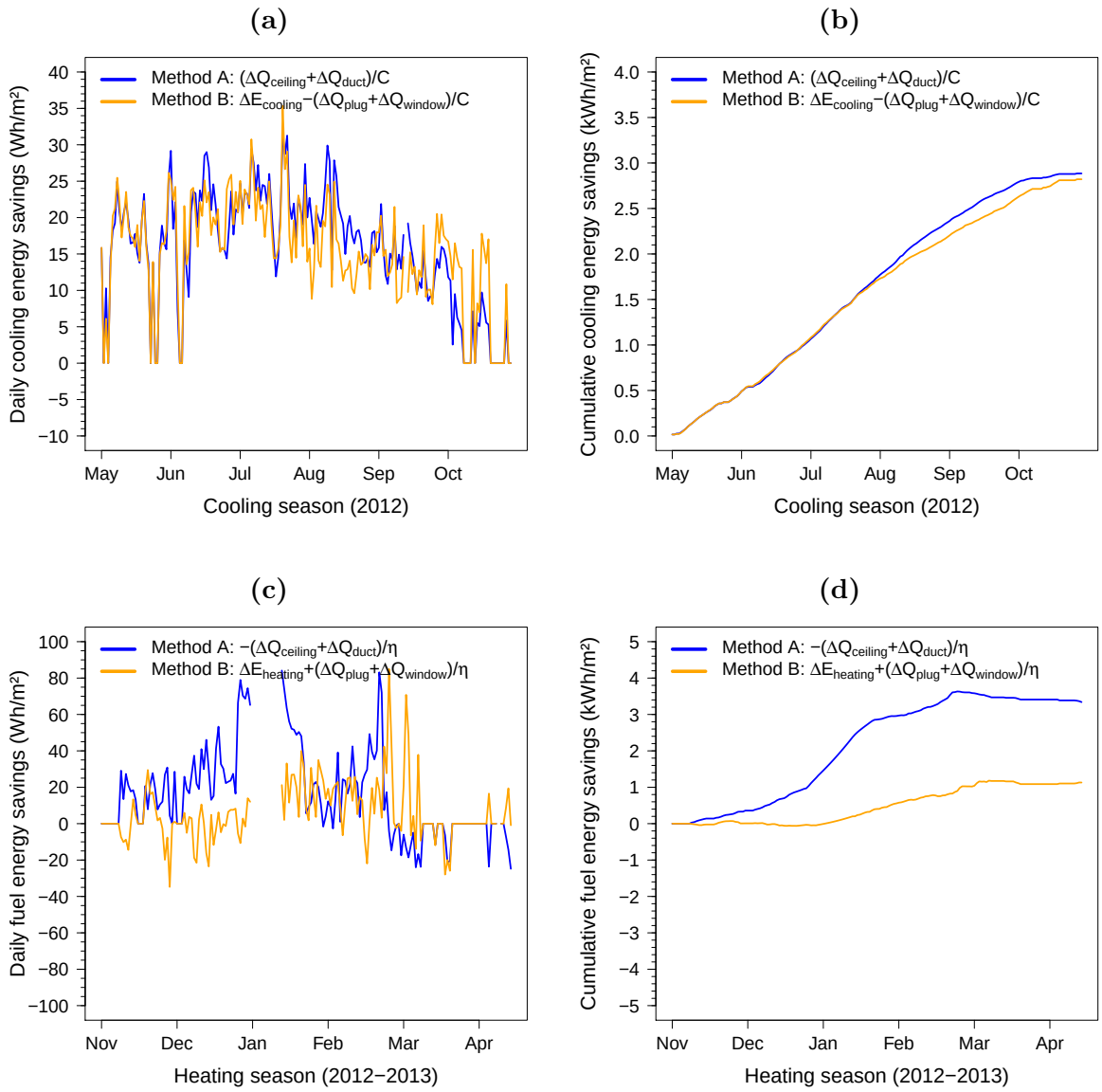

Figure 3.13: Values per unit ceiling area of (a) daily and (b) cumulative cooling (compressor + fan) energy savings in the cooling season; and (c) daily and (d) cumulative fuel energy savings in the heating season.

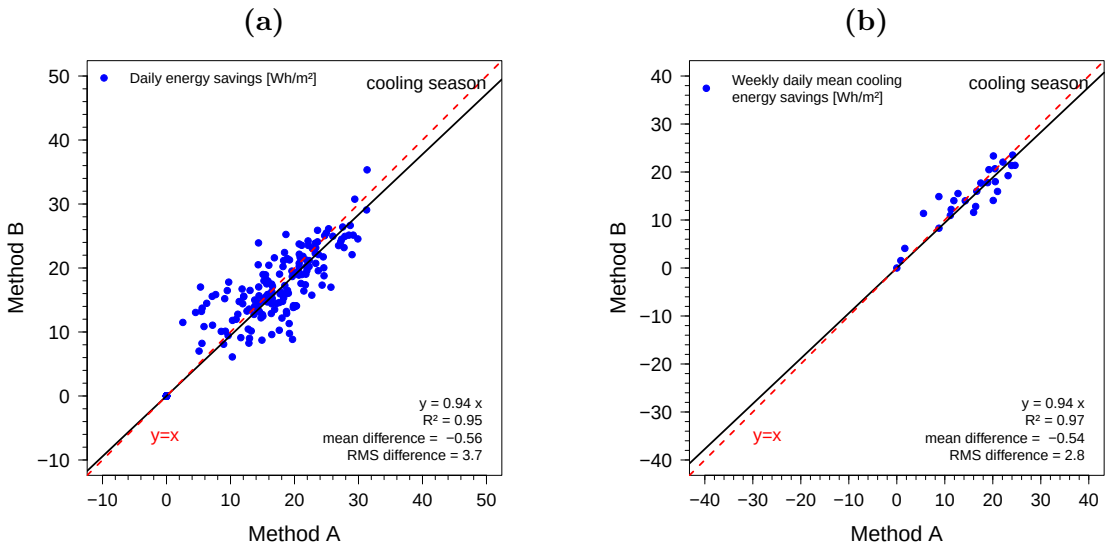

Figure 3.14: Cooling season comparisons of Method A and Method B estimates of (a) daily and (b) weekly mean values of daily cool-roof energy savings per unit ceiling area.

fuel energy savings from Method A (3.34 kWh/m^2) are three times greater than those from Method B (1.13 kWh/m^2) (Figure 3.13d).

Figure 3.16 shows per unit ceiling area the daily and cumulative values of cool-roof fan energy savings in the heating season. For each method (A,B), cool-roof fan energy savings are estimated by scaling daily fan energy savings by ratio of cool-roof heating fuel energy savings to raw heating fuel energy savings. Cumulative heating-season cool-roof fan energy savings from Method A (0.077 kWh/m^2) are 2.7 times higher than those from Method B (0.029 kWh/m^2).

Note that Methods A and B each yield positive fuel and fan energy savings in the heating season, which is attributed to the higher thermal capacitance of the tile roof.

3.4.5 Daily peak-hour cooling power demand reduction

Figure 10 shows daily values of peak-hour cooling power demand reduction, calculated on each weekday in the cooling season (May through October) as the mean value of cool-roof power demand reduction from 12:00 LDT to 18:00 LDT (11:00 LST - 17:00 LST). The seasonal mean demands reduction predicted by Method A (1.06 W/m^2) is about 20% higher than that calculated by Method B (0.88 W/m^2).

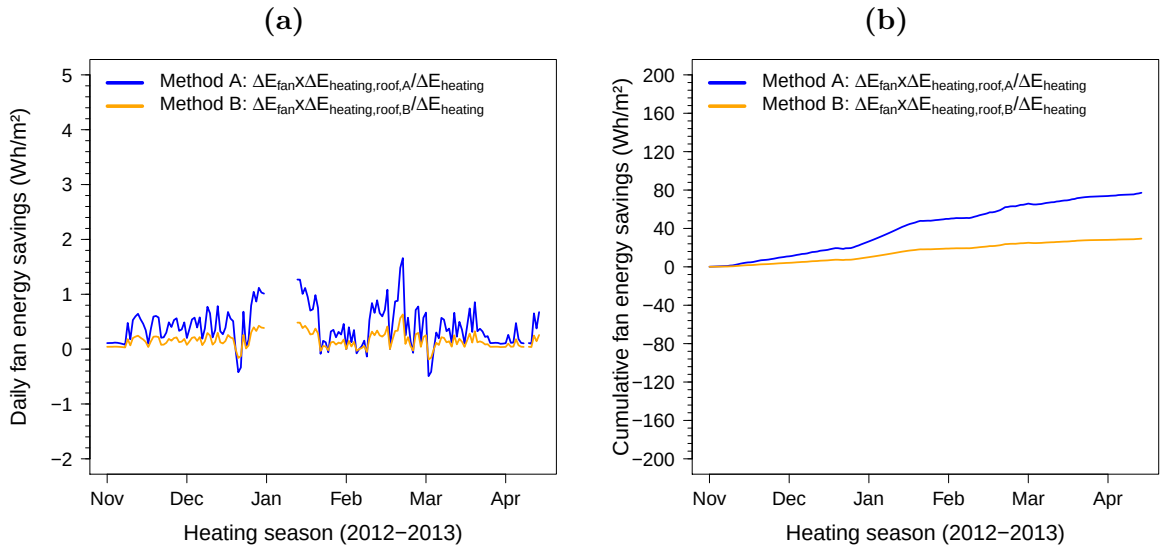

Figure 3.15: Values per unit ceiling area of (a) daily and (b) cumulative fan energy savings in the heating season.

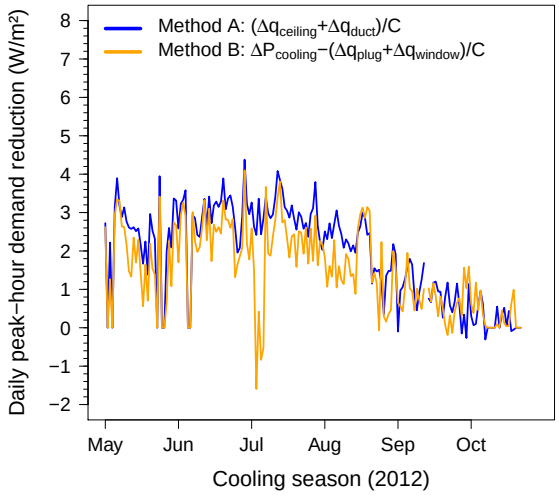

Figure 3.16: Daily peak-hour cooling power demand reduction in the cooling season.

3.4.6 Seasonal and annual cumulative conditioning site energy, source energy, energy cost, and emission savings

Table 3.6 summarizes Method A and Method B values of seasonal and annual site energy, source energy, energy cost, and emission savings, all per unit ceiling area. Since the earlier analysis showed substantial differences in heating-season fuel and fan energy savings, the following reports the more conservative Method B savings, which are based on measured energy savings adjusted for measured differences in plug load heat gain and estimated differences in window heat gain. Each parenthetical value is relative to use, cost, or emission in the standard home.

- **Annual cooling (compressor + fan) site energy savings** are 2.82 kWh/m^2 (26%).
- **Annual heating (furnace) fuel site energy savings** are 1.13 kWh/m^2 [0.0386 therm/m^2] (4%).
- **Annual heating (furnace) fan site energy savings** are 0.0294 kWh/m^2 (3%).
- **Annual conditioning (cooling + heating) source energy savings** are 10.7 kWh/m^2 (15%).
- **Annual conditioning energy cost savings** are 0.886 \$/m^2 (20%).
- **Annual conditioning CO_2 emission reduction** is 1.63 kg/m^2 (15%).
- **Annual conditioning NO_x emission reduction** is 0.621 g/m^2 (10%).
- **Annual conditioning SO_2 emission reduction** is 0.0462 g/m^2 (22%).
- **Peak-hour cooling (compressor + fan) power demand reduction** is 0.88 W/m^2 (37%).

Using the mean ceiling area of the two homes in this study (188 m^2), annual cooling, heating fuel, and heating fan site energy savings were 530 kWh, 212 kWh (7.25 therm), and 5.53 kWh, respectively. Annual conditioning source energy savings were 2010 kWh; annual energy cost savings were \$167. Emission reductions were 307 kg CO_2, 117 g NO_x, and 8.69 g SO_2; peak-hour power demand reduction was 165 W.

3.5 Discussion

3.5.1 Cooling and heating energy savings

Following Method B, the cool home with the reflective tile roof (initial SR 0.51; thermal capacity 40 kJ/m$^2\cdot$ K) used 26% less annual cooling (compressor + fan) energy, 4% less

Table 3.6: Daily, seasonal, and annual mean values of energy savings, energy cost savings, emission reduction, and peak-hour demand reduction per unit ceiling area. Method B fractional savings (relative to standard house) are shown in parentheses.

	Cooling season (May to Oct)		**Heating season (Nov to Apr)**		**Annual**	
Savings per unit ceiling area	Method A	Method B	Method A	Method B	Method A	Method B
Daily site cooling energy (Wh/m^2)	15.7	15.3				
Daily site heating fuel energy (Wh/m^2)			18.5	6.24		
Daily site heating fan energy (Wh/m^2)			0.426	0.162		
Seasonal or annual site electrical energy (kWh/m^2)	2.89	2.82 (26%)	0.0772	0.0294 (3%)	2.97	2.85
Seasonal or annual site fuel energy (kWh/m^2)	0	0	3.34	1.13 (4%)	3.34	1.13
Seasonal or annual source energy (kWh/m^2)	9.65	9.42	3.76	1.28	13.4	10.7 (15%)
Seasonal or annual conditioning energy cost ($\$/m^2$)	0.861	0.84	0.131	0.0454	0.993	0.886 (20%)
Seasonal or annual CO_2 (kg/m^2)	1.45	1.41	0.641	0.218	2.09	1.63 (15%)
Seasonal or annual NO_x (g/m^2)	0.468	0.456	0.484	0.164	0.95	0.62 (10%)
Seasonal or annual SO_2 (g/m^2)	0.0459	0.0448	0.00419	0.00147	0.0501	0.0462 (22%)
Peak-hour site electrical demand (W/m^2)	1.06	0.88 (37%)				

annual heating fuel energy, and 3% less annual heating fan energy than the standard home with the dark shingle roof (initial SR 0.07; thermal capacity 22 $kJ/m^2 \cdot K$).

The Fresno fractional annual cooling energy savings (26%) were 2.6 times the 10% daily cooling energy savings that Parker and Barkaszi [16] measured after applying a white coating to an RSI-3.3 asphalt shingle roof on a Palm Bay, Florida home, even though (a) all three homes (Fresno cool, Fresno standard, Palm Bay) had RSI-3.3 roof insulation; (b) the roof albedo increase in Fresno (0.44) was the same as that in Palm Bay; and (c) based on the TMY3 typical meteorological year, the cooling-season (May – Oct) mean global horizontal solar irradiance in Fresno is only about 25% greater than that in Melbourne, FL (near Palm Bay) [67]. Similarly, fractional peak-hour cooling power demand savings in Fresno were 37%, or 2.3 times the 16% savings measured in Palm Bay at 17:00 – 18:00 LDT.

While this study was not designed to isolate the effects of increasing roof thermal mass and adding above-sheathing ventilation from those of increasing roof albedo, some remarks can be made. First, basic physics suggests (a) that increasing roof albedo will tend to decrease roof temperature during the day (sunny), while minimally affecting that at night (no sun); (b) above-sheathing ventilation enhances roof heat transfer mostly during the day, because buoyant air flow in the space between the sheathing and roofing is driven by the temperature difference between roof and outside air; and (c) increasing roof thermal mass will

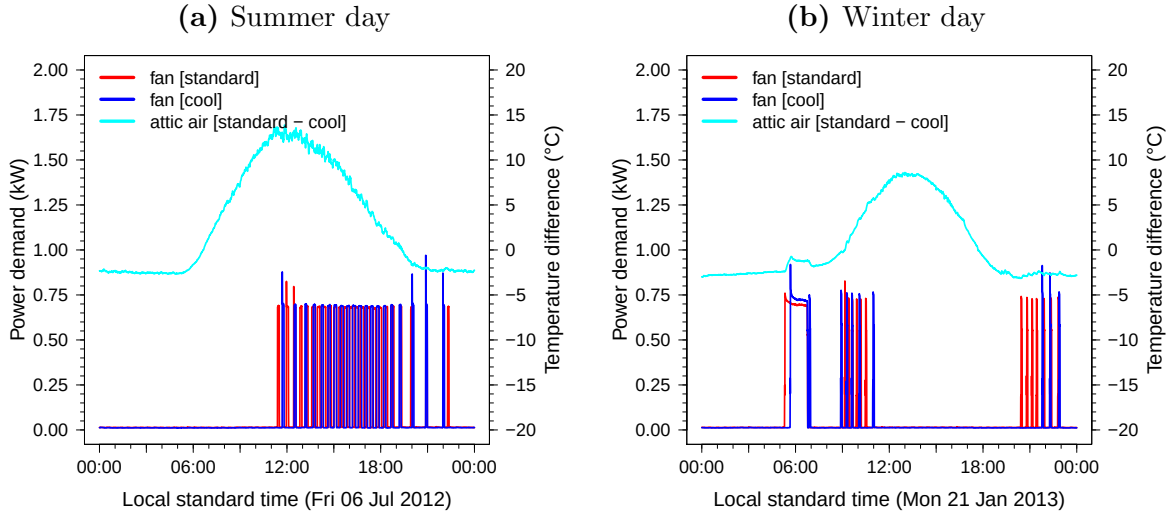

Figure 3.17: HVAC fan power demand on (a) the summer day and (b) the winter day.

tend to lower roof temperature during the day and raise it at night by slowing temperature change. On the representative summer day, the magnitude of the maximum roof bottom temperature difference (standard – cool), around 12:00 LST, was over 5 times greater than that of the minimum roof bottom temperature difference, near 00:00 LST (Figure 3.7a). Similarly, on that day the magnitude of the maximum ceiling heat gain difference (standard cool), around 14:00 LST, was over 4 times greater than that of the minimum ceiling heat gain difference, near 06:00 LST (Figure 3.8a). This indicates that daytime reductions in roof temperature and/or ceiling heat flux resulted predominantly from raising albedo and adding above-sheathing ventilation, rather than from increased thermal storage.

Second, while the tile roof's higher thermal mass (80% greater than that of the shingle roof) delayed peak ceiling + duct heat gain by about an hour (ESM Table C 3), this shift may not have substantially reduced summer cooling loads, because the cool homes AC operated well into the evening (Figure A.1). Thus, the improved fractional cooling energy savings (26% vs. 10%) and fractional peak demand reduction (37% vs. 16%) observed in Fresno likely resulted from the tile roofs above-sheathing ventilation (1.9 – 4.4 cm air gap below tiles; none below shingles), rather than its higher thermal mass. These boosts in savings are qualitatively consistent with the 50% ceiling heat flux reduction measured by Miller and Kosny [19] when comparing an SR 0.13 flat tile roof on double battens to an SR 0.09 shingle roof.

Third, the slightly positive fractional annual heating energy savings in Fresno (4%) differs in sign from the fractional annual heating energy savings (e.g., -5% in Los Angeles; -2% in Phoenix) simulated by Akbari et al. [12] for a 0.30 increase in the albedo of an RSI-3.3

asphalt shingle roof. Here the improvement likely results from the tile roofs high thermal capacity, which increases the overnight temperature of the attic air.

3.5.2 Importance of corrections to measured energy savings

Figure 3.12 shows that differences (standard – cool) in daily mean rates of ceiling, plug load, duct, and window heat gain were generally comparable in magnitude (-0.5 kW to +0.5 kW). This confirms the importance of correcting measured HVAC savings for differences in window and plug load heat gain, as shown in Method B equations 3.20 and 3.21.

3.5.3 Estimating cooling energy savings from temperature and heat flux measurements

The close agreement between Methods A and B in the cooling season suggest that Method A can be used to estimate cooling energy savings without measuring HVAC or plug load power demand. A minimalist and quite economical *cooling season* experiment would require in each building only seven temperature sensors—roof top, attic air, room air, supply duct inlet, supply duct outlet, return duct inlet, and return duct outlet—and one ceiling heat flux sensor. While not strictly needed to measure energy savings, multiple roof top temperature sensors would be warranted if the roof is not flat.

If the HVAC's cooling COP and fan-on air flow rate are known from equipment specifications, duct heat gain rate and Method A cooling power savings can be computed from Equations 3.4 and 3.18, respectively. For calculation of duct heat gain rate, the fan can be assumed on if the supply duct outlet air temperature is far from the room air temperature, and off otherwise.

Methods A and B each reference the heating and cooling COPs of the HVAC equipment. Note that the COP of an air conditioner or heat pump can vary with load factor, outside air temperature, and refrigerant charge [68].

3.6 Summary

Temperatures, heat flows, and energy were measured for a year in two side-by-side, single-story, single-family homes in Fresno, California. One house had a reflective concrete tile roof (initial SR 0.51; thermal capacity 40 kJ/m^2·K), and the other a standard dark asphalt shingle roof (initial SR 0.07; thermal capacity 22 kJ/m^2·K). The flat tiles were mounted on battens, creating an air gap between tile and deck; the shingles were nailed directly to deck. The buildings were otherwise similar in construction and occupancy, with some differences in heat gains from plug loads and windows.

On a representative summer day (6 Jul 2012), maximum roof top, roof bottom, and attic air temperatures in the cool home (tile roof) were 13.8, 14.3, and 10.5°C lower than in the standard house (shingle roof). Maximum rates of ceiling, duct, and ceiling + duct heat gain in the cool home were 1.50, 0.89, and 2.4 kW lower than in the standard house. Minimum roof top, roof bottom, and attic air temperatures in the cool roof home were 2.1, 2.4, and 2.4°C *higher* than in the standard house, likely resulting from the higher thermal capacitance of the tile roof.

On a representative winter day (21 Jan 2013), maximum roof top, roof bottom, and attic air temperatures in the cool home were 11.0, 10.6, and 6.9°C lower than in the standard house. Maximum ceiling, duct, and ceiling + duct rates of heat gain in the cool home were 0.83, 1.33, and 1.17 kW lower than in the standard house. Minimum roof top, roof bottom, and attic air temperatures in the cool home were 0.4, 2.1, and 2.3°C *higher* than in the standard house.

Seasonal mean reductions (standard – cool) in roof top, roof bottom, and attic air temperatures in the cooling season were about 3.4°C, 3.7°C, and 2.4°C, roughly twice those the heating season. Above-sheathing ventilation cooling the deck of the cool tile roof may have made the temperature difference (standard – cool) at roof bottom (underside of roof deck) larger than that at roof top (just below tile surface).

In the cooling season (May – October), the mean rates of ceiling and duct heat gain in the standard home were about 310 W and 130 W lower in the cool home than in the standard home. However, mean rates of ceiling and duct heat gain in the heating season (November – April) were about 46 W and 32 W *greater* in the cool home than in the standard home, likely resulting from the higher thermal capacity of the cool roof.

Relative to the standard home, annual cooling (compressor + fan), heating fuel, and heating fan energy savings at the site were 2.82 kWh/m^2 (26%), 1.13 kWh/m^2 (4%), and 0.0294 kWh/m^2 (3%), respectively. Annual conditioning source energy savings were 10.7 kWh/m^2 (15%); annual energy cost savings were 0.886 \$/m^2 (20%). Annual conditioning CO_2, NO_x, and SO_2 emission reductions were 1.63 kg/m^2 (15%), 0.621 g/m^2 (10%), and 0.0462 g/m^2 (22%). Peak-hour cooling (compressor + fan) power demand reduction was 0.88 W/m^2 (37%). For the studied homes with 188 m^2 ceilings, annual cooling, heating fuel, and heating fan site energy savings were 530 kWh, 212 kWh (7.25 therm), and 5.53 kWh, respectively. Annual conditioning source energy savings were 2010 kWh; annual energy cost savings were \$167. Emission reductions were 307 kg CO_2, 117 g NO_x, and 8.69 g SO_2; peak-hour power demand reduction was 165 W.

Fractional annual cooling energy savings (26%) were 2.6 times the 10% daily cooling energy savings measured in a previous study that used a white coating to increase the albedo of an asphalt shingle roof by the same amount (0.44). Fractional peak-hour cooling power demand savings (37%) were 2.3 times the 16% savings observed in the earlier study.

The improved cooling energy savings (26% vs. 10%) may be attributed to the cool tiles above-sheathing ventilation, rather than to its high thermal mass.

The work presented in this chapter covered the first topic studied in this dissertation. Additional concluding remarks on this topic are presented in Chapter 7. The second topic of the dissertation is the direct and indirect effects of cool pavements on building energy use. The following chapter – Chapter 4 – initiates the second topic by presenting an urban canyon model that can be used to correct temperature sensitivities obtained from climate models. The corrected temperature sensitivities will then be used to simulate the indirect effect of cool pavements.

CHAPTER 4

A Model that Estimates the Solar Downward and Upward Radiance in an Urban Canyon

4.1 Introduction

The climate in urban regions usually experiences higher air temperature and more detrimental air quality than the suburban and rural areas. Rapid urban growth and global climate change aggravate these environmental conditions. Meteorological models have been developed to predict the weather and to model regional climates. These tools are being used to understand the effects of climate change and urban growth on the environmental problems in urban areas, and to develop mitigation and adaptation strategies [25]. The weather research and forecasting model, WRF Model [69] is a model widely used in the field for these purposes.

Urban canyon models (UCMs) assess the geometry and the thermophysical properties of urban canyons. UCMs are used to study the influence that urban morphology, surface properties, and energy fluxes have on the local climate. The meteorological models are coupled with UCMs to assess the near-surface heat islands and their effect on the regional climate in an urban area [9, 25]. The accuracy of a coupled system depends on how accurate the urban morphology can be characterized in the urban canyon model and how well it can be integrated to the climate model.

The WRF model can use various urban models, each with a different level of complexity in the way it defines the urban morphology and the number of parameters required to model the influence of urban characteristics on the local climate. The simplest urban model used by WRF is the slab model, which treats the urban geometry as a flat rough surface. More sophisticated models used by WRF are the single-layer urban canopy model (SLUCM)

developed by Kusaka et al. [27, 28], and the multi-layer urban canopy model (MLUCM) developed by Martilli et al. [29]. These two models consider the three-dimensional nature of urban canyons, shadowing by canyon walls, and reflection from the canyon surfaces.

It is complicated to reproduce the heterogeneous nature of a real city and implement it in an WRF/urban modelling system. In many urban regions, urban planning data and remote-sensing (images) data are used to create urban maps that divide the urban region into different land-use types. The United States Geological Survey (USGS) National Land Cover Data (NLCD) provides such maps, and has three land-use categories for urban regions: low-intensity residential, high-intensity residential, and industrial/commercial [70].

WRF defines urban canyon parameters for these three urban land-use categories. The parameters include geometric dimensions of the canyons (wall height, road width, and roof width), surface albedos, and thermal surface properties (see Table 1 in Chen et al. [25]).

One application to WRF/urban modelling systems is to study how increasing the albedo of roads decreases convective heating of the urban air. However, in these urban canyon models the road extends from wall to wall, with no setback between wall and road—setbacks refer to the portions of the canyon floor that lie between the road and the canyon wall, such as sidewalks, planters, and front yards. Additionally, the road widths specified in the different WRF urban land-use categories may not accurately represent the different canyon widths found in real cities. Hence, when an WRF/urban modelling system is employed to investigate the influence of the wide spread adoption of cool roads on the urban climate, the results need to be adjusted to represent actual canyon geometries.

This study presents the design of a simple urban canyon model that calculates the solar downward and solar upward radiances through the canyon ceiling, and computes the canyon albedo as the ratio of upward to downward irradiance. The canyon geometry is treated as a canyon of infinite length with a canyon floor composed of a road and surrounding setbacks. The model allows the user to vary the dimension and albedo of each canyon surface (i.e., road, setback, and walls). The current version of the model can only be applied for canyons oriented either north-south or east-west. Other canyon orientations can be estimated by averaging the north-south and east-west orientations.

The proposed model is employed to demonstrate how the canyon geometry influences the change in solar radiance that enters and exits the canyon when the road albedo is modified. The model was written and developed using the Python programming language; the code is provided in Appendix F. Additionally, a method is presented to scale air temperature changes from citywide adoption of cool roads modelled in a WRF/urban system. The air temperature changes are scaled to represent the city's street construction standards and the city's building stock.

4.2 Theory

4.2.1 Concept

A model is developed to calculate the amount of downward solar irradiance that enters an urban canyon. The canyon can be oriented east-west or north-south. The model computes the solar irradiance that is reflected from the surfaces (i.e. walls, setbacks, and road) and exits through the ceiling as a function of the canyon geometry, surface albedos, and the solar position. The canyon albedo is computed as the ratio of upward to downward solar irradiance. The air between the surfaces is assumed non-absorbing.

Table 4.1 lists the parameters required by the model.

Table 4.1: Parameters required in the model.

Parameters	**Symbol**	**Units**
Canyon geometry		
wall height	h_w	m
road width	w_r	m
setback width	w_{sb}	m
Surface albedos		
left wall	ρ_3	NA
right wall	ρ_4	NA
road	ρ_0	NA
setback	ρ_0	NA
Solar position		
azimuth angle	ϕ	degrees
zenith angle	β	degrees
Solar irradiances		
global horizontal	I_g	W m^{-1}
diffuse horizontal	I_d	W m^{-1}
Canyon orientations		
east-west	NA	NA
north-south	NA	NA

4.2.2 Canyon geometry

The urban canyon model defines the canyon geometry as illustrated in Figure 4.1. The canyon floor (surface 1) includes a road (dashed gray line) and two equal setbacks (dashed green lines). The floor is divided into N segments, with any particular segment referred to as surface 0. Each segment is identified as part of the road or part of the setback based on the road and setback widths.

The model refers to the canyon ceiling as the sky (surface 2). Surfaces 3 and 4 are the left and right walls, assumed to be of equal height.

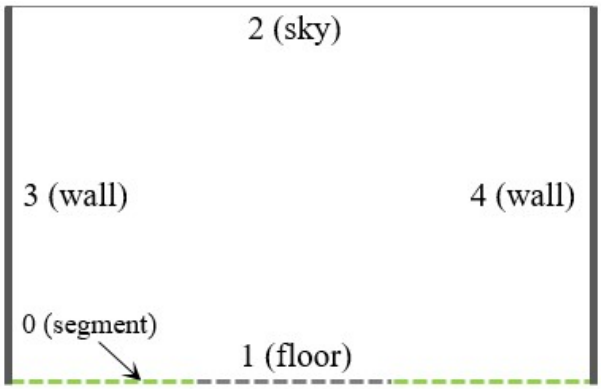

Figure 4.1: Canyon surfaces nomenclature.

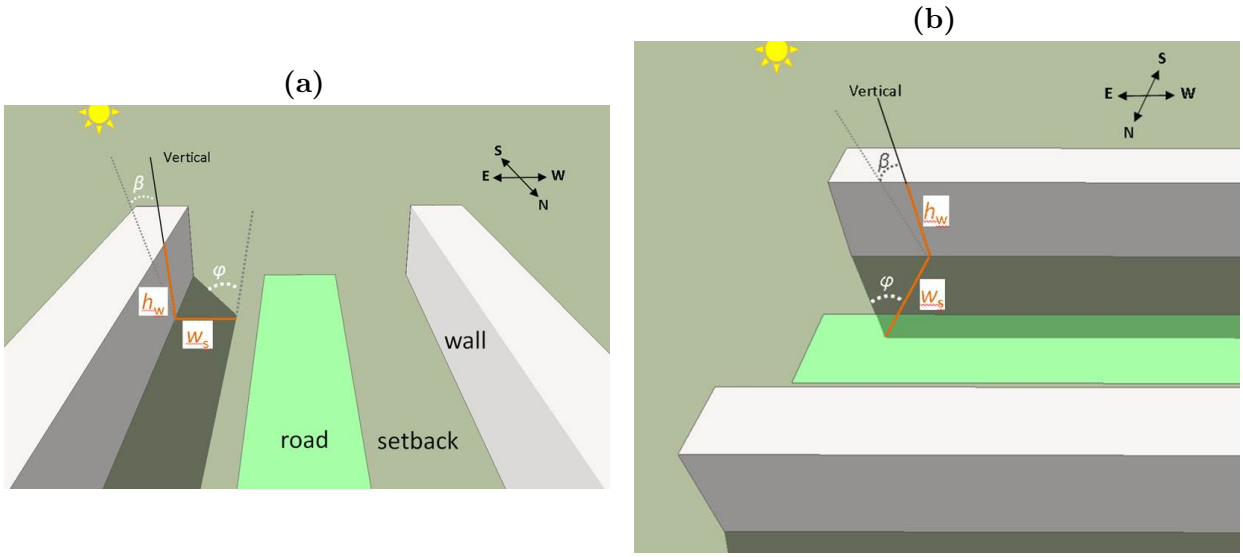

Figure 4.2: Representing shadow width when canyon is oriented a) north-south and b) east-west.

4.2.3 Shadow length on canyon floor

During the day, the canyon floor may be partially or completely shaded by the canyon walls. The width of the canyon floor is the sum of the road width w_r and twice the setback width w_{sb}. The width of the shadow w_s distance along the canyon floor from the wall to the point on the shadow furthest from the wall depends on sun location and canyon orientation. To demonstrate, Figure 4.2 shows the shadow being cast by a 10 m high wall over a 30 m wide floor (10 m road + 10 m setbacks × 2); the figure represents the scenario of a canyon located in Sacramento, California on October 21 at 08:00 LST. In Figure 4.2a and Figure 4.2b the road is oriented north-south and east-west respectively.

When the canyon is oriented north-south, w_s is calculated as

$$w_s = h_w \tan\beta \sin\phi \tag{4.1}$$

where h_w is height of the wall, β is the solar zenith, and ϕ is the solar azimuth (measured clockwise from south).

When the canyon runs east-west, w_s is calculated as

$$w_s = h_w \tan\beta \cos\phi. \tag{4.2}$$

4.2.4 Calculating solar radiances

The model calculates the solar irradiance that enters the canyon and is intercepted by the walls and floor. To do so, it uses the hourly global horizontal irradiance I_g [W/m^2] and hourly diffuse horizontal irradiance I_d [W/m^2], which can be obtained from NREL TMY3 datasets for different locations, dates and time. The beam horizontal irradiance I_b is then calculated as $I_b = I_g - I_d$.

$$I_b = I_g - I_d \tag{4.3}$$

and the beam normal solar irradiance I_{bn} is

$$I_{bn} = \frac{I_b}{\cos\beta}. \tag{4.4}$$

Using these solar irradiances and the algorithm detailed next, the model can then calculate the solar radiance that is reflected from the canyon back to the sky and calculate the canyon albedo as the ratio of radiance leaving the canyon to radiance entering the canyon.

4.2.4.1 Downward irradiance intercepted by the canyon walls

ASHRAE Fundamentals [71] specifies an algorithm for calculating the downward solar irradiance incident on a tilted surface, I_t. This irradiance is the sum of two components: 1) the beam tilt component $I_{t,b}$, and 2) diffuse component $I_{t,d}$.

The model treats the walls as surfaces with a tilt angle of 90° (vertical). For vertical surfaces, the beam component is calculated as

$$I_{t,b} = I_{b,n} \cos\theta \tag{4.5}$$

where θ is the angle of incidence. This relationship is valid when $\cos\theta > 0$. Otherwise, the surface is in shade and $I_{t,b} = 0$.

The diffuse component on vertical surfaces can be calculated as

$$I_{t,d} = I_b Y \tag{4.6}$$

where

$$Y = max(0.45, 0.55 + 0.437\cos\theta + 0.313\cos^2\theta). \tag{4.7}$$

The cosine of the incident angle is calculated as

$$\cos\theta = \cos(90^\circ - \beta)\cos(\phi - \Psi) \tag{4.8}$$

where ϕ is the solar azimuth and Ψ is the surface azimuth, in degrees.

The linear solar irradiance (incident solar power per unit canyon length) on each wall is

$$J_3 = h_w I_{t,b}\cos(\theta_3) + h_w I_{t,b} Y \tag{4.9}$$

and

$$J_4 = h_w I_{t,b}\cos(\theta_4) + h_w I_{t,b} Y. \tag{4.10}$$

The magnitudes of J_3 and J_4 depend on the walls' orientation and on solar position. For example, an urban canyon extending east-west has one wall facing north (surface azimuth of 180°) and the other south (0°). For canyons extending north-south, one wall faces east (-90°) and the other faces west (90°). Solar position (zenith and azimuth angles) can be obtained from NREL's Solar Position Algorithm [57] by location, date, and time.

The model assumes the walls are distant enough that they do not shade each other. It also ignores the wall-reflected radiance that strikes the other wall.

4.2.4.2 Solar irradiance intercepted by the canyon floor

Each segment of the canyon floor receives solar irradiance from the sky and from the walls.

The linear irradiance from the sky is calculated for each floor segment. Let us define $J_{X\to Y}$ as the linear irradiance on surface Y that comes from surface X, the linear irradiance on the segment that comes from the sky is

$$J_{2\to 0} = I \cdot w_0 \tag{4.11}$$

where w_0 is the segment width; $I = I_d$ if the segment is in shade or $I = I_g$ otherwise. The model uses the shadow width (w_s) and the segment distance from each canyon wall to determine if the segment is shaded.

As the model iterates through the segments to obtain each value of $J_{2\to0}$, it also calculates the fraction of the wall-reflected irradiance that intercepts each individual segment. It does so as follows

$$J_{3\to0} = J_3\rho_3 F_{3\to0} \tag{4.12}$$

and

$$J_{4\to0} = J_4\rho_4 F_{4\to0} \tag{4.13}$$

where ρ_3 and ρ_4 are the wall albedos; $F_{3\to0}$ and $F_{4\to0}$ are the view factors from the walls to a segment. The view factor (a.k.a. configuration factor or shape factor) from surface A to surface B (FAB) is the fraction of radiant energy leaving surface A that is intercepted by surface B. Section 4.2.5 details how the model calculates the view factors required in the model.

The total solar irradiance intercepted by a segment is

$$J_0 = J_{2\to0} + J_{3\to0} + J_{4\to0}. \tag{4.14}$$

4.2.4.3 Solar radiance reflected from the canyon

Segment-reflection to sky Some of the canyon floor irradiance is reflected to the sky. The reflected radiance exits the canyon two ways: directly through the ceiling, and by reflection from the walls. From each floor segment, the radiance that is reflected to the sky is calculated as

$$J_{0\to2} = J_0\rho_0(F_{0\to2} + F_{0\to3}\rho_3 F_{3\to2} + F_{0\to4}\rho_4 F_{4\to2}). \tag{4.15}$$

Here ρ_0 is the albedo of the segment (road or setback), while $F_{0\to2}$, $F_{0\to3}$, $F_{3\to2}$, $F_{0\to4}$, and $F_{4\to2}$ are the view factors.

The total radiance reflected from the floor that exits the canyon is

$$J_{1\to2} = \sum_{i=1}^{N} J_{0_i\to2} \tag{4.16}$$

where N is the number of segments.

Wall-reflection to sky The solar radiance reflected from each wall to the sky is

$$J_{3\to2} = J_3\rho_3 F_{3\to2} \tag{4.17}$$

and

$$J_{4\to2} = J_4\rho_4 F_{4\to2}. \tag{4.18}$$

Upward radiance through the canyon ceiling The total linear upward radiance is

$$J_{out} = J_{1\to 2} + J_{3\to 2} + J_{4\to 2}. \tag{4.19}$$

The upward radiance I_{out} by unit of road width can be obtained by normalizing J_{out} by the width of the road w_r:

$$I_{out} = \frac{J_{out}}{w_r} \tag{4.20}$$

The model is designed to compute the mean upward linear radiance over a period of time by receiving as input M values of global and diffuse horizontal solar irradiances as well as M values of the solar coordinates (solar zenith and azimuth angles) that correspond to the solar irradiances:

$$J_{out\_total} = \frac{\sum_{h=1}^{M} J_{out_h}}{M} \tag{4.21}$$

Hence, the model can calculate the daily mean upward linear radiance when provided with solar irradiances and solar position angles over a day.

4.2.4.4 Canyon albedo

The model calculates the mean downward linear radiance entering the canyon over the given timeframe as

$$J_{in,mean} = \frac{w_2 \sum_{h=1}^{M} I_{g_h}}{M} \tag{4.22}$$

where w_2 is the width of the canyon ceiling (sky). The canyon albedo ρ_c (ratio of mean upward radiance to mean downward radiance) is then calculated as

$$\rho_c \equiv \frac{J_{out,mean}}{J_{in,mean}}. \tag{4.23}$$

The user can instruct the model to return the mean upward linear radiance, mean upward radiance by road width, or canyon albedo (Table 4.2).

Table 4.2: Optional outputs of the present model.

Output	Symbol	Units
mean upward linear radiance	$J_{out,mean}$	W m^{-1}
mean upward radiance by road width	$I_{out,mean}$	W m^{-2}
canyon albedo	ρ_c	NA

4.2.5 View factor calculations

View factors depend only on geometry. As such, view factors have been published in the engineering literature for common geometric configurations, many of which are readily available in an online catalog of configuration factors [72].

The urban canyons analyzed with the model have simple geometries, which simplify the view factor calculations to pre-existing geometric configuration equations. An example of simple geometry would be two finite identical planes parallel to each other and separated by a finite distance.

4.2.5.1 Sky to walls

To obtain the sky to walls view factors, the tool first calculates the view factor from sky (surface 2) to floor (surface 1), $F_{2\to1}$. The sky and the floor can be considered as two infinitely long, directly opposed parallel plates of the same width ($w_1 = w_2$) and separated by the wall height h_w. The equation (section C-1 in [72]) used to calculate the view factor for this type of configuration is

$$F_{2\to1} = \sqrt{1 + H^2} - H \tag{4.24}$$

where $H = h_3/w_c$.

The sum of view factors from a given surface is unity. All the view factors leaving the sky (surface 2) can then be expressed as

$$F_{2\to1} + F_{2\to2} + F_{2\to3} + F_{2\to4} = 1. \tag{4.25}$$

By symmetry, $F_{2\to3} = F_{2\to4}$. Meanwhile, $F_{2\to2}$ is zero since the surface 2 does not see itself. Hence, the view factors from the sky to each wall (surfaces 3 and 4) are

$$F_{2\to3} = F_{2\to4} = \frac{1 - F_{1\to2}}{2}. \tag{4.26}$$

4.2.5.2 Segment to sky

The view factor from a floor segment to sky varies by segment. As the model iterates through the segments, it calculates their view factor to the sky using the "crossed-string

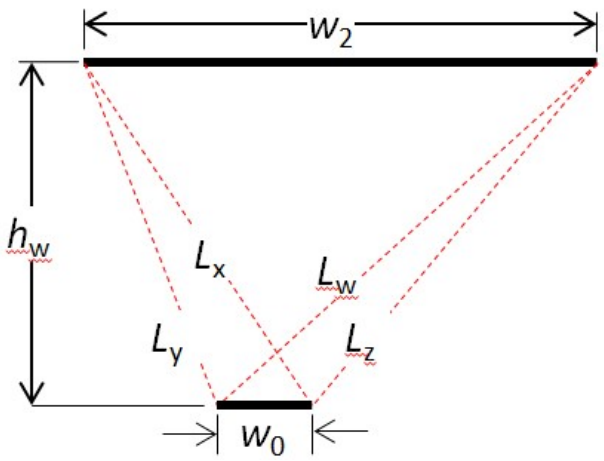

Figure 4.3: Crossed-string method applied to segment-to-sky view factors.

method" [73]. Figure 4.3 illustrates how the method is applied to calculate the segment-to-sky view factor. The model calculates the distances L_x, L_w, L_y, and L_z for each segment.

The equation (section C-2a in [72]) is derived from this method and used to calculate the segment-to-sky view factors:

$$F_{0\to2} = \frac{L_x + L_w - L_y - L_z}{2w_0}. \tag{4.27}$$

4.2.5.3 Segment to wall

As the model iterates through the segments, it also calculates the view factors from each segment to the walls ($F_{0\to3}$ and $F_{0\to4}$). By calculating the distance of each segment to both walls, the model can then use a pre-existing view factor equation (section C-5a in [72]), which was derived for two non-adjacent infinitely long plates of finite width. Equations 4.28 and 4.29 show a simplified version of the equation used to obtain $F_{0\to3}$ and $F_{0\to4}$ respectively. Figure 4.4 illustrates the dimensions used in the $F_{0\to3}$ and $F_{0\to4}$ calculations. Note that x_1 and x_2 vary by segment.

$$F_{0\to3} = \frac{({x_1}^2 - {h_w}^2)^{\frac{1}{2}} - ({x_2}^2 - {h_w}^2)^{\frac{1}{2}} + (x_2 - x_1)}{2(x_2 - x_1)} \tag{4.28}$$

and

$$F_{0\to4} = \frac{[w_2 - {x_1}^2 - {h_w}^2]^{\frac{1}{2}} - [w_2 - {x_2}^2 - {h_w}^2]^{\frac{1}{2}} - (x_2 - x_1)}{2(x_2 - x_1)}. \tag{4.29}$$

View factor reciprocity relates view factors (F) and areas (A), such that

$$A_A F_{AB} = A_B F_{BA}. \tag{4.30}$$

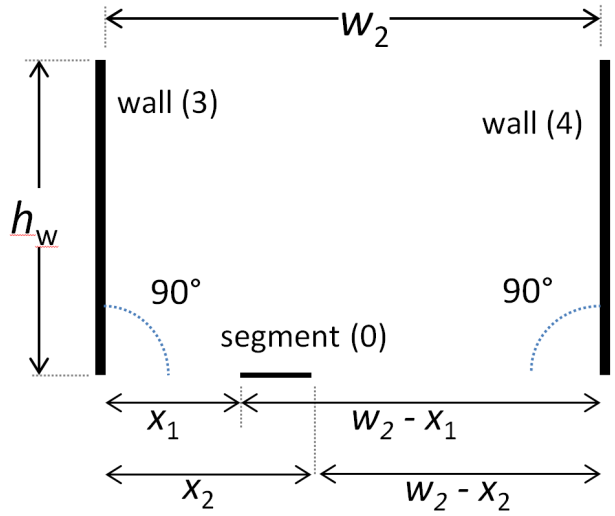

Figure 4.4: Diagram of dimensions and variables used to calculate $F_{0\to3}$ and $F_{0\to4}$.

Applying view factor reciprocity, the model calculates the wall-to-segment view factors as

$$F_{3\to0} = \frac{w_0 F_{0\to3}}{w_3} \tag{4.31}$$

and

$$F_{4\to0} = \frac{w_0 F_{0\to4}}{w_4}. \tag{4.32}$$

4.2.6 Uses for the model

4.2.6.1 Canyon transmittance

The canyon geometry influences the amount of sunlight that enters the canyon and reaches the floor. This means that the sunlight that reaches the road in a narrow canyon and is reflected back to the sky will change if the same road is placed in a wide canyon. The ability of sunlight on reaching the road in a canyon and being reflected back to the sky can be described with the canyon transmittance τ.

Canyon transmittance is defined as the ratio of the increase in sunlight reflected from canyon to sky upon raising the albedo of a road in the canyon, to the increase in sunlight reflected to the sky upon raising the albedo of the same road not in a canyon. It can be interpreted as the transmittance of sunlight from sky to road to sky. Canyon transmittance should approach one as canyon height approaches zero, and should never exceed one.

For a road not in a canyon (*outside* of a canyon), the reflected solar irradiance $I_{outside}$ is

$$I_{outside} = I_g \cdot \rho_r. \tag{4.33}$$

Hence, the change in reflected solar irradiance from a change in the road albedo outside the canyon is

$$\Delta I_{outside} = I_g \cdot \rho_{r,modified} - I_g \cdot \rho_{r,original} \tag{4.34}$$

or

$$\Delta I_{outside} = I_g \cdot \Delta\rho_r. \tag{4.35}$$

where $\Delta\rho_r$ is the change in road albedo.

If the same road is inside a canyon, the solar irradiance reflected from the road and exits the canyon (I_{inside}) can be computed with I_{out} [Eq. 4.20]. The change in canyon-reflected solar radiance from a change in road albedo is

$$\Delta I_{inside} = I_{out}(\rho_{r,modified}) - I_{out}(\rho_{r,original}). \tag{4.36}$$

The canyon transmittance can then be obtained as

$$\tau = \frac{\Delta I_{inside}}{\Delta I_{outside}}. \tag{4.37}$$

4.2.6.2 Scaling factor

The reduction in the air temperature in a canyon is proportional to the reduction in the canyon's solar heat gain, which in turn is proportional to the decrease in the canyon's solar absorptance. The solar absorptance of the canyon can be reduced by increasing the irradiance reflected from the road ΔI_{inside}. Hence, the reduction in air temperature is proportional to the increase in radiance reflected from the canyon, or simply

$$\Delta T \propto \Delta I_{inside}. \tag{4.38}$$

Climate modeling can be used to predict the reduction in air temperature upon increasing the road albedo in a canyon. However, the change in air temperature applies only to a city having the canyon geometry defined in the climate model, and must be adjusted to describe air temperature changes that will occur in a city composed with different canyon geometries.

To illustrate, assume the climate model was used to obtain the air temperature change from modifying the road albedo in a city composed of narrow canyons. The narrow-canyon temperature change ΔT_n may need to be scaled to estimate a wide-canyon temperature change ΔT_w—subscripts n and w refer to narrow and wide canyon respectively. Since ΔT is proportional to ΔI_{inside}, the scaling factor is

$$\sigma_{n\to w} \equiv \frac{\Delta T_w}{\Delta T_n} = \frac{\Delta I_{inside,w}}{\Delta I_{inside,n}}. \tag{4.39}$$

The change in canyon-reflected radiation ΔI_{inside}, upon increasing road albedo by $\Delta\rho_r$ is proportional to the canyons transmittance τ . Thus for a given increase in road albedo,

$$\sigma_{n\to w} = \frac{\Delta I_{inside,w}}{\Delta I_{inside,n}} = \frac{\tau_w \cdot \Delta\rho_r}{\tau_n \cdot \Delta\rho_r} = \frac{\tau_w}{\tau_n}. \tag{4.40}$$

Thus the ratio of canyon transmittances can be used to calculate the scaling factor to adjust between canyons with different geometries.

Since ΔI_{inside} is proportional to ΔT, the change in air temperature in a narrow canyon can be scaled to air temperatures in a wide canyon with

$$\Delta T_w = \sigma_{n\to w} \cdot \Delta T_n. \tag{4.41}$$

Citywide scaling factor. A city's urban morphology is composed of canyons with different geometries. However, they can be estimated with the street design standards and the building stock composition of the city. First, multiple wide canyons are defined, each with geometries that describe a particular city region (e.g. a residential wide canyon can be defined with wall heights of a home and residential street standards). Next, a scaling factor can be computed for each of the newly defined wide canyons. Each building of the city is then mapped to one of the newly defined wide canyons. Finally, a citywide scaling factor ($\sigma_{n\to\bar{w}}$) can be calculated as the average of the scaling factors of each wide canyon weighted by the number of buildings mapped to each wide canyon. The $\sigma_{n\to\bar{w}}$ can be used in Eq. 4.41 to scale the changes in air temperature of a city modelled with the narrow canyon to the city composed of the more realistic wide canyons.

4.3 Simulations

4.3.1 Impact of setbacks in reflection from road

The proposed model allowed us to obtain the increase in canyon-reflected solar radiance upon raising the albedo of the road. The canyon is first modelled with the road having the original low albedo. It is later modelled with the higher road albedo. The difference between the two results gives the change in canyon-reflected radiance.

To demonstrate the impact of canyon dimensions in the reflected radiation, a canyon that has a 10 m high wall and 10 m wide road with no setback is compared to a canyon having the same wall and road dimensions and 10 m wide setbacks (Table 4.3). The road albedo was raised to 0.40 from 0.10.

Figure 4.5 compares the difference in diurnal upward radiance between a canyon with no setbacks and a canyon with setbacks, both modelled in Sacramento (using the citys solar

Table 4.3: Geometries of canyon without setback and canyon with setback.

Canyon version	Wall height [m]	Road width [m]	Setback width [m]	Floor width [m]	Wall to floor width ratio
No setback	10	10	0	10	1.00
With setback	10	10	10	30	0.33

position and irradiation). The plots include results for canyons oriented east-west and north-south, and are representing each season of the year. A representative day of each season is obtained by calculating the hourly diurnal mean solar irradiances (global horizontal and diffuse horizontal) of 21 days around the solstices (for summer and winter) and the equinoxes (for spring and fall).

4.3.2 Adjusting climate modelling results with the proposed model

In this section the proposed model is applied on a canyon with dimensions of the high-density residential land-use category from NLCD. A set of canyon geometries are also defined using Sacramento street design standards to represent realistic canyon dimensions. Finally, it is demonstrated how Sacramento's air temperature changes obtained from a WRF/urban modelling system can be scaled to represent the city's street construction standards and its building stock. The two cases being compared are

- Case 1 – employ the proposed model on a canyon with NLCD high-residential geometries.
- Case 2 – apply the proposed model on canyons having (a) setback and street dimensions that follow design standards of Sacramento and (b) wall height obtained from various building prototypes used to represent US current building stock and simulate building energy use.

4.3.2.1 Defining canyon geometries

Canyons based on NLCD. The three urban land-use categories defined in the USGS National Land Cover Dataset, or USGS NLCD [74] are low-intensity residential, high-intensity residential, and industrial/commercial. These categories define canyon geometry with no setback and the canyon floor width equals the road width. This study will only employ the canyon geometry specify for the high-intensity land-use category; this geometry is the one used for our *narrow* canyon (Table 4.4).

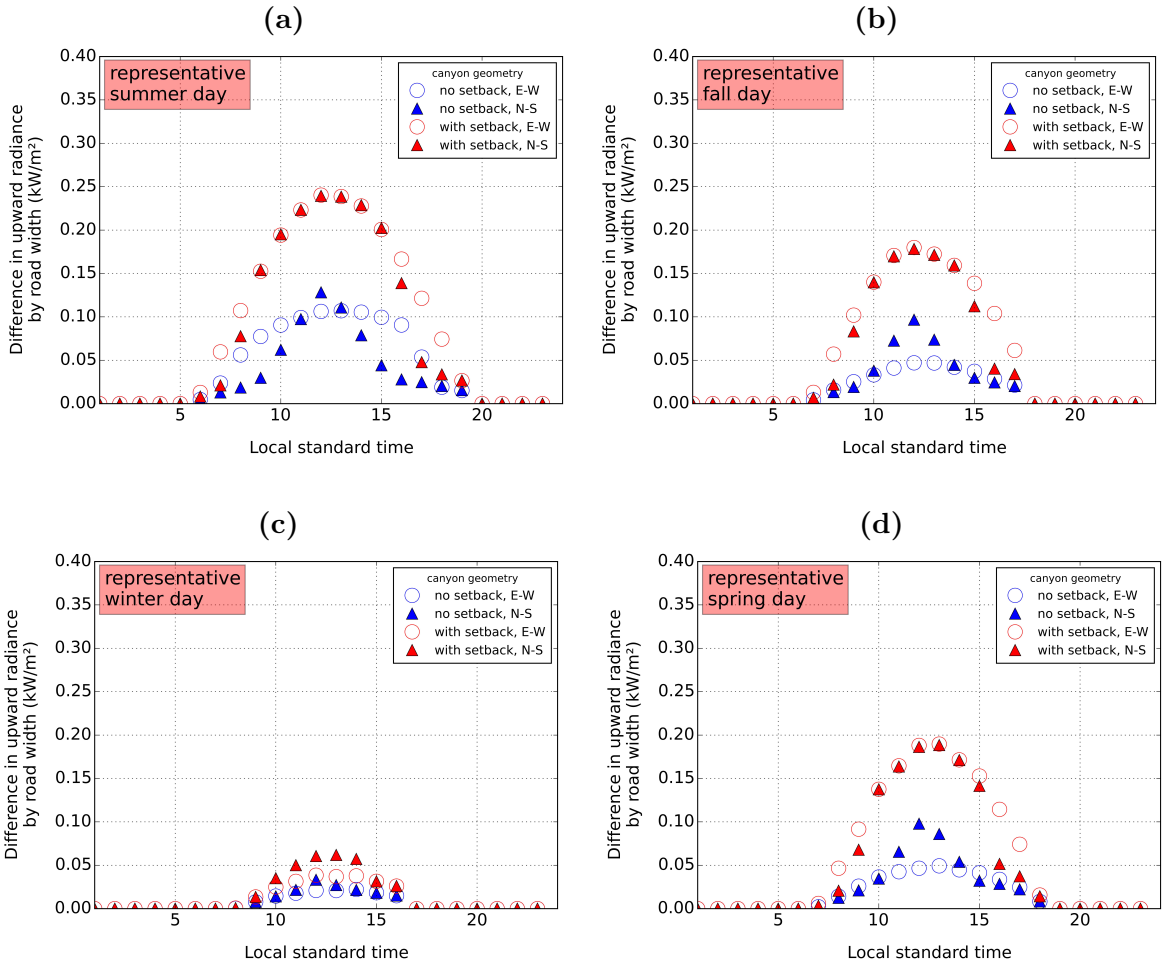

Figure 4.5: Comparing the difference in diurnal upward radiance of cases 1 and 2 when raising the road albedo to 0.40 from 0.10 in the representative day of (a) summer (b) fall, (c) winter, and (d) spring.

Canyons with wide geometries. Ten additional canyons were defined to represent actual wall, road, and setback dimensions obtained from building prototypes and city streets construction standards. They are referred to as the *wide* canyons.

The wall height of two residential scenarios single-family home and multi-family building were obtained from the building models provided by US-DOE's Building Energy Codes Program [75]. The wall heights of eight commercial scenarios were obtained from the US Department of Energys commercial reference building models [76].

The road widths vary according to street design standards. Each building prototype was mapped to a street type depending on the building use and size. The dimensions and lane configurations of each street type were obtained from Sacramento's Street Design Standards [77].

The setback widths follow street design guidelines specified in the Zoning Code of Sacramento County, ZCSC [78] and in the Street Design Standards for the City of Sacramento [77]; they vary also by building type.

Table 4.4 details the dimensions of the wide canyons.

Table 4.4: Dimensions for the narrow canyon and for each wide canyon.

Canyon type	Canyon name	Wall height [m]	Road width [m]	Setback width [m]	Floor width [m]	Wall to floor width ratio
Narrow canyon	NLCD high-intensity	7.5	9.4	0.0	9.4	0.80
Wide canyon	Single-family home	5.2	9.1	9.6	28.3	0.18
	Multi-family building	7.8	9.1	11.1	31.3	0.25
	Large hotel	21.6	16.5	19.7	55.9	0.39
	Large office	37.5	16.5	12.0	40.5	0.93
	Medium office	11.9	11.0	11.1	33.2	0.36
	Primary school	4.0	9.1	11.1	31.3	0.13
	Fast-food restaurant	3.1	11.0	18.7	48.4	0.06
	Retail stand-alone	6.1	22.0	64.5	151.0	0.04
	Strip mall retail	5.2	16.5	18.7	53.9	0.10
	Sit-down restaurant	3.1	9.1	18.7	46.5	0.07

4.3.2.2 Comparing canyon transmittances

The narrow canyon and wide canyons were modelled for Sacramento, CA to calculate the canyon transmittance when raising the road albedo to 0.40 from 0.10. The canyon transmittances were calculated for each season and averaged over the two orientations (Figure 4.6).

4.3.2.3 Scaling factor for city composed of the wide canyons

Consider a WRF/urban system that was employed to study the change in Sacramento's local climate when increasing the albedo of all public roads by 0.30; all canyons were defined

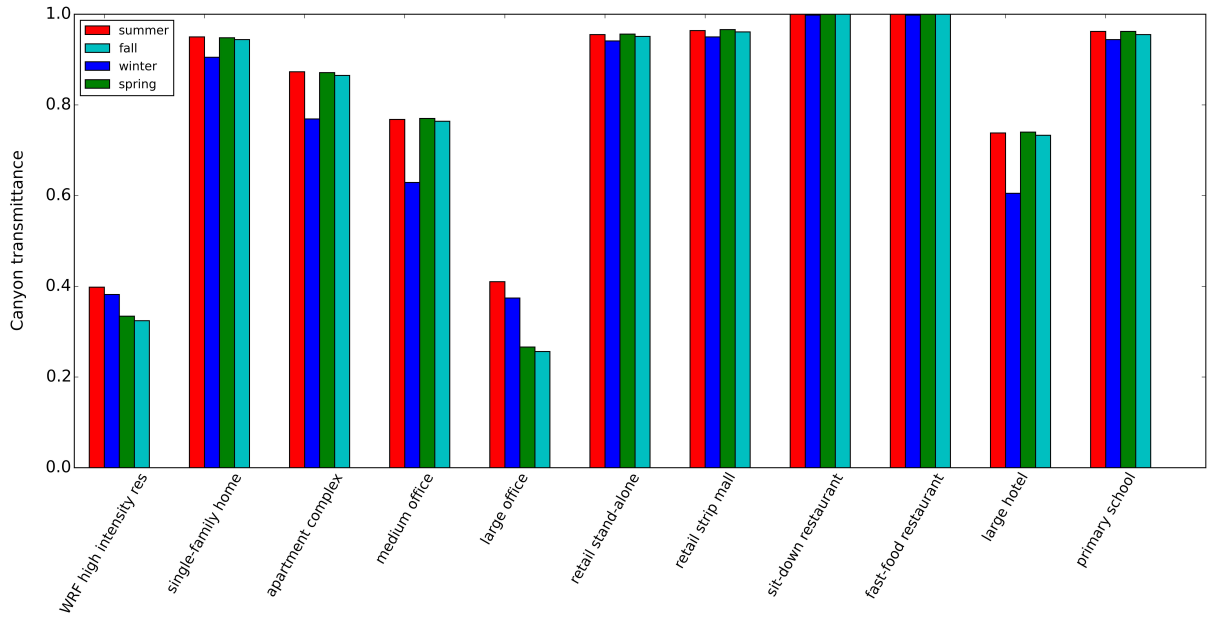

Figure 4.6: Canyon transmittances of narrow and wide canyons for each season.

in the system with the geometry of NLCD's high density residential urban type. This section demonstrates a method to scale the air temperature changes obtained from the WRF/urban model by considering the building stock of Sacramento and assuming the city is composed of the wide canyons.

Sacramento's building stock. Sacramentos building stock was obtained from the County Assessor's office of Sacramento. The Assessor's office is responsible for the discovery and assessment of all the properties within their jurisdiction. Their public property records provide useful information for each of the properties, which include location (county, city, and zip code) and property type (e.g., single-family home, office building).

All properties in the Sacramento's building stock data are classified into 63 property types. The properties were first grouped by property types and then added up to obtain the number of properties of each property type. Nearly half of the property types, including such types as vacant land and agricultural fields, are not relevant for purposes of our study. That left 32 relevant property types. Each remaining property type was mapped to one of the wide geometry canyons to represent all the relevant buildings in Sacramento (Table 4.5).

Table 4.5: Mapping of stock property types to the wide canyons.

Building prototype	Stock property types	Building prototype	Stock property types
Single-family home	Single family residence Duplex Triplex Mobile home Trailer park Miscellaneous residential Fraternal organization	Apartment building	Multi-family dwelling (2-4 units) Multi-family res (5+ units) Quadruplex Timeshare Condominium Planned unit development (PUD) Cooperative
Large hotel	Hotel Motel Casino Hospital Convalescent home	Medium office	Store/office combo Medical building Miscellaneous commercial Nursery Veterinary Governmental
Retail stand-alone	Department store Food store Market Bowling alley	Strip mall retail	Shopping center Stores Retail outlet
Fast-food restaurant	Laundry Dry cleaning	Sit-down restaurant	Restaurant Bar Food service
Large office	Financial building Office building	Primary school	School

4.4 Results

4.4.1 Impact of setbacks in reflection from road

The solar irradiance that is reflected from the canyon road to the sky depends on canyon orientation and season (Figure 4.5). However, the road reflects much more when the canyon has setbacks. The changes in daily mean radiance reflected from the canyon with no setbacks when increasing the road albedo by 0.30 are 0.06 kW (representative summer day), 0.04 kW (fall), 0.02 kW (winter), and 0.03 kW (spring). These values represent the average of having the canyon oriented east-west and north-south. Similarly, for the canyon with setbacks, the values were 0.14 kW (summer), 0.11 kW (fall), 0.03 kW (winter), and 0.11 kW (spring). The results from the canyon with setbacks were 2.39 (summer), 3.10 (fall), 1.95 (winter), and 3.04 (spring) times greater than the canyon with no setback.

4.4.2 Adjusting climate modelling results with the proposed model

4.4.3 Comparing canyon transmittances

The canyon transmittance of the narrow canyon averaged over the four seasons is 0.32 and for all wide canyons combined is 0.86. The only wide canyon with similar average

transmittance as the narrow canyon is the large office (0.33), which has very tall walls compared to the other wide canyons. The summer transmittances of the narrow and large office canyons are 0.41, which is greater than in the other seasons. Their spring and fall transmittances are the smallest transmittances.

The transmittances of the canyons associated with the single-family home, two restaurants, two retail buildings, and the primary school are 0.95 or higher. The transmittance in these canyons vary very little by season. This means that no matter the season, the sunlight that strikes the road and is subsequently reflected back to the sky is barely affected by the canyon geometry.

4.4.3.1 Scaling factor to represent Sacramento

A citywide scaling factor ($\sigma_{n\to\bar{w}}$) for Sacramento was computed by calculating the scaling factors from the narrow canyon to each wide canyon and doing a weighted average by the number of the buildings in the city mapped to each wide canyon (Table 4.6). The weighted citywide scaling factor is 2.97. Thus changes in air temperature in Sacramento ($\Delta T_{n,city}$) obtained from a climate modeling that used as the urban geometry the narrow canyon, can be scaled using

$$\Delta T_{w,city} = 2.97 \cdot \Delta T_{n,city} \tag{4.42}$$

where $\Delta T_{w,city}$ is the corrected city's temperature change. Note that since residential buildings is the most common building type in the city, the weighted citywide scaling factor is dominated by residential canyons.

Table 4.6: Estimated canyon transmittances and scaling factors, and number of buildings mapped to each wide canyon.

Wide canyon name	**Canyon transmittance, τ**	**Narrow to wide canyon scaling factor, $\sigma_{n\to w}$**	**Number of buildings in Sacramento**
Single-family home	0.95	3.02	202,567
Multi-family building	0.87	2.76	11,946
Large hotel	0.74	2.35	299
Large office	0.41	1.30	2,194
Medium office	0.77	2.44	6,339
Primary school	0.96	3.05	422
Fast-food restaurant	1.00	3.17	0
Retail stand-alone	0.95	3.02	187
Strip mall retail	0.96	3.05	1,899
Sit-down restaurant	1.00	3.17	581

4.5 Summary

When the floor of the canyon includes setbacks, the road is able to reflect more of the entering sunlight back to the sky. A canyon that had a 5 m wide road with no setback

was compared to a canyon with the same road and 5 m wide setbacks. Although the daily average sunlight reflected to the sky from a canyon road varies by season, the road with surrounding setbacks reflected two to three times more sunlight.

The term canyon transmittance, τ, was introduced to define the ability of sunlight on reaching the road in a canyon and being reflected back to the sky. This concept was tested in one narrow canyon (no setbacks) and 10 wide canyons (with setbacks). The canyon transmittance is more season-dependent on very tall canyons (i.e. large office canyon) and canyons without setbacks—the highest τ occurs during summer, while the lowest τ occurs during spring and fall. Six of the canyons had annual averaged transmittance above 0.95 and had little variation by season.

This study revealed the importance of considering realistic canyon geometries in urban canyon models since the effect of incoming sunlight that enters the canyon and is absorbed by the surfaces is highly dependent on geometry. Furthermore, when studying the effect of cooler roads in an urban climate, it is crucial to consider the setbacks since the air temperature change obtained from increasing the road albedo is underestimated when setbacks are not included.

A method to scale air temperature changes obtained from a WRF/urban modelling system was presented using the building stock of Sacramento and the street dimension standards of the city. It is a simple method that can be applied to any city if the building stock is known. It is also applicable for the various canyon geometries used in the WRF/urban modelling system and other urban canyon models.

The next chapter – Chapter 5 – presents the methodology followed to simulate the direct and indirect effect of cool pavements on building energy use. The proposed urban canyon model and the method presented here for scaling air temperature changes are employed in Chapter 5 to scale the temperature changes obtained from a climate model. The scaled temperature changes are then used to modify the weather files used in the building energy simulations.

CHAPTER 5

Effect of Cool Pavements on Building Energy Use – Methodology

5.1 Introduction

This chapter describes the method used to simulate the direct and indirect effects of cool pavements on the cooling, heating, and lighting annual energy uses of buildings throughout California. The building energy simulations were performed with 10 different building prototypes that comply with 2008 Title 24 Standards. The prototypes were modified to add horizontal surfaces mimicking "roads" adjacent to the buildings, and vertical surfaces mimicking neighboring buildings. The roads added to the prototypes are meant to represent only public roads; private roads and parking areas around a building are not simulated in this study.

The direct effect of cool pavements adjacent to a building was simulated by varying the albedo of the neighboring roads. The indirect effect of changes to the city mean pavement albedo to the building's energy use was evaluated by modifying the weather files used in the simulations. These modified weather files incorporate air temperature changes induced by cool pavements, which in turn were obtained from the urban climate modeling activity.

The results from the building energy simulations were used to fit coefficients to physical models relating the annual site cooling, heating, and lighting energy uses of each prototype to local and city-mean pavement albedos.

To calculate citywide changes in building energy use, California's current building stock was first assessed and later mapped to the modelled building prototypes.

The coefficients of the physical model solutions and the results of the building stock assessment are later used by the pavement LCA tool to calculate the site use-phase changes

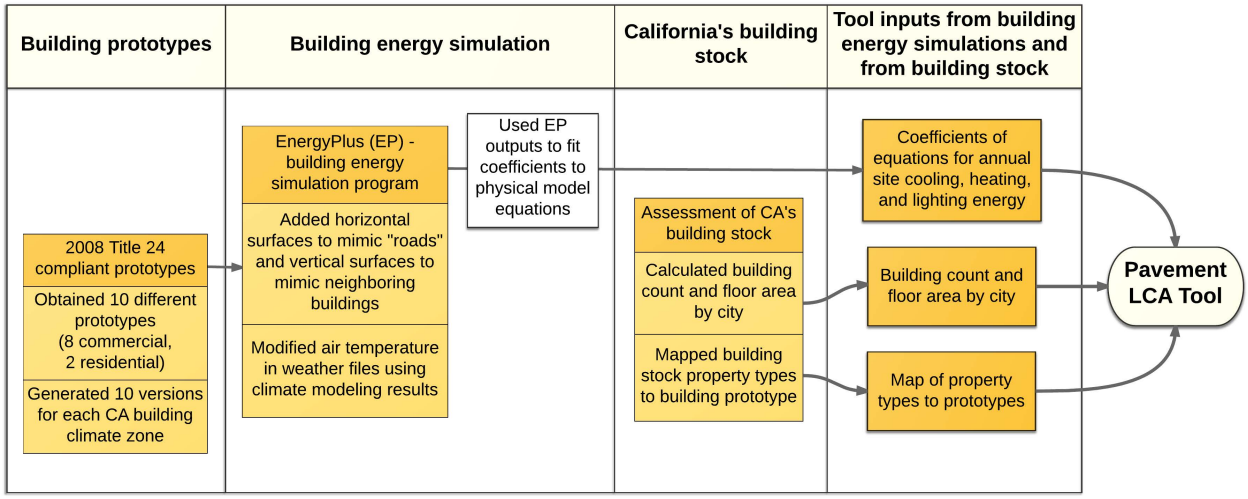

Figure 5.1: Flowchart of building energy modeling and building stock methodology.

to building energy consumption in each city. Figure 5.1 summarizes the methodology that is described in detail in this chapter.

5.2 Building prototypes

EnergyPlus [79] was employed for running the building energy simulations (see Section 5.3). To simulate a building's energy use, EnergyPlus requires the input of a building prototype, which includes details on the buildings physical construction, internal loads, and HVAC system, and thermal control schedule and setpoints. The program then calculates the heating and cooling loads necessary to maintain the thermal control settings, as well as many other details to ensure the simulation performs like an actual building.

5.2.1 Source of residential building prototypes

The United States Department of Energy's Building Energy Codes Program uses two prototypes—single-family home and multi-family apartment building—to evaluate published versions of their code and proposed code changes [75]. These two prototypes were modified to meet the California 2008 Title 24 residential building energy efficiency standards [80], creating one version of each prototype for each of California's 16 building climate zones, BCZ (Figure 5.2). The building properties modified to meet the Title 24 standards include

- thermal resistances of wall and ceiling;

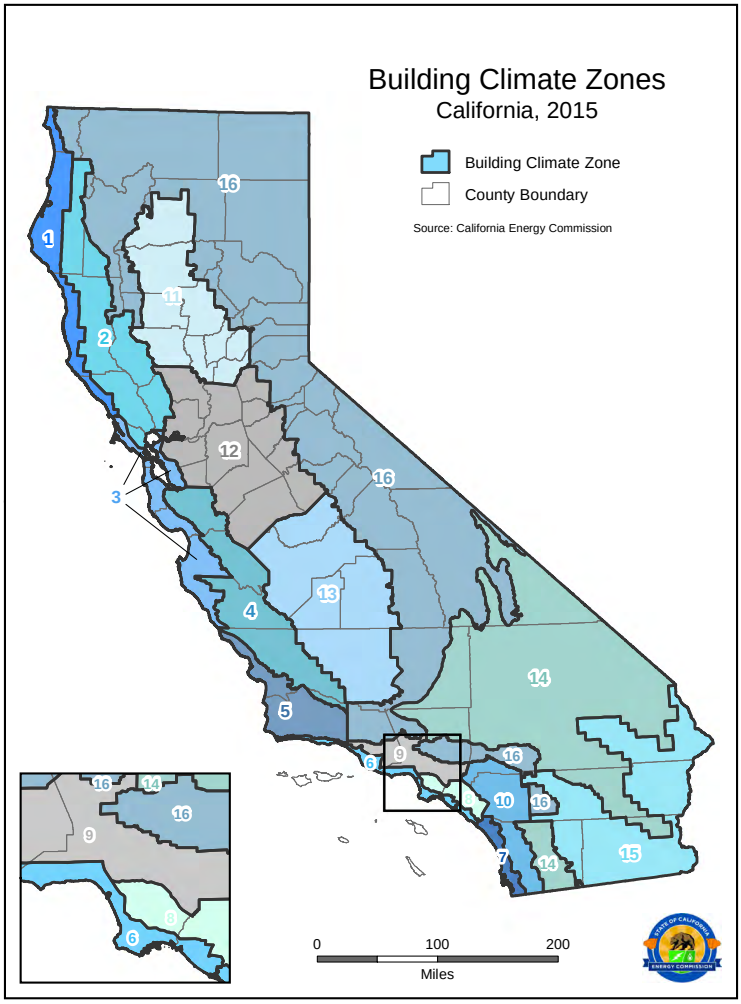

Figure 5.2: Map of California building climate zones [81].

- thermal transmittance (U-factor), solar heat gain coefficient (SHGC), and visible transmittance of windows;
- cooling efficiency (seasonal energy efficiency ratio, SEER) and heating efficiency (annual fuel utilization efficiency, AFUE); and
- HVAC schedule (hours and setpoints).

5.2.2 Source of commercial building prototypes

Past United States Department of Energy (DOE) efforts to assess building energy efficiency used a suite of 15 commercial building prototypes [76]. Each prototype complies with

ASHRAE 90.1-2004 (Energy Standard for Buildings Except Low-Rise Residential Buildings) and ASHRAE 62.1-2004 (Ventilation for Acceptable Indoor Air Quality), which provide standards for energy use, ventilation, and indoor air quality in U.S. commercial buildings.

The California Energy Commission (CEC) supplied eight of the 15 DOE commercial building prototypes, adapted to meet 2008 Title 24 nonresidential standards [82]. Our collection includes 16 versions of each commercial building prototype, one for each of Californias building climate zones (Figure 5.2).

5.2.3 Prototype characteristics

Prototype dimensions and construction properties are summarized in Table 5.1.

Table 5.2 lists the HVAC system(s) used in each prototype.

Table 5.1: Geometries of the prototype buildings.

Building prototype	**Floors**	**Conditioned floor area [1000 m^2]**	**Footprint area [1000 m^2]**	**Roof area [1000 m^2]**	**Wall+window area [1000 m^2]**	**Wall area [1000 m^2]**	**Window-to-wall ratio[a](%)**
Single-family home	2	0.22	0.11	0.12	0.27	0.24	14.1
Apartment building	3	2.01	0.67	0.79	0.25	1.50	16.4
Large hotel	6	11.4	1.89	1.98	5.24	4.03	30.2
Large office	13	46.3	3.56	3.56	16.2	11.6	40.0
Medium office	3	4.98	1.66	1.66	2.63	1.98	33.0
Primary school	1	6.87	6.80	6.87	3.39	2.51	35.0
Fast-food restaurant	1	0.23	0.23	0.26	0.21	0.19	14.0
Retail stand-alone	1	2.29	2.29	2.29	1.26	1.18	7.1
Strip mall retail	1	2.09	2.09	2.09	1.31	1.18	10.5
Sit-down restaurant	1	0.51	0.51	0.57	0.32	0.28	17.1

[a] In calculating the window-to-wall ratio, the denominator (wall area) omits window area.

Table 5.2: HVAC systems of the prototype buildings.

Building prototype	**Cooling**	**Heating**	**Air distribution**
Single-family home	DX unitary system	Gas heating coil	Single zone constant air volume (SZ CAV)
Apartment building	DX unitary system	Gas heating coil	CAV
Large hotel	Chiller (2) air cooled	Boiler	FCU (fan coil unit) and VAV (variable air volume)
Large office	Chiller (2) water cooled	Boiler	MZ (multizone) VAV
Medium office	Precision air conditioning unit (PACU)	Electrical resistance and furnace	MZ VAV
Primary school	PACU	Boiler	CAV
Fast-food restaurant	PACU	Furnace	SZ CAV
Retail stand-alone	PACU	Furnace	SZ CAV
Strip mall retail	PACU	Furnace	SZ CAV
Sit-down restaurant	PACU	Furnace	SZ CAV

5.2.4 Adding external surfaces to the prototypes

5.2.4.1 Neighboring buildings

EnergyPlus has a feature, called *external shading surfaces*, to calculate the solar radiation that is reflected from exterior surfaces (e.g. neighboring buildings) and then strikes the building. The feature also simulates the shadow from the exterior surfaces.

Vertical external shading surfaces were added to each prototype to represent neighboring buildings.

The distances from the building to the added vertical shading surfaces follow design guidelines specified in the Zoning Code of Sacramento County, or ZCSC [78]. These guidelines specify the widths of the side yards around a building, which depend on building type. The distance from each building prototype to the added vertical shading surfaces (or "neighboring buildings") was determined from the side yard widths. Assuming the neighboring structure has a use similar to that of the modeled building, the distance between a building and its neighbor is twice the side yard.

Table 5.3 summarizes the distance between each prototype building and its vertical shading surfaces.

Table 5.3: Side and front yard distances from the building prototypes.

Building prototype	**Building type category in Sacramentos zoning code**	**Distance between neighboring buildings [m]**	**Front yard [m]**
Single-family home	Single-family	3	6
Apartment building	Multiple-family dwellings	12.2	7.6
Large hotel	Commercial, business, or professional use	15.2	15.3
Large office	Business and professional uses in residential zones	12.2	7.6
Medium office	Business and professional uses in residential zones	12.2	7.6
Primary school	Institutional use	3.7	7.6
Fast-food restaurant	Commercial, business, or professional use	15.2	15.3
Retail stand-alone	Commercial, business, or professional use	15.2	15.3
Strip mall retail	Commercial, business, or professional use	15.2	15.3
Sit-down restaurant	Commercial, business, or professional use	15.2	15.3

5.2.4.2 Representing local roads

EnergyPlus treats the entire ground around the modeled building as one homogeneous surface. The software is not capable of segmenting the ground into different surface types (e.g. road and sidewalk). Hence, to isolate the effect of roads on the building energy use,

external shading surfaces were placed horizontally around the buildings to represent the local "roads". They were placed at a distance from the building that complies with street design standards.

The front yard is the distance from the building to the street's right-of-way. The right-of-way includes the road, road verge (also known as a planting strip, sidewalk buffer, or utility strip, among other names), and sidewalk. The front setback distance is the sum of widths of the front yard, road verge, and sidewalk. The front setback width equals the distance from the building to the road. The widths of the front yards were obtained from the ZCSC, while the widths of the sidewalk and the road verge were obtained from the Street Design Standards for the City of Sacramento [77]. Table 5.4 summarizes these distances for all building prototypes.

In the city of Sacramento (35^{th} largest US city by population) [83], a standard city block is 120 m × 120 m (14,400 m^2). In other major US cities like Manhattan, NY (1st), Houston, TX (4^{th}), and Portland, OR (24^{th}) the average city block size ranges from 6,000 m^2 to 22,000 m^2 [84]. Since the size of city blocks vary widely in the country, Sacramento's standard city block area (14,000 m^2) was used to represent the size of city blocks in California. Unless a building occupies an entire city block, the building is expect to face a road on one or two sides. The footprint area of each building prototype was compared to the size of a typical city block to estimate the number of the building sides facing a public road. Table 5.4 lists the number of sides (out of four) each building prototype was modified with public "roads".

The roads added to the prototypes varied in width according to street design standards used in various cities in California. Each building prototype was mapped to a street type based on building use and building size. After reviewing lane configuration and dimension standards for different street types in Sacramento [77], Los Angeles [85], and San Jose [86], very little difference was observed among them. Hence, the street design standards of Sacramento were selected as they are closest to the average of the three cities. Table 5.5 details the dimensions and lane configurations of each street type used in each prototype.

Appendix C illustrates the 10 modified building prototypes, including the shading surfaces that represent neighboring walls and roads.

5.2.4.3 Effect of trees

Trees may have a significant effect on the cooling and heating load of a building [87, 88]. The presence of trees near buildings can reduce the solar flux reflected to walls and windows from pavements, thus changing the direct effect of cool pavements. However, this study does not include the effect of trees.

Table 5.4: Distances from building to road and number of sides facing a road, for each prototype building.

Building prototype	Street type	Front yard [m]	Sidewalk and planter [m]	Building to road distance [m]	Building sides facing road
Single-family home	Residential	6.1	3.5	9.6	1
Apartment building	Residential	7.6	3.5	11.1	1
Large hotel	Boulevard, Commercial	15.2	4.4	19.7, 11.1	2
Large office	Boulevard, Commercial	7.6	4.4	12.0, 11.1	2
Medium office	Commercial	7.6	3.5	11.1	1
Primary school	Residential	7.6	3.5	11.1	3
Fast-food restaurant	Commercial	15.2	3.5	18.7	1
Retail stand-alone	Boulevard	15.2	4.4	64.5	1
Strip mall retail	Boulevard, Commercial	15.2	4.4	64.5, 18.7	2
Sit-down restaurant	Commercial	15.2	3.5	18.7	1

Table 5.5: Road descriptions and dimensions assumed for each building prototype.

Building prototype	Street type	Parking lane width [m]	Bike lane width [m]	Travel lane width [m]	Number of travel lanes	Total road width[a][m]
Single-family home	Residential	0	0	4.6	2	9.1
Apartment building	Residential	0	0	4.6	2	9.1
Large hotel	Boulevard, Commercial	2.1	1.8	3.5	4	22.0, 11.0
Large office	Boulevard, Commercial	2.1	1.8	3.5	4	22.0, 11.0
Medium office	Commercial	2.1	0	3.4	2	11
Primary school	Residential	0	0	4.6	2	9.1
Fast-food restaurant	Commercial	2.1	0	3.4	2	11
Retail stand-alone	Boulevard	2.1	1.8	3.5	4	22
Strip mall retail	Boulevard, Commercial	2.1	1.8	3.5	4	22.0, 11.0
Sit-down restaurant	Commercial	2.1	0	3.4	2	11

[a] Some prototypes were modified with roads of different width. In pairs of values, the first is the width of the road added south of the building. The second is the width of the road located in the west side.

5.3 Building energy simulation

5.3.1 Simulation tools

EnergyPlus [79] is a free building energy simulation program, funded by the US Department of Energy (DOE) Building Technologies Office. EnergyPlus version 8.1 was used to simulate the cooling, heating, lighting, and other building energy uses for each hour of the year. jEPlus [89], a parametric EnergyPlus simulation manager, helped simplify the process of simulating each model with six different road albedos (0.10, 0.15, 0.20, 0.30, 0.40, and 0.50). The study required simulating 300 models (see Section 5.4.2). A Python script was written to automatically run jEPlus on all models.

5.3.2 Original weather files

An EnergyPlus simulation requires a weather file that represents the climate in the location specified in the EnergyPlus prototype. The most recent California weather files developed by White Box Technologies, WBT [90] were used. These were released in February 2015, and characterize weather records spanning 1998 to 2009. WBT developed these 85 weather files, collectively called CZ2010, for Title 24 compliance simulations, and provides the CZ2010 weather files in epw file format, which is the format required by EnergyPlus. (Before the CZ2010 files were released, energy simulations for prototypes in CA used 'CTZ2' weather files, one per building climate zone (BCZ), characterizing weather records from the 1950s to the 1980s.)

A CZ2010 weather file consists of hourly values over a period of a "typical year". This typical year is an artificial weather year reflecting average conditions between 1998 and 2009. Each month in the weather file consists of actual weather data collected from the weather station and it represents the most typical weather of that month among the 12-year span.

One weather file from the CZ2010 set was chosen per BCZ, selecting the same weather stations used to generate CTZ2.

5.3.3 Modified weather files

Researchers from University of Southern California (USC) were one of the teams that collaborated in this Pavement Life Cycle Assessment Decision Tool project. The USC team simulated the local urban climate and air quality in cities throughout California, and investigated the influence of wide spread adoption of cool pavements using three scenarios, each with a different city mean pavement albedo. The control scenario assumes a baseline pavement albedo of 0.10. The small perturbation scenario assumed cool pavements with albedo 0.20 were deployed in all urban grid cells in California. The large perturbation scenario assumed deployment of cool pavements with albedo 0.50.

These climate modeling results were incorporated into the building energy simulations through the weather files. The control scenario uses the original CZ2010 weather files. To represent the small and large perturbation scenarios, two modified versions of the original weather files were generated. The new versions reflect the hourly urban air temperature differences that results from citywide deployment of cool pavements obtained from the climate modeling.

5.3.3.1 Results from climate modeling

Results provided from the USC team included seasonal hourly values of mean air temperature difference ΔT. The climate modeling team calculated ΔT in each hour of the year by subtracting the air temperature in the control scenario (pavement albedo 0.10) from the air temperature in the large perturbation scenario (pavement albedo 0.50). The seasonal hourly values are obtained by averaging each hour of the day over every day of the season; the seasons are defined as summer (Jun, Jul, Aug), fall (Sep, Oct, Nov), winter (Jan, Feb, Dec), and spring (Mar, Apr, May). The accuracy of the urban climate modeling is greater in large, high density (high impervious surface fraction) urban areas. These urban areas are also more sensitive to the climate effect of cool pavements. Hence, the USC team provided ΔT values for only 9 urban areas of California, each representing a different BCZ. The BCZs included are 4, 7, 8, 9, 10, 12, 13, 14, and 15. Table 5.6 lists some of the major cities in these BCZs.

The climate modeling also generated ΔT values that correspond to the small perturbation scenario minus the control scenario. Since these temperature differences were comparable to noise in the climate model, ΔT in the small perturbation scenario was instead calculated by scaling the high perturbation scenario by the ratio of pavement albedo changes, $0.10/0.40 = 0.25$.

Table 5.6: California's major cities in the represented building climate zones (BCZs).

Representative cities	**BCZ**
San Jose	4
San Diego	7
Irvine, Anaheim, Santa Ana, Garden Grove	8
Los Angeles	9
Riverside	10
Sacramento	12
Fresno	13
Lancaster	14
Palm Springs	15

5.3.3.2 Urban canyon geometry used in the climate model

The climate modeling was performed using an urban canyon geometry characteristic of medium-intensity urban areas as defined in the National Land Cover Dataset, or NLCD [74].

This canyon geometry has a road width of 9.4 m that extends from wall to wall, with no setback between wall and road. The geometry has a wall height of 7.5 m. The canyons length (dimension along the long axis of the road) is treated as infinite. These dimensions were used to represent every urban grid cell in the climate modeling. The dimensions of this NLCD canyon geometry are summarized in Table 5.7.

In reality, roads do not extend from wall to wall in an urban canyon. The road and wall are separated by a setback, which can include a front yard, sidewalk, and/or road verge, as described in Section 5.2.4. The roads are also typically wider than 9.4 m. Hence, this NLCD canyon geometry (9.4 m wide road, 7.5 m high walls, no setbacks) will be referred to as the *narrow* canyon.

Another key disparity between the NLCD canyon geometry and the urban geometry of actual cities is the height of the canyon walls, which depends on the type of buildings forming the canyon. While a canyon wall height of 7.5 m is usually a good approximation of a two-level building, a city is composed of buildings that vary widely in height.

Table 5.7: Urban canyon dimensions used in the climate modeling. These dimensions are specified in the National Land Cover Dataset.

Canyon	**Setback width [m]**	**Road width [m]**	**Canyon width [m]**	**Wall height [m]**
narrow (NLCD) canyon	0	9.4	9.4	7.5

5.3.3.3 Defining new canyon geometries

A new canyon geometry for each of the 10 building prototypes was created to better represent a city's morphology. Each canyon was defined using the road and setback widths used when adding "roads" to the building prototypes (Section 5.2.4). Figure 5.3 shows a general geometry of these urban canyons, and Table 5.8 defines the dimensions of the 10 canyons.

These canyons (hereafter, *wide* canyons) are wider than the narrow canyon because their canyon floors include wide roads and setbacks.

5.3.3.4 Adjusting ΔT obtained from climate modeling

The amount of sunlight that enters and subsequently escapes the canyon depends on the canyon's location, which affects climate and hourly solar position, and the canyon's geometry, which determines how much of the sunlight entering the canyon reaches the floor. This means that canyon albedo (ratio of sunlight leaving the canyon to sunlight entering the canyon) will differ between a narrow canyon and a wide canyon. Therefore, the air temperature differences

Table 5.8: Dimensions for canyons defined from modeled building prototypes and roads.

Canyon	Setback width [m]	Road width [m]	Canyon width [m]	Wall height [m]
Single-family home	6.1	9.1	21.3	5.2
Apartment building	7.6	9.1	24.3	7.8
Large hotel	15.2	22	52.4	21.6
Large office	7.6	22	37.2	37.5
Medium office	7.6	11	26.2	11.9
Primary school	7.6	9.1	24.3	4
Fast-food restaurant	15.2	11	41.4	3.1
Retail stand-alone	15.2	22	52.4	6.1
Strip mall retail	15.2	22	52.4	5.2
Sit-down restaurant	15.2	11	41.4	3.1

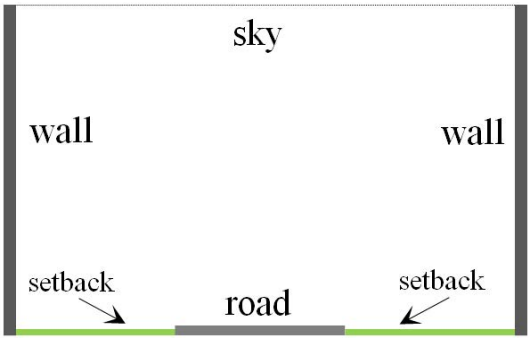

Figure 5.3: Urban canyon geometry.

ΔT predicted by the climate modeling applies only to cities populated with narrow canyons, and must be scaled to describe air temperature changes from wide canyons.

Chapter 4 presented a model to calculate canyon albedo as a function of canyon geometry and location. It also introduced a method to scale air temperature changes obtained from simulations that used one canyon geometry to temperature changes that would be obtained with a different canyon geometry. This new method was used to calculate the scaling factors $\sigma_{n\to w}$ (see section 4.2.6.2) for going from the NLCD narrow canyon to each of the 10 wide canyons.

In California, the building stock is approximately 80% residential and 20% commercial (Table 5.9). The 10 building prototypes were used to represent this building stock distribution by assigning 60% to single-family home, 20% to apartment building, and 20% as the mean of all commercial prototypes. As mentioned before, the wide canyons have geometries that resemble canyons that would be formed by the 10 modified building prototypes.

The assigned building stock distribution and the scaling factor ($\sigma_{n\to w}$) of each wide canyon were used to calculate a weighted citywide scaling factor, $\sigma_{n\to\bar{w}}$, which describes the

factor to adjust from a city composed of only the narrow canyon to a city composed of the wide canyons.

Since the albedo of the canyon varies by location, the citywide scaling factor was calculated for each of the BCZs represented by the climate modeling. Table 5.10 lists $\sigma_{n\to\bar{w}}$ by BCZ and season. Note that $\sigma_{\bar{w}}$, the average value of $\sigma_{n\to\bar{w}}$ over the 9 BCZs, rounds to 2.85 in summer, fall, and spring, and to 2.66 in winter.

The corrected air temperature difference of a city $\Delta T_{\bar{w}}$ can now be estimated as

$$\Delta T_{\bar{w}} = \sigma_{n\to\bar{w}} \cdot \Delta T_n. \tag{5.1}$$

In this way, new values of $T_{\bar{w}}$ for the 9 BCZs were estimated from the ΔT_n provided by the project collaborators from USC.

Table 5.9: Comparing Assessor's Office building floor areas for California with 2009 Residential Energy Consumption Survey (RECS) and 2006 Commercial End-Use Survey (CEUS).

Source	**Category**	**Floor area [km^2]**	**Fraction [%]**
Assessor's Office	Residential	1659	78
	Commercial	469	22
	Total	2128	100
RECS 2009 and CEUS 2006	Residential (RECS)	1844	80
	Commercial (CEUS)	457	20
	Total	2301	100

Table 5.10: Scaling factors $\sigma_{n\to\bar{w}}$ from city composed of narrow canyon to city composed of the wide canyons.

Season	**Scaling factors, $\sigma_{n\to\bar{w}}$, by building climate zone**											
	4	**7**	**8**	**9**	**10**	**12**	**13**	**14**	**15**	**Min**	**Max**	**Mean**
Fall	2.84	2.84	2.85	2.84	2.83	2.83	2.83	2.79	2.82	2.79	2.85	2.83
Winter	2.59	2.66	2.70	2.66	2.63	2.69	2.76	2.60	2.62	2.59	2.76	2.66
Spring	2.84	2.84	2.86	2.84	2.83	2.85	2.84	2.82	2.82	2.82	2.86	2.84
Summer	2.87	2.87	2.89	2.88	2.87	2.86	2.86	2.84	2.85	2.84	2.89	2.87

5.3.3.5 Create modified weather files with adjusted ΔTs

The two modified versions of the weather files were created using the new $\Delta T_{\bar{w}}$ to modify their dry-bulb air temperature. Each weather file consists of hourly values over the period of a "typical year" (see Section 5.3.2). The ΔT_n values obtained for a particular climate zone consists of hourly ΔT_n values to describe one representative day of a season. Hence, for each climate zone, there are 96 ΔT_n values (24 hours in a day $\times$ 4 seasons).

When modifying the dry-bulb air temperature in the weather files, the same 24 hourly ΔT_n values of a representative seasonal day were applied to every day of the season. In the end, the collection of weather files consisted of

- Original weather files – used in building energy simulations to represent the control scenario;
- Modified weather files, small perturbation – used to represent the small perturbation scenario ($\Delta\rho_p = 0.10$); and
- Modified weather files, large perturbation – used to represent the large perturbation scenario ($\Delta\rho_p = 0.40$).

5.4 Physical model

5.4.1 Physical model equations

Before continuing with the physical model, it is important to distinguish between two terminologies used here concerning pavements. The *local road* refers to the pavement adjacent to any specific building being analyzed. This local road is the one described in Section 5.2.4.2. The second is the *city pavement*, which refers to the entire pavement system of a city.

A physical model is proposed to describe the effects of modifying local road albedo and city pavement albedo on the cooling, heating, and lighting energy uses of a building. This model considers two different effects of cool pavements on a buildings energy use. The first, or "direct", effect is the result from modifying the local road albedo, ρ_r, meaning that of the road (or roads) adjacent to the building. Raising local road albedo increases the solar flux incident on walls and windows, which can increase the cooling load and decrease the heating load. The second, or "indirect" effect happens when increasing the city-mean pavement albedo, ρ_p, reduces the convective heating of the city air. This lowers the city air temperature and changes the air temperature difference across the building envelope. The indirect effect is expected to reduce cooling loads and increase heating loads.

Cooling energy includes both the energy used to chill air and the ventilation energy used to distribute chilled air. Increasing the local road albedo raises the solar flux incident on the walls and windows, which increases the cooling load. Assuming the change in the site cooling energy use scales linearly with the change in local road albedo, it can be expressed as

$$\frac{\partial E_C}{\partial \rho_r} = a_1. \tag{5.2}$$

Increasing the city-mean pavement albedo lowers the city air temperature by reducing convective heating of the air. Cooler air decreases the cooling load. Assuming the change in the site cooling energy use scales linearly with the change in city-mean pavement albedo, it can be expressed as

$$\frac{\partial E_C}{\partial \rho_p} = a_2. \tag{5.3}$$

Solving the partial differential equations 5.2 and 5.3 yields the linear equation

$$E_C = a_0 + a_1 \cdot \rho_r + a_2 \cdot \rho_p. \tag{5.4}$$

The coefficients a_0, a_1, and a_2 are assumed constants specific to building and location.

Heating energy includes both the energy used to warm air, and the ventilation energy used to distribute warmed air. The prototypes used in this study are heated with natural gas, electricity, or both. *Gas heating* energy includes only gas used to warm air, while *electric heating* energy includes both electricity used to warm air, and electricity used to distribute air that was warmed with either natural gas or electricity.

An increase in the incident solar flux on walls and windows from more reflective local roads can also decrease the heating load. The change in the site gas heating energy use (G_H) is assumed to scale linearly with the change in ρ_r and can be expressed as

$$\frac{\partial G_H}{\partial \rho_r} = b_1. \tag{5.5}$$

Cooler air from the "indirect" effect of cool pavements can also increase the heating load. The change in the site gas heating energy use (G_H) is assumed to scale linearly with the change in ρ_p and can be expressed as

$$\frac{\partial G_H}{\partial \rho_p} = b_2. \tag{5.6}$$

Solving the partial differential equations 5.5 and 5.6 yields the linear equation

$$G_H = b_0 + b_1 \cdot \rho_r + b_2 \cdot \rho_p. \tag{5.7}$$

Similarly, a derived linear equation for the site electric heating energy use is:

$$E_H = c_0 + c_1 \cdot \rho_r + c_2 \cdot \rho_p. \tag{5.8}$$

The coefficients b_0, b_1, b_2, c_0, c_1, and c_2 are assumed constants specific to building and location.

Increasing the local road albedo increases the solar flux that is reflected from the road and enters through the windows. This rise in sunlight entering through the windows may decrease the need for artificial lighting. Assuming the change in the site lighting energy use (E_L) scales linearly with the change in ρ_r, it can be expressed as

$$\frac{\partial E_L}{\partial \rho_r} = d_1. \tag{5.9}$$

The indirect effect of cool pavements will have no effect on lighting energy use. Hence, simply by solving equation 5.9, yields the linear equation

$$E_L = d_0 + d_1 \cdot \rho_r. \tag{5.10}$$

As it was assumed for the previous coefficients, d_0 and d_1 are treated as constants specific to building and climate.

5.4.2 Validate physical model equations with the EnergyPlus simulations

A multivariate linear regression analysis was applied to the EnergyPlus simulations to test the energy equations derived from the physical model and estimate their coefficients. The simulations returned hourly values of energy use for the various HVAC system components over a period of a year.

One of the fields from the simulation outputs is the electric cooling energy use. Depending on the prototype, this output of electric cooling energy could refer to any or a combination of chiller, precision air conditioning unit (PACU), or direct exchange (DX) unitary system.

Another field is the gas heating energy use, which refers only to the gas used to heat the conditioned space. Depending on the prototype, the gas heating may involve a boiler or furnace. With the exception of the medium office, all prototypes used gas as their main source for heating. Although the medium office used a small amount of gas for heating, it mainly used electric heating coils. The simulation output also provided a field for electric heating energy use.

Another output field is the ventilation energy use. The ventilation system distributed air for both cooling and heating. The ventilation energy had to be separated into that used to distribute cooled air and that used to distribute heated air. In some prototypes (single-family home, sit-down restaurant, and strip mall retail), the cooling and heating system

never ran simultaneously. Hence, it was easy to separate the cooling and heating ventilation energiesduring the hours when the building was being cooled, ventilation energy was assigned to cooling; while heating, ventilation energy is assigned to heating.

In the other seven prototypes, the cooling and heating system sometimes ran simultaneously. When this happened, the amount of ventilation energy allotted to cooling and heating depended on the fractions of HVAC heat transfer associated with each application. Simply as an illustration, assume that at a given hour in the medium office prototype, the cooling coils remove 1 MJ of heat while the heating coils add 3 MJ of heat. The cooling fraction is 0.25 [1 MJ / (1 MJ + 3 MJ)]; hence, in that hour, 25% of the ventilation energy is assigned to electric cooling and 75% is assigned to electric heating.

Two other output fields of EnergyPlus are the hourly indoor and outdoor lighting energy uses. Only the indoor lighting energy was used in this study.

The annual site cooling energy use is the sum of the annual electric energy consumed by the cooling system plus the annual ventilation energy allotted to cooling. The annual site gas heating energy use includes gas heating energy, but no ventilation energy. In the case of the medium office, the annual site electric heating is the sum of the electricity used to warm the air and the ventilation energy allotted to heating. For every other prototype, the annual electric heating energy use is equal to the ventilation energy for heating.

The annual site energy uses were analyzed to find coefficients for the cooling, heating, and lighting site energy use equations proposed in the physical model. This was done for each of the building prototypes and for the different building climate zones. Each prototype was simulated for six different local road albedos (0.10, 0.15, 0.20, 0.30, 0.40, and 0.50). To model the indirect effect of cool pavements, these simulations were executed three times using the three versions of each location's weather file. The total number of simulations was 1,620 (10 building prototypes $\times$ 9 building climate zones $\times$ 6 local road albedo $\times$ 3 weather file versions).

5.5 Building-to-road view factors

Assuming an unobstructed view from wall to road (no trees), the view factors from the building prototype to the roads were calculated using common geometric configurations. The view factor (a.k.a. configuration factor or shape factor) from surface A to surface B ($F_{A \to B}$) is the fraction of radiant energy leaving surface A that is intercepted by surface B. View factors depend only on geometry. As such, view factors have been published in the engineering literature for common geometric configurations, many of which are readily available in John Howell's online catalog of configuration factors [72].

Each road-facing wall of a building was treated as a rectangular surface of height H_w and length L_w, with a setback to the road of width W_s. The road is treated as an infinitely

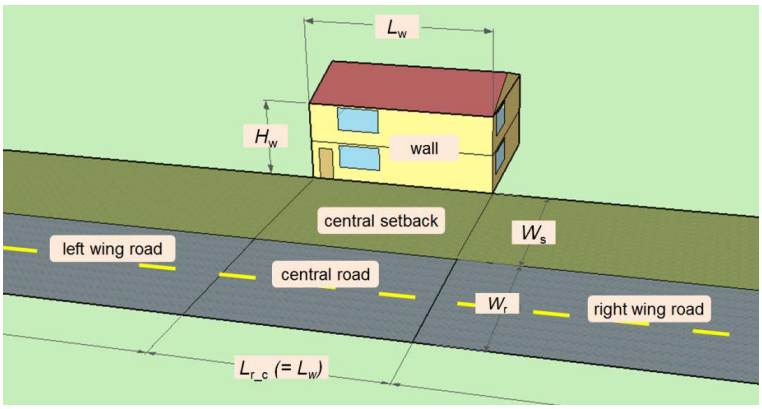

Figure 5.4: Diagram of single-family home with setback and road.

long rectangle of width W_r. Figure 5.4 illustrates the dimensions of the single-family home, setback, and road.

Calculations of the wall-to-road view factor $F_{w\to r}$ were done using two standard radiation configurations. One configuration was used to find the view factor from the wall to the portion of the road directly in front of the wall (hereafter, central road). The second configuration was employed to calculate the view factor from the wall to the left and right wings of the road. See Figure 5.4 for a diagram of the wall, setback, and road sections used for the view factor calculations.

The first configuration [91] is used for two finite rectangles of same length, having one common edge, and at an angle of 90° of each other. Hence, the view factor from the wall to the central road portion ($F_{w\to r_c}$) was obtained by subtracting the view factor to the central setback ($F_{w\to s_c}$) from the view factor to the central setback + road ($F_{w\to(s+r)_c}$):

$$F_{w\to r_c} = F_{w\to(s+r)_c} - F_{w\to s_c}. \tag{5.11}$$

The second configuration [92] is commonly used for a rectangle to a rectangle in a perpendicular plane, with all boundaries being parallel or perpendicular. Thus this configuration helped obtain the view factors from the wall to the left ($F_{w\to r_l}$) and right ($F_{w\to r_r}$) wings of the road. The total wall-to-road view factor ($F_{w\to r}$) was obtained as

$$F_{w\to r} = F_{w\to r_c} + F_{w\to r_l} + F_{w\to r_r}. \tag{5.12}$$

As explained in Section 5.2.4, the modified prototypes do not have roads on all four sides of the building. Using the number of building sides (N) facing a road (Table 5.4) the estimated overall building-to-road view factor $F_{b\to r}$ is

$$F_{b\to r} = F_{w\to r} \times \frac{N}{4}. \tag{5.13}$$

Table 5.11 lists the view factors from the wall to setback, setback + road, and road. These were calculated using the setback distances (Table 5.4) and the widths of the roads (Table 5.5) assigned to each prototype.

Table 5.11: View factors by building prototype.

Prototype	**Wall to setback** ($F_{w\to s}$)	**Wall to (setback + road)** ($F_{w\to(s+r)}$)	**Wall to road** ($F_{w\to r}$)	**Building to road** ($F_{b\to r}$)
Single-family home	0.373	0.326	0.057	0.014
Apartment building	0.342	0.358	0.064	0.016
Large office	0.277	0.212	0.137	0.069
Medium office	0.133	0.330	0.090	0.023
Fast-food restaurant	0.413	0.398	0.014	0.004
Sit-down restaurant	0.434	0.42	0.013	0.003
Retail stand-alone	0.458	0.422	0.038	0.010
Retail strip mall	0.422	0.442	0.034	0.017
Primary school	0.282	0.438	0.037	0.028
Large hotel	0.277	0.356	0.079	0.040

5.6 Assessment of California's building stock

The results from the modeled prototypes help understand the effect that cool pavements have on the energy use in a single building. But to understand the building energy use effect of cool pavements in a city, it is important to know the building stock in that location. In each county, the Assessor's office is responsible for the discovery and assessment of all the properties within their jurisdiction. The entire state's building stock was evaluated using a statewide collection of property records from the Assessor's offices.

5.6.1 Obtaining source data

California Air Resources Board (ARB) acquired the public records of commercial and residential properties in the state from each County Assessor's office in California. ARB provided the records for this study, which were used to assess the state's building stock. The entire collection includes property data entries up to 2013. Each record provides useful information for each of the properties, including the location (county, city, and ZIP code), floor area, property type (e.g., single-family home, office building), and age. The number of records obtained were 12,552,241.

5.6.2 Cleaning data

The Assessor's Office in each county locates and assesses all taxable properties in their jurisdiction. In many cases, the property information is collected and recorded manually.

This often leads to misspelled information, including the city's name. To correct the inconsistency in city names, the Zip Code Database [93] was used to pair the zip codes reported in the property records to the corresponding city and then renamed the misspelled city names.

5.6.3 Calculating building count, floor area, and age

To estimate the citywide impact of cool pavements, it is necessary to understand the building stock in the city of interest, such as the size, floor area, and age distributions by property type and location. The building stock data collection provides sufficient information to do this sort of analysis.

The building stock was first grouped by county and later by city and property type. The data contains information for all 58 counties in California, and nearly 1,500 cities and towns are represented. All properties are classified into 63 property types.

Once the records were grouped, it was possible to calculate the total floor area of each property type by city. A small fraction of the building records do not include floor area—e.g., state-wide, 12% of single-family homes do not report floor area. Hence, to calculate the total floor area of each property type in each city, the mean floor area in that city (from the subset of records that report floor area) was multiplied by the number of buildings to obtain the total floor area. The statewide mean floor area of a particular property type was assigned as the floor area for all the records of the same type that did not report the floor area.

The building stock collection also classifies all properties into six general categories (residential, commercial, agricultural, vacant land, industrial, and miscellaneous). The entire building stock was grouped by category to obtain the state-wide floor areas of the residential and commercial buildings—1659 km^2 (640.5 mi^2) (78%) for residential and 469 km^2 (180 mi^2) (22%) for commercial. These values are comparable with the floor area calculated from the 2009 Residential Energy Consumption Survey (RECS) [94] for residential buildings, and from 2006 California Commercial End-Use Survey (CEUS) [95] for commercial. Table 5.9 summarizes California's floor area.

The average age of the property types relevant to this study are summarized in Appendix D.

5.6.4 Mapping property type to building prototype

A total of 63 property types are represented in the public records of the County Assessor's offices. Nearly half, including such types as vacant land and agricultural fields, are not relevant for purposes of this study. That left 32 relevant property types. Each of these remaining property types were mapped to one of the building prototypes to represent all the relevant buildings in any particular city (Table 5.12).

Table 5.12: Mapping of stock property types to building prototypes.

Building prototype	Stock property types	Building prototype	Stock property types
Single-family home	Single family residence Duplex Triplex Mobile home Trailer park Miscellaneous residential Fraternal organization	Apartment building	Multi-family dwelling (2-4 units) Multi-family res (5+ units) Quadruplex Timeshare Condominium Planned unit development (PUD) Cooperative
Large hotel	Hotel Motel Casino Hospital Convalescent home	Medium office	Store/office combo Medical building Miscellaneous commercial Nursery Veterinary Governmental
Retail stand-alone	Department store Food store Market Bowling alley	Strip mall retail	Shopping center Stores Retail outlet
Fast-food restaurant	Laundry Dry cleaning	Sit-down restaurant	Restaurant Bar Food service
Large office	Financial building Office building	Primary school	School

5.7 Methodology to assess citywide energy and environmental consequences of urban pavements

As described in Sections 1.5 and 1.6, the work presented in this chapter and Chapter 6 forms part of a larger collaboration effort that is developing the Pavement Life Cycle Assessment Decision Tool. The results from the building energy simulations and from the states building stock assessment will be used by the pavement LCA tool to compute the energy and environmental impacts of urban pavements during their use phase. This section presents a method that uses a user-defined city of interest, the fraction of urban pavement being modified, and the albedo of the new pavement to compute the citywide impacts on two life-cycle indicators – global warming potential (GWP) and Smog Potential – and a life-cycle flow—Primary Energy Demand (PED).

5.7.1 Site energy use

The physical model equations solved in Section 5.4 are used to calculate a prototype's annual site energy use as a function of local road albedo ρ_r and city-mean pavement albedo ρ_p. Let $e_{i,j}(\rho_r,\ \rho_p)$ [kWh/m^2·y] and $g_{i,j}(\rho_r,\ \rho_p)$ [therm/m^2·y] be the city-specific annual electric and gas energy equations coefficients (Section 5.4.2) normalized by conditioned floor area for prototype i and for energy function j (cooling, heating, or lighting).

These equations can then be employed to calculate the direct, indirect, and combined (direct + indirect) effect of cool pavements to the site energy uses of a city's building stock. In these calculations, it is assumed that: a) the modified pavement is distributed evenly across the city which causes the city to experience a uniform air temperature change; and b) the fraction f of the city's building stock that "sees" the modified pavement is the same fraction of the city's pavement that has been modified.

5.7.1.1 City-mean surface albedo

Let $\rho_{r,modified}$ represent the local road albedo for the fraction f of city buildings that "see" the modified road; and $\rho_{r,original}$ represent the local road albedo for the $1-f$ portion of the buildings in the city that do not see a modified road. The city-mean local road albedo $\rho_{r,m}$ is calculated as

$$\rho_{r,m} = f \cdot \rho_{r,modified} + (1-f) \cdot \rho_{r,original}. \tag{5.14}$$

Similarly, let $\rho_{p,modified}$ represent the albedo for the fraction f of the city's pavement that has been modified; and $\rho_{p,original}$ the albedo of the unmodified pavement. The city-mean pavement albedo $\rho_{p,m}$ is calculated as

$$\rho_{p,m} = f \cdot \rho_{p,modified} + (1-f) \cdot \rho_{p,original}. \tag{5.15}$$

5.7.1.2 Citywide energy effects

If A_i is the total floor area of the buildings in a city mapped to prototype i, the city's site electric [kWh/y] and gas [therm/y] use for function j can be calculated for a period of Y years as

$$E_j = Y \times \sum_i A_i \cdot e_{i,j}(\rho_{r,m}, \rho_{p,m}) \tag{5.16}$$

and

$$G_j = Y \times \sum_i A_i \cdot g_{i,j}(\rho_{r,m}, \rho_{p,m}). \tag{5.17}$$

Let ρ_0 be the original albedo of local road and city pavements and ρ_1 the modified albedo of local roads and city pavements. Eqs 5.16 and 5.17 can be used to assess the different citywide energy effects by applying ρ_0 and ρ_1 following Table 5.13.

Table 5.13: Albedo assignments for equations 1 and 2 to calculate the different effects.

Effect	$\rho_{r,modified}$	$\rho_{p,modified}$	$\rho_{r,original}$	$\rho_{p,original}$
Direct	ρ_1	ρ_0	ρ_0	ρ_0
Indirect	ρ_0	ρ_1	ρ_0	ρ_0
Direct + indirect	ρ_1	ρ_1	ρ_0	ρ_0

5.7.2 LCA metrics

The team collaborators from the University of California Pavement Research Center (UCPRC) provided factors to compute life-cycle impact metrics (Global Warming Potential, Smog Potential, and Primary Energy Demand) from site energy use [96]. These factors were estimated based on CA's grid mix projections for year 2020.

Let m_e and m_g represent the factors to compute each life-cycle metric per unit site electricity and per unit site gas energy use. Using the factors in Table 5.14, the life-cycle impact on metric M of a city's building stock over Y years for function j (cooling, heating, or lighting) is

$$M_j = (E_j \cdot m_e + G_j \cdot m_g). \tag{5.18}$$

Table 5.14: Factors to compute life-cycle impact indicators and flows from site energy use.

Impact metrics	per MJ electricity (m_e)	per therm gas (m_g)
Global Warming Potential, GWP [kg CO_2e]	1.07E-01	2.41E-02
Photochemical Ozone Creation (Smog) Potential, POCP [kg O_3e]	3.53E-03	5.30E-04
Primary Energy Demand, PED [MJ]	3.49E+00	3.84E-01

5.8 Quality assurance

5.8.1 Manual inspection of prototype definitions

To make sure the prototypes were defined accurately to the Title 24 Standards and were simulating properly, a thorough inspection was conducted on the construction properties of each prototype and on the simulation output files.

5.8.2 Validate energy use results from the EnergyPlus simulations

5.8.2.1 Comparison of modeled and actual building energy use

The EnergyPlus outputs included results for annual cooling and heating energy uses. To test the validity of the model outputs, the annual cooling and heating energy uses of commercial buildings were compared with those reported in the Commercial Building Energy Consumption Survey (CBECS) [97] and Commercial End-Use Survey (CEUS) [95], and residential buildings with those reported in the Residential Energy Consumption Survey (RECS) [94].

CBECS is a national sample survey on the stock of US commercial buildings, including their energy-related building characteristics and end-use energy consumption. CBECS uses

an engineering model to estimate the amount of electricity, natural gas, and other fuels used for several end-uses, including space heating, cooling, ventilation, lighting, and others. CBECS also includes buildings that may traditionally not be considered commercial, such as schools. The latest full version currently available is CBECS 2003. The smallest level of geographic detail available in CBECS is the US Census division. Thus California is represented with the Pacific division, which includes California (75% of the Pacific division population), Alaska (1.4%), Oregon (7.7%), Washington (14%), and Hawaii (2.7%). Note that values do not sum to 100% because of rounding. The population was obtained from the US Census.

RECS is the residential analog of CBECS. The latest available version is RECS 2009. RECS data can be segregated by US state, which facilitated access to their California data.

The historical end-use consumption and age of the building stock was extracted from these two sources (CBECS and RECS). The data was then disaggregated by building type and selected only the building types that best matched our 10 building prototypes. Table 5.15 shows the mapping of CBECS and RECS building stock to the modeled prototypes.

The CEC's Commercial End-Use Survey, CEUS [95] is an energy use study of California's commercial sector. The survey captures detailed electricity and gas energy use by building type. CEUS was used as a second source to validate the modeled energy uses of the commercial prototypes. Table 5.15 shows the mapping of CEUS building stock to the modeled prototypes.

Table 5.15: Mapping of modeled prototypes to CBECS, RECS, and CEUS building stock.

Prototypes	**CBECS**	**RECS**	**CEUS**
Retail strip mall	Strip shopping	NA	Retail
Primary school	Elementary school	NA	School
Large hotel	Hotel	NA	Lodging
Large office	Professional or government office of similar floor area	NA	Large office
Medium office	Professional or government office of similar floor area	NA	Mean of small and large office
Sit-down restaurant	Restaurant	NA	Restaurant
Fast-food restaurant	Fast food	NA	Restaurant
Retail stand-alone	Retail store	NA	Retail
Apartment building	NA	Apartment in building with 2 - 4 units; Apartment in building with 5+ units	NA
Single-family home	NA	Single-family detached	NA

The cooling and heating energy intensities (annual site energy use per unit floor area, in kWh/m^2) reported by CBECS, RECS, and CEUS were compared to the intensities calculated from the building energy modeling. Since the Pacific division includes three states that experience colder climates than California throughout the year (Alaska, Washington, and Oregon), the Pacific conditioning energy use reported by CBECS may underestimate California's cooling load and overestimate its heating load.

Table 5.16 reports California's mean annual site cooling energy use intensities (energy per unit floor area, in kWh/m^2) calculated from the EnergyPlus simulations. Population varies widely across the state's climate zones. Hence, the cooling energy use intensities obtained from the simulations were weighted by climate zone population. These are compared with values reported in CBECS and RECS for new stock (CBECS period 1990-2003; RECS period 2000-2009) and all stock. The table also compares the modeled commercial buildings to CEUS.

Table 5.16: Comparing electric cooling energy intensity of modeled prototypes to CBECS, RECS and CEUS.

Building type	**California's site cooling energy intensity [kWh/m^2]**					
	EnergyPlus models weighted by BCZ population	**CBECS new stock[a]**	**RECS new stock**	**CBECS all stock**	**RECS all stock**	**CEUS all stock**
Retail strip mall	26.4	23.9	NA	24.4	NA	23.8
Primary school	18.8	40.4	NA	25.6	NA	12.6
Large hotel	21.9	7.70	NA	13.9	NA	25.9
Large office	15.7	20.8	NA	17.2	NA	38.4
Medium office	25.4	20.8	NA	17.2	NA	33.3
Sit-down restaurant	43.1	36.9	NA	25.8	NA	62.0
Fast-food restaurant	56.5	244	NA	151	NA	62.0
Retail stand-alone	22.3	12.3	NA	13.9	NA	23.8
Apartment building	6.90	NA	6.90	NA	7.60	NA
Single-family home	6.00	NA	10.1	NA	8.20	NA

[a] CBECS values describe commercial buildings from the Pacific division of the U.S. Census.

Table 5.17 reports California's mean site gas and electric heating energy use intensities. The medium office prototype is the only one that uses electricity as its main source for heating. Thus the table reports electric heating intensity for the medium office and gas heating intensity for all other prototypes.

5.8.2.2 Base energy use versus degree days

To verify the simulated HVAC systems were properly responding to the climate, their annual cooling and heating energy uses were compared to annual cooling and heating degree days. The cooling energy use is expected to increase with cooling degree days and heating energy use is expected to increase with heating degree days.

Figure 5.5 show plots of cooling source energy use intensities versus cooling degree days at 18°C (CDD18C). The 10 prototypes were paired by the use of the building–retail, residential, restaurant, office, and others (hotel and school). Note that in each plot, both curves follow the same trend and increase with CDD18C. In each pair of prototypes, the curves have similar slopes, but the difference in magnitudes is due to differences in plug loads and internal loads.

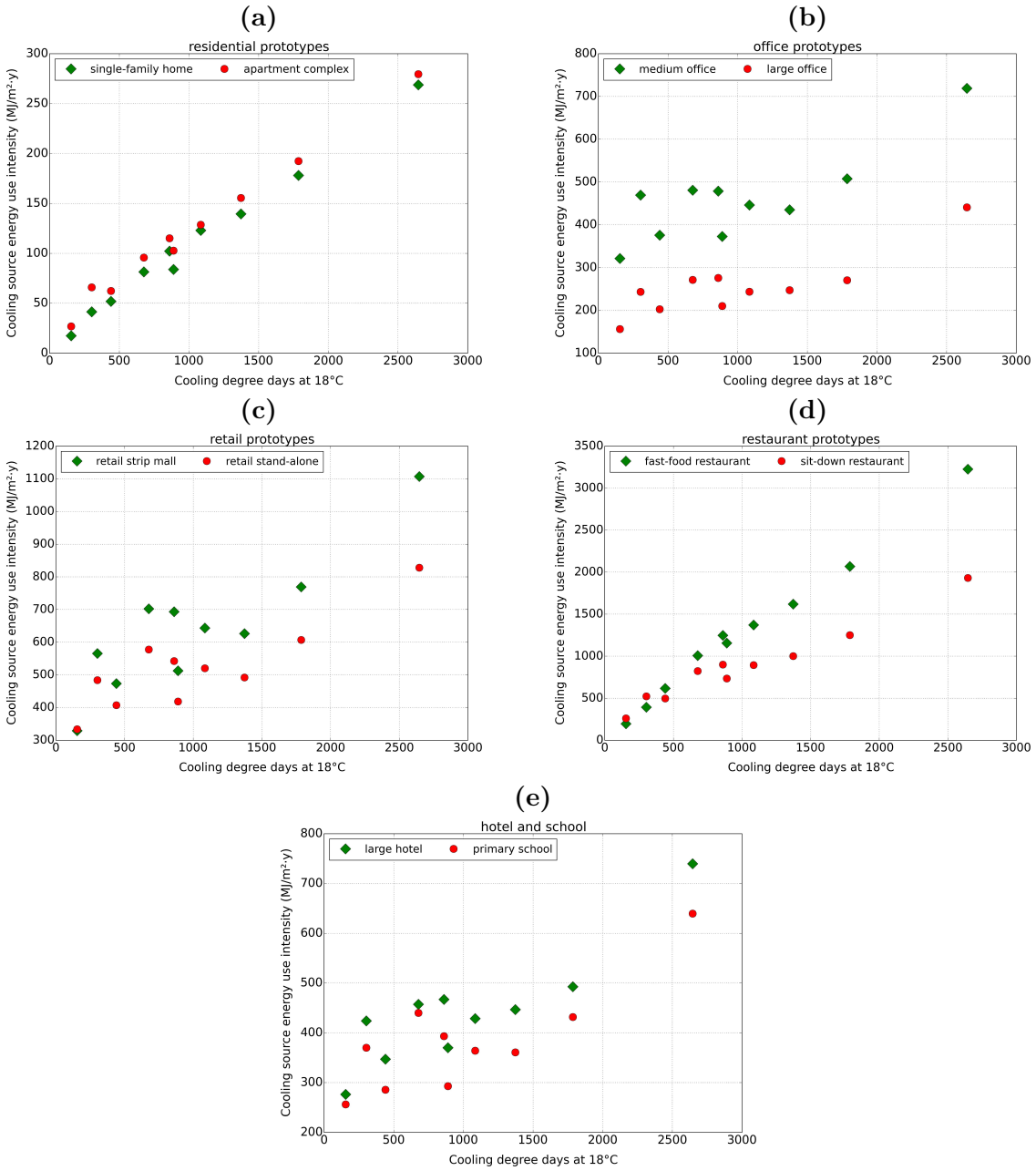

Figure 5.5: Cooling source energy use intensity versus cooling degree days (CDD18C) for a) residential, b) office, c) retail, d) restaurant, and e) other prototypes.

Table 5.17: Comparing heating energy intensity of modeled prototypes to CBECS 2003, RECS and CEUS.

Building type	California's site gas or electric heating energy intensity [kWh/m^2·y]					
	EnergyPlus models weighted by CZ population	CBECS new stock	RECS new stock	CBECS all stock	RECS all stock	CEUS all stock
Retail strip mall	8.00	42.2	NA	93.7	NA	9.50
Primary school	6.60	63.9	NA	156	NA	31.5
Large hotel	24.8	17.6	NA	14.1	NA	23.0
Large office	7.40	46.5	NA	66.1	NA	54.3
Medium office (electric heating)	5.4	6.5	NA	14.1	NA	3.70
Sit-down restaurant	92.1	25.3	NA	49.7	NA	24.3
Fast-food restaurant	195	18.8	NA	10.6	NA	24.3
Retail stand-alone	12.3	20.5	NA	38.6	NA	9.50
Apartment building	3.50	NA	64.9	NA	54.4	NA
Single-family home	13.4	NA	64.9	NA	42.6	NA

Figure 5.6 shows plots of heating source energy use intensity versus heating degree days at 18°C (HDD18C). In Figure 5.6 the 10 prototypes were paired the same way as in Figure 5.5. As expected, the heating energy use intensity increases with HDD18C.

5.9 Discussion

Comparison of modeled and actual building energy use Comparing the energy intensities modeled in this study with EnergyPlus to the energy intensities reported in CBECS, RECS, and CEUS surveys served to corroborate the prototypes output are comparable to the state's documented energy. For each building type, the energy intensities vary widely within the surveys, which provide a range of realistic energy intensities. For cooling, the modeling results nearly match either or both of the survey results.

For heating, the modeling results are generally much lower than the CBECS and RECS results. One reason for this is that in the case of commercial buildings, CBECS values include much colder states like Alaska, Washington, and Oregon. When comparing the heating from the modeling with the CEUS results, the energy intensities match better; this was expected since CEUS is a study done solely for California.

Another reason the heating energy intensities from the EnergyPlus simulations were lower than those reported in the surveys is the stricter construction standards on insulation and greater airtightness of the prototypes, thus requiring lower heating power demand. The modeling results of the two restaurants are 4 (sit-down restaurant) to 10 (fast-food restaurant) times larger than the survey values, but the CBECS survey suggest many restaurants also use electric heating. There was an excellent match between the gas heating source energy of the modeled restaurants and the CBECS' restaurants electric heating source energy.

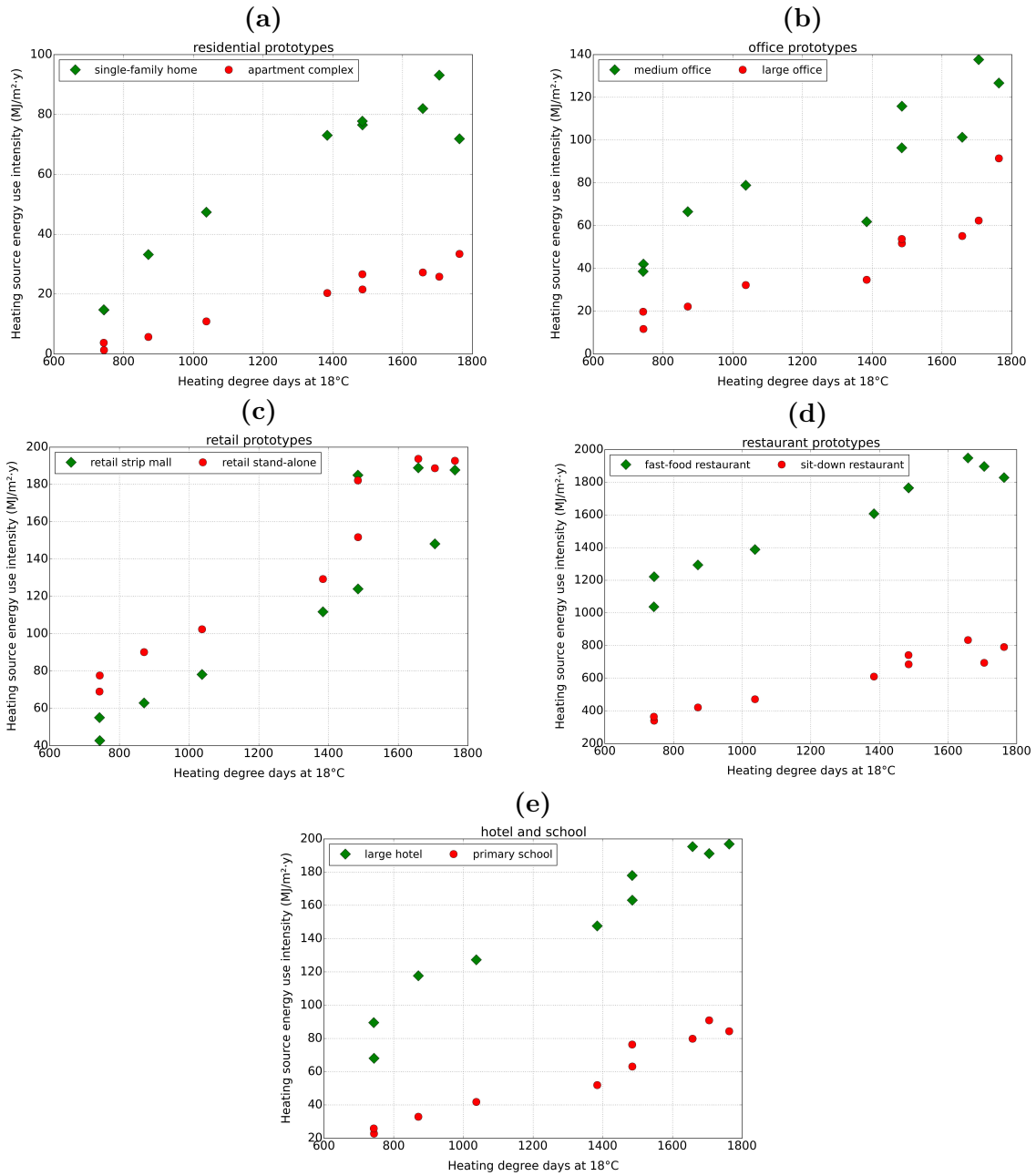

Figure 5.6: Heating source energy use intensity versus heating degree days (HDD18C) for a) residential, b) office, c) retail, d) restaurant, and e) other prototypes.

Represent vintage of California's building stock The most common period of construction of California's building stock is between 1970 and 1979 (Appendix D). The building prototypes do not precisely represent the current building stock because the prototypes were simulated following 2008 Title 24 Standards. The prototypes were modeled with higher HVAC efficiency and better envelope insulation than what is found in typical current buildings. Hence, the simulations may have underestimated the direct and indirect building energy effects of cool pavements. Hence, the results will likely underestimate the cool pavement effects on the energy use of the current building stock.

5.10 Summary

This chapter detailed the methodology followed to assess the direct and indirect effects of cool pavements during their use phase on a building's energy use. The chapter also presented a method to estimate the citywide impact of cool pavements by assessing a city's building stock.

The results from the building energy simulations were validated by comparing them with actual building energy uses as reported by nationwide and state-specific building energy consumption surveys. To further validate the simulations, the modeled cooling and heating energy uses were compared to the annual cooling and heating degree days of the different California climate zones.

The next chapter – Chapter 6 – uses the results obtained from the building energy simulations to evaluate the direct and indirect effects of cool pavements on the energy use of individual buildings and on different California cities.

CHAPTER 6

Effect of Cool Pavements on Building Energy Use – Results and Discussion

6.1 Introduction

The present chapter complements Chapter 5 by presenting the results obtained from the building energy simulations and utilizing them to analyse the energy and environmental impacts of cool local roads and city pavements (see Section 5.4 for explanation of local roads and city pavements). First, the chapter presents the energy uses of the base cases for the 10 prototypes in the 9 California building climate zones (BCZs) listed in Table 5.6; the base cases consider the local road and city mean pavement albedos as 0.10. Later, the base energies are used to proof the relationship between the direct effect of local road albedo and building-to-road view factor. The chapter continues by showing the changes in cooling, heating, and lighting energy uses versus changes in local road and city pavement albedos. The plots of energy changes versus albedo changes demonstrated the linearity that exists between energy change and albedo change. These results were used to solve the physical model equations derived in Section 5.4.2.

The coefficients of the physical model equations were employed to compute and analyse the direct and indirect effects of cool pavements by prototype and BCZ. Finally, two case studies are defined to assess a conservative (case study 1) and more aggressive (case study 2) state-wide initiative to implement cool pavements in 9 major California cities. The case studies explore citywide energy and environmental impacts of cool pavements over a 50-year period.

6.2 Base energy use by prototype and building climate zone

As described in Section 5.3, the cooling, heating, and lighting energy use of 10 different prototypes were simulated in 9 different BCZs (4, 7, 8, 9, 10, 12, 13, 14, and 15), giving a total of 90 building models. Before continuing further in this chapter presenting the cooling and heating energy changes obtained from the simulations, Tables 6.1 and 6.2 give for each prototype and BCZ the base electric cooling (Table 6.1) and gas heating (Table 6.2) energy intensities (energy per unit of floor area). These base cases consider the local road albedo and the city-mean pavement albedo to be 0.10. As it will be demonstrated later in the chapter, changes to local road albedo had a negligible effect on the prototypes' lighting demand. Thus the base lighting energy uses are not included here. Note that these base energy uses are the values used throughout the chapter when calculating the absolute and relative energy savings and penalties from cool pavements.

Table 6.1: Base site cooling energy use intensity by prototype and building climate zone.

	Site electric cooling energy intensity by building climate zone [kWh/m^2·y]								
Prototype	**4**	**7**	**8**	**9**	**10**	**12**	**13**	**14**	**15**
Single-family home	1.40	4.30	3.40	6.80	8.50	10.2	11.6	14.8	22.3
Apartment building	2.20	5.20	5.50	8.00	9.60	10.7	12.9	16.0	23.2
Large office	13.0	16.8	20.2	22.6	22.9	20.2	20.5	22.5	36.7
Medium office	26.7	31.2	39.0	40.0	39.8	37.1	36.2	42.2	59.8
Retail stand-alone	27.8	33.9	40.2	48.0	45.1	43.3	40.9	50.5	68.9
Strip mall retail	27.4	39.4	47.0	58.4	57.7	53.5	52.1	63.9	92.1
Sit-down restaurant	21.6	41.3	43.3	68.4	74.8	74.4	83.2	104	161
Fast-food restaurant	16.3	51.3	32.6	83.7	104	114	135	172	268
Large hotel	23.0	28.9	35.3	38.0	38.8	35.6	37.1	41.0	61.5
Primary school	23.8	30.8	36.6	32.7	30.3	24.4	30.0	35.9	53.2

Table 6.2: Base site gas heating energy use intensity by prototype and building climate zone.

	Site gas heating energy intensity by building climate zone [therm/m^2·y]								
Prototype	**4**	**7**	**8**	**9**	**10**	**12**	**13**	**14**	**15**
Single-family home	0.712	0.571	0.108	0.243	0.341	0.533	0.571	0.532	0.103
Apartment building	0.188	0.152	0.009	0.039	0.073	0.14	0.182	0.236	0.024
Large office	0.381	0.317	0.062	0.131	0.192	0.204	0.337	0.639	0.124
Medium office (electric [kWh/m^2·y])	11.4	9.60	3.50	5.50	6.60	5.10	8.00	10.3	3.20
Retail stand-alone	0.532	0.455	0.206	0.251	0.291	0.395	0.580	0.714	0.233
Strip mall retail	0.338	0.271	0.048	0.093	0.126	0.246	0.509	0.588	0.108
Sit-down restaurant	3.63	3.75	1.63	1.98	2.26	3.18	4.08	4.59	1.83
Fast-food restaurant	8.22	7.38	4.47	4.88	5.31	6.67	7.86	8.64	3.99
Large hotel	1.03	0.916	0.359	0.662	0.702	0.831	1.03	1.23	0.543
Primary school	0.239	0.091	0.135	0.153	0.208	0.342	0.315	0.402	0.117

6.3 Building-to-road view factors

Figure 6.1 shows the relationship of the cooling and heating energy of the building prototypes to the building-to-road view factors, in BCZs 9, 12, and 13. Since each prototype had a different window-to-wall ratio, the cooling and heating energies were normalized by the window-to-wall ratio. Once normalized, it was possible to find a climate-specific relationship between the direct effect and the building-to-road view factor. The slope of the curves varied slightly throughout the 9 BCZs; for cooling, it ranged between 2.3% and 3.2% per 0.10 increase in local road albedo. For the effect on heating energy use, the slopes were opposite in sign, and smaller in magnitude (-2.5% to -0.6% per 0.10 albedo).

Building-to-road view factor is not the only geometrical parameter that influences the direct effect of cool pavements. Other important ones are the wall-to-floor area ratio and window-to-wall ratio. The HVAC thermostat schedule of a building and the HVAC efficiency are additional relevant parameters as well. Thus although it would be too complicated to precisely predict the direct effect on any particular building, Figure 6.1 shows that the building-to-road view factor and window-to-wall ratio are effective parameters to estimate the direct effect.

6.4 Annual energy use vs local road and city pavement albedos

Each building model was simulated with six different local road albedos, r (0.10, 0.15, 0.20, 0.30, 0.40, and 0.50) and with 3 different weather file versions, each representing a different citywide pavement albedo, p [original (p=0.10), small perturbation (p=0.20), and large perturbation (p=0.50)]. The simulation results were plotted as annual energy use (cooling, gas heating, electric heating, or lighting) versus local road albedo. Each curve in the plot represents a different city-mean pavement albedo. The results were converted to source energies to be able to compare between electric and gas energy uses.

Figure 6.2 shows the annual source cooling, gas heating, and lighting energy uses for the single-family home in BCZs 12 and 15. BCZ 12 experiences very hot summers as well as long and cold winters. BCZ 15 represents an arid region in CA with longer summers and shorter winters than BCZ 12. Hence, cooling degree days in BCZ 15 are three times more than in BCZ 12, while heating degree days in BCZ 15 are half than in BCZ 12. For that reason, the single-family home in BCZ 12 used 1.3 times more cooling than heating energy use while in BCZ 15 was 20-25 times.

The plots demonstrate the multivariate linear relationship of the building energies to the local road and city pavement albedos. The slopes of the plots describe the energy sensitivity to local road albedo. Cooling energy use is proportional to local road albedo and inversely

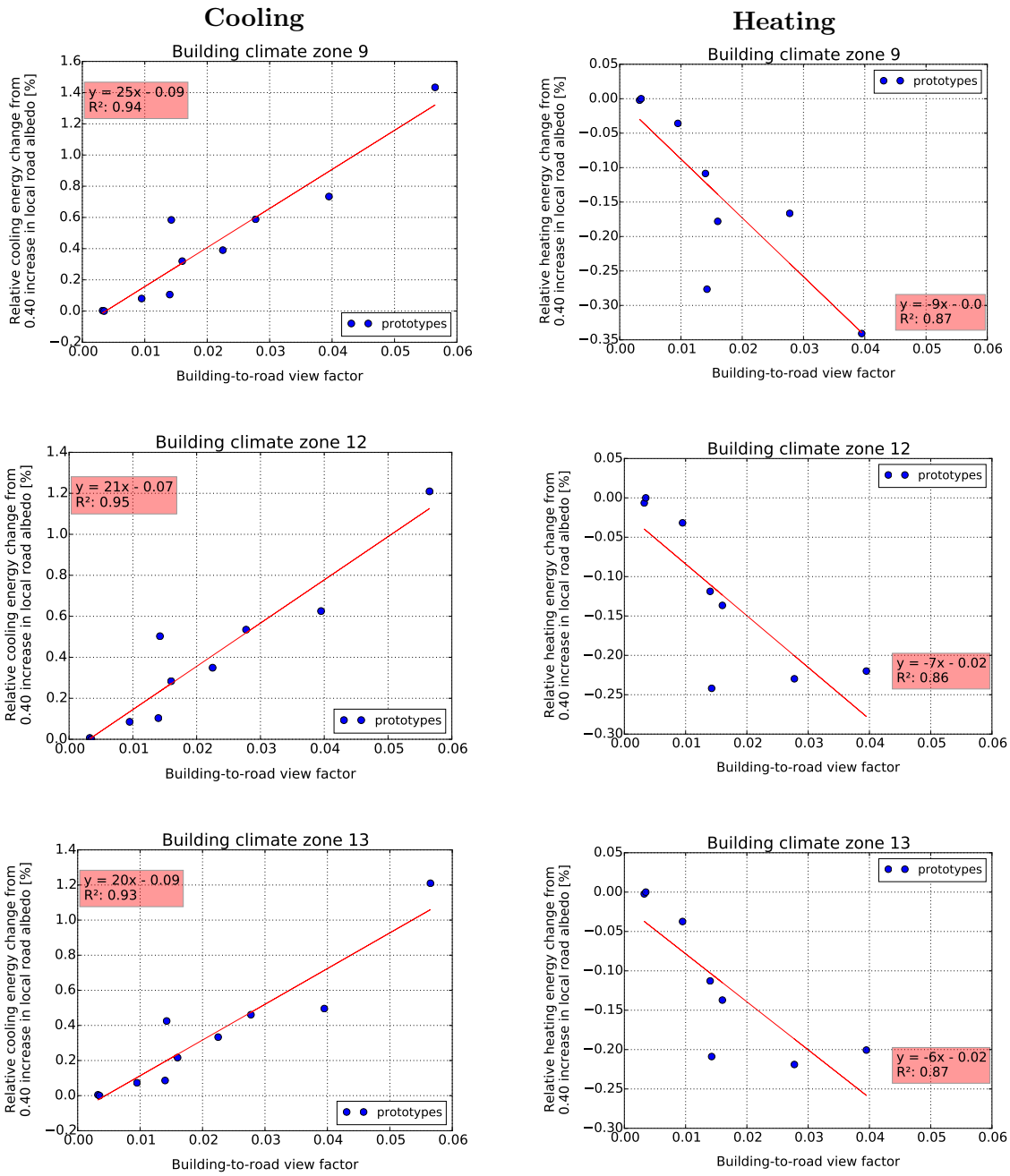

Figure 6.1: Direct effect from cool pavements normalized by window-to-wall ratio versus building-to-road view factor, for BCZs 9, 12, and 13.

proportional to city-mean pavement albedo. The sensitivity of cooling energy to local road albedo increases in climates with hot and long summers (e.g. BCZ 15).

Heating energy use is proportional to city-mean pavement albedo and is inversely proportional to local road albedo. The sensitivity of heating energy to local road is greater in climates with long cold periods (e.g. BCZ 12).

Although not shown in Figure 6.2, electric heating also changed linearly with albedos and proportional to gas heating. However, the magnitudes of electric heating changes were much smaller than changes from electric cooling. Only the medium office prototype used electricity as its main source of heating. The electric heating in all other prototypes is related to the ventilation used to circulate warm air, which is only a small fraction of the total HVAC electric energy of a building.

Lighting energy use is not affected by the air temperature changes obtained from changes in city-mean pavement albedo. It may only be affected by changes to the local road. However, the changes in the local road albedo had no appreciable effect on the single-family home's lighting energy use.

Figure 6.3 shows the source annual cooling, heating, and lighting energy uses as a function of local road and city pavement albedos for the large office in BCZs 12 and 15. The results are different to the single-family home in that the heating energy increases with both local road and city pavement albedos. The HVAC in the large office includes a reheat system to regulate the cooled air differently in different building zones, hence, it consumes gas for the reheat system during the cooling season. In addition, the building occupancy is high during daytime and low during nighttime, thus the HVAC system experiences high cooling demand during the day and low heating demand at night. For these reasons, the net heating demand in the large office increases with cooling demand.

Another major difference between the large office and the single-family home is their window-to-wall ratio. Since the large office has a large (40%) window-to-wall ratio, a large fraction of the road-reflected sunlight is transmitted through the windows, which may reduce the need for artificial light. However, the results showed that the sensitivity of lighting energy to the local road albedo is negligible compared to the sensitivities of cooling and heating energy (Figure 6.3). The only two additional prototypes in which lighting energy changed with local road albedo change were the medium office and the primary school.

6.5 Coefficients of physical model solutions

Figures 6.2 and 6.3 demonstrate the linear relationship that exists between the building energies and the local road and city-mean albedos. As discussed in Section 5.4.2, a multivariate linear regression analysis was applied to the simulation results to test the energy

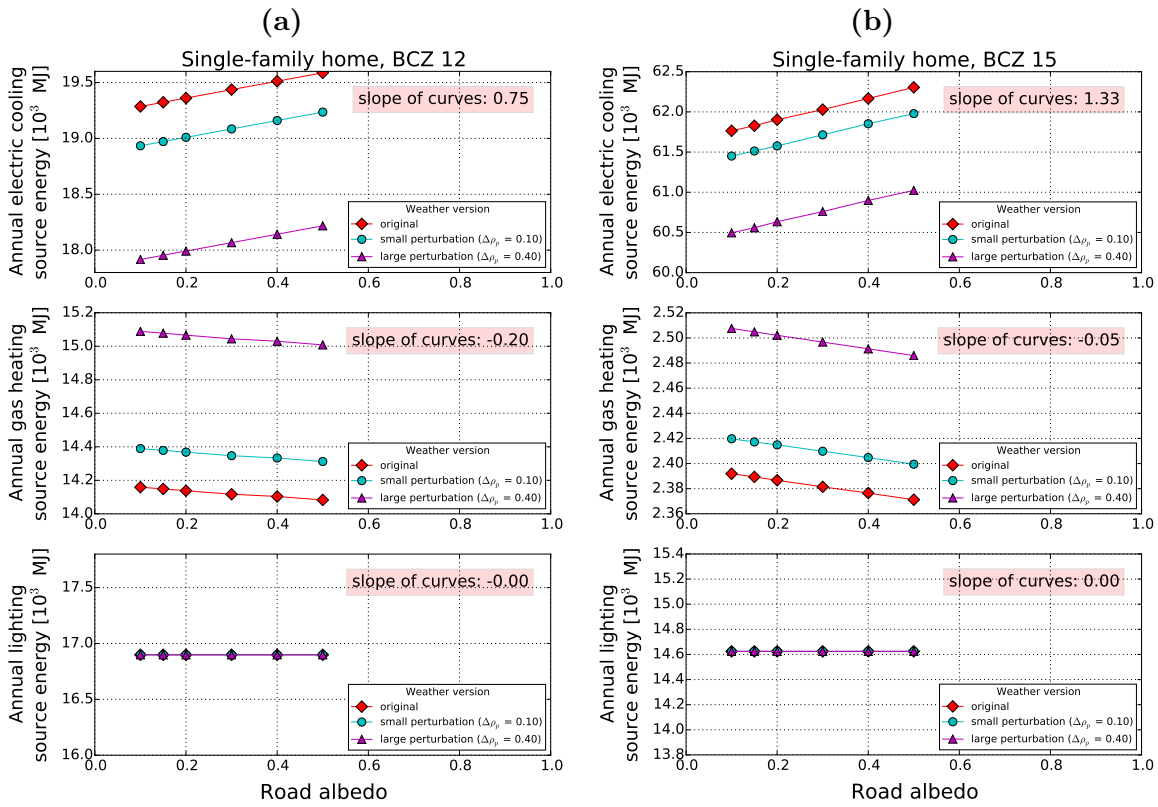

Figure 6.2: Annual cooling, heating, and lighting energy uses as a function of local road albedo and city-mean pavement albedo for the single-family home in BCZ a) 12 and b) 15.

equations derived from the physical model and estimate their coefficients. These equations and their coefficients facilitate predictions to building energy changes given a change in local road albedo and/or city-mean pavement albedo.

Table 6.3 shows the site cooling, heating, and lighting coefficients for the single-family home, medium office, and retail stand-alone prototypes in climate zone 9. The coefficients labelled e represent electric site energy use in units of MWh/y, and the coefficients g are for gas site energy use in units of therm/y. Site energies can be expressed in MJ using conversion factors of 3,600 MJ/kWh or 105.5 MJ/therm. This table is a subset of a complete coefficient table that includes the 10 building prototypes and 9 modelled BCZs. The full table can be found in Appendix E.

6.6 Direct vs indirect effect

The solutions to the physical model equations were employed to study the individual energy impact from changes to either the local road albedo or city-mean pavement albedo.

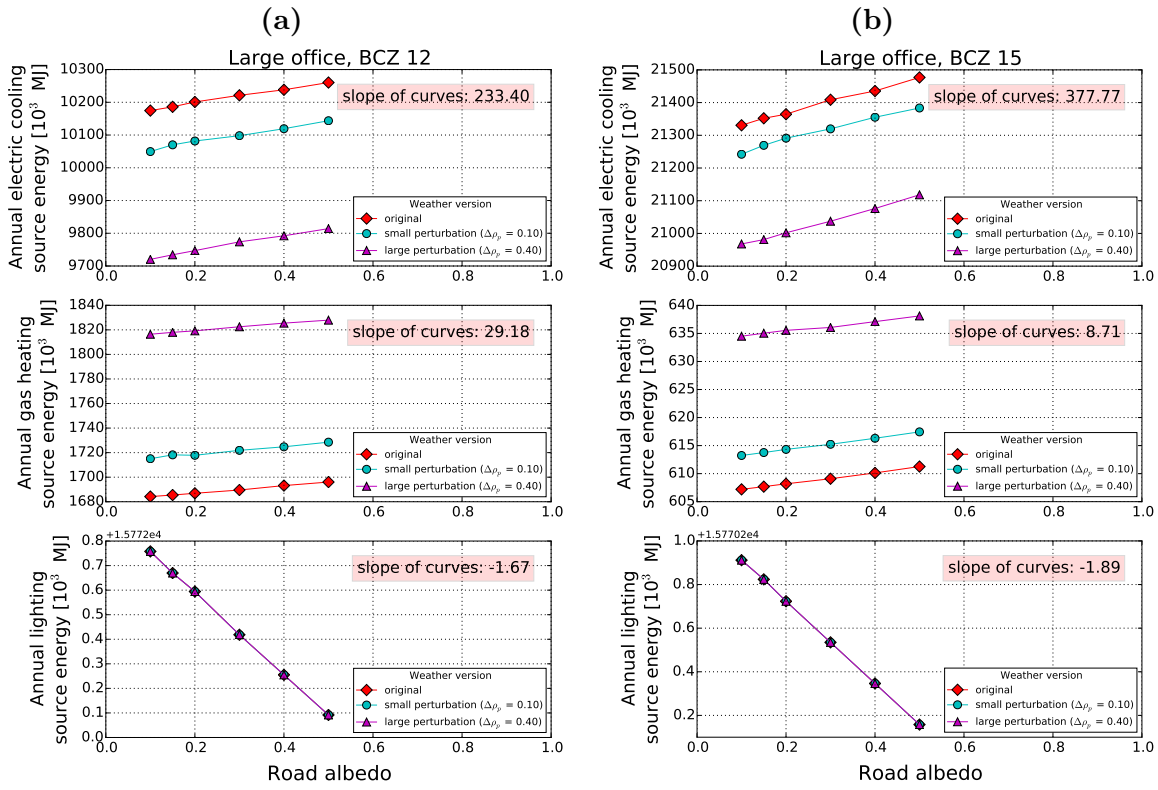

Figure 6.3: Annual cooling, heating, and lighting energy uses as a function of local road albedo and city-mean pavement albedo for the large office in BCZ a) 12 and b) 15.

Table 6.3: Coefficients of the physical model equations for the single-family home, medium office, and retail stand-alone prototypes in BCZ 9.

Prototype	Use	e_0 [MWh/y]	e_1 [MWh/y]	e_2 [MWh/y]	g_0 [therm/y]	g_1 [therm/y]	g_2 [therm/y]
Single-family home	cooling	1.91	0.085	-0.451	0.000	0.000	0.000
	heating	0.131	0.001	0.048	72.5	-1.42	26.3
	lighting	1.35	0.000	0.000	0.000	0.000	0.000
Medium office	cooling	201	2.07	-24	0.000	0.000	0.000
	heating	31.8	0.655	8.01	0.000	0.000	0.000
	lighting	135	-0.017	0.000	0.000	0.000	0.000
Retail stand-alone	cooling	105	0.286	-12.2	0.000	0.000	0.000
	heating	12.7	-0.004	3.3	647	-0.798	199
	lighting	61.7	0.000	0.000	0.000	0.000	0.000

As described in Section 5.4, a change to the local road albedo causes a direct effect on a building's energy use while a change to the city-mean pavement albedo has an indirect effect.

Consider a simple scenario in which the albedo of 50% of a city's pavement was raised by 0.20. According to Equation 5.15, the new change in city-mean pavement albedo ends up being 0.10. To estimate the maximum potential direct effect that this scenario can have on the 10 simulated prototypes, let us assume that the local roads seen by the prototypes were part of the modified city pavement. The physical model equation solutions of all 9 BCZs were employed using a change in local road albedo of 0.20 and a change in city-mean pavement albedo of 0.10.

Figure 6.4 shows the (a) absolute and (b) relative annual site cooling energy intensity savings (savings per conditioned floor area) obtained from this scenario when evaluated in BCZ 12. All prototypes experienced cooling penalties[1] from the direct effect and cooling savings from the indirect effect. However, the magnitudes of the indirect savings strongly dominated the direct penalties.

The absolute cooling intensity savings from the indirect effect were smallest for the residential prototypes (single-family home and apartment building). Thus they experienced the smallest total (direct + indirect) absolute change in energy intensity. The total cooling intensity saving in each residential prototype is 0.07 kWh/m^2·y, which translates to 15.4 kWh/y (0.99%) in the single-family home and 141 kWh/y (0.85%) in the apartment building. On the other hand, the relative direct penalties and relative indirect savings were largest for the residential buildings. The total relative savings were 0.99% (single-family home) and 0.85% (apartment building).

The two restaurants had the largest absolute site cooling energy intensity savings (0.82 kWh/m^2·y for the sit-down restaurant and 1.37 kWh/m^2·y for the fast-food restaurant). With building-to-road view factors of less than 0.01, the restaurants did not experience a direct effect. Hence, their cooling changes are attributed only to the indirect effect.

The human occupancy in the residential buildings is low during daytime and high at nighttime. Hence, during daytime, the interior of commercial buildings are maintained cooler than residential buildings, requiring more cooling energy during the day than the residential buildings. For that reason, absolute cooling intensity savings in the commercial buildings are larger than the residential buildings.

Figure 6.5 shows the absolute changes in gas heating intensity for all prototypes in BCZ 12. The direct and indirect effects had the opposite impact on heating that they had on cooling. However, the direct heating benefits were very small. The magnitudes of the direct

[1]Most figures in this chapter present changes in energy use as energy savings. Thus negative values represent energy penalties and are referred as such throughout the chapter (e.g. -5 kWh in savings would be described as 5 kWh in energy penalty).

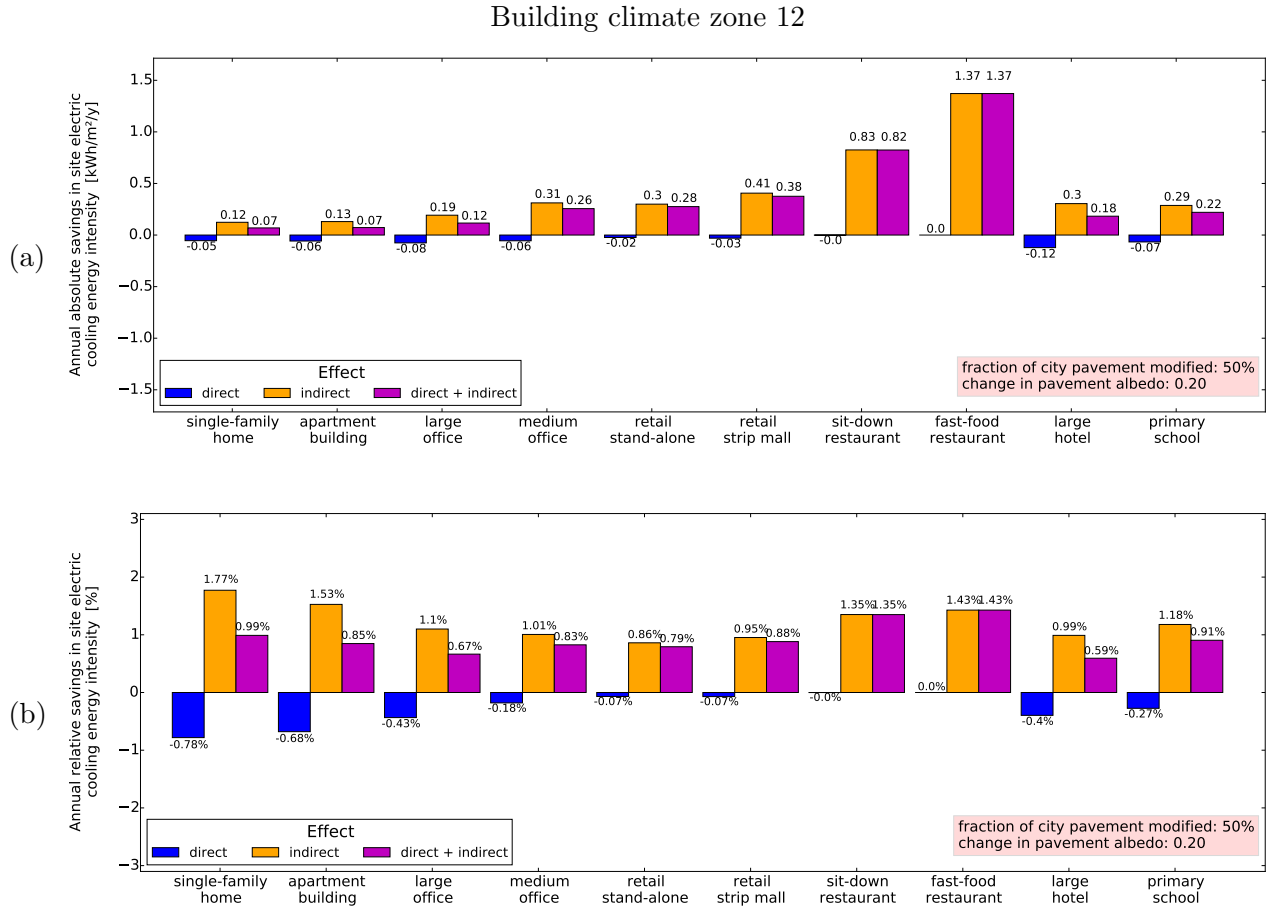

Figure 6.4: a) Absolute and b) relative savings in site cooling energy use of all prototypes in BCZ 12 from the direct, indirect, and direct + indirect effects of cool pavements.

heating savings are far smaller than the magnitudes of the indirect heating penalties. The medium office shows no gas heating effects because the prototype uses electric heating.

To compare across BCZs, Figure 6.6 compares the single-family home's annual site a) absolute savings on cooling energy intensity and b) relative savings. The direct effect has little variation across BCZs. The indirect benefits are greater than the direct penalties except in BCZ 14.

As described in Section 5.3, the USC team simulated the urban climate in different California cities while varying the albedo of all city pavements. The greatest air temperature reductions increased with city size and impervious surface fraction. As such, the greatest air temperature reductions were obtained in BCZ 9 (represented by Los Angeles). The indirect effects in Figure 6.6d are proportional to the air temperature reductions obtained in the climate simulations.

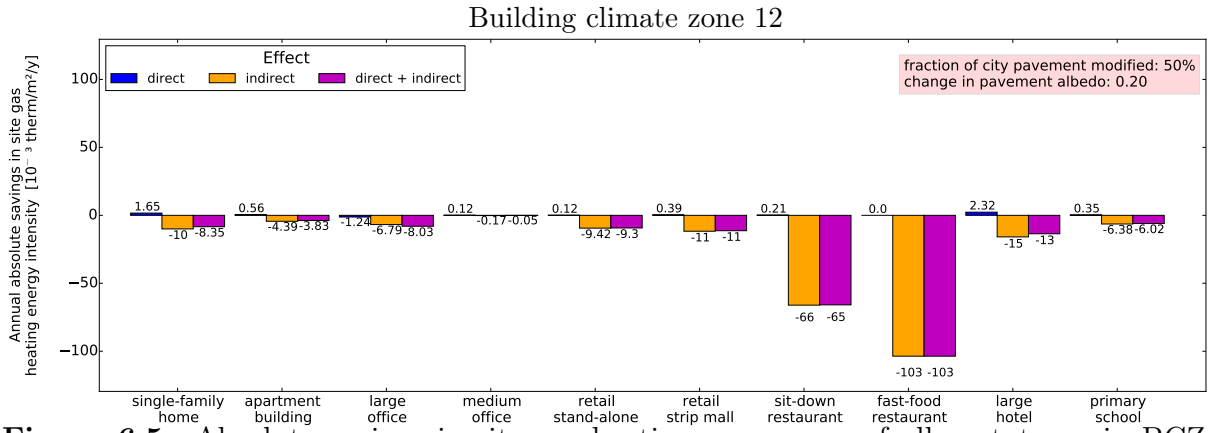

Figure 6.5: Absolute savings in site gas heating energy use of all prototypes in BCZ 12 from the direct, indirect, and direct + indirect effects of cool pavements.

A building's cooling energy demand is proportional to cooling degree days, which in turn is proportional to the outdoor air temperature. Hence, the base cooling energy use of the prototypes is greater in the BCZs with a warm and long summer. Figure 6.6f shows the relative savings in each BCZ and compare them with the cooling degree days at 18°C (CDD18C). The total relative savings were greatest in BCZ 4 (2.2%) and decreased inversely with CDD18C. The relative savings reduced with CDD18C because although the absolute cooling savings may be similar across climate zones, the base cooling energy increased with CDD18C.

Figure 6.7 shows the relative changes in the gas heating energy use of the single-family home in all climate zones and compares them with heating degree days at 18°C (HDD18C). The direct benefits are similar across climate zones and very small, ranging between 0.27% (BCZ 12) to 0.63% (BCZ 7). Relative penalties from the indirect effect are much greater than the direct benefits, especially in climate zones 7, 8, and 9. Similar to cooling, the absolute changes in heating energy do not vary much across climate zones. However, since the base heating energy use increases with heating degree days, the relative indirect penalties reduce inversely proportional to heating degree days.

6.7 Case studies

6.7.1 Overview

This section presents two case studies with the intention to evaluate the potential energy and environmental effects of a cool pavement choice over a 50-year period installed on the public roads of different California cities. These case studies evaluate only the use phase of the pavements' life-cycle. As such, the surface albedo is the only property of a pavement that affects a city's building stock energy use and energy-related environmental impact. In

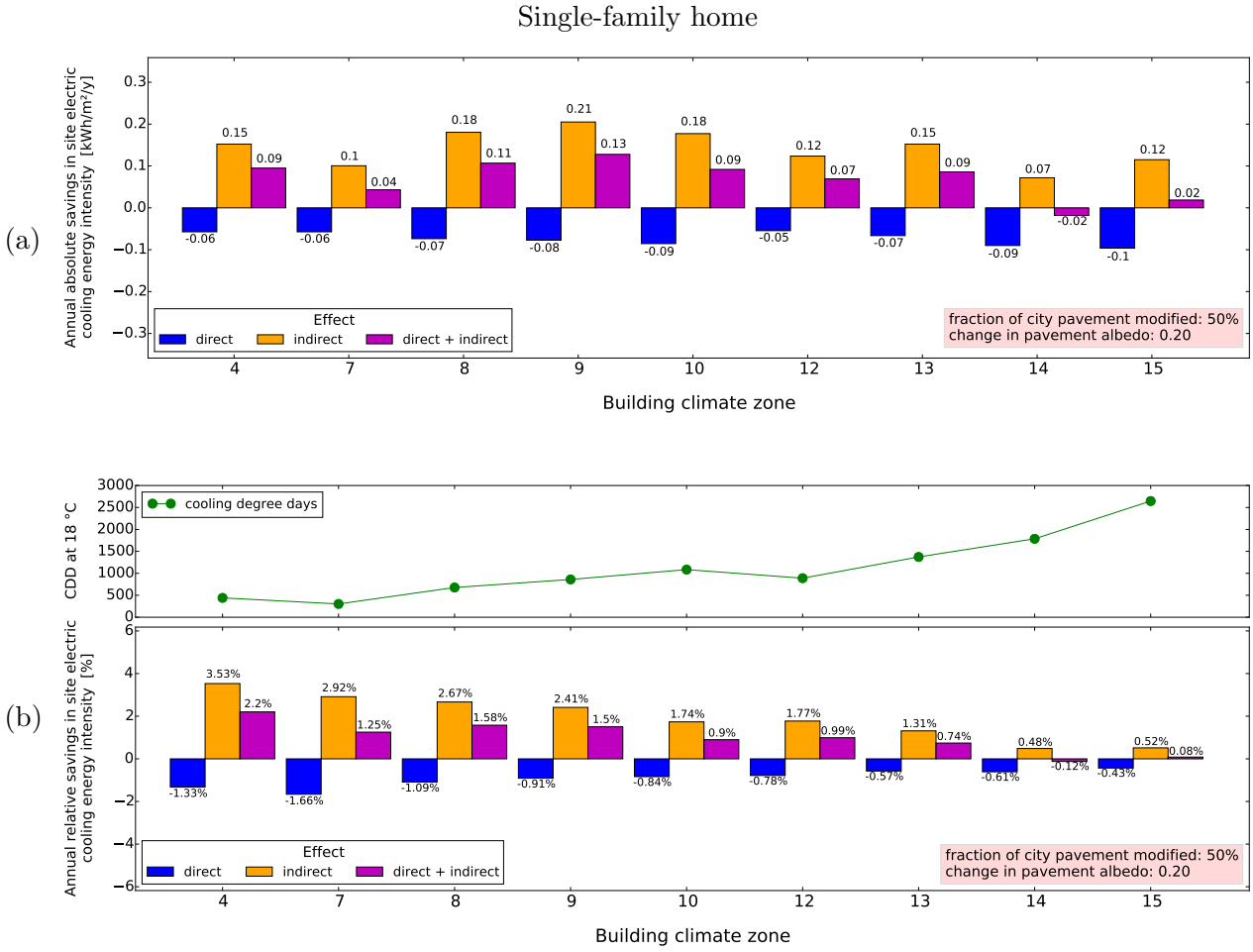

Figure 6.6: a) Absolute and b) relative savings in site cooling energy use of the single-family home in all BCZs from the direct, indirect, and direct + indirect effects of cool pavements.

each case study, a typical pavement practice (scenario A') is compared to a non-typical and cooler practice (scenario B').

In California there are many surface treatment practices used for routine maintenance of city pavements. These practices are applied solely at the surface to protect the underlying pavement structure. In a survey of local California governments, *slurry seal* was identified as the most typical surface treatment used in the state. Slurry seal usually has an initial albedo of 0.05 and aged albedo of 0.10. An example of a non-typical surface treatment is *chip seal*, which consists of a layer of asphalt with aggregate pressed on the top. The aged albedo of the chip seal can vary between 0.10 and 0.25, depending on the aggregate used. Another non-typical surface treatment is the application of a *reflective coating*, which can have an aged albedo between 0.20 and 0.30.

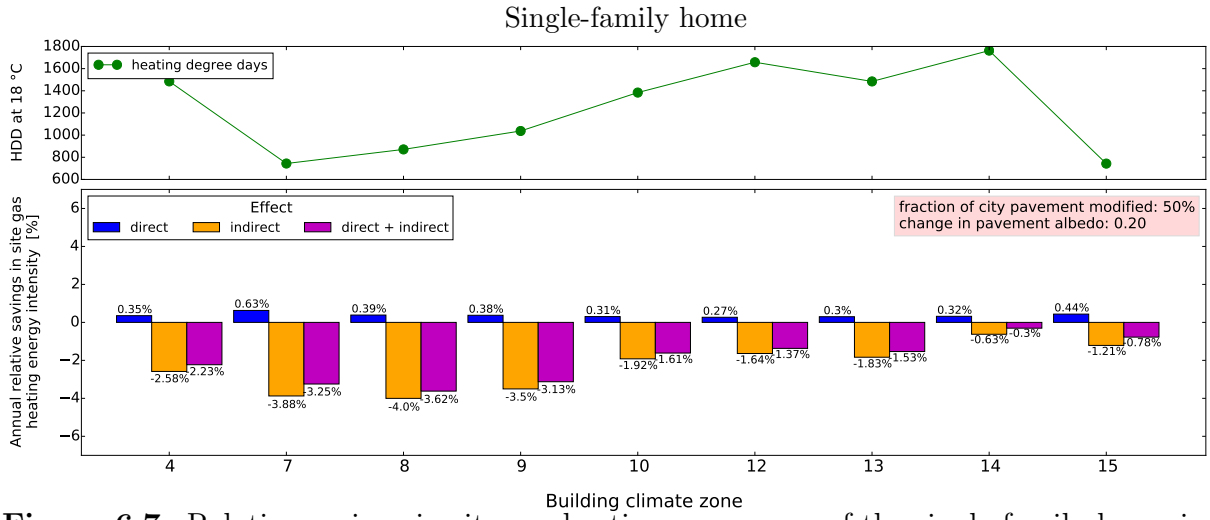

Figure 6.7: Relative savings in site gas heating energy use of the single-family home in all BCZs from the direct, indirect, and direct + indirect effects of cool pavements.

6.7.2 Defining the case studies

Case study 1 was generated to assess a conservative initiative to implement citywide cool pavements on public roads. Slurry seal was selected as scenario A and was assigned an albedo of 0.10. Scenario B consists of chip seal with albedo 0.23. Since case study 1 represents a more conservative approach, it was evaluated by modifying only 50% of a city's public pavement.

Case study 2 assesses a more aggressive initiative and evaluates the impact from modifying 100% of a city's public pavement. Slurry seal with albedo 0.10 was again assigned as Scenario A. Scenario B consists of a reflective coating with albedo 0.30.

The case studies evaluate nine major cities in California, each located in a different BCZ (Table 6.4). Assessing cities in different climates provide insights on the effect of climate and city size on the results.

In the climate simulations, the USC team modified all pavements (public + private). Hence, the city-mean pavement albedo referred to in the physical model (Section 5.4) includes public and private urban pavements. Since these case studies assess only the public pavements, it is necessary to calculate the fraction of the city's total pavement that is public.

The total pavement area for each city is calculated as the product of the city's total area, the city's impervious area fraction, and the ratio of total pavement area to impervious area. The cities' total areas (land + water) were obtained from the 2010 US Census [98]; the LBNL team calculated the cities' impervious area fractions with ESRI ArcMap 10.2 [99]; and the ratio of total pavement area to impervious area was set to 0.50 at the recommendation of the USC team.

Table 6.4: Major California cities and BCZs assessed in the case studies.

City	Building climate zone
San Jose	4
San Diego	7
Anaheim	8
Los Angeles	9
Riverside	10
Sacramento	12
Fresno	13
Lancaster	14
Palm Springs	15

The public pavement area was calculated using a survey conducted from the project team members at University of California Pavement Research Center (UCPRC). Their survey reports the public pavement lane miles for some California cities, including San Jose, Los Angeles, Sacramento, and Fresno [96]. The total public pavement area in each city was then calculated as the product of pavement lane miles times lane width, assumed 3.7 m wide (Table 6.5).

For the cities in which the public pavement area is available, the fraction of total pavement that is public is now easily obtained by dividing the public pavement area by total pavement area. Los Angeles has the largest public to total pavement fraction at 62% and it has also the largest public pavement area with 165 km^2. For the other cities, the fraction ranges between 28% to 33%. Therefore, for the cities in which public pavement area was not available, the fraction of public to total pavement area was estimated as 30% (Table 6.5).

Table 6.5: Land area and pavement areas (total and public) for each city.

City (BCZ)	Total area (land+water) [km^2]	Land area [km^2]	Total pavement area [km^2]	Total public pavement area [km^2]	Fraction of land area that is pavement [%]	Fraction of total pavement that is public [%]
San Jose (4)	466.1	457.2	90.4	25.1	20	28
San Diego (7)	964.5	842.2	151	45.3[a]	18	30[b]
Anaheim (8)	131.6	129.1	34.1	10.2[a]	26	30[b]
Los Angeles (9)	1302	1214	266	165	22	62
Riverside (10)	210.9	210.2	32.9	9.90[a]	16	30[b]
Sacramento (12)	259.3	253.6	54.2	18.0	21	33
Fresno (13)	290.9	290.0	60.8	20.0	21	33
Lancaster (14)	244.9	244.2	14.9	4.50[a]	6.0	30[b]
Palm Springs (15)	246.0	243.8	13.5	4.00[a]	6.0	30[b]

[a] Estimated from the assumption that 30% of total pavement area is public.
[b] The total public pavement area was not available. The fraction of total pavement that is public was assumed as 30%.

The fraction of total pavement that is public is used in Equation 5.15 to compute the city-mean pavement albedo, $\rho_{p,m}$. In study case 1, fraction f for Equation 5.15 is the public pavement fraction $\times$ 0.50. In case study 2, f equals the public pavement fraction (Table 6.6).

Table 6.6: City-mean pavement albedos for each city.

City (BCZ)	$\rho_{p,m}$ for case study 1	$\rho_{p,m}$ for case study 2
San Jose (4)	0.12	0.16
San Diego (7)	0.12	0.16
Anaheim (8)	0.12	0.16
Los Angeles (9)	0.14	0.22
Riverside (10)	0.12	0.16
Sacramento (12)	0.12	0.17
Fresno (13)	0.12	0.17
Lancaster (14)	0.12	0.16
Palm Springs (15)	0.12	0.16

6.7.3 Air temperature change

The city-mean pavement albedo change in each city was calculated using 0.10 as the original city-mean pavement albedo. Section 5.3.3 details how the adjusted seasonal hourly temperature differences obtained for each BCZ scale with change in city-mean pavement albedo. Thus the temperature differences of each city and in each case study were obtained using this linear relationship.

Figure 6.8 plot the seasonal hourly temperature differences in San Diego and Los Angeles for case studies 1 and 2. These two cities were selected because Los Angeles had the largest temperature differences of all cities and the differences in San Diego are similar to those experienced by the other seven cities. In case study 1, temperature reductions in San Diego were never more than 0.05°C and were very similar between all seasons. In case study 2, all seasons in San Diego reached a maximum temperature reduction of 0.08°C at some time between 17:00 and 20:00 LST. In case study 1 for Los Angeles, temperature reductions averaged 0.05°C with the summer having the largest reduction at 10:00 and 19:00 LST. Temperature reductions in case study 2 varied more between seasons with winter averaging the lowest reductions and summer experiencing the largest reductions nearly at all times. In all seasons, the maximum reduction happened between 17:00 and 19:00 LST; spring, fall, and summer also had large reductions in the morning between 8:00 and 10:00 LST.

The hours between 14:00 and 16:00 LST are often the times of a day in any given city when temperatures are the highest. However, as seen in Figure 6.8, maximum temperature reductions happened most of the time during late afternoon or early evening. Figure 6.9 plots the temperature changes at 15:00 and 20:00 LST for all cities and by season. During winter, temperature reduction was larger at 15:00 LST in most cities. However, temperature reduction was larger at 20:00 LST in all the other seasons and in most of the cities.

6.7.4 Direct and indirect effects

Figure 6.4 through Figure 6.7 compared direct and indirect effects for a scenario in which the prototypes "see" modified local roads. However, in a scenario where only a fraction

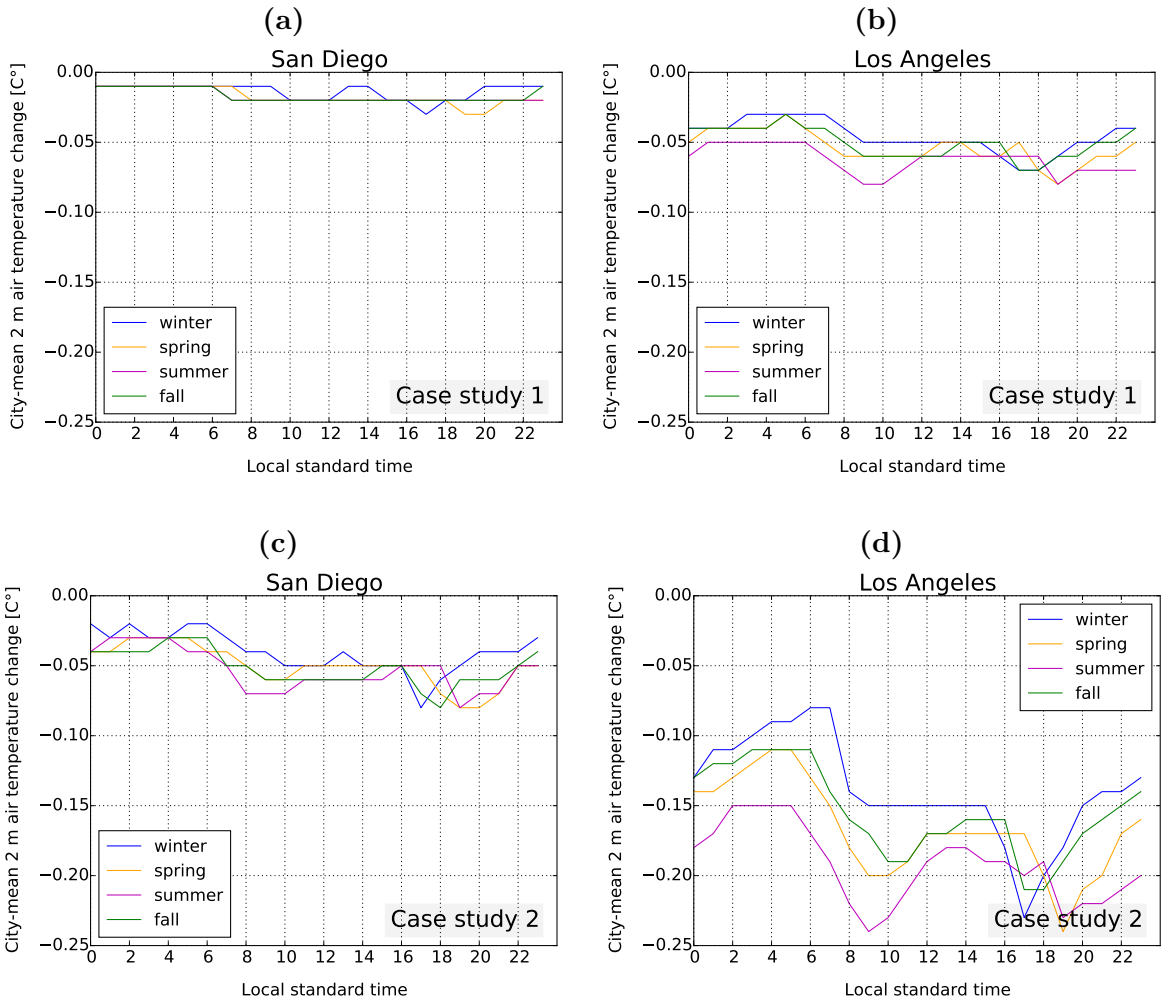

Figure 6.8: Seasonal hourly temperature differences for San Diego and Los Angeles in case studies 1 and 2.

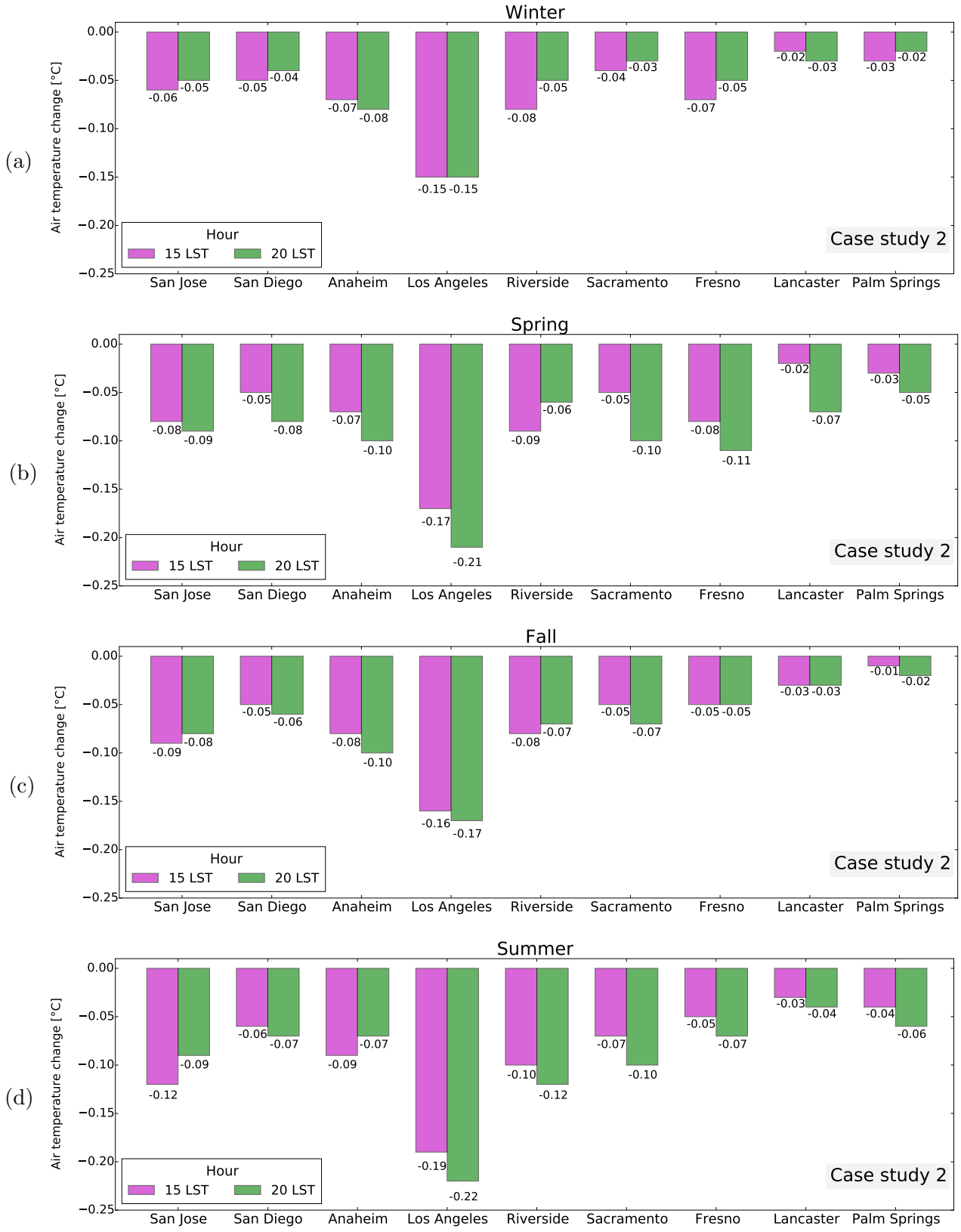

Figure 6.9: Temperature reductions at 15:00 and 20:00 LST for all cities by season.

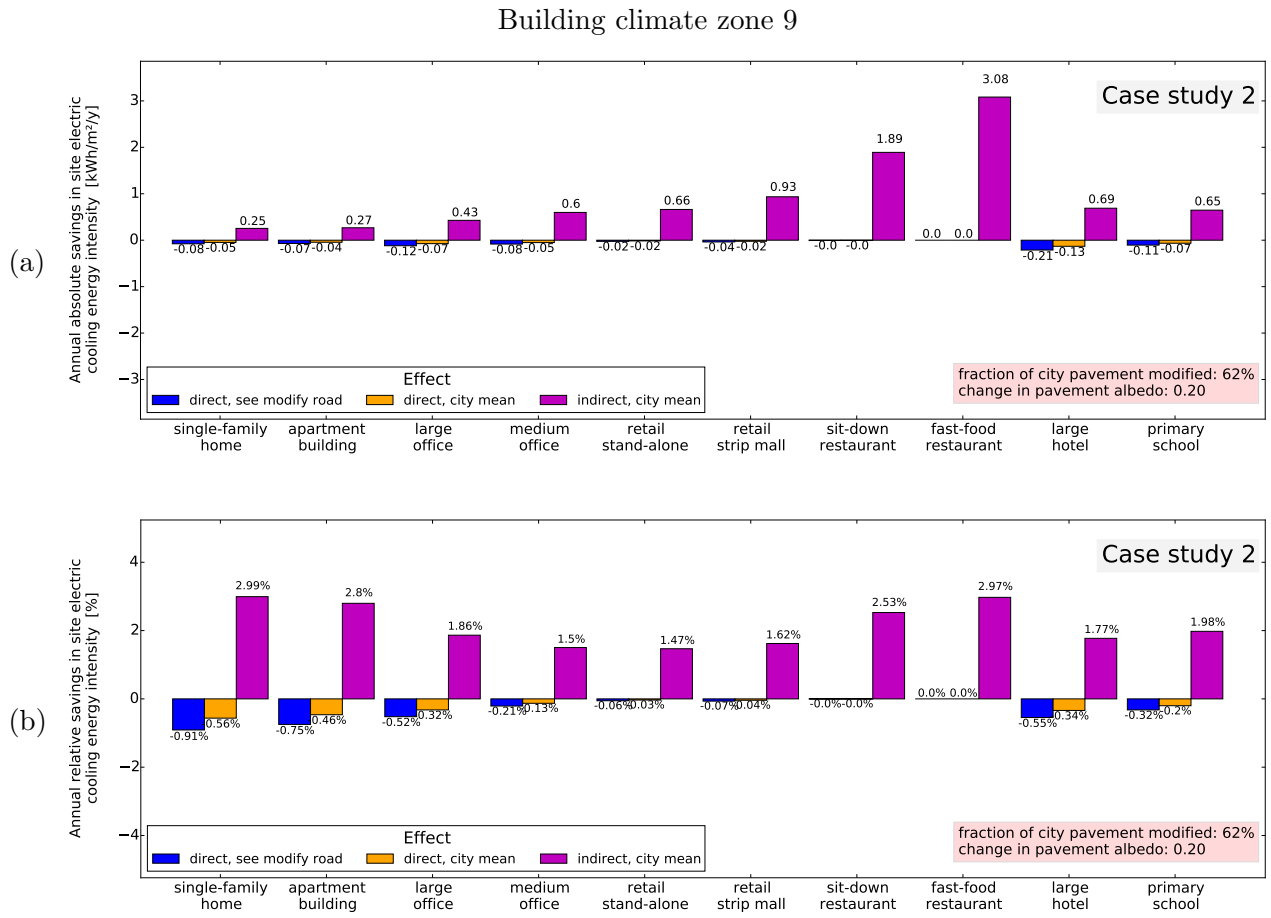

Figure 6.10: Annual a) absolute and b) relative savings in site cooling energy intensity of all prototypes in BCZ 12.

of the urban pavement is modified, some buildings will not see modified pavements. Thus Equation 5.14 can be used to estimate a city-mean local road albedo, in which f is the fraction of all buildings that see modified local road and equals the fraction of a city's urban pavement that is modified.

Figure 6.10 compares the direct and indirect effects on site cooling energy intensity on all prototypes in BCZ 9 (Los Angeles) for case study 2. The plots show the direct effect for the cases in which the prototypes see modified road as well as the city mean direct effect. The results in direct and indirect effects showed the same behavior as seen in Figure 6.4. Figure 6.10 also illustrates that when considering an entire city, the direct effect may impact only a portion of the building stock, hence, the city mean direct impact is lower than what can be estimated for a single building.

Figure 6.11 compares between BCZs the single-family home's annual a) absolute and b) relative site cooling intensity changes for case study 2. The indirect savings were greatest

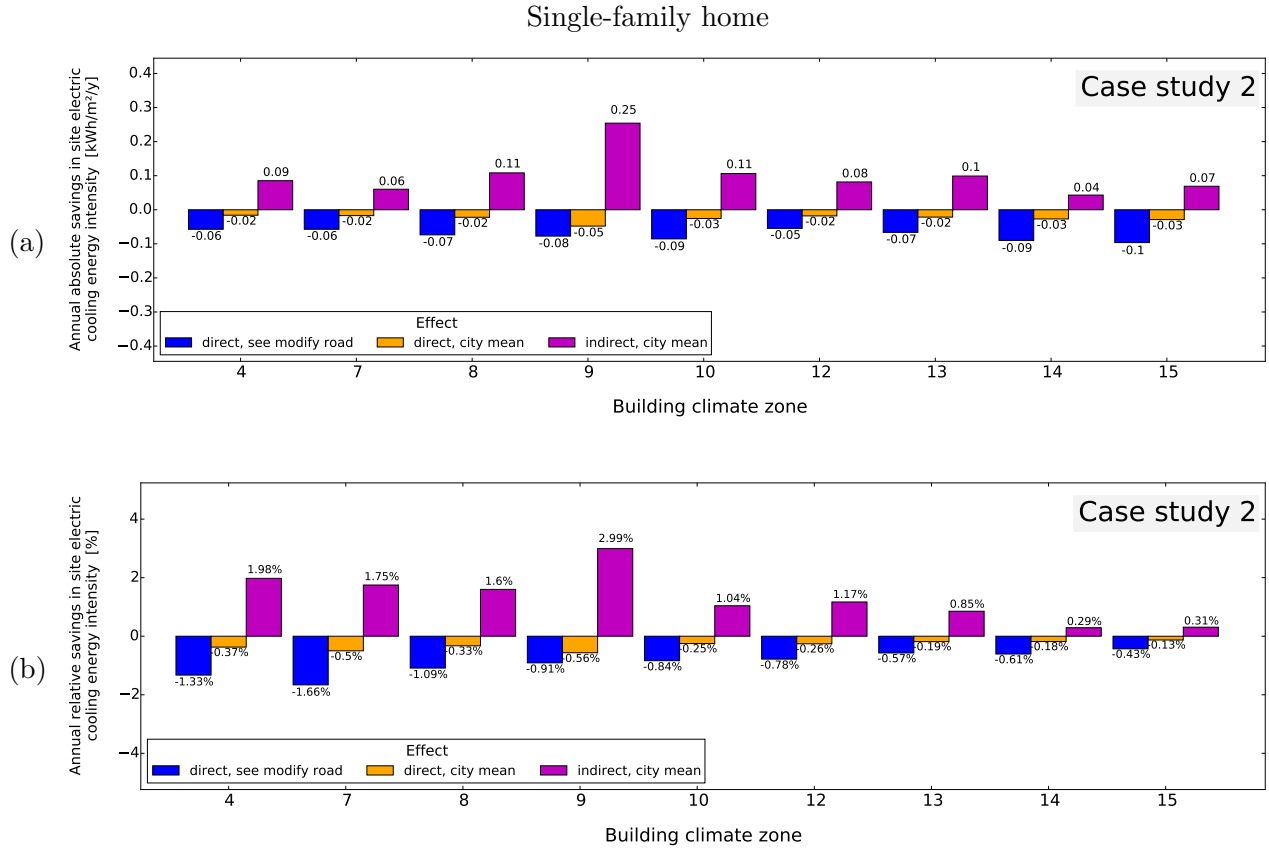

Figure 6.11: a)Absolute and b)relative site cooling intensity savings in single-family home for all BCZs.

in BCZ 9 (0.25 kWh/m^2, 2.99%) and were smallest in BCZ 14 (0.04 kWh/m^2, 0.29%). The magnitudes of direct penalties from seeing the modified road are equal or greater than the indirect savings only in BCZs 7, 14, and 15, resulting in net cooling penalty. However, when considering the city mean results, the indirect cooling benefits always outweigh the direct penalties. Citywide, the net cooling benefits ranged from 0.01 kWh/m^2 (0.11%) in BCZ 14 to 0.20 kWh/m^2 (2.43%) in BCZ 9.

Figure 6.12 compares between BCZs the single-family home's annual a) absolute and b) relative site gas heating intensity changes for case study 2. The indirect penalties were greatest in BCZ 9 (14×10^{-3} therm/m^2, 4.34%) and were smallest in BCZ 15 (0.75×10^{-3} therm/m^2, 0.73%). The direct effect had a lesser impact than it did on cooling energy; in all BCZs the direct benefits on buildings seeing modified road never outweighed the indirect penalties. Citywide, the net heating penalties ranged from 0.62×10^{-3} therm/m^2 (0.60%) in BCZ 15 to 13.21 $\times10^{-3}$ therm/m^2 (4.11%) in BCZ 9.

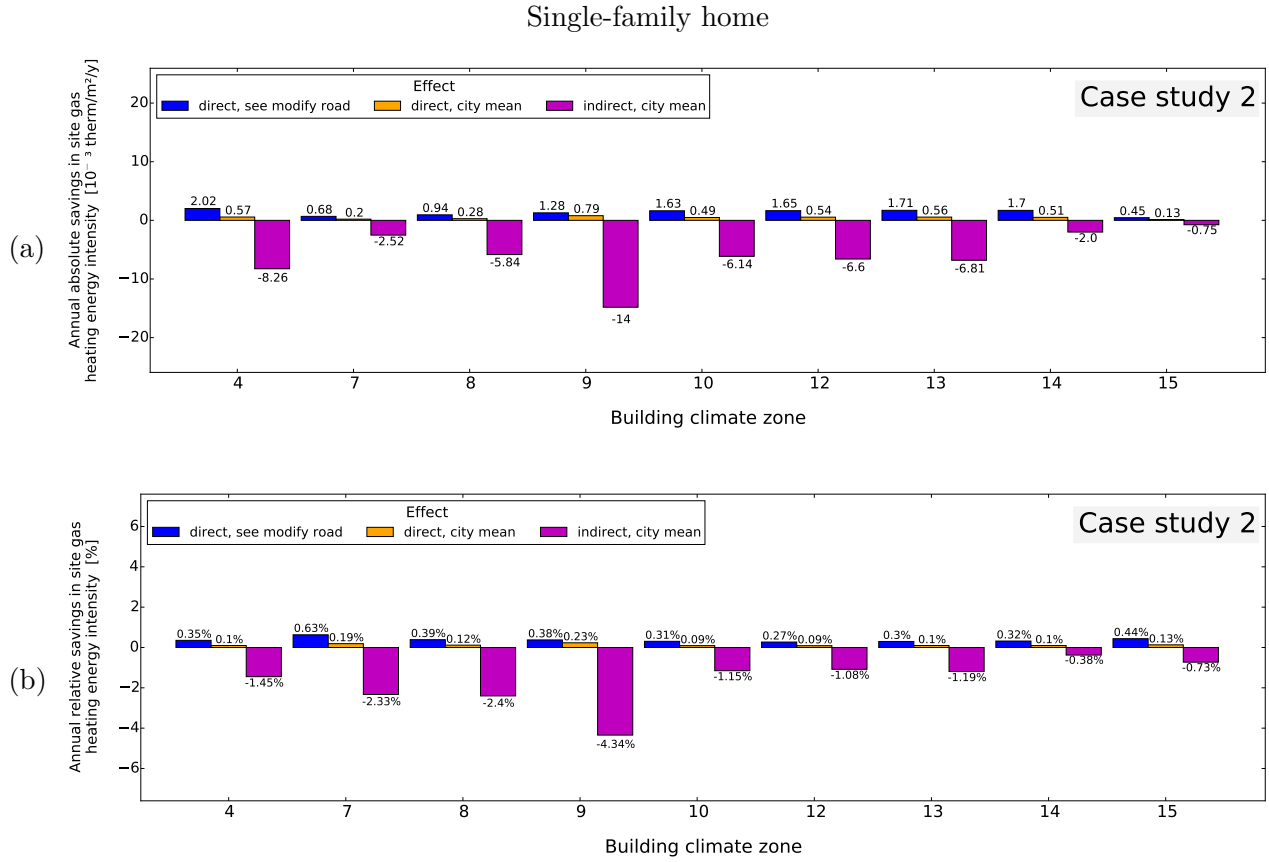

Figure 6.12: a)Absolute and b)relative site gas heating intensity savings in single-family home for all BCZs.

6.7.5 Citywide impact

6.7.5.1 Building stock mapped to prototypes

Section 5.7 details a simple method to calculate the citywide energy and environmental consequences of cool pavements. Section 5.6 described how California's building stock was assessed to obtain the total citywide floor area of each property type in each city. The relevant property types were then mapped to one of the building prototypes to obtain the total city floor area mapped to each prototype.

Tables 6.7 and 6.8 gives the number of buildings and total floor area mapped to each prototype for each of the cities. A predominant characteristic of all cities is that residential buildings hugely dominate the building stock. The fraction of buildings that are residential in these cities range between 94% (Los Angeles) to 98% (Lancaster). The fraction of total floor area that is residential ranges between 78% (Anaheim) to 96% (Riverside). Single-family home is the most common building type, being as much as 94% of buildings (Lancaster) and covering up to 89% of the floor area (Riverside).

Even though the building records from the Assessor's Offices in California include the majority of buildings in the state, not every record thoroughly describes the property type and floor area. For that reason and the fact that the records do not include 100% of California properties, some cities in Tables 6.7 and 6.8 list some prototypes as not having any buildings mapped to them.

6.7.5.2 Site energy use

The energy intensity savings obtained for each prototype and BCZ as well as the total floor areas were applied to Equations 5.16 and 5.17 to calculate the citywide site energy impact over a 50-year period to match the 50-year cycle the pavement LCA tool is designed for.

Figure 6.13 plots for each city in case study 2, the absolute savings over 50 years per modified pavement area (Figure 6.13a) and as city total (Figure 6.13b). The direct cooling penalties are far less than the cooling benefits. Penalties range between 1.2 and 2.7 kWh per m^2 of modified pavement. The largest possible indirect savings happened in Anaheim, Riverside, and Los Angeles with 9.3 to 9.4 kWh/m^2. When considering the city total cooling savings, Los Angeles far dominates over all other cities due its large public pavement area, producing net (direct + indirect) cooling savings of $1{,}315\times10^6$ kWh. Other large cities like San Jose, San Diego, Sacramento, and Fresno produced net cooling savings that range between 118×10^6 and 256×10^6 kWh. Lancaster and Palm Springs were the cities with the smallest temperature reductions and the smallest modified area (4 to 4.5 km^2 of public pavement), thus they only experienced 9.9×10^6 (Lancaster) and 16×10^6 kWh (Palm Springs) of net cooling savings.

Figure 6.14 shows the gas heating savings in the same fashion as cooling energy savings were presented in Figure 6.13. However, the direct effects were dwarfed by the indirect effect. All cities experienced direct gas heating savings that ranged between 0.01 to 0.04 therm/m^2. On the other hand, the indirect penalties were as much as 0.51 therm/m^2 in Sacramento and 0.55 therm/m^2 in San Jose. When considering the city total gas heating changes, all cities experienced net penalties, ranging between 0.14×10^6 therm in Palm Springs to 47×10^6 therm in Los Angeles.

Figure 6.13 and Figure 6.14 demonstrate the highest possible site cooling savings and gas heating penalties that are obtainable under case study 2. Table 6.9 and Table 6.10 include a complete set of savings and penalties including those obtained from electric heating as well as the relative changes of all savings and penalties. The tables also show the cooling, gas heating, and electric heating changes under case study 1.

Due to the linear relationship of the energy changes to albedo changes, estimating the savings and penalties under case study 1 is very simple. The results per modified pavement area for case study 1 are obtained by multiplying the values in case study 2 by the ratio of

Table 6.7: Number of buildings, total floor area, fraction of buildings, and fraction of floor area attributed to each prototype in BCZs 4, 7, 8, 9, and 10.

City (BCZ)	Prototype	Number of buildings	Total floor area [m^2]	fraction of buildings [%]	fraction of floor area [%]
San Jose (4)	Single-family home	182648	29671670	77.2	66.7
	Apartment building	48090	11413061	20.3	25.6
	Large hotel	114	258667	0.0	0.6
	Large office	2111	1037768	0.9	2.3
	Medium office	3152	1579470	1.3	3.5
	Primary school	158	81575	0.1	0.2
	Fast-food restaurant	0	0	0.0	0.0
	Retail stand-alone	447	470556	0.2	1.1
	Strip mall retail	0	0	0.0	0.0
	Sit-down restaurant	0	0	0.0	0.0
San Diego (7)	Single-family home	208988	35343448	61.6	60.5
	Apartment building	120564	17166517	35.5	29.4
	Large hotel	879	375003	0.3	0.6
	Large office	0	0	0.0	0.0
	Medium office	1962	1013282	0.6	1.7
	Primary school	0	0	0.0	0.0
	Fast-food restaurant	0	0	0.0	0.0
	Retail stand-alone	115	182402	0.0	0.3
	Strip mall retail	5970	4066300	1.8	7.0
	Sit-down restaurant	665	259283	0.2	0.4
Anaheim (8)	Single-family home	51914	7254330	76.3	54.3
	Apartment building	13275	3167281	19.5	23.7
	Large hotel	0	0	0.0	0.0
	Large office	2	1300	0.0	0.0
	Medium office	2882	2925112	4.2	21.9
	Primary school	0	0	0.0	0.0
	Fast-food restaurant	0	0	0.0	0.0
	Retail stand-alone	0	0	0.0	0.0
	Strip mall retail	1	551	0.0	0.0
	Sit-down restaurant	0	0	0.0	0.0
Los Angeles (9)	Single-family home	275362	45530404	70.8	47.2
	Apartment building	91710	38504750	23.6	40.0
	Large hotel	1388	1223986	0.4	1.3
	Large office	3699	2261120	1.0	2.3
	Medium office	7160	3727395	1.8	3.9
	Primary school	830	689481	0.2	0.7
	Fast-food restaurant	2	612	0.0	0.0
	Retail stand-alone	350	381447	0.1	0.4
	Strip mall retail	7261	3589683	1.9	3.7
	Sit-down restaurant	1431	461927	0.4	0.5
Riverside (10)	Single-family home	88955	14659324	87.5	88.7
	Apartment building	8053	1166385	7.9	7.1
	Large hotel	0	0	0.0	0.0
	Large office	0	0	0.0	0.0
	Medium office	4643	708058	4.6	4.3
	Primary school	0	0	0.0	0.0
	Fast-food restaurant	0	0	0.0	0.0
	Retail stand-alone	0	0	0.0	0.0
	Strip mall retail	1	551	0.0	0.0
	Sit-down restaurant	0	0	0.0	0.0

Table 6.8: Number of buildings, total floor area, fraction of buildings, and fraction of floor area attributed to each prototype in BCZs 12, 13, 14, and 15.

City (BCZ)	Prototype	Number of buildings	Total floor area [m^2]	fraction of buildings [%]	fraction of floor area [%]
Sacramento (12)	Single-family home	202567	24483741	89.5	80.4
	Apartment building	11946	1204071	5.3	4.0
	Large hotel	299	74126	0.1	0.2
	Large office	2194	301323	1.0	1.0
	Medium office	6339	3338117	2.8	11.0
	Primary school	422	30806	0.2	0.1
	Fast-food restaurant	0	0	0.0	0.0
	Retail stand-alone	187	203593	0.1	0.7
	Strip mall retail	1899	605842	0.8	2.0
	Sit-down restaurant	581	196901	0.3	0.6
Fresno (13)	Single-family home	128265	20261473	88.1	78.5
	Apartment building	12989	2529599	8.9	9.8
	Large hotel	131	194159	0.1	0.8
	Large office	1525	1040431	1.0	4.0
	Medium office	541	326589	0.4	1.3
	Primary school	107	96279	0.1	0.4
	Fast-food restaurant	0	0	0.0	0.0
	Retail stand-alone	207	78946	0.1	0.3
	Strip mall retail	1476	1131321	1.0	4.4
	Sit-down restaurant	371	139125	0.3	0.5
Lancaster (14)	Single-family home	44950	7735208	93.7	82.6
	Apartment building	1973	949958	4.1	10.1
	Large hotel	62	72882	0.1	0.8
	Large office	311	176583	0.6	1.9
	Medium office	188	82816	0.4	0.9
	Primary school	22	19056	0.0	0.2
	Fast-food restaurant	0	0	0.0	0.0
	Retail stand-alone	14	14039	0.0	0.1
	Strip mall retail	340	278736	0.7	3.0
	Sit-down restaurant	89	30936	0.2	0.3
Palm Springs (15)	Single-family home	14998	2819430	30.7	38.4
	Apartment building	32239	4177131	66.0	56.9
	Large hotel	0	0	0.0	0.0
	Large office	0	0	0.0	0.0
	Medium office	1576	339943	3.2	4.6
	Primary school	0	0	0.0	0.0
	Fast-food restaurant	0	0	0.0	0.0
	Retail stand-alone	0	0	0.0	0.0
	Strip mall retail	0	0	0.0	0.0
	Sit-down restaurant	0	0	0.0	0.0

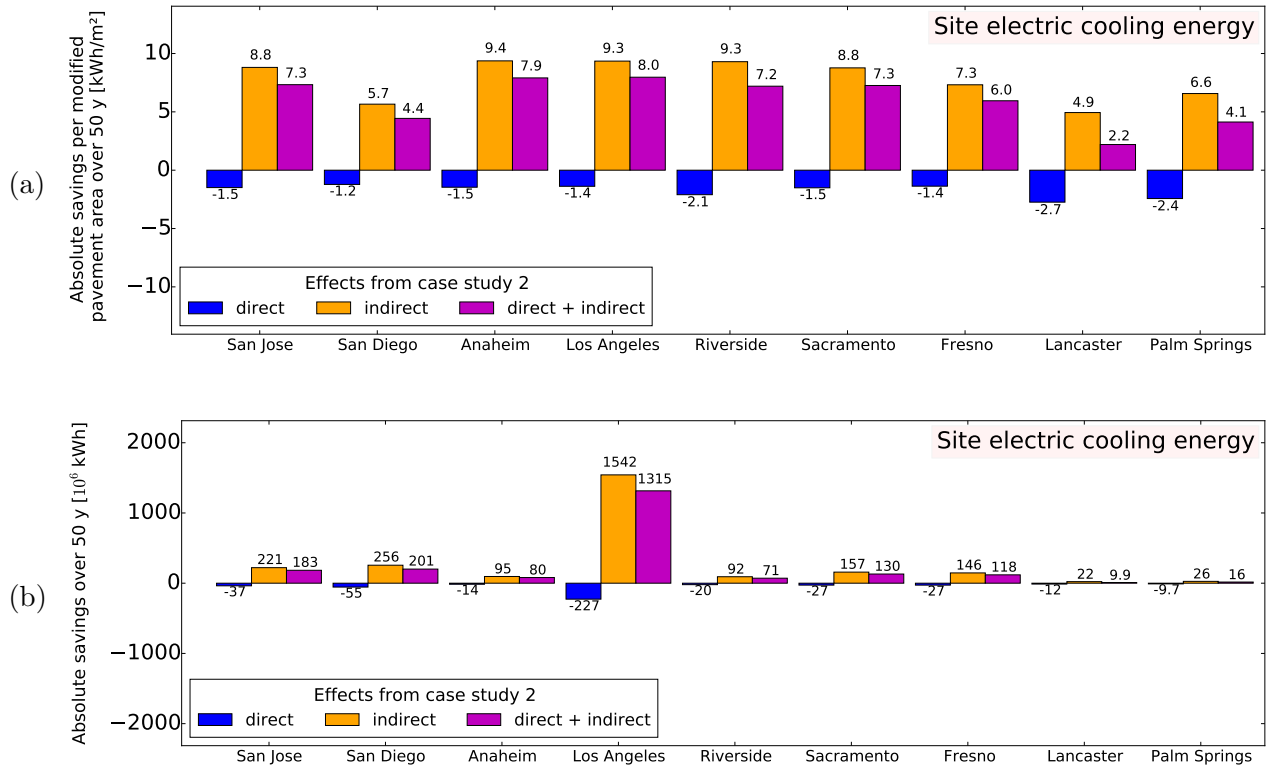

Figure 6.13: Absolute cooling savings over 50 years a) per modified pavement area and b) as city total, for each city in case study 2.

albedo change of case study 1 to albedo change of case study 2 (0.13 / 0.20 = 0.65). To obtain the citywide absolute changes and the relative changes for case study 1, the ratio of albedo changes is multiplied by the ratio of fraction of city pavement modified (0.65 × [0.50 / 1.00] = 0.33).

Since cooling required electric energy and heating required mainly gas energy, the total conditioning (cooling + heating) impact can be adequately compared by converting all energies to Primary Energy Demand, PED, which will be covered in the following section (Section 6.7.5.3).

6.7.5.3 Life-cycle impacts

This section continues to examine the 50-year impact of case study 2, particularly using the LCA metrics listed in Section 5.7 (PED, GWP, and Smog Potential) The site energy changes are converted to these life-cycle impacts using the factors in Table 5.14 with Equation 5.18. The 50-year impact under case study 1 can be obtain once again by multiplying the case study 2 results by the corresponding factors (0.65 for results per unit of pavement and 0.33 for citywide results and relative results).

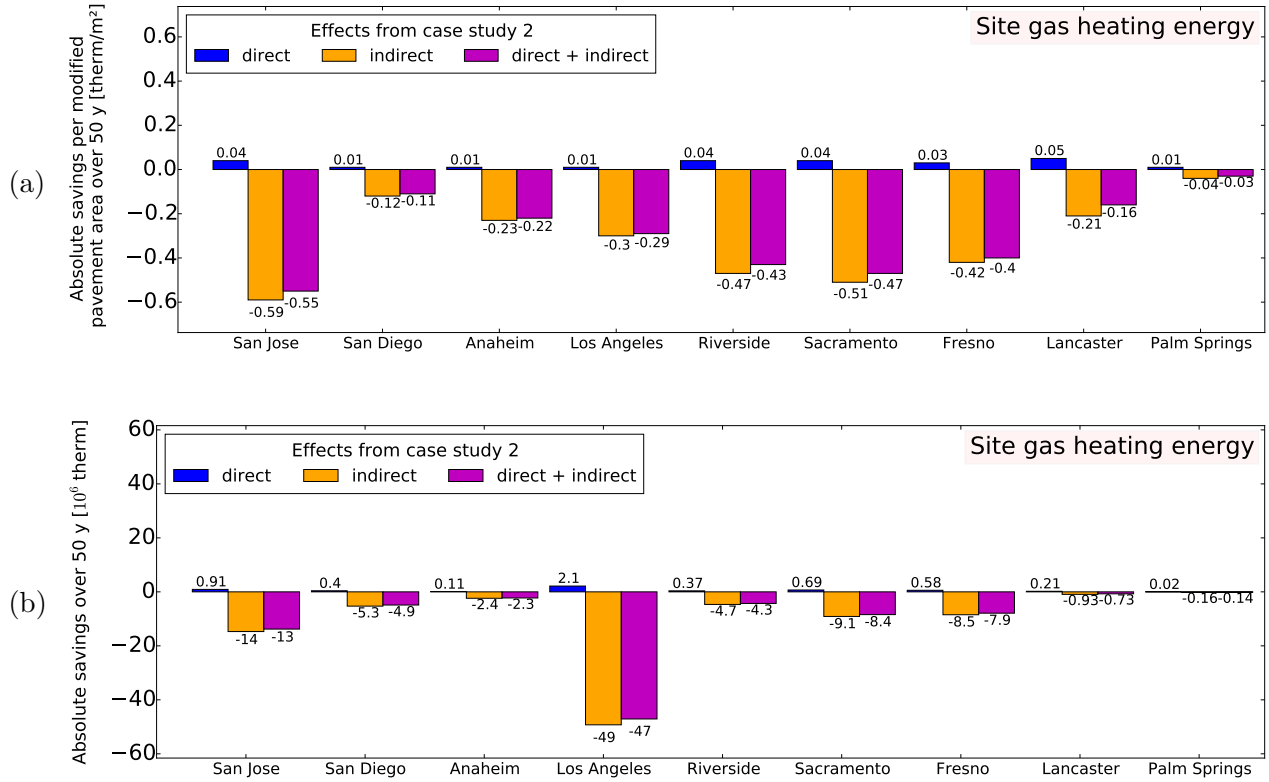

Figure 6.14: Absolute gas heating savings over 50 years a) per modified pavement area and b) as city total, for each city in case study 2.

Table 6.9: Citywide site absolute savings per modified pavement area.

Case study	City	Citywide site absolute savings per modified pavement area								
		Electric cooling [kWh/m^2]			Electric heating [kWh/m^2]			Gas heating [therm/m^2]		
		Direct	Indirect	Direct + indirect	Direct	Indirect	Direct + indirect	Direct	Indirect	Direct + indirect
1	San Jose	-0.97	5.73	4.76	-0.04	-0.87	-0.91	0.02	-0.38	-0.36
	San Diego	-0.79	3.68	2.89	0.01	-0.27	-0.27	0.01	-0.08	-0.07
	Anaheim	-0.95	6.09	5.14	-0.07	-1.04	-1.11	0.01	-0.15	-0.14
	Los Angeles	-0.90	6.08	5.18	-0.02	-0.70	-0.71	0.01	-0.19	-0.19
	Riverside	-1.37	6.04	4.68	-0.03	-0.68	-0.71	0.02	-0.31	-0.28
	Sacramento	-0.98	5.70	4.72	0.02	-1.05	-1.03	0.03	-0.33	-0.31
	Fresno	-0.89	4.76	3.87	0.00	-0.64	-0.65	0.02	-0.28	-0.26
	Lancaster	-1.78	3.21	1.43	0.00	-0.30	-0.30	0.03	-0.14	-0.10
	Palm Springs	-1.58	4.27	2.69	-0.01	-0.12	-0.12	0.00	-0.03	-0.02
2	San Jose	-1.49	8.81	7.33	-0.06	-1.34	-1.40	0.04	-0.59	-0.55
	San Diego	-1.22	5.66	4.44	0.01	-0.42	-0.41	0.01	-0.12	-0.11
	Anaheim	-1.46	9.37	7.91	-0.11	-1.60	-1.71	0.01	-0.23	-0.22
	Los Angeles	-1.38	9.35	7.97	-0.02	-1.07	-1.09	0.01	-0.30	-0.29
	Riverside	-2.10	9.30	7.20	-0.05	-1.05	-1.10	0.04	-0.47	-0.43
	Sacramento	-1.51	8.77	7.26	0.03	-1.62	-1.59	0.04	-0.51	-0.47
	Fresno	-1.37	7.32	5.95	0.00	-0.99	-0.99	0.03	-0.42	-0.40
	Lancaster	-2.74	4.94	2.20	0.00	-0.46	-0.46	0.05	-0.21	-0.16
	Palm Springs	-2.43	6.57	4.13	-0.01	-0.18	-0.19	0.01	-0.04	-0.03

Table 6.10: Citywide site absolute and relative savings.

Case study	City	Citywide site absolute savings (relative savings)								
		Electric cooling [10^6 kWh (%)]			Electric heating [10^6 kWh (%)]			Gas heating [10^6 therm (%)]		
		Direct	Indirect	Direct + indirect	Direct	Indirect	Direct + indirect	Direct	Indirect	Direct + indirect
1	San Jose	-12.1 (-0.02)	71.9 (0.10)	59.8 (0.08)	-0.50 (-0.01)	-10.9 (-0.48)	-11.4 (-0.49)	0.30 (0.07)	-4.79 (-1.18)	-4.50 (-1.11)
	San Diego	-17.9 (-0.02)	83.3 (0.06)	65.3 (0.04)	0.10 (0.09)	-6.10 (-1.89)	-6.00 (-1.80)	0.13 (0.67)	-1.73 (-11.5)	-1.59 (-10.8)
	Anaheim	-4.90 (-0.01)	31.1 (0.03)	26.2 (0.03)	-0.40 (0.00)	-5.30 (-0.59)	-5.70 (-0.59)	0.04 (0.21)	-0.77 (-5.28)	-0.74 (-5.07)
	Los Angeles	-73.9 (-0.01)	501 (0.07)	427 (0.06)	-1.20 (0.00)	-57.3 (-1.71)	-58.5 (-1.70)	0.70 (0.30)	-16.0 (-7.78)	-15.3 (-7.48)
	Riverside	-6.80 (-0.01)	29.9 (0.03)	23.2 (0.02)	-0.20 (-0.02)	-3.40 (-0.39)	-3.50 (-0.41)	0.12 (0.10)	-1.52 (-0.93)	-1.40 (-0.83)
	Sacramento	-8.80 (-0.01)	51.3 (0.03)	42.5 (0.03)	0.20 (0.02)	-9.50 (-0.16)	-9.30 (-0.15)	0.22 (0.09)	-2.97 (-0.72)	-2.74 (-0.63)
	Fresno	-8.90 (0.00)	47.6 (0.02)	38.7 (0.01)	0.00 (0.00)	-6.40 (-0.25)	-6.50 (-0.25)	0.19 (0.06)	-2.76 (-0.79)	-2.58 (-0.73)
	Lancaster	-4.00 (0.00)	7.20 (0.01)	3.20 (0.00)	0.00 (0.00)	-0.70 (-0.09)	-0.70 (-0.09)	0.07 (0.06)	-0.30 (-0.25)	-0.23 (-0.19)
	Palm Springs	-3.20 (0.00)	8.50 (0.00)	5.40 (0.00)	0.00 (0.02)	-0.20 (-1.12)	-0.20 (-1.10)	0.01 (1.29)	-0.05 (-5.60)	-0.04 (-4.61)
2	San Jose	-37.3 (-0.05)	221 (0.30)	184 (0.24)	-1.50 (-0.03)	-33.7 (-1.47)	-35.2 (-1.50)	0.91 (0.21)	-14.7 (-3.63)	-13.8 (-3.42)
	San Diego	-55.2 (-0.05)	256 (0.19)	201 (0.14)	0.30 (0.29)	-18.8 (-5.83)	-18.5 (-5.54)	0.40 (2.11)	-5.29 (-35.0)	-4.88 (-32.8)
	Anaheim	-14.9 (-0.02)	95.6 (0.10)	80.6 (0.08)	-1.10 (0.00)	-16.3 (-1.83)	-17.4 (-1.83)	0.11 (0.64)	-2.38 (-16.3)	-2.27 (-15.6)
	Los Angeles	-227 (-0.04)	1540 (0.21)	1320 (0.17)	-3.80 (0.01)	-176 (-5.25)	-180 (-5.25)	2.15 (0.92)	-49.3 (-23.9)	-47.1 (-23.0)
	Riverside	-20.8 (-0.02)	92 (0.09)	71.3 (0.07)	-0.50 (-0.05)	-10.4 (-1.21)	-10.8 (-1.26)	0.37 (0.32)	-4.66 (-2.70)	-4.29 (-2.38)
	Sacramento	-27.2 (-0.02)	158 (0.10)	131 (0.08)	0.60 (0.05)	-29.2 (-0.50)	-28.6 (-0.45)	0.69 (0.27)	-9.11 (-2.17)	-8.43 (-1.90)
	Fresno	-27.5 (-0.01)	146 (0.05)	118.9 (0.04)	0.00 (0.00)	-19.8 (-0.76)	-19.9 (-0.76)	0.58 (0.18)	-8.48 (-2.42)	-7.90 (-2.24)
	Lancaster	-12.3 (-0.01)	22.2 (0.02)	9.90 (0.01)	0.00 (0.00)	-2.10 (-0.29)	-2.10 (-0.29)	0.21 (0.17)	-0.93 (-0.76)	-0.73 (-0.59)
	Palm Springs	-9.70 (0.00)	26.3 (0.01)	16.5 (0.01)	0.00 (0.07)	-0.70 (-3.47)	-0.70 (-3.40)	0.02 (3.17)	-0.16 (-16.6)	-0.14 (-13.3)

Figure 6.15 presents for case study 2, the Primary Energy Demand, PED, savings and penalties obtained in each city from cooling and heating (PED from heating includes electric and gas heating). These plots are helpful for comparing cooling energy versus heating energy. Figure 6.15a shows that in all cities, the cooling PED savings are greater than the heating PED penalties. However, conditioning (cooling + heating) savings were small. Lancaster experienced a conditioning (cooling + heating) saving of only 4.69 MJ per m^2 of modified pavement area. The largest conditioning savings were in Palm Springs (45 MJ/m^2), Anaheim (53 MJ/m^2), and Los Angeles (56 MJ/m^2). San Diego and Palm Springs were the only cities in which the cooling benefits were substantially greater than the heating penalty. These two cities are characterized by having mild and short winters requiring lesser heating demand compared to the other cities.

When considering the total absolute changes in each city, Los Angeles dwarfs again the results of every other city; it experienced a conditioning PED saving of 9.3×10^9 MJ (Figure 6.15b). The plot includes the temperature change at 15:00 LST during winter and summer. The large temperature decrease in Los Angeles – as a result of the large modified pavement area and high urban density – is the reason the city has the largest cooling, heating, and conditioning PED savings.

Figure 6.15c shows the relative PED savings and penalties for each city. The largest conditioning saving in PED is 0.60% (Los Angeles). In the other cities, the conditioning savings are at most only 0.30%, and goes down even to zero (Lancaster).

The Global Warming Potential (GWP) savings over 50 years are plotted in Figure 6.16. In this case, only San Diego, Anaheim, Los Angeles, and Palm Springs experienced conditioning savings in GWP. These are the cities with the fewest heating degree days (Figure 6.7). In the other cities, GWP penalties from heating are greater than the cooling GWP savings. San Jose had the largest conditioning GWP penalties per modified pavement area with 1.37 kg CO_2e/m^2, followed by Sacramento with a penalty of 1.00 kg CO_2e/m^2 (Figure 6.16a). When considering the total GWP change in each city, Los Angeles experienced the largest conditioning GWP savings with 124×10^6 kg CO_2e, which is more than 3 times greater than the next largest conditioning GWP saving—San Diego with 38×10^6 kg CO_2e (Figure 6.16b). The largest net penalty was in San Jose with 34×10^6 kg CO_2e. The relative savings for GWP are not plotted in Figure 6.16 but are very similar to PED. The relative GWP saving in Los Angeles was 0.30%; the penalty in San Jose was 0.20%.

Figure 6.17 plots the Smog Potential savings and penalties over 50 years for each city. The only city having conditioning Smog Potential penalty is San Jose with 0.01 kg O_3e/m^2 per modified pavement area (Figure 6.17a) and citywide total of 0.1×10^6 kg O_3e (Figure 6.17b). Once more, Los Angeles dominates all other cities in conditioning savings with 0.01 kg O_3e/m^2 per modified area and city total of 7.5×10^6 kg O_3e. The relative savings for Smog Potential are not plotted in Figure 6.17 but are also similar to PED. The relative Smog

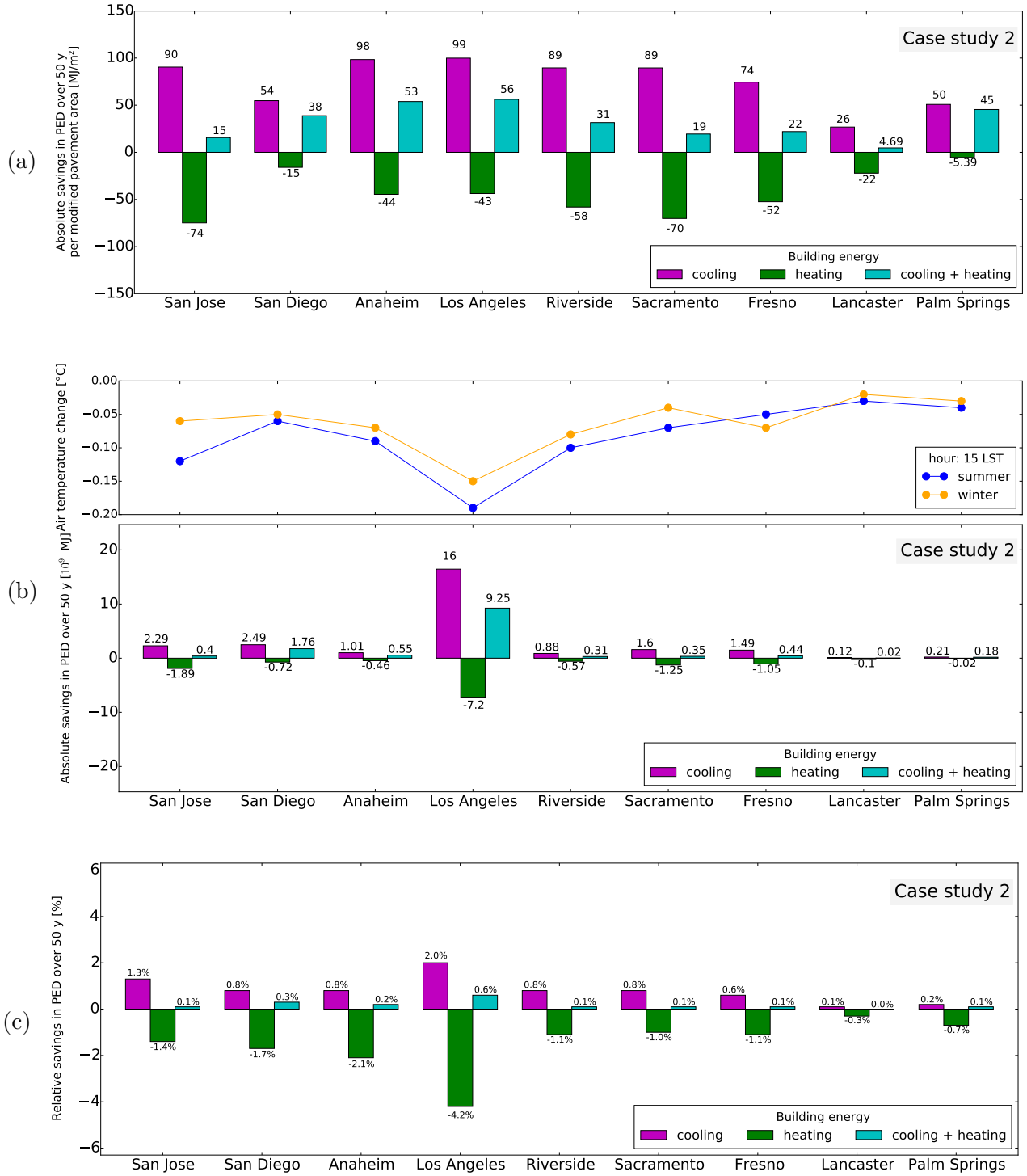

Figure 6.15: Primary Energy Demand savings over 50 years a) per modified pavement area, b) as city total, and c) as relative savings, for each city in case study 2.

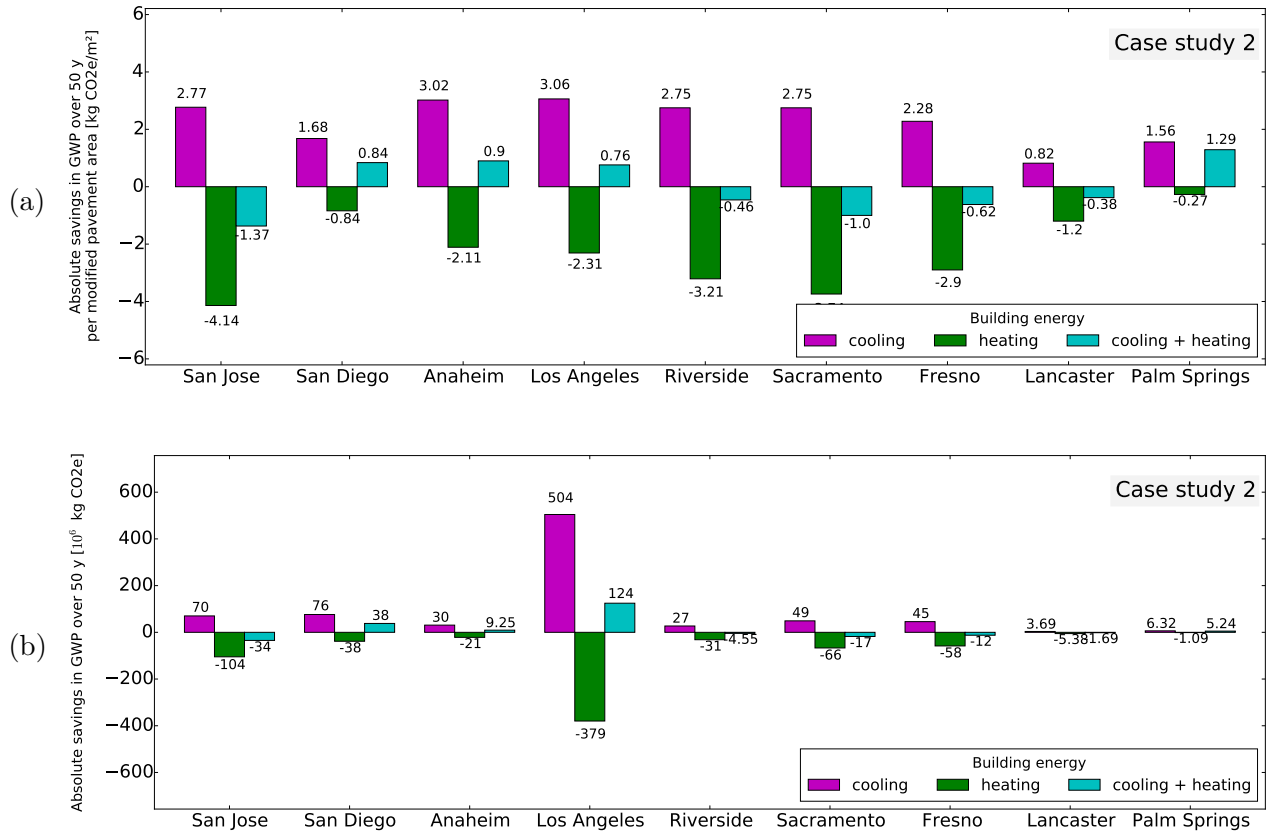

Figure 6.16: Global Warming Potential savings over 50 years a) per modified pavement area and b) as city total, for each city in case study 2.

Potential saving in Los Angeles was 0.50%; the other cities had relative savings not greater than 0.20%.

6.8 Summary and discussion

This chapter utilized the simulation results of 10 building prototypes to investigate the energy and environmental impacts during the use phase of cool pavements. Electric cooling and gas heating were the energy uses affected the most. Electric heating changed proportional to gas heating. However, the magnitudes of electric heating change were much smaller than changes from electric cooling.

In the case of lighting energy, only the two offices and the primary school prototypes had lighting change with local road albedo, but the changes were negligible compared to the other energy changes.

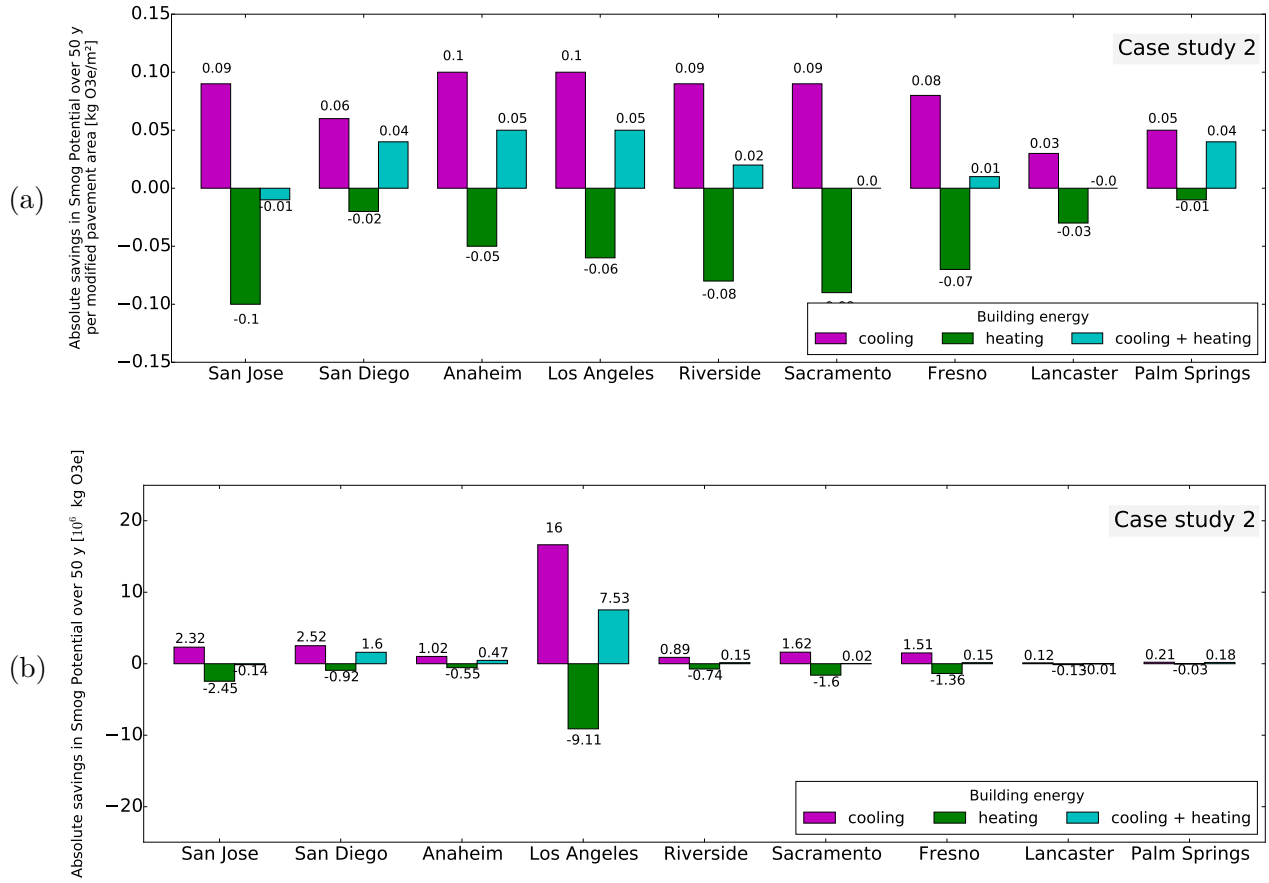

Figure 6.17: Smog Potential savings over 50 years a) per modified pavement area and b) as city total, for each city in case study 2.

6.8.1 Direct effect and indirect effect

The direct effect of cool pavements depends on the view factor from the building to the local roads. The view factor increases with building height, road width, and proximity of the road to the building. In addition to building-to-road view factor, other geometrical and building-related parameters that influence the direct effect are the window-to-wall ratio, wall-to-floor area ratio, and HVAC thermostat settings. Given these and other influential parameters, it would be very challenging to precisely predict the direct effect of a cool pavement on any specific building. However, it was proven that the building-to-road view factor and window-to-wall ratio can be combined to generate climate-specific linear relationships to predict the direct effect.

As expected, the prototypes with the largest building-to-road view factor had the largest direct effect. Even then, the direct effect was always overshadowed by the indirect effect, which dominated the cooling as well as the heating energy changes. Indirect cooling and

heating intensities were smallest in the residential buildings. As a result, the single-family home and apartment building had the smallest net (direct + indirect) cooling intensity savings and heating intensity penalties.

6.8.2 Temperature reductions

Although the warmest time of the day is usually between 14:00 to 15:00 LST, the temperature reductions peaked between 16:00 and 20:00 LST in the majority of BCZs and seasons. The peak power demand occurs during these late afternoon hours during which residential power demand is high and daytime cooling demand in commercial buildings is decreasing.

6.8.3 California building stock

Residential buildings strongly dominate the building stock in all of the evaluated cities, comprising between 94 to 98% of all city buildings (78 to 96% of city floor area). With such a large fraction, the cool pavement effects on residential buildings dominate the citywide effects.

To compare, consider the cool house used in the cool roof study (Chapter 3). The floor area of the cool house was 188 m^2 and was located in Fresno (BCZ 13). Assuming case study 2 and that the cool house sees modify road, the annual site cooling savings would be 5.6 kWh and the gas heating penalties would be 1 therm. Assuming the cool house does not see a modified road, the annual site cooling savings under case study 2 would increase by 10 kWh and gas heating penalties increase by 0.2 therm. In contrast, the annual savings from the cool roof were 530 kWh for cooling and 7.3 therm for heating. Thus the cooling savings from cool pavements would be 1% of the cool roof savings if seeing modified road and 3% if not; in heating, the cool roof yielded savings while the cool pavements yielded small penalties.

6.8.4 Citywide energy and environmental impacts

With a total pavement area of 266 km^2 and 62% of it being public pavement, Los Angeles experienced by far the largest air temperature reduction, which yielded the largest net indirect effect. The net (direct + indirect) citywide site electric cooling savings in case study 2 were 1,315 GWh (0.17%) and the electric heating penalties were 180 GWh (5.25%). For gas heating, the net penalties were 47×10^6 therm (23%). Results for case study 1 were only 33% of case study 2. Los Angeles experiences only about 1,000 heating degree days a year, which results in low heating energy demand. Thus the relative heating penalties were high because of the small base heating energy.

Annually, the electric (cooling + heating) savings in Los Angeles for case study 2 were 22.7 GWh. In 2014, approximately 175 small hydro power plants produced energy in California,

with an average annual generation of 16 GWh [100]. Thus the annual electric savings in Los Angeles is comparable to the energy generated over a year by an average-sized small hydro power plant.

Converting the results to Primary Energy Demand allows comparing cooling with heating (gas and electric) changes. Los Angeles experienced net PED 50-year savings of 3.05×10^9 MJ (0.20%) for case study 1 and 9.25×10^9 MJ (0.60%) for case study 2. While these savings in Los Angeles dwarfed the citywide results in the other 8 cities, they constitute a very small percent of the city's conditioning energy.

The two life-cycle impact metrics investigated were the GWP and Smog Potential. However, the two case studies had a very small impact on these two metrics, saving less than 1% for each one. The maximum savings (case study 2) were 124×10^6 kg CO_2e of GWP and 7.53×10^6 kg O_3e of Smog Potential. For the case of GWP, only four cities experienced net savings (San Diego, Anaheim, Riverside, and Palm Springs). The remaining five cities experienced net penalties—San Jose had the largest penalty with a GWP increase of 0.20%.

With the exception of Los Angeles, the average total fraction of city pavement that is public is 30%. Thus the temperature reductions in these other eight cities were much less than in Los Angeles, leading to even smaller indirect effects and net savings. Hence, the results for Los Angeles represent the largest savings obtainable in a California city under a scenario like case study 1 or 2. However, this study indicated that savings increased with fraction of pavement modified. Hence, modifying a larger portion of a city's pavement (public + pavement) would result in greater savings.

From what has been discussed thus far, it can be concluded that a major reason HVAC savings from cool pavements are so small is that the building stock in all cities is dominated by residential buildings, which are the building types affected the least by the indirect effect. Additionally, the indirect effect is generally greater than the direct effect; although the indirect effect causes cooling savings, it will also yield heating penalties.

CHAPTER 7

Conclusions

Several questions were posed at the beginning of this dissertation: (a) what are the annual benefits or penalties of a cool tile roof over a dark shingle roof; (b) can the results from urban climate simulations be adjusted to values obtained from realistic urban geometries; and (c) what are the building-specific and citywide effects of cool pavements on cooling, heating, and lighting energy use.

The short answers are: (a) the cool tile roof provided energy savings during the cooling as well as the heating season, which translated to peak-power cooling demand reductions and emission reductions; (b) a simple urban canyon model was developed, which proved how canyon albedo is dependent on geometry; and (c) cool pavements had a small building energy impact and the indirect effect predominated over the direct effect, leading to small annual net savings in most building types and in all cities.

7.1 Benefits of a cool tile roof over standard dark roof

Cool-roof energy savings in the cooling and heating seasons were computed two ways. Method A divides by HVAC efficiency the difference (standard – cool) in ceiling + duct heat gain. Method B measures the difference in HVAC energy use, corrected for differences in plug and window heat gains. Methods A and B agreed extremely well during the cooling season, proving that a simplified experimental configuration without power meters (Method A) can be used in future cool roof experiments.

Fractional annual cooling energy savings (26%) were 2.6 times the 10% daily cooling energy savings measured in a previous study that used a white coating to increase the albedo of an asphalt shingle roof by the same amount (0.44). Fractional peak-hour cooling power demand savings (37%) were 2.3 times the 16% savings observed in the earlier study. The improved cooling energy savings (26% vs. 10%) may be attributed to the cool tile's above-sheathing ventilation, rather than to its high thermal mass.

Previous studies which researched the annual effects from simply increasing roof albedo, reported heating penalties during the heating season. However, the cool tile roof yielded fractional annual gas heating savings of 4% and electric heating savings of 3%. The slightly positive fractional annual heating energy savings likely resulted from the tile roof's high thermal capacitance, which increased the overnight temperature of the attic air. Thus cool tile roofs should be perceived as a technology that provides energy and environmental benefits during the cooling season as well as the heating season.

7.2 Building-specific and citywide impacts of cool pavements

Increasing the local road albedo around a building will have a small direct effect on a building's energy, causing cooling demand to increase and heating demand to decrease. This direct effect is proportional to the building-to-road view factor and window-to-wall ratio; the HVAC thermostat schedule is another major parameter affecting the direct effect. The direct effect had the greatest impact on the residential prototypes—increasing the local road albedo by 0.20 had the largest direct effect in the single-family home of BCZ 7, causing a cooling penalty of 1.7% and a gas heating saving of 0.60%.

The indirect effect from a citywide adoption of cool pavements generally caused an opposite and greater energy impact than the direct effect. The indirect effect is proportional to the temperature reduction induced by citywide cool pavements, which in turn is proportional to the area of modified pavement. The residential buildings experienced less base cooling power demand by floor area compared to the commercial buildings, which caused them to have the smallest indirect cooling savings. As a result, the residential buildings had the smallest net (direct + indirect) cooling savings by floor area. However, heating power demand by floor area in the residential buildings is comparable to the demand in commercial buildings, yielding similar indirect heating penalties between residential and commercial buildings.

Residential buildings strongly dominate the building stock in all of the evaluated cities, having a strong influence on the citywide impact of cool pavements. Therefore, even though most cities yielded conditioning (cooling + heating) energy savings, they were small due to the minuscule net savings from the residential buildings. In the case of Global Warming Potential (GWP), only four cities (San Diego, Anaheim, Los Angeles, and Palm Springs) experienced small but positive savings. These four cities are characterized by having mild winters with small heating demand. The other five cities experienced net GWP penalties. Hence, cities with long heating seasons throughout the year may experience GWP penalties from the increased demand for heating from the indirect effect of cool pavements.

It is also worth noting that since the indirect effect dominates the direct effect, modifying

a larger fraction of a city's paved surface than the areas modified in this study, will likely result in slightly greater net energy savings.

7.3 Merits of the urban canyon model

7.3.1 Strengths

The model presented in Chapter 4 has several attractive features. First, it is a simple method that can be converted to run with any programming language. Second, the ability to individually characterize the dimension and albedo of each canyon surface type (walls, road, and setbacks), allows the user to define realistic canyon geometries.

The application of the proposed model is not limited to canyon roads, but can also be applied to similar studies that explore the impact from changing the albedo of other surfaces from the canyon floor. Finally, the simplicity and adaptability of the tool allows it to be used as a stand-alone tool in a similar fashion as employed in this dissertation, or it can be incorporated into other more complex urban canyon models.

7.3.2 Weaknesses

Simplicity came with a small price. First, in reality, the solar radiation entering a canyon is reflected multiple times between surfaces. The model only considers the first two reflections. However, the amount of radiation reflected each time is only a small fraction of the previous reflection, especially for low surface albedos. Thus considering the first two surface reflections is a great approximation to the canyon reflections. Another shortcoming is that when the sun is low in the sky, a canyon wall may partially shade the other wall. The model currently treats partially shaded walls as fully shaded.

Another shortcoming is that the model treats partially shaded walls as fully shaded. In reality, one wall may partially shade the other, thus the solar radiation reflected from the wall is greater under these circumstances. However, this usually happens during the hours when solar radiation is low.

Finally, a canyon may have an orientation other than north-south or east-west.

7.4 Directions for future research

Some of the topics investigated in this dissertation deserve further research:

1. **Improvements to the urban canyon tool.** Enhance the tool by considering the partial shadow of the canyon walls. By improving how the walls are treated, the tool

can then be used to assess the changes in canyon albedo from changes in wall albedo. The next version of the tool will also be able to handle any canyon orientation.

2. **Better represent actual vintage of a building stock.** Although the building prototypes were simulated following construction standards of 2008, the most common period of construction of California's current building stock is between 1970 and 1979. Older buildings were designed with inferior standards on wall insulation, window properties, and HVAC efficiencies, affecting the impact from the direct and indirect effects of cool pavements. Future work should simulate old vintage prototypes.

3. **Explore further the direct effects of pavements.** Neighbouring buildings are not the only external urban surfaces that may alter the direct effect of pavements. The presence of trees and vehicles may affect the solar irradiation striking the pavements as well as the pavement-reflected sunlight incident on walls and windows. Additionally, buildings usually have private pavements in one or more of its sides. Future building simulations should address the influence of other shading surfaces (i.e. trees and cars) and of private pavements.

4. **Consider all urban pavements.** Evaluate the net impact of modifying public as well as private pavements.

5. **Life-cycle impact of pavements.** This dissertation investigated the impact of pavements during their use phase. The results need to be integrated to the pavement LCA decision tool to assess the life-cycle energy and environmental impact of deploying higher-albedo pavement materials instead of business-as-usual pavement practices.

Appendix A

HVAC Operation Patterns

Figure B.1 shows HVAC fan power demand in the standard and cool houses on sunny summer and winter days. The difference (standard – cool) in attic air temperature is overlaid on each graph because difference in attic air temperature drives differences in ceiling and duct heat gains.

On the summer day, the HVAC systems (cooling) are completely off from about 22:30 LST (late night) to 11:30 LST (just before noon),and cycle on/off at other times. On the winter day, the HVAC systems (heating) are completely off from 23:00 LST (late at night) to 05:30–06:00 LST (early morning), from 07:00 to 09:00 LST (mid-morning), and from 11:00 to 20:30–22:00 LST (late morning to late night), running continuously for about 1.5 h in the

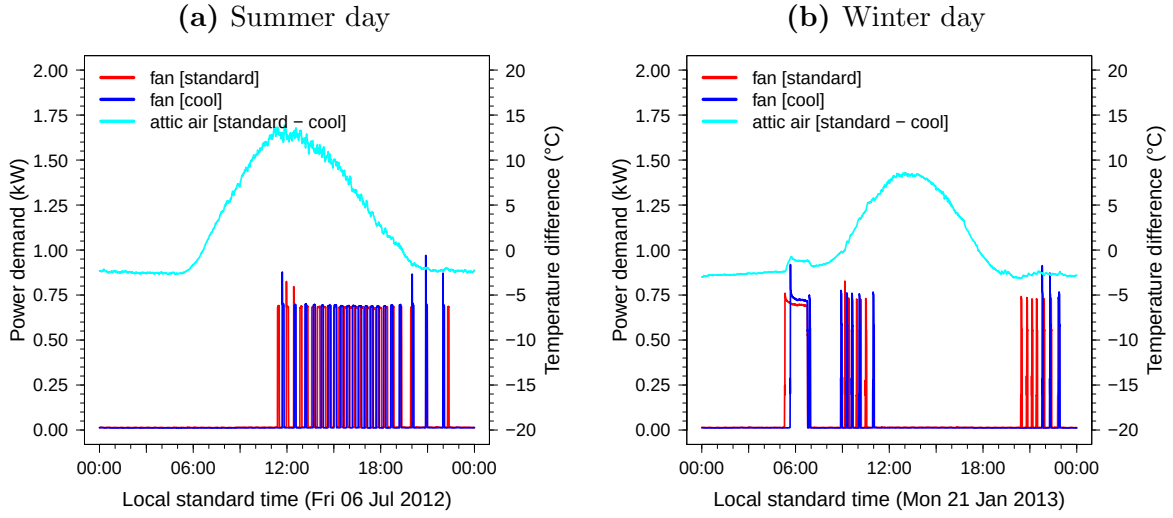

Figure A.1: HVAC fan power demand on the summer day and the winter day.

early morning and cycling on/off for another 4–5 h in the mid-morning and late evening.

The HVAC performance observed on the summer day supports the premise of including all hours of day when integrating cooling power savings, because the period of non-operation in which there is a substantial difference in attic air temperature (about 08:00–11:00 LST) is immediately followed by about 7 h of operation. The winter-day HVAC operation suggests that including all hours of day when integrating heating power savings may over-estimate the heating energy penalty, because the primary heating period (early morning, following the nighttime setback of the thermostat) begins about 10 h after the attic air temperature difference falls to a small nighttime value.

Appendix B

Differences Between North and South Side Building Temperatures

On a clear summer day, the south face of the roof receives less direct solar irradiance than the north face in the early morning and early evening, but more in the middle of the day. On a clear winter day, the south face roof receives more direct irradiance throughout the day (see Section 3.3.3).

Figure B.1 shows the temperature differences between the south and north sides of the standard home on sunny summer and winter days. On the summer day, the difference (south north) was about 5 to +6°C at the roof top, 3 to +4°C at the roof bottom, 1to +1°C at the attic air, and 0 to 2°C at the attic floor.

On the winter day, roof top and roof bottom differences were much larger, ranging from 1 to +24°C at the roof top and 0 to 13Cat the roof bottom. Winter-day attic air temperature differences were close to zero. The southnorth attic floor temperature differences on that day were up to 4°C because the south-side attic floor temperature sensor was close to a supply register, while its north-side counterpart was not. (Proximity to a supply register has little effect on attic floor temperature in summer, when the cold supply air falls, but strong influence in winter, when the warm supply air rises.)

Similar results were observed in the cool home on the summer and winter days (Figure B.2).

The north and south side temperature measurements suggest that (a) as expected, it is important to measure roof top and roof bottom temperatures on all faces of a sloped roof; (b) while good practice, measuring attic air and attic floor temperatures at more than one point is not strictly necessary; and (c) attic floor temperature sensors should be placed away from supply registers.

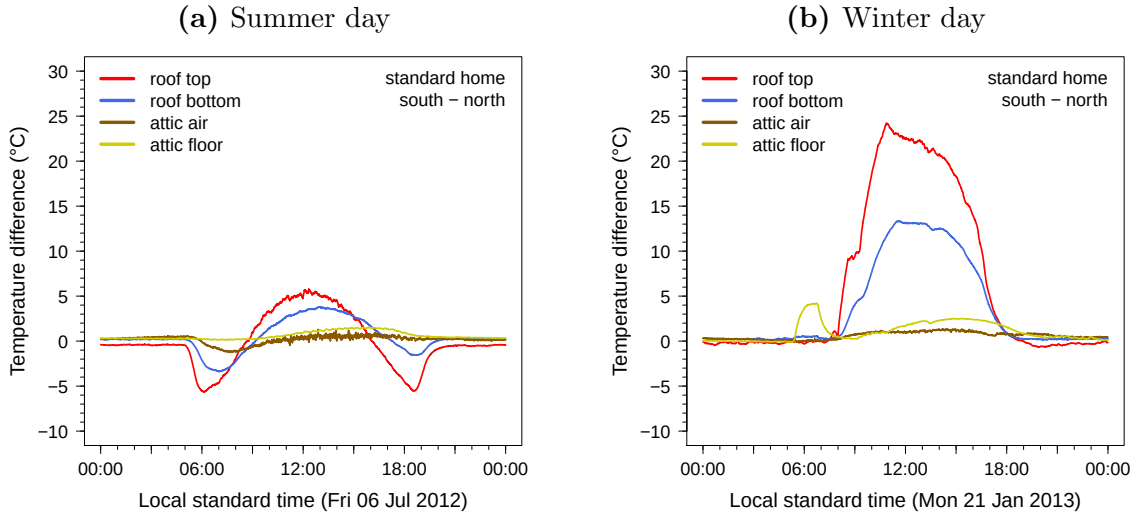

Figure B.1: Roof top, roof bottom, attic air, and attic floor temperature differences between south and north sides of the standard home on (a) the summer day and (b) the winter day. As expected, it is important to measure roof top and roof bottom temperatures on all faces of a sloped roof.

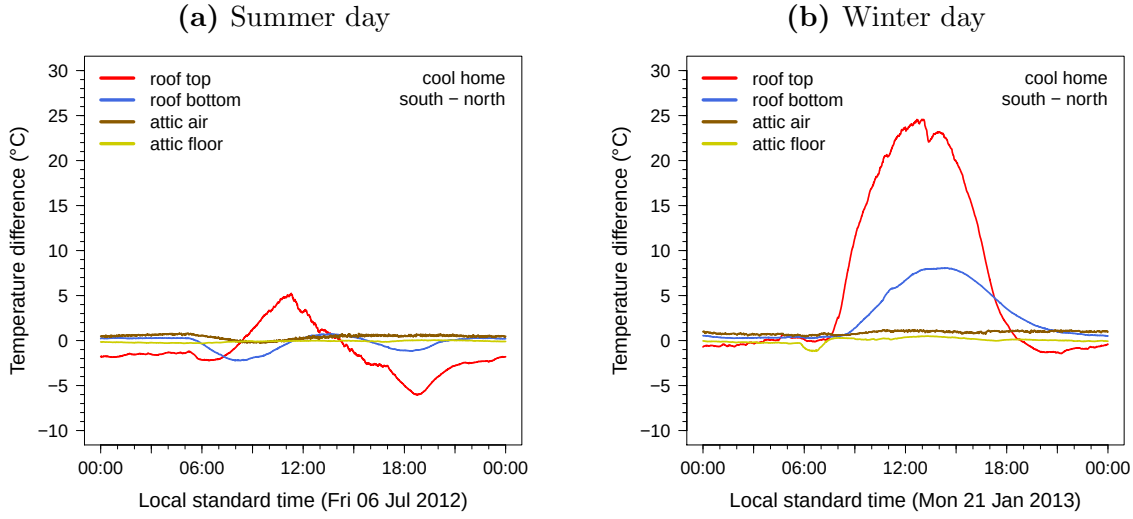

Figure B.2: Roof top, roof bottom, attic air, and attic floor temperature differences between south and north sides of the cool home on (a) the summer day and (b) the winter day.

Appendix C

Prototype Schematics

Table C.2 shows schematics of the 10 modified building energy model prototypes. The vertical purple surfaces represent the wall of a neighboring building of the same height as the modeled prototype. The horizontal purple surfaces represent the local roads. The widths of the roads and side and front setbacks follow the design standards of Zoning Code of Sacramento County (ZCSC) and Street Design Standards for the City of Sacramento (see Section 5.2.4). Note that the illustrations of the large hotel and large office do not show the horizontal and vertical purple surfaces; these two prototypes were simulated with the walls and roads, but the buildings were not rendering correctly in our 3-D modeling software.

Single-family home

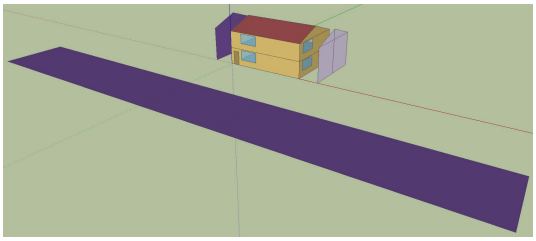

Apartment building

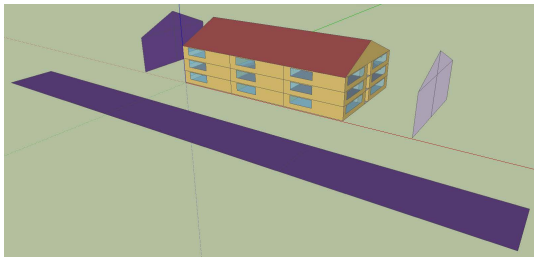

Stand-alone retail

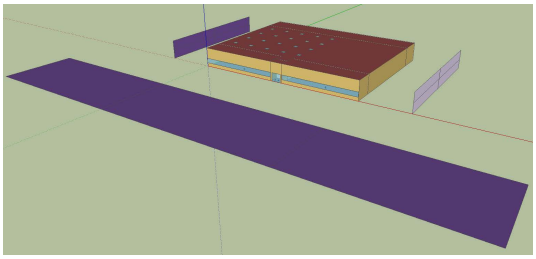

Strip mall retail

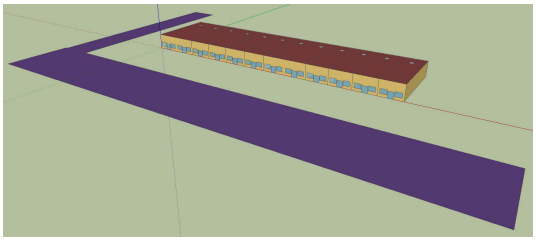

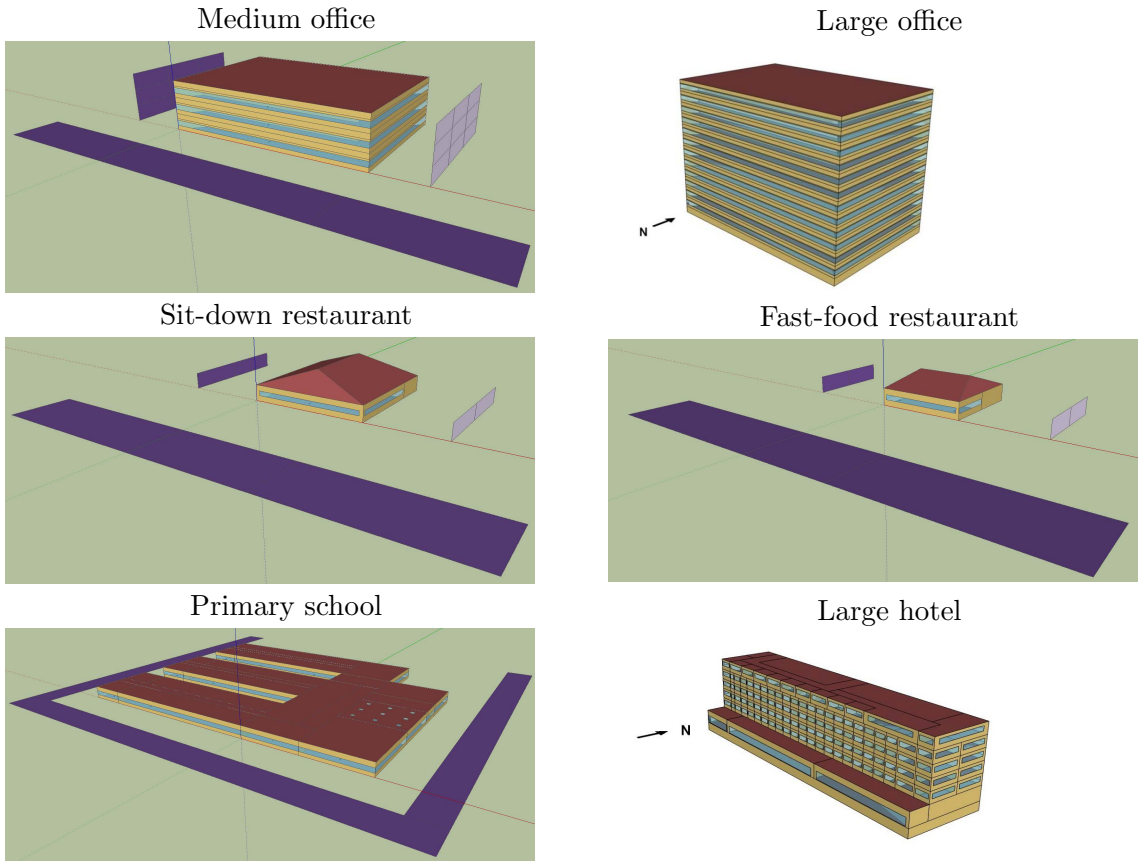

Figure C.2: Illustration of modified prototypes. The purple surfaces represent the roads (horizontal surfaces) and neighboring buildings (vertical surfaces). The illustrations of the large hotel and large office omit the horizontal and vertical surfaces because they were not rendering correctly in our 3D modeling software.

Appendix D

Assessing the Age of California's Building Stock

The Commercial Building Energy Consumption Survey (CBECS) groups the year of construction for commercial building stock into 10-year periods. The Residential Energy Consumption Survey (RECS) is the residential analog of CBECS and does a similar classification for residential buildings. Table D.1 gives the mean period of construction as obtained by CBECS and RECS for the building types that were mapped to the EnergyPlus prototypes that were used for the study (see Section 4.5).

The age of the state's building stock was also calculated using the property data collection from California's Assessor's Office. The collection includes over 12.5 million records of properties in the state.

Table D.2 lists the relevant property types for this study and their state-wide age.

Table D.1: Mean period of construction for different building types as reported by CBECS and RECS.

Building type	**Mean period of construction**
Professional office	1970 to 1979
Government office	1970 to 1979
Mixed-use office	1980 to 1989
Elementary school	1970 to 1979
Fast food	1980 to 1989
Restaurant	1970 to 1979
Hotel	1980 to 1989
Retail store	1970 to 1979
Strip shopping mall	1980 to 1989
Single-family detached	1970 to 1979
5+ units apartment complex	1970 to 1979

Source: CBECS 2003.
Source: RECS 2009.

Table D.2: Average year of construction of building stock reported by the Assessor's Office.

Building type	**Average year of construction**
Bowling alley	1970
Clubs, fraternal organizations	1954
Condominium, PUD	1982
Cooperative	1944
Department store	1970
Duplex	1958
Financial building	1971
Food store, market	1973
Governmental, public	1950
Hospitals, convalescent homes	1965
Hotel/motel	1958
Laundry, dry cleaning	1959
Medical buildings	1972
Miscellaneous commercial	1953
Miscellaneous residential	1951
Mobile home	1973
Mobile home parks, trailer parks	1981
Multi-family dwelling (2-4 units)	1984
Multi-family res (5+ units)	1957
Nursery	1961
Office building	1968
Quadruplex	1962
Restaurant, bar, food service	1967
School	1960
Shopping center	1980
Single-family residence	1969
Store/office combo	1961
Stores, retail outlet	1958
Timeshare	1991
Triplex	1943
Veterinary	1962

Appendix E

Coefficients of physical model solutions

Tables E.1 thru E.10 give the coefficients of the physical model solutions to all prototypes by building climate zone (BCZ).

Table E.1: Coefficients for all prototypes in BCZ 3.

Prototype	Use	e_0 [MWh/y]	e_1 [MWh/y]	e_2 [MWh/y]	g_0 [therm/y]	g_1 [therm/y]	g_2 [therm/y]
Single-family home	cooling	0.328	0.036	-0.136	0.000	0.000	0.000
	heating	0.174	0.003	0.034	154	-2.92	30
	lighting	1.35	0.000	0.000	0.000	0.000	0.000
Apartment building	cooling	4.61	0.406	-1.57	0.000	0.000	0.000
	heating	0.623	-0.014	0.176	367	-6.42	104
	lighting	7.29	0.000	0.000	0.000	0.000	0.000
Large hotel	cooling	263	8.28	-31.8	0.000	0.000	0.000
	heating	65.8	-1.14	9.51	11500	-144	1550
	lighting	402	0.000	0.000	0.000	0.000	0.000
Large office	cooling	610	17.9	-100	0.000	0.000	0.000
	heating	67.5	-0.02	12.4	17300	30.2	3450
	lighting	1250	-0.183	0.000	0.000	0.000	0.000
Medium office	cooling	135	1.72	-15.9	0.000	0.000	0.000
	heating	56.1	0.876	8.56	0.000	0.000	0.000
	lighting	135	-0.017	0.000	0.000	0.000	0.000
Primary school	cooling	149	3.07	-32.7	0.000	0.000	0.000
	heating	31.3	0.112	9.75	1980	-22.4	402
	lighting	274	-0.025	0.000	0.000	0.000	0.000
Fast-food restaurant	cooling	3.98	0.000	-2.1	0.000	0.000	0.000
	heating	17.9	0.000	1.3	1880	0.000	237
	lighting	10.7	0.000	0.000	0.000	0.000	0.000
Retail stand-alone	cooling	64.5	0.316	-9.19	0.000	0.000	0.000
	heating	23.7	-0.028	4.01	1200	-1.85	222
	lighting	62.2	0.000	0.000	0.000	0.000	0.000
Strip mall retail	cooling	58.2	0.384	-10.3	0.000	0.000	0.000
	heating	18.5	-0.065	3.69	688	-3.36	189
	lighting	94.4	0.000	0.000	0.000	0.000	0.000
Sit-down restaurant	cooling	11.4	0.001	-3.35	0.000	0.000	0.000
	heating	11.3	0.002	1.88	1820	-0.073	299
	lighting	20.3	0.000	0.000	0.000	0.000	0.000

Table E.2: Coefficients for all prototypes in BCZ 4.

Prototype	Use	e_0 [MWh/y]	e_1 [MWh/y]	e_2 [MWh/y]	g_0 [therm/y]	g_1 [therm/y]	g_2 [therm/y]
Single-family home	cooling	0.976	0.063	-0.335	0.000	0.000	0.000
	heating	0.172	0.002	0.046	123	-2.22	32.4
	lighting	1.35	0.000	0.000	0.000	0.000	0.000
Apartment building	cooling	10.7	0.581	-3.38	0.000	0.000	0.000
	heating	0.607	-0.006	0.246	294	-5.74	119
	lighting	7.29	0.000	0.000	0.000	0.000	0.000
Large hotel	cooling	331	9.27	-49.2	0.000	0.000	0.000
	heating	51.8	-0.645	10.4	10200	-77	2180
	lighting	402	0.000	0.000	0.000	0.000	0.000
Large office	cooling	792	24.8	-146	0.000	0.000	0.000
	heating	54.7	0.701	14.1	14200	389	4150
	lighting	1250	-0.193	0.000	0.000	0.000	0.000
Medium office	cooling	158	2.09	-23.3	0.000	0.000	0.000
	heating	46.9	0.947	9.61	0.277	-0.154	0.064
	lighting	135	-0.02	0.000	0.000	0.000	0.000
Primary school	cooling	166	3.51	-34.5	0.000	0.000	0.000
	heating	19.4	0.158	6.29	1600	-8.62	464
	lighting	274	-0.028	0.000	0.000	0.000	0.000
Fast-food restaurant	cooling	12.3	0.000	-4.4	0.000	0.000	0.000
	heating	17.2	0.000	1.64	1680	0.000	305
	lighting	10.7	0.000	0.000	0.000	0.000	0.000
Retail stand-alone	cooling	78.8	0.306	-11.7	0.000	0.000	0.000
	heating	18.4	-0.021	3.68	1020	-1.08	247
	lighting	62.4	0.000	0.000	0.000	0.000	0.000
Strip mall retail	cooling	83.7	0.361	-15	0.000	0.000	0.000
	heating	15.7	-0.058	3.71	545	-2.34	207
	lighting	94.2	0.000	0.000	0.000	0.000	0.000
Sit-down restaurant	cooling	21.7	0.008	-5.83	0.000	0.000	0.000
	heating	10.3	-0.001	1.76	1880	-0.804	391
	lighting	20.3	0.000	0.000	0.000	0.000	0.000

Table E.3: Coefficients for all prototypes in BCZ 7.

Prototype	Use	e_0 [MWh/y]	e_1 [MWh/y]	e_2 [MWh/y]	g_0 [therm/y]	g_1 [therm/y]	g_2 [therm/y]
Single-family home	cooling	0.774	0.063	-0.221	0.000	0.000	0.000
	heating	0.036	-0.001	0.014	22.9	-0.751	9.21
	lighting	1.35	0.000	0.000	0.000	0.000	0.000
Apartment building	cooling	11.2	0.645	-2.52	0.000	0.000	0.000
	heating	0.041	-0.001	0.031	16	-0.477	12
	lighting	7.29	0.000	0.000	0.000	0.000	0.000
Large hotel	cooling	403	9.81	-41.9	0.000	0.000	0.000
	heating	24	-1.25	6.16	4040	-169	577
	lighting	402	0.000	0.000	0.000	0.000	0.000
Large office	cooling	945	27.6	-111	0.000	0.000	0.000
	heating	16.5	0.486	6.21	2750	170	922
	lighting	1250	-0.165	0.000	0.000	0.000	0.000
Medium office	cooling	196	2.1	-13	0.000	0.000	0.000
	heating	17	0.536	3.92	0.000	0.000	0.000
	lighting	135	-0.017	0.000	0.000	0.000	0.000
Primary school	cooling	214	3.92	-28.1	0.000	0.000	0.000
	heating	6.66	0.046	2.97	606	-2.01	159
	lighting	274	-0.024	0.000	0.000	0.000	0.000
Fast-food restaurant	cooling	7.88	0.000	-3.19	0.000	0.000	0.000
	heating	13.3	0.000	1.68	1020	0.000	137
	lighting	10.7	0.000	0.000	0.000	0.000	0.000
Retail stand-alone	cooling	93.1	0.49	-8.99	0.000	0.000	0.000
	heating	9.97	-0.036	2.34	460	-1.3	127
	lighting	62.1	0.000	0.000	0.000	0.000	0.000
Strip mall retail	cooling	99.2	1.01	-10.7	0.000	0.000	0.000
	heating	6.34	-0.003	1.12	96.4	-1.18	44.8
	lighting	93.1	0.000	0.000	0.000	0.000	0.000
Sit-down restaurant	cooling	22.7	0.012	-5.62	0.000	0.000	0.000
	heating	6.24	0.003	0.77	821	-0.286	119
	lighting	20.3	0.000	0.000	0.000	0.000	0.000

Table E.4: Coefficients for all prototypes in BCZ 8.

Prototype	Use	e_0 [MWh/y]	e_1 [MWh/y]	e_2 [MWh/y]	g_0 [therm/y]	g_1 [therm/y]	g_2 [therm/y]
Single-family home	cooling	1.52	0.081	-0.397	0.000	0.000	0.000
	heating	0.083	0.000	0.035	51.4	-1.03	21.4
	lighting	1.35	0.000	0.000	0.000	0.000	0.000
Apartment building	cooling	16.3	0.701	-4.03	0.000	0.000	0.000
	heating	0.175	-0.003	0.131	72.8	-1.55	54.6
	lighting	7.29	0.000	0.000	0.000	0.000	0.000
Large hotel	cooling	437	11.7	-62.9	0.000	0.000	0.000
	heating	37	-0.572	9.34	7380	-87.4	1460
	lighting	402	0.000	0.000	0.000	0.000	0.000
Large office	cooling	1060	28.7	-150	0.000	0.000	0.000
	heating	25.2	0.624	9.68	5790	262	2380
	lighting	1250	-0.166	0.000	0.000	0.000	0.000
Medium office	cooling	201	2.05	-21.1	0.000	0.000	0.000
	heating	26.8	0.63	6.94	0.000	0.000	0.000
	lighting	135	-0.016	0.000	0.000	0.000	0.000
Primary school	cooling	255	3.82	-39.8	0.000	0.000	0.000
	heating	9.25	0.087	5.16	894	-1.08	308
	lighting	275	-0.02	0.000	0.000	0.000	0.000
Fast-food restaurant	cooling	20	0.000	-5.64	0.000	0.000	0.000
	heating	13.7	0.000	2.49	1110	0.000	217
	lighting	10.7	0.000	0.000	0.000	0.000	0.000
Retail stand-alone	cooling	111	0.308	-12.8	0.000	0.000	0.000
	heating	11.2	-0.011	3.6	556	-0.59	184
	lighting	61.4	0.000	0.000	0.000	0.000	0.000
Strip mall retail	cooling	124	0.44	-16.4	0.000	0.000	0.000
	heating	8.78	0.035	2.58	185	-0.756	106
	lighting	93.1	0.000	0.000	0.000	0.000	0.000
Sit-down restaurant	cooling	35.8	0.011	-8.01	0.000	0.000	0.000
	heating	7.92	0.001	1.34	987	-0.099	241
	lighting	20.3	0.000	0.000	0.000	0.000	0.000

Table E.5: Coefficients for all prototypes in BCZ 9.

Prototype	Use	e_0 [MWh/y]	e_1 [MWh/y]	e_2 [MWh/y]	g_0 [therm/y]	g_1 [therm/y]	g_2 [therm/y]
Single-family home	cooling	1.91	0.085	-0.451	0.000	0.000	0.000
	heating	0.131	0.001	0.048	72.5	-1.42	26.3
	lighting	1.35	0.000	0.000	0.000	0.000	0.000
Apartment building	cooling	19.6	0.719	-4.34	0.000	0.000	0.000
	heating	0.364	-0.005	0.218	139	-2.88	83.7
	lighting	7.29	0.000	0.000	0.000	0.000	0.000
Large hotel	cooling	446	12	-63	0.000	0.000	0.000
	heating	41.7	-0.737	8.96	7800	-113	1780
	lighting	402	0.000	0.000	0.000	0.000	0.000
Large office	cooling	1080	27.6	-160	0.000	0.000	0.000
	heating	36.3	0.653	11.5	8540	296	3240
	lighting	1250	-0.171	0.000	0.000	0.000	0.000
Medium office	cooling	201	2.07	-24	0.000	0.000	0.000
	heating	31.8	0.655	8.01	0.000	0.000	0.000
	lighting	135	-0.017	0.000	0.000	0.000	0.000
Primary school	cooling	228	3.63	-35.8	0.000	0.000	0.000
	heating	13.1	0.13	5	1020	-4.46	357
	lighting	274	-0.023	0.000	0.000	0.000	0.000
Fast-food restaurant	cooling	24.6	0.000	-5.77	0.000	0.000	0.000
	heating	14.5	0.000	2.39	1210	0.000	244
	lighting	10.7	0.000	0.000	0.000	0.000	0.000
Retail stand-alone	cooling	105	0.286	-12.2	0.000	0.000	0.000
	heating	12.7	-0.004	3.3	647	-0.798	199
	lighting	61.7	0.000	0.000	0.000	0.000	0.000
Strip mall retail	cooling	122	0.397	-15.8	0.000	0.000	0.000
	heating	10.7	0.021	2.65	251	-1.14	129
	lighting	93.1	0.000	0.000	0.000	0.000	0.000
Sit-down restaurant	cooling	39	0.006	-7.8	0.000	0.000	0.000
	heating	8.63	0.003	1.34	1130	-0.032	287
	lighting	20.3	0.000	0.000	0.000	0.000	0.000

Table E.6: Coefficients for all prototypes in BCZ 10.

Prototype	Use	e_0 [MWh/y]	e_1 [MWh/y]	e_2 [MWh/y]	g_0 [therm/y]	g_1 [therm/y]	g_2 [therm/y]
Single-family home	cooling	2.28	0.094	-0.39	0.000	0.000	0.000
	heating	0.19	0.002	0.038	115	-1.79	22.5
	lighting	1.35	0.000	0.000	0.000	0.000	0.000
Apartment building	cooling	21.8	0.755	-3.43	0.000	0.000	0.000
	heating	0.634	-0.008	0.213	273	-5.03	92.1
	lighting	7.29	0.000	0.000	0.000	0.000	0.000
Large hotel	cooling	408	10.1	-42.2	0.000	0.000	0.000
	heating	46.9	-0.919	6.36	9300	-162	1440
	lighting	402	0.000	0.000	0.000	0.000	0.000
Large office	cooling	946	20.2	-103	0.000	0.000	0.000
	heating	40.7	0.504	6.92	9190	162	2450
	lighting	1260	-0.145	0.000	0.000	0.000	0.000
Medium office	cooling	187	1.62	-19	0.000	0.000	0.000
	heating	25	0.237	5.59	2.86	-0.685	1.91
	lighting	135	-0.015	0.000	0.000	0.000	0.000
Primary school	cooling	210	2.64	-26.4	0.000	0.000	0.000
	heating	15.4	0.098	3.58	1400	-7.67	332
	lighting	275	-0.039	0.000	0.000	0.000	0.000
Fast-food restaurant	cooling	26.9	0.000	-4.58	0.000	0.000	0.000
	heating	15.8	0.000	1.22	1530	0.000	200
	lighting	10.7	0.000	0.000	0.000	0.000	0.000
Retail stand-alone	cooling	100	0.293	-9.63	0.000	0.000	0.000
	heating	15.6	-0.007	2.49	888	-1.13	170
	lighting	66.8	0.000	0.000	0.000	0.000	0.000
Strip mall retail	cooling	113	0.444	-12.8	0.000	0.000	0.000
	heating	14.2	0.037	2.27	500	-2.16	152
	lighting	101	0.000	0.000	0.000	0.000	0.000
Sit-down restaurant	cooling	38.6	0.002	-5.87	0.000	0.000	0.000
	heating	10	-0.003	0.82	1600	-0.107	249
	lighting	20.4	0.000	0.000	0.000	0.000	0.000

Table E.7: Coefficients for all prototypes in BCZ 12.

Prototype	Use	e_0 [MWh/y]	e_1 [MWh/y]	e_2 [MWh/y]	g_0 [therm/y]	g_1 [therm/y]	g_2 [therm/y]
Single-family home	cooling	1.56	0.06	-0.272	0.000	0.000	0.000
	heating	0.19	-0.004	0.031	132	-1.82	22
	lighting	1.35	0.000	0.000	0.000	0.000	0.000
Apartment building	cooling	17.4	0.583	-2.62	0.000	0.000	0.000
	heating	0.827	-0.005	0.196	372	-5.61	88.2
	lighting	7.29	0.000	0.000	0.000	0.000	0.000
Large hotel	cooling	352	6.91	-34.6	0.000	0.000	0.000
	heating	58.8	-0.948	6.28	12700	-131	1800
	lighting	402	0.000	0.000	0.000	0.000	0.000
Large office	cooling	817	17.6	-89.1	0.000	0.000	0.000
	heating	56.3	0.704	7.4	15600	288	3150
	lighting	1260	-0.133	0.000	0.000	0.000	0.000
Medium office	cooling	156	1.39	-15.5	0.000	0.000	0.000
	heating	41.1	0.41	5.8	28.4	-2.99	8.25
	lighting	135	-0.013	0.000	0.000	0.000	0.000
Primary school	cooling	169	2.3	-19.7	0.000	0.000	0.000
	heating	22.4	0.193	2.86	2300	-12.2	438
	lighting	276	-0.042	0.000	0.000	0.000	0.000
Fast-food restaurant	cooling	22.6	0.000	-3.18	0.000	0.000	0.000
	heating	17.6	0.000	0.768	2020	0.000	240
	lighting	10.7	0.000	0.000	0.000	0.000	0.000
Retail stand-alone	cooling	80.4	0.274	-6.87	0.000	0.000	0.000
	heating	22.5	0.001	2.25	1440	-1.32	216
	lighting	67	0.000	0.000	0.000	0.000	0.000
Strip mall retail	cooling	89.9	0.317	-8.49	0.000	0.000	0.000
	heating	21.5	-0.016	2.67	1120	-4.14	244
	lighting	102	0.000	0.000	0.000	0.000	0.000
Sit-down restaurant	cooling	31.6	0.002	-4.22	0.000	0.000	0.000
	heating	11.7	-0.001	0.821	2400	-0.535	338
	lighting	20.4	0.000	0.000	0.000	0.000	0.000

Table E.8: Coefficients for all prototypes in BCZ 13.

Prototype	Use	e_0 [MWh/y]	e_1 [MWh/y]	e_2 [MWh/y]	g_0 [therm/y]	g_1 [therm/y]	g_2 [therm/y]
Single-family home	cooling	2.58	0.073	-0.335	0.000	0.000	0.000
	heating	0.195	0.000	0.036	124	-1.89	23
	lighting	1.35	0.000	0.000	0.000	0.000	0.000
Apartment building	cooling	26.2	0.655	-2.99	0.000	0.000	0.000
	heating	0.852	-0.004	0.231	358	-5.35	96.4
	lighting	7.29	0.000	0.000	0.000	0.000	0.000
Large hotel	cooling	424	6.96	-36.4	0.000	0.000	0.000
	heating	54.2	-0.83	5.34	11500	-108	1730
	lighting	402	0.000	0.000	0.000	0.000	0.000
Large office	cooling	959	19.4	-89.7	0.000	0.000	0.000
	heating	54.3	0.652	7.06	15200	291	3530
	lighting	1260	-0.137	0.000	0.000	0.000	0.000
Medium office	cooling	182	1.55	-15.9	0.000	0.000	0.000
	heating	39.1	0.392	5.9	15.9	-2.22	7.04
	lighting	135	-0.015	0.000	0.000	0.000	0.000
Primary school	cooling	208	2.59	-21.4	0.000	0.000	0.000
	heating	22.2	0.184	3.01	2120	-11	483
	lighting	277	-0.045	0.000	0.000	0.000	0.000
Fast-food restaurant	cooling	31.6	0.000	-3.5	0.000	0.000	0.000
	heating	16.2	0.000	0.962	1800	0.000	257
	lighting	10.7	0.000	0.000	0.000	0.000	0.000
Retail stand-alone	cooling	94.5	0.314	-7.28	0.000	0.000	0.000
	heating	21.6	0.022	2.08	1310	-1.62	229
	lighting	66.9	0.000	0.000	0.000	0.000	0.000
Strip mall retail	cooling	110	0.358	-9.11	0.000	0.000	0.000
	heating	21.5	-0.03	2.78	1040	-4.14	274
	lighting	102	0.000	0.000	0.000	0.000	0.000
Sit-down restaurant	cooling	43	0.002	-4.64	0.000	0.000	0.000
	heating	11.1	0.002	0.904	2050	-0.147	345
	lighting	20.4	0.000	0.000	0.000	0.000	0.000

Table E.9: Coefficients for all prototypes in BCZ 14.

Prototype	Use	e_0 [MWh/y]	e_1 [MWh/y]	e_2 [MWh/y]	g_0 [therm/y]	g_1 [therm/y]	g_2 [therm/y]
Single-family home	cooling	3.26	0.099	-0.158	0.000	0.000	0.000
	heating	0.174	0.000	0.01	116	-1.88	7.31
	lighting	1.16	0.000	0.000	0.000	0.000	0.000
Apartment building	cooling	32.2	0.839	-1.45	0.000	0.000	0.000
	heating	0.964	-0.004	0.078	471	-5.5	38.4
	lighting	6.31	0.000	0.000	0.000	0.000	0.000
Large hotel	cooling	466	6.78	-16.6	0.000	0.000	0.000
	heating	50.2	-0.951	2.15	13900	-121	689
	lighting	402	0.000	0.000	0.000	0.000	0.000
Large office	cooling	1040	22.1	-37.3	0.000	0.000	0.000
	heating	63.7	0.251	2.99	29400	155	2000
	lighting	1260	-0.146	0.000	0.000	0.000	0.000
Medium office	cooling	211	1.87	-7.08	0.000	0.000	0.000
	heating	51.1	0.403	2.9	108	-6.51	12.8
	lighting	135	-0.017	0.000	0.000	0.000	0.000
Primary school	cooling	247	2.81	-9.58	0.000	0.000	0.000
	heating	21.2	0.147	1.3	2740	-8.37	213
	lighting	277	-0.091	0.000	0.000	0.000	0.000
Fast-food restaurant	cooling	40.1	0.000	-1.99	0.000	0.000	0.000
	heating	15.7	0.000	0.52	1990	0.000	102
	lighting	10.7	0.000	0.000	0.000	0.000	0.000
Retail stand-alone	cooling	116	0.344	-3.56	0.000	0.000	0.000
	heating	20.6	-0.019	1.56	1630	-1.59	99.6
	lighting	70.1	0.000	0.000	0.000	0.000	0.000
Strip mall retail	cooling	134	0.434	-4.55	0.000	0.000	0.000
	heating	20.5	-0.018	1.48	1220	-3.59	105
	lighting	101	0.000	0.000	0.000	0.000	0.000
Sit-down restaurant	cooling	53.4	0.005	-2.41	0.000	0.000	0.000
	heating	10.8	0.000	0.382	2330	-0.113	131
	lighting	20.4	0.000	0.000	0.000	0.000	0.000

Table E.10: Coefficients for all prototypes in BCZ 15.

Prototype	Use	e_0 [MWh/y]	e_1 [MWh/y]	e_2 [MWh/y]	g_0 [therm/y]	g_1 [therm/y]	g_2 [therm/y]
Single-family home	cooling	4.93	0.106	-0.253	0.000	0.000	0.000
	heating	0.048	0.000	0.007	22.4	-0.493	2.74
	lighting	1.16	0.000	0.000	0.000	0.000	0.000
Apartment building	cooling	46.9	0.841	-2.26	0.000	0.000	0.000
	heating	0.146	-0.001	0.026	48.2	-0.65	8.49
	lighting	6.31	0.000	0.000	0.000	0.000	0.000
Large hotel	cooling	700	8.26	-27.3	0.000	0.000	0.000
	heating	24.3	-0.451	1.59	6140	-70.7	352
	lighting	402	0.000	0.000	0.000	0.000	0.000
Large office	cooling	1700	28.7	-72.9	0.000	0.000	0.000
	heating	19.7	0.243	1.9	5680	92.1	648
	lighting	1260	-0.151	0.000	0.000	0.000	0.000
Medium office	cooling	299	2.03	-12.1	0.000	0.000	0.000
	heating	15.8	0.172	1.36	1.78	-0.508	0.509
	lighting	135	-0.016	0.000	0.000	0.000	0.000
Primary school	cooling	366	4	-14.9	0.000	0.000	0.000
	heating	6.88	0.043	0.786	796	-2.65	76.1
	lighting	276	-0.05	0.000	0.000	0.000	0.000
Fast-food restaurant	cooling	62.6	0.000	-3.47	0.000	0.000	0.000
	heating	10.9	0.000	0.581	920	0.000	51.3
	lighting	10.7	0.000	0.000	0.000	0.000	0.000
Retail stand-alone	cooling	158	0.335	-5.59	0.000	0.000	0.000
	heating	7.9	-0.004	0.743	528	-0.546	53.6
	lighting	67.8	0.000	0.000	0.000	0.000	0.000
Strip mall retail	cooling	193	0.483	-7.29	0.000	0.000	0.000
	heating	7.33	-0.012	0.544	222	-0.875	26.8
	lighting	101	0.000	0.000	0.000	0.000	0.000
Sit-down restaurant	cooling	82.5	0.006	-4.2	0.000	0.000	0.000
	heating	6.37	0.000	0.197	928	-0.032	62.8
	lighting	20.4	0.000	0.000	0.000	0.000	0.000

Appendix F

Urban Canyon Model

The following figures are screenshots of the individual functions that compose the urban canyon model described in detail in Chapter 4. The model was coded in the Python programming language.

```
''' Function to calculate view factor (VF) from canyon floor to sky (or vice versa)
    VF configuration description: Two infinitely long, directly opposed parallel plates of the same finite width.
    source: http://www.thermalradiation.net/sectionc/C-1.html
'''

def VF_floor_to_sky_same_width (canyon_width, canyon_height):
    height_to_width_ratio = canyon_height / canyon_width
    VF_floor_to_sky = math.sqrt( 1 + height_to_width_ratio**2 ) - height_to_width_ratio
    return VF_floor_to_sky
```

Figure F.1: Function to calculate view factor from canyon floor to sky (or vice versa).

```
''' Function that calculates floor segment to sky view factor using the cross-string method
    VF configuration description: Cross-string method = Two infinitely long parallel plates of
    different widths contained in parallel planes.
    source: http://www.thermalradiation.net/sectionc/C-2a.htm
'''

def VF_floor_segment_to_sky(canyon_width, canyon_height, segment_width, wall_to_segment_distance):

    L1 = math.sqrt( canyon_height**2 + (wall_to_segment_distance + segment_width)**2 )
    L2 = math.sqrt( canyon_height**2 + (canyon_width - wall_to_segment_distance)**2 )
    L3 = math.sqrt( canyon_height**2 + (wall_to_segment_distance)**2 )
    L4 = math.sqrt( canyon_height**2 + (canyon_width - wall_to_segment_distance - segment_width)**2 )
    VF_segment_to_sky = (L1 + L2 - L3 - L4) / (2 * segment_width)

    return VF_segment_to_sky
```

Figure F.2: Function that calculates floor segment to sky view factor using the cross-string method.

```
''' Function that calculates view factor from a floor segment of specified width to a wall
    VF configuration description: Two infinitely long plates of unequal width without a common edge
                                  with an included angle α.
                                  In our case, angle = 90°, cos(α) = 0
    source: http://www.thermalradiation.net/sectionc/C-5a.html
'''

def VF_floor_segment_to_wall (canyon_height, segment_width, wall_to_segment_distance):

    # x1,x2, y1, y2 are defined in the thermal radiation catalog
    x1 = wall_to_segment_distance
    x2 = x1 + segment_width
    y1 = 0
    y2 = canyon_height

    # VF from floor segment to wall
    VF_segment_to_wall = ( math.sqrt(x1**2 + y2**2) + math.sqrt(x2**2 + y1**2) -
                           math.sqrt(x2**2 + y2**2) - math.sqrt(x1**2 + y1**2) ) / (2 * (x2 - x1))

    return VF_segment_to_wall
```

Figure F.3: Function that calculates view factor from a floor segment of specified width to a wall.

```
''' Function to calculate width of shadow of a canyon wall '''

def calculate_shadow_width (
                            wall_height,
                            road_orientation, # input either 'NS' (North-South) or 'EW' (East-West)
                            zenith_angle, # zenith angle (in degrees) of a specific hour
                            azimuth_angle # azimuth angle (in degrees) of a specific hour
                            ):

    tan_zenith = math.tan(math.radians(zenith_angle))

    if road_orientation == 'NS':
        sin_azimuth = math.sin(math.radians(azimuth_angle))
        shadow_width = abs(wall_height * tan_zenith * sin_azimuth)
        return shadow_width

    elif road_orientation == 'EW':
        cos_azimuth = math.cos(math.radians(azimuth_angle))
        shadow_width = abs(wall_height * tan_zenith * cos_azimuth)
        return shadow_width

    else:
        print "Select orientation as either NS or EW"
        return
```

Figure F.4: Function to calculate width of shadow of a canyon wall.

```
''' MAIN Function: calculates the reflected sunlight in [kWh/m2] from the road on the canyon floor.

    The incoming sunlight is treated as provided in the weather files (global sunlight for unshaded surfaces;
    diffuse sunlight for shaded surfaces).

    The road width is divided into N segments, and then iterate through hour and segment to calculate
    hourly radiation (energy) reflected from each segment.

    Weather files: The TMY3 weather files can be used (like the ones used in EnergyPlus simulations),
    but converted to CSV format.

    Solar position (zenith and azimuth angles) were obtained from NREL's Solar Position Algorithm.
    Source: http://www.nrel.gov/midc/solpos/spa.html

    Canyon dimensions:
        Width: distance between the walls forming the canyon
        Height: Height of the building wall forming the canyon
        Length: Here we treat the length of the canyon as infinite. It is the length along the long axis of the road.

    Nomenclature:   I refers to sunlight as energy per area [kWh/m2]
                    J refers to sunlight energy per unit of canyon length [kWh/m]
                    The output of the function returns daily reflected sunlight I
'''
```

```
def sunlight_reflected_from_wide_canyon (
       ''' Inputs names that end in _by_hour refers to each hour of the day '''
       wall_height,
       road_width,
       setback_width,
       road_orientation, # input either 'NS' (North-South) or 'EW' (East-West)
       zenith_angle_by_hour, # Array of zenith angles (in degrees)
       azimuth_angle_by_hour, # Array of azimuth angles (in degrees)
       diffuse_sunlight_by_hour, # Array of diffused sunlight [Wh/m2] as obtained from the weather file
       global_sunlight_by_hour, # Array of global sunlight [Wh/m2] as obtained from the weather file
       sunlight_west_wall_by_hour, # Array of calculated direct sunlight [Wh/m2] striking the WEST wall
       sunlight_east_wall_by_hour, # Array of calculated direct sunlight [Wh/m2] striking the EAST wall
       sunlight_north_wall_by_hour, # Array of calculated direct sunlight [Wh/m2] striking the NORTH wall
       sunlight_south_wall_by_hour, # Array of calculated direct sunlight [Wh/m2] striking the SOUTH wall
       wall_albedo,
       road_albedo,
       setback_albedo = 0.1
       ):

    ''' Calculate additional canyon dimensions and properties '''
    canyon_width = road_width + 2* setback_width
    setback_plus_road_width = setback_width + road_width # Calculate width of setback + road

    ''' View factor calculations
        Let VF_AB = view factor from A to B, or fraction of radiation leaving surface A that is intercepted by surface B
        Here, the canyon is represented with 4 surfaces: (1) ground, (2) sky, (3) left wall, and (4) right wall:
                2
          ----------------
          |              |
        3 |              | 4
          |              |
          ----------------
                1
    '''
```

Figure F.5: This is the main function to calculate the reflected sunlight in [kWh/m^2] from the road on the canyon floor.

```
    VF_12 = VF_floor_to_sky_same_width (canyon_width = canyon_width, canyon_height = wall_height)
    VF_21 = VF_12
    VF_42 = canyon_width / wall_height * ( (1 - VF_12) / 2 )
    VF_32 = VF_42
    VF_31 = VF_42
    VF_41 = VF_42
    VF_23 = (1 - VF_21) / 2
    VF_24 = VF_23
    VF_13 = VF_23
    VF_14 = VF_24

    ''' Segments into which the floor of the canyon is divided '''
    number_of_segments = 2000
    segment_width = canyon_width / float(number_of_segments)
    distances_from_wall = [canyon_width * float(i) / number_of_segments for i in range(number_of_segments)]
    reflected_sunlight_by_hour = []  # Radiation (power) escaping the canyon

    ''' Iterate through each hour of the day '''
    for h, hour in enumerate(range(0,24)):

        ''' Verify if it is daytime or nighttime. If nighttime, skip the hour and go to next. '''
        is_night = zenith_angle_by_hour[hour] > 90
        if is_night:
            reflected_sunlight_this_hour = 0
        else:

            ''' Call function that calculates the width of the shadow '''
            shadow_width = calculate_shadow_width (wall_height = wall_height,
                                                   zenith_angle = zenith_angle_by_hour[hour],
                                                   azimuth_angle = azimuth_angle_by_hour[hour],
                                                   road_orientation = road_orientation )

            ''' Loop through the segments of the ground '''
            sunlight_from_all_segments_to_sky_this_hour = []
```

```
            for distance_from_wall in distances_from_wall:

                ''' Assign segment albedo depending on segment location '''
                if setback_width <= distance_from_wall < setback_plus_road_width: # If TRUE, segment is where the road is.
                    albedo = road_albedo
                else:
                    albedo = setback_albedo

                ''' Segment view factor calculations
                    Here, the canyon is represented with 4 surfaces: (0) floor segment, (2) sky, (3) left wall,
                    and (4) right wall, as shown below:
                            2
                      ----------------
                      |              |
                    3 |              | 4
                      |  _           |
                         0
                '''

                VF_02 = VF_floor_segment_to_sky(canyon_width = canyon_width,
                                                canyon_height = wall_height,
                                                segment_width = segment_width,
                                                wall_to_segment_distance = distance_from_wall
                                               ) # Function that calculates sky view factor from segment

                VF_20 = (segment_width / canyon_width) * VF_02
                VF_03 = VF_floor_segment_to_wall (canyon_height = wall_height,
                                                  segment_width = segment_width,
                                                  wall_to_segment_distance = distance_from_wall
                                                 )
                VF_04 = VF_floor_segment_to_wall (canyon_height = wall_height,
                                                  segment_width = segment_width,
                                                  wall_to_segment_distance = canyon_width-distance_from_wall-segment_width
                                                 )
                VF_30 = (segment_width / wall_height) * VF_03
                VF_40 = (segment_width / wall_height) * VF_04

                width_of_sunlit_area = canyon_width - shadow_width # Calculate width of ground that is NOT in shade
```

Figure F.6: Continuation of function to calculate the reflected sunlight from the road on the canyon floor.

```
            if road_orientation == 'NS':  # Road oriented North-South (N-S)

                ''' Obtain sunlight that strikes the West and East walls '''
                I_3 = sunlight_west_wall_by_hour[hour] * Wh_to_kWh
                I_4 = sunlight_east_wall_by_hour[hour] * Wh_to_kWh

                ''' Determining if sun is positioned east or west '''
                sun_is_east = azimuth_angle_by_hour[hour] < 180
                if sun_is_east:
                    segment_in_shade = distance_from_wall >= width_of_sunlit_area
                else:
                    segment_in_shade = distance_from_wall < shadow_width

            elif road_orientation == 'EW':  # Road oriented East-West (E-W)

                ''' Obtain sunlight that strikes the South and North walls '''
                I_3 = sunlight_south_wall_by_hour[hour] * Wh_to_kWh
                I_4 = sunlight_north_wall_by_hour[hour] * Wh_to_kWh

                ''' Determining if sun is positioned north or south '''
                sun_is_north = azimuth_angle_by_hour[hour] < 90 or azimuth_angle_by_hour[hour] >= 270
                if sun_is_north:
                    segment_in_shade = distance_from_wall >= width_of_sunlit_area
                else:
                    segment_in_shade = distance_from_wall < shadow_width

            else:
                print "Select road orientation as either NS or EW"
                return

            if segment_in_shade:
                I_20 = diffuse_sunlight_by_hour[hour] * Wh_to_kWh
            else:
                I_20 = global_sunlight_by_hour[hour] * Wh_to_kWh

            J_20 = I_20 * segment_width

            ''' At walls '''
            J_3 = I_3 * wall_height
            J_4 = I_4 * wall_height
            J_30 = J_3 * wall_albedo * VF_30
            J_40 = J_4 * wall_albedo * VF_40
```

```
            ''' Calculate the total radiation that strikes the segment this hour.
            Then calculate how much of it is reflected from the canyon '''
            # J_0 is the total sunlight that strikes the segment (from sky and walls)
            J_0 = J_20 + J_30 + J_40

            # radiation reflected from segment to sky this hour
            sunlight_segment_to_sky_this_hour = J_0 * albedo * (VF_02 + VF_03 * wall_albedo *
                                                    VF_32 + VF_04 * wall_albedo * VF_42 )

            # radiation reflected from segments to sky this hour
            sunlight_from_all_segments_to_sky_this_hour.append(sunlight_segment_to_sky_this_hour)

        # Radiation from all segments reflected to sky
        all_sunlight_from_segments_to_sky_this_hour = sum(sunlight_from_all_segments_to_sky_this_hour)

        # radiation reflected from wall back to sky this hour
        sunlight_from_wall_to_sky_this_hour = J_3 * wall_albedo * VF_32 + J_4 * wall_albedo * VF_42

        # total radiation reflected from canyon to sky this hour
        reflected_sunlight_this_hour = all_sunlight_from_segments_to_sky_this_hour + sunlight_from_wall_to_sky_this_hour

    # total radiation reflected from canyon to sky by hour
    reflected_sunlight_by_hour.append( reflected_sunlight_this_hour )

    ''' Calculate the daily reflected radiation '''
    # Calculate daily reflected radiation by the sum of each hour's reflected radiation
    daily_reflected_sunlight = sum(reflected_sunlight_by_hour)

    # Normalized daily reflected radiation by road width [kWh/m2]
    reflected_sunlight_per_unit_road_area = daily_reflected_sunlight / road_width

return reflected_sunlight_per_unit_road_area
```

Figure F.7: Continuation of function to calculate the reflected sunlight from the road on the canyon floor.

Bibliography

[1] D. Parker, J. Sonne, and J. Sherwin. "Comparative evaluation of the impact of roofing systems on residential cooling energy demand in Florida". In: *Proceedings of 2002 ACEEE Summer Study on Energy Efficiency in Buildings, Teaming for Efficiency.* 2002.

[2] Dev Millstein and Surabi Menon. "Regional climate consequences of large-scale cool roof and photovoltaic array deployment". In: *Environmental Research Letters* 6 (2011). URL: http://iopscience.iop.org/1748-9326/6/3/034001.

[3] M. Santamouris. "Cooling the cities - A review of reflective and green roof mitigation technologies to fight heat island and improve comfort in urban environments". In: *Solar Energy* 103 (), pp. 682–703. ISSN: 0038.

[4] Arthur H. Rosenfeld et al. "Cool communities: strategies for heat island mitigation and smog reduction". In: *Energy and Buildings* 28.1 (1998), pp. 51 –62. ISSN: 0378-7788. DOI: http://dx.doi.org/10.1016/S0378-7788(97)00063-7.

[5] Hashem Akbari, Surabi Menon, and Arthur H. Rosenfeld. "Global cooling: increasing world-wide urban albedos to offset CO2". In: *Climatic Change* 94 (2009), pp. 275–286. ISSN: 0165-0009 (Print), 1573-1480 (Online). DOI: 10.1007/s10584-008-9515-9.

[6] Surabi Menon et al. "Radiative forcing and temperature response to changes in urban albedos and associated CO2 offsets". In: *Environmental Research Letters* 5 (2010). DOI: 10.1088/1748-9326/5/1/014005.

[7] Hashem Akbari, H Damon Matthews, and Donny Seto. "The long-term effect of increasing the albedo of urban areas". In: *Environmental Research Letters* 7.2 (2012), p. 024004. URL: http://stacks.iop.org/1748-9326/7/i=2/a=024004.

[8] H Akbari, M Pomerantz, and H Taha. "Cool surfaces and shade trees to reduce energy use and improve air quality in urban areas". In: *Solar Energy* 70.3 (2001). Urban Environment, pp. 295 –310. ISSN: 0038-092X. DOI: http://dx.doi.org/10.1016/S0038-092X(00)00089-X.

[9] Haider Taha. "Modifying a mesoscale meteorological model to better incorporate urban heat storage: a bulk-parameterization approach". In: *Journal of Applied Meteorology* 38.4 (1999). Added to JabRef: 2010.04.21, pp. 466–473. DOI: doi:10.1175/1520-0450(1999)038<0466:MAMMMT>2.0.CO;2.

[10] Hashem Akbari and Steven J. Konopacki. "Calculating energy-saving potentials of heat-island reduction strategies". In: *Energy Policy* 33.6 (2005), pp. 721–756. DOI: 10.1016/j.enpol.2003.10.001.

[11] H. Taha, S. Konopacki, and S. Gabersek. "Impacts of Large-Scale Surface Modifications on Meteorological Conditions and Energy Use: A 10-Region Modeling Study". In: *Theoretical and Applied Climatology* 62.3 (), pp. 175–185. ISSN: 1434-4483. DOI: 10.1007/s007040050082.

[12] Hashem Akbari, Steven J. Konopacki, and Melvin Pomerantz. "Cooling energy savings potential of reflective roofs for residential and commercial buildings in the United States". In: *Energy - The International Journal* 25.5 (1999), pp. 391–407. URL: http://www.sciencedirect.com/science/article/pii/S0360544298001054.

[13] A. Synnefa, M. Santamouris, and H. Akbari. "Estimating the effect of using cool coatings on energy loads and thermal comfort in residential buildings in various climatic conditions". In: *Energy and Buildings* 39.11 (2007), pp. 1167–1174.

[14] S.A. Klein and et al. *TRNSYS 17: A Transient System Simulation Program*. 2010. URL: http://sel.me.wisc.edu/trnsys.

[15] R Levinson and H Akbari. "Potential benefits of cool roofs on commercial buildings: conserving energy, saving money, and reducing emission of greenhouse gases and air pollutants". In: *Energy Efficiency* 3.1 (2010), pp. 53–109.

[16] Danny S. Parker and Stephen F. Barkaszi Jr. "Roof solar reflectance and cooling energy use: field research results from Florida". In: *Energy and Buildings* 25.2 (1997), pp. 105–115.

[17] W.A. Miller et al. *California Home Demonstrations Showcasing the Energy Savings of Tile, Painted Metal and Asphalt Shingle Roofs with Cool Color Pigments*. Tech. rep. CEC-500-2006-067-AT7. California Energy Commission, 2006. URL: http://www.energy.ca.gov/2006publications/CEC-500-2006-067/CEC-500-2006-067-AT7.pdf.

[18] G De With, N Cherry, and J Haig. "Thermal Benefits of Tiled Roofs with Above-sheathing Ventilation". In: *Journal of Building Physics* 33.2 (2009), pp. 171–194. DOI: http://dx.doi.org/10.1177/1744259109105238.

[19] William Miller and Jan Kony. "Next generation roofs and attics for homes". In: *2008 ACEEE Summer Study on Energy Efficiency in Buildings*.

[20] Melvin Pomerantz, Pablo J. Rosado, and Ronnen M. Levinson. "A simple tool for estimating city-wide annual electrical energy savings from cooler surfaces". In: *Urban Climate* 14, Part 2 (2015), pp. 315 –325. ISSN: 2212-0955. DOI: http://dx.doi.org/10.1016/j.uclim.2015.05.007.

[21] Haider Taha. "Modeling the impacts of large-scale albedo changes on ozone air quality in the South Coast Air Basin". In: *Atmospheric Environment* 31.11 (1997), pp. 1667 – 1676. ISSN: 1352-2310. DOI: http://dx.doi.org/10.1016/S1352-2310(96)00336-6.

[22] Melvin Pomerantz et al. "Paving materials for heat island mitigation". In: (1997). DOI: doi:10.2172/291033.

[23] Neda Yaghoobian and Jan Kleissl. "Effect of reflective pavements on building energy use". In: *Urban Climate* 2 (2012), pp. 25 –42. ISSN: 2212-0955. DOI: http://dx.doi.org/10.1016/j.uclim.2012.09.002.

[24] D. Sailor et al. "Building energy use implications of ground-level albedo modification". In: *8th International Conference on Urban Climates in UCD, Dublin, Ireland*. 2012.

[25] Fei Chen et al. "The integrated WRF/urban modelling system: development, evaluation, and applications to urban environmental problems". In: *International Journal of Climatology* 31.2 (). ISSN: 1097-0088.

[26] Valery Masson. "A physically-based scheme for the urban energy budget in atmospheric models". In: *Boundary-Layer Meteorology* 94 (2000), pp. 357–397.

[27] Hiroyuki Kusaka et al. "A Simple Single-Layer Urban Canopy Model For Atmospheric Models: Comparison With Multi-Layer And Slab Models". English. In: *Boundary-Layer Meteorology* 101.3 (2001), pp. 329–358. ISSN: 0006-8314. DOI: 10.1023/A:1019207923078.

[28] Hiroyuki Kusaka and Fujio Kimura. "Coupling a Single-Layer Urban Canopy Model with a Simple Atmospheric Model: Impact on Urban Heat Island Simulation for an Idealized Case". In: *Journal of the Meteorological Society of Japan. Ser. II* 82.1 (2004), pp. 67–80. DOI: 10.2151/jmsj.82.67.

[29] Alberto Martilli, Alain Clappier, and MathiasW. Rotach. "An Urban Surface Exchange Parameterisation for Mesoscale Models". English. In: *Boundary-Layer Meteorology* 104.2 (2002), pp. 261–304. ISSN: 0006-8314. DOI: 10.1023/A:1016099921195.

[30] K. Fortuniak. "Numerical estimation of the effective albedo of an urban canyon". In: *Theoretical and Applied Climatology* 91.1 (2007), pp. 245–258. ISSN: 1434-4483. DOI: 10.1007/s00704-007-0312-6.

[31] Pablo J. Rosado et al. "Measured temperature reductions and energy savings from a cool tile roof on a central California home". In: *Energy and Buildings* 80 (2014), pp. 57 –71. ISSN: 0378-7788. URL: http://www.sciencedirect.com/science/article/pii/S037877881400334X.

[32] US Environmental Information Administration. *Residential Energy Consumption Survey (RECS)*. 2011. URL: http://www.eia.gov/consumption/residential/reports/2009/square-footage.cfm.

[33] Akbari Hashem. "Cool roofs save energy". In: *ASHRAE Transactions* 104.1B (1998), pp. 783–788.

[34] Hashem Akbari et al. "Cool Colored Roofs to Save Energy and Improve Air Quality". In: *Proceedings of the 2004 ACEEE Summer Study on Energy Efficiency in Buildings*. 2004. URL: http://www.osti.gov/scitech/servlets/purl/860746.

[35] J. Konopacki Steven and Akbari Hashem. *Simulated impact of roof surface solar absorptance, attic, and duct insulation on cooling and heating energy use in single-family new residential buildings*. Tech. rep. 1998.

[36] R Levinson et al. "Inclusion of cool roofs in nonresidential Title 24 prescriptive requirements". In: *Energy Policy* 33.2 (2005), pp. 151–170.

[37] W. Miller et al. *Experimental analysis of the natural convection effects observed withinthe closed cavity of tile roofs*. 2005.

[38] Danny S. Parker and John Sherwin. "Comparative summer attic thermal performance of six roof constructions". In: *ASHRAE Transactions 104 (Part 2)* 104.2 (1998), pp. 1084–1092.

[39] William Miller et al. "Natural convection heat transfer in roofs with above-sheathing ventilation". In: *Proceedings of Thermal Performance of the Exterior Envelopes of Buildings X*. 2007.

[40] Marc Dodson. *Residential market: the western steep-slope market*. 2007.

[41] Marc Dodson. *Reader survey & western market share*. 2015.

[42] H Akbari et al. *Inclusion of Solar Reflectance and Thermal Emittance Prescriptive Requirements for Residential Roofs in Title 24*. 2006.

[43] F Incropera and D DeWitt. "Internal flow". In: *Fundamentals of Heat and Mass Transfer*. 5th Edition. Wiley and Sons, 2002. Chap. Section 8.3.3.

[44] R Hendron and C Engenbrecht. *United States DOE Building America House Simulation Protocols (Revised October 2010)*. Tech. rep. U.S. DOE Buildng Technologies Program, 2010. URL: http://www.nrel.gov/docs/fy11osti/49246.pdf.

[45] Pacific Gas and Electric. *Time of use pricing*. 2013. URL: http://www.pge.com/mybusiness/energysavingsrebates/timevaryingpricing/timeofusepricing.

[46] *ASTM Standard C1549-09: Standard Test Method for Determining Solar Reflectance Near Ambient Temperature Using a Portable Solar Reflectometer*. Tech. rep. West Conshohocken, PA: American Society for Testing and Materials, 2010.

[47] *Cool Roof Rating Council Rated Product Directory*. Tech. rep. URL: http://coolroofs.org/products/search.php.

[48] R Levinson, H Akbari, and P Berdahl. "Measuring solar reflectancePart I: Defining a metric that accurately predicts solar heat gain". In: *Solar Energy* 84.9 (2010), pp. 1717–1744.

[49] R Levinson, H Akbari, and P Berdahl. "Measuring solar reflectancePart II: Review of practical methods". In: *Solar Energy* 84.9 (2010), pp. 1745–1759.

[50] CertainTeed. *CertainTeed Shingle Applicators Manual, Grand Manor and Carriage House, Chapter 16*. 2012. URL: http://www.certainteed.com/resources/CarriageHouseInstall.pdf.

[51] Tile Roofing Institute. *Concrete and clay roof tile: installation manual for moderate climate regions – part 2*. March 2010. URL: http://www.eagleroofing.com/pdf/ProductLiturature/InstallationGuides/TRIModerateClimateGuide2010_part2.pdf.

[52] *2011 American Housing Survey, Table C-11-AO*. 2011. URL: http://www.census.gov/housing/ahs/files/ahs11/National2011.xls.

[53] I Walker. "Technical background for default values used for forced air systems in proposed ASHRAE Standard 152P". In: *ASHRAE Transactions* 104 (1998), pp. 1360–1375.

[54] ASHRAE. *2009 ASHRAE Handbook – Fundamentals (SI Edition)*. Chapter 26, Table 4. 2009.

[55] *Installation Instructions*. Lennox Merit Series 14ACX Units. 2011. URL: http://www.lennox.com/pdfs/installation_maintenance/Lennox_14ACX_IOM.pdf.

[56] *Unit Information*. Lennox G51MP Series, revised 11-2006. 2006. URL: http://0190acd.netsolhost.com/manuals/G51MP_Series.pdf.

[57] National Renewable Energy Laboratory. *Measurement and Instrumentation Data Center Solar Position and Intensity (SOLPOS) Calculator*. 2013. URL: http://www.nrel.gov/midc/solpos/solpos.html.

[58] University of Oregon Solar Radiation Monitoring Laboratory. *Polar sun chart program*. 2008. URL: http://solardat.uoregon.edu/PolarSunChartProgram.html.

[59] Sustainable by Design. *Windows heat gain*. Seattle, Washington. 2009. URL: http://susdesign.com/windowheatgain/.

[60] Windows and Daylighting Group. *WINDOW sofware version 6.3*. Lawrence Berkeley National Laboratory, Berkeley, California. 2009. URL: http://windows.lbl.gov/software/window/window.html.

[61] US Environmental Protection Agency. *ENERGY STAR performance ratings - methodology for incorporating source energy use*. 2011. URL: http://www.energystar.gov/ia/business/evaluate_performance/site_source.pdf.

[62] Pacific Gas and Electric. *Gas and electric rates*. 2013. URL: http://www.pge.com/nots/rates/tariffs/rateinfo.shtml.

[63] US Environmental Protection Agency. *eGRID2012 Version 1.0 Year 2009 Summary Tables*. April 2012. URL: http://www.epa.gov/cleanenergy/documents/egridzips/eGRID2012V1_0_year09_SummaryTables.pdf.

[64] US Environmental Protection Agency. *Compilation of air pollutant emission factors, volume I - Stationary point and area source - AP 52, 5th edn.* 2005. URL: http://www.epa.gov/ttnchie1/ap42.

[65] *History of Fresno, CA*. 2013. URL: http://www.wunderground.com/history/airport/KFAT/MonthlyHistory.html\#calendar.

[66] *Daily averages for Fresno, CA*. 2013. URL: http://www.weather.com/weather/wxclimatology/daily/USCA0406?climoMonth=7.

[67] National Renewable Energy Laboratory. *National solar radiation data base, 1991 - 2005 update: typical meteorological year 3*. 2013. URL: http://rredc.nrel.gov/solar/old_data/nsrdb/1991-2005/tmy3.

[68] M Farzad and D L O'Neal. "System performance characteristics of an air conditioner over a range of charging conditions". In: *International Journal of Refrigeration* 14.6 (1991), pp. 321–328.

[69] William C. Skamarock et al. *A description of the advanced research WRF version 3*. Tech. rep. NCAR Technical Note NCAR/TN475+STR. Boulder, Colorado. National Center for Atmospheric Research, Mesoscale and Microscale Meteorology Division, 2008. URL: http://www2.mmm.ucar.edu/wrf/users/docs/arw_v3.pdf.

[70] Collin Homer et al. "Completion of the 2001 National Land Cover Database for the Conterminous United States". In: *Photogrammetric Engineering and Remote Sensing* 73.4 (2007), pp. 337–341.

[71] ASHRAE. *2009 ASHRAE Handbook – Fundamentals (SI Edition)*. Chapter 14. 2009.

[72] J R Howell. *A catalog of radiation configuration factors*. 1982. URL: http://www.thermalradiation.net/tablecon.html.

[73] HC Hottel. "Radiant heat transmission". In: *Heat Transmission*. 3rd Edition. McGraw-Hill Book Co., 1954, pp. 55–125.

[74] United States Geological Survey Multi-Resolution Land Characteristics Consortium. *National Land Cover Dataset (NLCD) 2006 Percent Developed Imperviousness (2011 Edition)*. 2011. URL: http://gisdata.usgs.gov/TDDS/DownloadFile.php?TYPE=nlcd2006\&FNAME=nlcd_2006_impervious_2011_edition_2014_10_10.zip.

[75] Pacific Northwest National Laboratory. *Building Energy Codes Program – Residential Prototype Building Models*. 2014. URL: https://www.energycodes.gov/development/residential/iecc_models.

[76] M Deru et al. *US Department of Energy commercial reference building models of the national building stock*. Tech. rep. National Renewable Energy Laboratory, 2011.

[77] *Design and Procedures Manual: Section 15 - Street Design Standards*. City of Sacramento CA. 2015. URL: http://portal.cityofsacramento.org/Public-Works/Resources/Publications.

[78] *Zoning Code of Sacramento County*. Sacramento County, CA. 2015. URL: http://www.per.saccounty.net/LandUseRegulationDocuments/Pages/.

[79] *EnergyPlus version 8.1*. 2003. URL: https://energyplus.net/.

[80] *Residential compliance manual*. Tech. rep. CEC-400-2008-016-CMF-Rev 1. California Energy Commission, 2008. URL: http://www.energy.ca.gov/title24/standards_archive/.

[81] *California Building Climate Zone Areas*. 2015. URL: http://www.energy.ca.gov/maps/renewable/building_climate_zones.html.

[82] *Nonresidential compliance manual*. Tech. rep. CEC-400-2008-017-CMF-Rev 1. California Energy Commission, 2008. URL: http://www.energy.ca.gov/title24/standards_archive/.

[83] Infoplease. *Top 50 cities in the U.S. by population and rank*. 2015. URL: http://www.infoplease.com/ipa/a0763098.html.

[84] *City block*. 2015. URL: https://en.wikipedia.org/wiki/City_block.

[85] *Los Angeles County Model Design Manual for Living Streets*. Los Angeles County, CA. 2015. URL: http://www.modelstreetdesignmanual.com/.

[86] *Geometric Design Guidelines*. Department of Transportation, City of San Jose, CA. 2015. URL: https://www.sanjoseca.gov/index.aspx?NID=1882.

[87] Geoffrey H. Donovan and David T. Butry. "The value of shade: Estimating the effect of urban trees on summertime electricity use". In: *Energy and Buildings* 41.6 (2009), pp. 662 –668. ISSN: 0378-7788. DOI: http://dx.doi.org/10.1016/j.enbuild.2009.01.002.

[88] James R. Simpson and E. Gregory McPherson. "Potential of tree shade for reducing residential energy use in California". In: *Journal of Arboriculture* 22.1 (1996), pp. 10–18.

[89] Yi Zhang. *jEPlus – An EnergyPlus simulation manager for parametrics*. 2012.

[90] White Box Technologies. *Weather data for energy calculations*. 2011. URL: http://weather.whiteboxtechnologies.com/.

[91] F Incropera and D DeWitt. "Radiation Exchange between surfaces". In: *Fundamentals of Heat and Mass Transfer*. 6th Edition. Wiley and Sons, 2007. Chap. Section 13.1.1.

[92] JR Ehlert and TF Smith. "View factors for perpendicular and parallel rectangular plates". In: *Journal of Thermophysics and Heat Transfer* 7.1 (1993), pp. 175–173.

[93] *United States Zip Code Database*. 2015. URL: http://www.unitedstateszipcodes.org/zip-code-database/.

[94] US Environmental Information Administration. *Residential Energy Consumption Survey (RECS) - public use microdata*. 2009. URL: http://www.eia.gov/consumption/residential/data/2009/.

[95] Itron Incorporated. *California commercial end-use survey (CEUS)*. Tech. rep. CEC-400-2006-005. California Energy Commission, 2006. URL: http://www.energy.ca.gov/ceus.

[96] H Gilbert et al. *Life Cycle Assessment and Co-Benefits of Cool Pavements*. Tech. rep. Technical report in progress. California Air Resources Board and California Environmental Protection Agency, 2016.

[97] US Environmental Information Administration. *Commercial Building Energy Consumption Survey (CBECS) - public use microdata*. 2003. URL: http://www.eia.gov/consumption/commercial/data/2003/.

[98] *Table GCT-PH1 Population, Housing Units, Area, and Density: 2010 - State – Place and (in selected states) County Subdivision*. 2010. URL: http://www.census.gov/cgi-bin/geo/shapefiles2010/main.

[99] *ArcGIS Desktop Help 10.2 Geostatistical Analyst*. 2014. URL: http://resources.arcgis.com/en/help/main/10.2/index.html.

[100] *California Hydroelectric Statistics & Data*. 2016. URL: http://energyalmanac.ca.gov/renewables/hydro/index.php.